# University of Southampton

Faculty of Environmental Life Sciences

School of Biological Sciences

**Tau Gene Structure-Function Relationships:**

**How do Genetic Variations in the Tau Gene *MAPT* Influence Tau-Mediated Degeneration?**

By

**Amber Skye Cooper**

**BSc in Biomedical Sciences**

**MRes in Advanced Biological Sciences**

ORCID ID: 0000-0003-2525-0148

Thesis for the degree of Doctor of Philosophy

2026

# University of Southampton

## Abstract

Faculty of Environmental Life Sciences
Doctor of Philosophy

**How do Genetic Variations in the Tau Gene *MAPT* Influence Tau-Mediated Degeneration?**

Amber Skye Cooper

The microtubule associated protein Tau plays a critical pathogenic role in multiple neurodegenerative diseases, called Tauopathies, which manifest as sporadic or familial dementias. Tauopathies have significant clinical, microscopic and molecular heterogeneity, which poses challenges for diagnosis and treatment. Tau hyperphosphorylation and aggregation are two hallmarks of Tauopathies and represent common therapeutic targets. However, the extent to which these mechanisms independently contribute towards neurotoxicity and drive disease heterogeneity remains unclear.

Leveraging the genetic tractability of *Drosophila*, this thesis investigates the relative contributions of phosphorylation and aggregation towards Tau-mediated neurodegeneration. This was achieved by using novel designer human transgenes with altered phosphorylation status and/or aggregation propensity by deleting the $^{306}$VQIVYK$^{311}$ motif. By assessing Tau accumulation, neurodegeneration, neuronal function and survival in the aging *Drosophila* nervous system, I evaluated the utility of $^{306}$VQIVYK$^{311}$ as a therapeutic target through genetic deletion and pharmacological inhibition with RI-AG03 *in vivo*.

This evaluation demonstrated that hyperphosphorylation-induced toxicity is dependent on the $^{306}$VQIVYK$^{311}$ motif, where its deletion completely abolishes severe neurotoxicity, Tau accumulation, mis-localisation and functional deficits caused by phospho-mimicking Tau at 14 disease associated epitopes (TauE14). Studies to investigate the mechanisms underlying this rescue in toxicity imply that $^{306}$VQIVYK$^{311}$ does not mediate protection by altering Tau's microtubule binding ability or phosphorylation propensity. The rescue could also not be explained purely through a reduction of Tau aggregation as measured by the amount of insoluble Tau species formed in animals with and without the $^{306}$VQIVYK$^{311}$ domain. However, using the conformation-specific MC1 antibody, my results indicate that $^{306}$VQIVYK$^{311}$ may mediate toxicity by controlling the misfolding of Tau into pathogenic conformations.

Furthermore, I show that $^{306}$VQIVYK$^{311}$ represents a broad therapeutic target which can reduce toxicity not just of hyperphosphorylated Tau, but also of the disease-associated R406W mutant. Pharmacological inhibition using RI-AG03 selectively reduced the accumulation of phospho-mimicking Tau, showing good translation of *in vivo* efficacy, although optimisation of delivery and dose are needed.

This thesis establishes $^{306}$VQIVYK$^{311}$ as a central mediator of Tau toxicity across multiple pathological contexts and highlights a focal shift for future studies to design therapies that target pathological conformations rather than Tau aggregate abundance alone.

# Table of Contents

# Table of Tables

# Table of Figures

## Research Thesis: Declaration of Authorship

Print name: Miss Amber Skye Cooper

Title of thesis: How do Genetic Variations in the Tau Gene *MAPT* Influence Tau-Mediated Degeneration?

I declare that this thesis and the work presented in it are my own and has been generated by me as the result of my own original research.

I confirm that:

1. This work was done wholly or mainly while in candidature for a research degree at this University;
2. Where any part of this thesis has previously been submitted for a degree or any other qualification at this University or any other institution, this has been clearly stated;
3. Where I have consulted the published work of others, this is always clearly attributed;
4. Where I have quoted from the work of others, the source is always given. With the exception of such quotations, this thesis is entirely my own work;
5. I have acknowledged all main sources of help;
6. Where the thesis is based on work done by myself jointly with others, I have made clear exactly what was done by others and what I have contributed myself;
7. Parts of this work have been published as: Aggregation promoting sequences rather than phosphorylation are essential for Tau-mediated toxicity in *Drosophila* in BioRxiv DOI: 2024.12.22.629946; doi: https://doi.org/10.1101/2024.12.22.629946. (Cooper et al., 2024)

Signature: .....Date:.....

# Acknowledgements

I am deeply grateful to my supervisor, Professor Amritpal Mudher for her continued support, mentorship and guidance throughout my PhD journey. I would also like to thank my secondary supervisor Dr Herman Wijnen and my collaborators Professor Douglas Allan and Dr Makis Skoulakis for their guidance, discussion and valuable input throughout the project.

To my Lab members past and present: Dr Eva Ruiz Ortega, Dr Bradley Richardson, Dr Ben Batchelor, Dr George Devitt, Dr Miguel Ramirez-Moreno, Yongrui Zhang, Ray Price, Aran Mohan and Dr Dipita Bhattacharyya. Thank you all for being my teachers, collaborators, friends and support network. I would also like to thank Jazmine Williams and Georgia Millner for being excellent students.

I would like to thank all the other people in Biological Sciences who have supported me, with a special thanks to the Crispin Lab for adopting me as their honorary member. Thank you to the research technicians and staff at the imaging faculty, particularly Dr Mark Willett. I would like to also say a huge thankyou to the Gerald Kerkut Trust for their generous financial support throughout my studies.

Finally, I wish to thank my fiancé Anoir, for his unwavering support throughout my PhD. You are my rock. To my parents Steve and Andrea thank you for everything you have done and sacrificed for me, I love you both very dearly. I am also grateful to my siblings, Oliver and Joshua, and my dear friend Izzy, for nurturing me and helping me into the best version of myself. I could not have done it without you all!

# Definitions and Abbreviations

aa ..... Amino Acid

AAV ..... Adeno-associated virus

AD ..... Alzheimer's disease

AGD ..... Argyrophilic grain disease

AL ..... Antennal lobe

APP ..... Amyloid precursor protein

BBB ..... Blood brain barrier

CBD ..... Corticobasal degeneration

CNS ..... Central nervous system

Cryo-EM ..... Cryogenic electron microscopy

CSF ..... Cerebrospinal fluid

CTE ..... Chronic traumatic encephalopathy

EM ..... Electron microscopy

FRET ..... Forster resonance energy transfer

FTDP-17(*MAPT*) ..... Frontotemporal dementia and parkinsonism linked to chromosome 17 (*MAPT*)

GFP ..... Green fluorescent protein

GOF ..... Gain-of-function

GTO ..... Granular Tau Oligomer

GSK-3β ..... Glycogen synthase kinase 3β

HMW ..... High molecular weight

HNRP ..... Heterogenous nuclear ribonucleoprotein

HSP ..... Heat shock protein

hTau ..... Human Tau

hTau2N4R-DEL ..... Human Tau 2N4R-ΔVQIVYK

hTau2N4R-E14,DEL ..... Human Tau 2N4R-E14+ΔVQIVYK

IDP ..... Intrinsically disordered protein

iPSC ..... Induced pluripotent cells

KO ..... Knock-out

LOF ..... Loss-of-function

MAPs ..... Microtubule associated proteins

MAPT ..... Microtubule associated protein Tau

MARKs ..... Microtubule-affinity regulating kinases

MBRD ..... Microtubule binding repeat domain

MCI ..... Mild cognitive function

MT ..... Microtubules

NFT ..... Neurofibrillary tangle

Or47b ..... Olfactory receptor 47b
ORN ..... Olfactory receptor neurons
PD ..... Picks disease
PHF ..... Paired helical filament
PNS ..... Peripheral nervous system
PP2A ..... Protein phosphatase 2A
PRD ..... Proline rich domain
PSP ..... Progressive supranuclear palsy
PTM ..... Post-translational modification
p-Tau ..... Phosphorylated Tau
RNA ..... Ribonucleic acid
SEM ..... Scanning electron microscopy
SF ..... Straight filament
SIM ..... Structured illumination microscopy
WT ..... Wildtype
VBFDA ..... Value-based feeding decision assay

# Chapter 1 Introduction

## 1.1 Dementia and Neurodegenerative diseases

Dementia is an umbrella term used to describe various cognitive impairment disorders caused by neuronal degeneration. These complex neurodegenerative diseases affect the brain and nervous system as a result of neuron and synapse death. Consequentially, patients experience deficits in cognitive functioning including thinking, reasoning, language, learning and memory. These symptoms lead to a devastating loss of ability to perform activities of daily living.

Currently the World Health Organization (WHO) estimate there are 50 million people living with dementia globally (WHO 2020), which is expected to triple to more than 153 million by 2050 (GBD 2019 Dementia Forecasting collaborators DOI: https://doi.org/10.1016/S2468-2667(21)00249-8). Age is the biggest risk factor for developing dementia (BMJ 2019), however there are significant lifestyle, environmental and genetic factors which contribute towards the likelihood of developing dementia. Recent reports from the Lancet Commission (2024) have identified 14 modifiable risk factors that manifest at different life stages which could account for up to 45% of all cases of dementia **(Figure 1).**

As age-related diseases, the likelihood of developing dementia after the age of 60 doubles every 5 years (Prince 2014, NHS England 2024). It is reported that 1 in 2 people will be affected by dementia in their life, either directly or indirectly as form of family members or carers(NHS England 2024). Aside from huge economic pressures that dementia has on the NHS, there are many relational and social implications for living with or caring for someone with dementia.

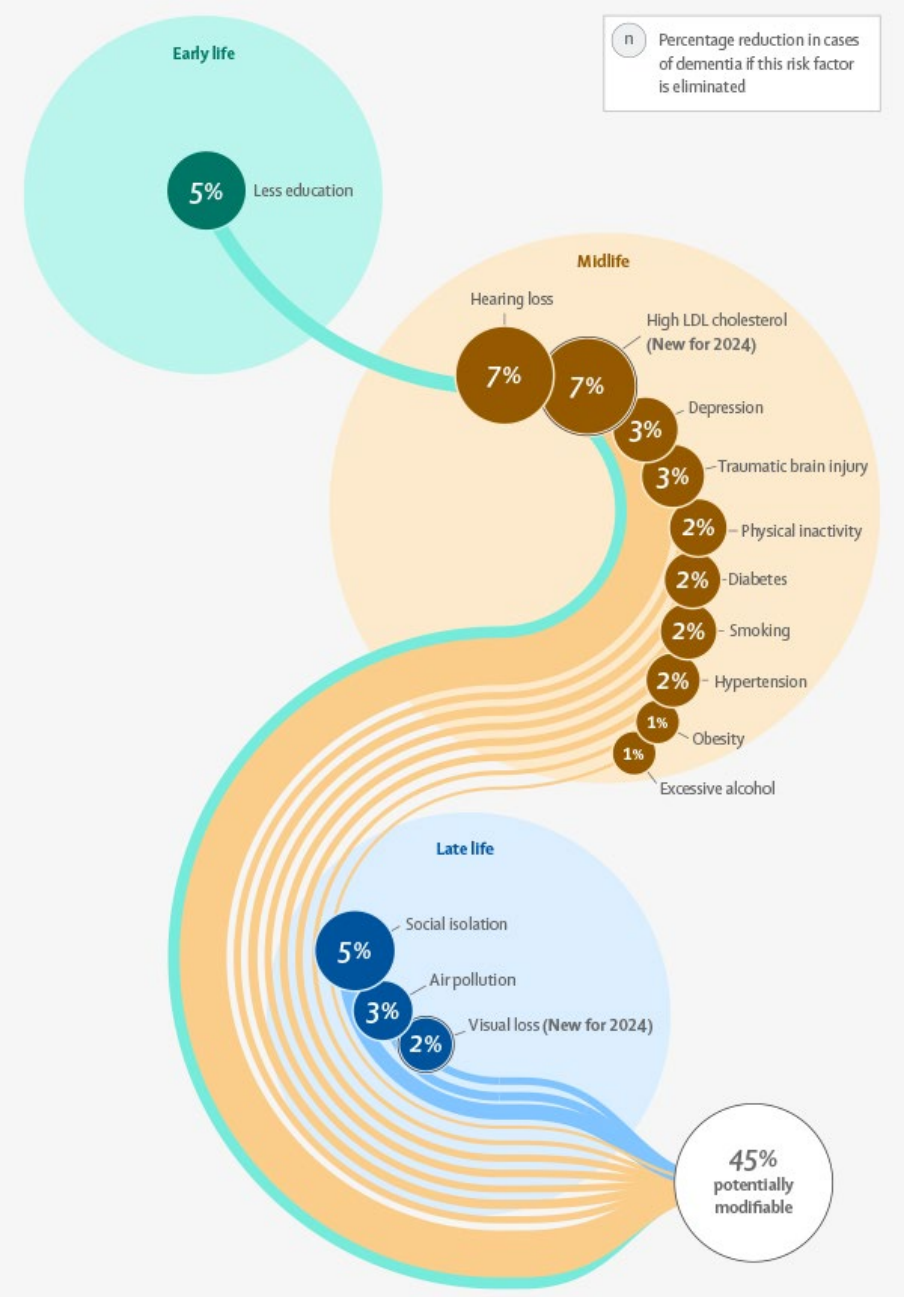


**Figure 1. Risk factors of dementia.**

Modifiable, lifestyle risk factors associated with dementia taken from the 2024 update to the standing Lancet Commission on dementia prevention https://www.thelancet.com/infographics-do/dementia-risk accessed June 10.2025

### 1.1.1 Alzheimer's disease and Tauopathies

Alzheimer's disease (AD) is the most common form of dementia. First discovered by Alois Alzheimer in 1906 (Möller and Graeber, 1998), AD has been researched for over 100 years. Like dementia, the most significant risk factor to developing AD is age, however there are also genetic and lifestyle risk factors. Genetic risk factors include mutations in

genes such as amyloid precursor protein (APP), presenilin-1 and presenilin-2, or carriers of alleles like Apolipoprotein-ε4 which is strongly associated with increased risk (Karagas et al., 2025). In contrast, recent genome-wide association studies of cognitively healthy centenarians (individuals aged >100 years old) have identified an enrichment of protective alleles associated with resilience to AD. These findings highlight genes that may confer neuroprotection against cognitive decline and disease, and offer potential new therapeutic targets (Tesi et al., 2024). Other controllable lifestyle factors are also strongly linked to AD incidence, including cardiovascular disease, obesity, type 2 diabetes, smoking, physical inactivity and high blood pressure (Abubakar et al., 2025). Overall, AD is considered to be a multifactorial disease which likely develops from multiple factors over a persons lifetime, which makes it inherently difficult to predict.

AD belongs to a subcategory of dementias called Tauopathies, which are primarily caused by abnormal Tau protein deposits within the brain. Tauopathies are a large heterogenous group of neurodegenerative diseases defined by the presence of filamentous, highly phosphorylated Tau inclusions within the neurons and/or glia (Goedert et al., 2017, Spillantini et al., 1998, Crowther and Goedert, 2000). This pathology produces a diverse range of diseases including AD, Pick's disease (PiD), Progressive supranuclear palsy (PSP), Corticobasal degeneration (CBD), Chronic traumatic encephalopathy (CTE), Argyrophilic grain disease (AGD) and Frontotemporal dementia linked to chromosome 17 (FTDP-17). Tauopathies are typically sporadic, eg. AD, PSP, PD, however some are environmentally implicated eg. CTE through brain injury, and some are linked to familial genetic mutations eg. FTDP-17(*MAPT*). Nonetheless, all of these diseases are defined characteristically by significant neuronal loss, paired with abnormal Tau protein accumulation and aggregation, and as such are often referred to as proteinopathies (Harris et al., 2025).

Despite primarily being caused by the same proteins, the diseases are heterogenous at the clinical, neuropathological and molecular level. The clinical diversities of Tauopathies

varies dependent on the Tau isoforms and species present in the aggregates within the brain, and the cell types and anatomical regions affected by protein accumulation (Chung et al., 2021, Horie et al., 2022). Most recently, the structures of several brain-derived Tau fibrils from distinct Tauopathies have been solved using cryogenic electron microscopy (cryo-EM) (Shi et al., 2021, Scheres et al., 2020, Qi et al., 2025, Schweighauser et al., 2025). Cryo-EM has significantly increased our understanding about the atomic structures of mature Tau fibrils, directly visualising the fibrillar cores and their differences and similarities between the most prominent Tauopathies. Importantly this work demonstrates that down to the molecular level there are distinct fibril conformations between distinct Tauopathies (Shi et al., 2021, Scheres et al., 2020). This raises the underlying question as to how the Tau fibril structure and conformation influences pathological mechanisms mediating degeneration differently between Tauopathies.

### 1.1.2 Frontotemporal linked dementia

A small subset of familial Tauopathies are caused by genetic dysfunction within the *MAPT* gene encoding Tau. Missense, deletion, and splice mutations within the *MAPT* gene were first described in 1998 following human DNA sequence analysis of families with autosomal dominant frontotemporal dementia (FTD) (Hutton et al., 1998, Poorkaj et al., 1998, Spillantini et al., 1998). This category of diseases provides clear evidence that dysfunction of the Tau gene directly results in neurodegenerative disorders. Despite familial FTDP-17(*MAPT*) cases being a particularly rare form of dementia (Onyike and Diehl-Schmid, 2013), over 50 different pathogenic *MAPT* mutations have been reported (Strang et al., 2019a). The most common mutations include P301S/L, R406W, V337M and IV10+ (Schweighauser et al., 2025). The differential toxicity of these mutations are discussed in **section 1.5.4.**

Alike all Tauopathies, carriers of *MAPT* mutations are also clinically, pathologically, and genetically heterogenous, although carriers typically present with earlier age of onset and more aggressive clinical progression (Bugiani et al., 1999). Immunohistochemical slices of Tauopathy patients show distinct isoform composition and distinct lesion morphologies (Spillantini et al., 1998). Neuroimaging studies have also shown that *MAPT* mutations generate distinct progression patterns of regional atrophy related to their clinical phenotypes (Young et al., 2021, Whitwell et al., 2009a).

The significant clinical and molecular heterogeneity between Tauopathies creates challenges in understanding of the pathological mechanisms underlying Tau-mediated degeneration. Currently there is no cure for dementia or Tauopathies. Available treatments target the cognitive, behavioural and motor symptoms associated with the disease however there are no current Tau-targeting therapies which treat the underlying pathology (Congdon et al., 2023). Clear understanding of the mechanisms contributing towards neuronal degeneration and pathological gain-of-function from toxic proteins is essential for better design of therapeutic strategies against these conditions, and will form the main focus on the research in this thesis.

## 1.2 Tau

Tau is a microtubule-associated protein that in its physiological state, plays important roles in neuronal function. However, in Tauopathies, abnormal Tau deposits are a pathological hallmark. The hyperphosphorylation of Tau and its subsequent aggregation are the two most prominent pathogenic mechanisms that influence Tau-mediated toxicity and are therefore the primary targets for the development of modern Tau-based therapeutics. I will first describe Tau in its physiological state and later in **section 1.3** describe its roles in disease.

### 1.2.1 Tau Isoforms

Human Tau protein is encoded by the *MAPT* gene on chromosome 17 arm 21.31(Leveille et al., 2021). Tau protein is comprised of 16 exons, which through alternative splicing of pre-mRNA at exon 2, 3 and 10 generates 6 distinct Tau isoforms expressed in the central nervous system (CNS). The nomenclature of Tau isoforms are based on their inclusion of either 0, 1 or 2 N-terminal repeat inserts (0N, 1N, or 2N), and either 3 or 4 (3R or 4R) microtubule binding repeat inserts (R'), which range in size between 441-352 amino acids and weigh between 60-74kDa (Goedert et al., 1989) **(Figure 2).** Within the *MAPT* gene exons 2 and 3 encode for the N-terminal inserts (N1 and N2 respectively) **(Figure 2).** Exon 10 encodes for the second (R2) of the four repeat sequences that makes up the microtubule binding repeat domain (MBRD). In the peripheral nervous system (PNS), additional isoforms referred to as "Big Tau" associated to their high molecular weight have also been identified (Goedert et al., 1992, Fischer, 2023). These are generated from splicing of exons 4A and 6, but have significantly less pathogenic potential when compared to the CNS isoforms expressed in cells or an AVV-mouse model (Goedert et al., 1992, Fischer, 2023, Chung et al., 2024).

Tau isoforms are expressed differentially during development and aging. For example, 0N3R Tau, also known as foetal Tau, is only expressed during development. However, the isoform composition of Tau expressed changes dramatically after birth. In the adult human brain, the expression pattern of 3R:4R Tau isoforms is equimolar (Goedert et al., 1989) and the 1N and 2N isoforms also increase postnatally. While all six isoforms are present in the adult brain the relative abundance can vary regionally and can be difficult to directly measure *in vivo* as *MAPT* splicing and isoform expression are differentially regulated across different brain regions and in different cell types (Trabzuni et al., 2012). However, *in vitro* a 3D culture model of iPSC-derived neurons has demonstrated there are

relative differential expression patterns of 0N(37%), 1N(54%) and 2N(9%) of total Tau (Miguel et al., 2019, Wang and Mandelkow, 2016).

Isoform composition plays a critical role in pathology and diagnosis. Alterations to the 3R:4R Tau isoform expression patterns and are directly implicated in neurodegenerative diseases. For example, AD is characterized by a shift towards increased 4R Tau production (Cherry et al., 2021). These changes are disease specific and may classify different Tauopathies from the isoform composition signatures within the Tau accumulates (Spillantini et al., 1998). For example, AD, CTE and FTDP-17(*MAPT*), are associated with mixed 3R and 4R Tau compositions, whereas PSP, AGD and CBD feature predominantly 4R Tau, but PD only features 3R Tau(Kovacs, 2015). These isoforms have distinct roles in disease development, conformation and diagnosis and will be explored later in **sections 1.5 and 1.5.6.**

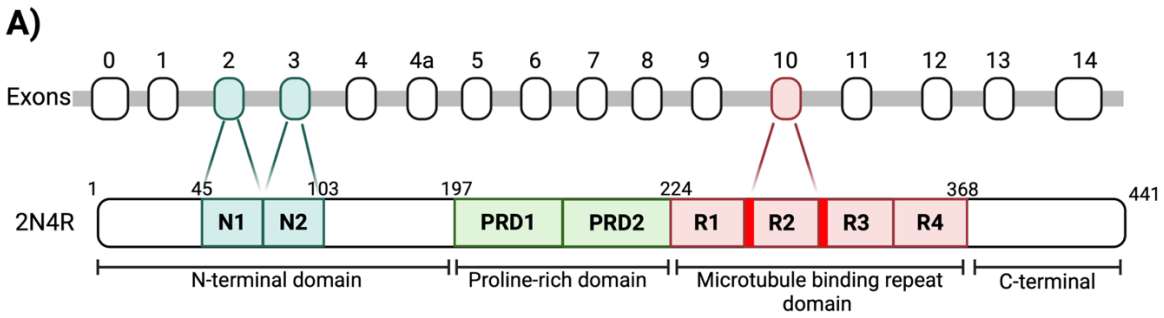


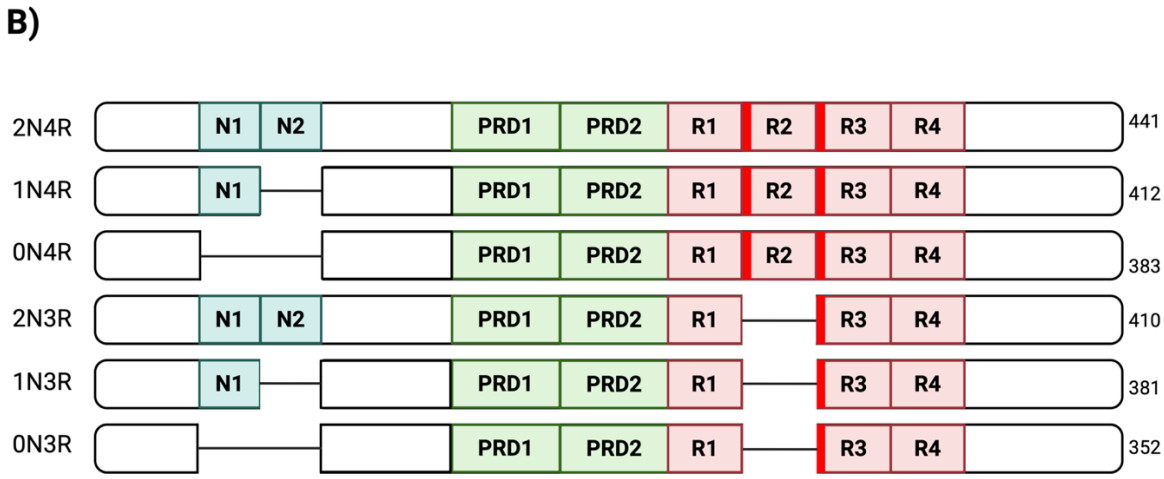


C)

```
  1 MAEPRQEFEV MEDHAGTYGL GDRKDQGGYT MHQDQEGDTD AGLKESPLQT
 51 PTEDGSEEPG SETSDAKSTP TAEDVTAPLV DEGAPGKAQQ QAPHTEIPEG
101 TTAEEAGIGD TPSLEDEAAG HVTQARMVSK SKDGTGSDDK KAKGADGKTK
151 IATPRGAAPP GQKGQANATR IPAKTPPAPK TPPSSGEPPK SGDRSGYSSP
201 GSPGTPGSRS RTPSLPTPPT REPKKVAVVR TPPKSPSSAK SRL
244 QTAPVPMPDLKNVKSKIGSTENLKHQPGGGK
275 VQIINKKLDLSNVQSKCGSKDNIKHVPGGGS
306 VQIVYKPVDLSKVTSKCGSLGNIHHKPGGGQ
337 VEVKSEKLDFKDRVQSKIGSLDNITHVPGGN
369 KKIETHKLTF RENAKAKTDH GAEIVYKSPV VSGDTSPRHL SNVSSTGSID
419 MVDSPQLATL ADEVSASLAK QGL
```

**Figure 2. Tau structural domains, isoforms and sequence.**

A) Splicing of the *MAPT* gene at exons 2, 3 and 10 produces B) 6 distinct isoforms of Tau protein. Tau has 4 main structural domains: the N-terminal domain containing two repeat inserts (N1, N2), proline-rich domain(PRD), the microtubule-binding domain containing 4 repeats (R1-4), and the C-terminal domain. C) Domains highlighted in corresponding colours in sequence of full length Tau2N4R.

### 1.2.2 Tau Structural Domains

Tau is an intrinsically disordered protein (IDP), mostly hydrophilic and locally repetitive (Mandelkow and Mandelkow, 1998). This means that Tau does not have a defined structure under physiological conditions, and in healthy adults. Structurally, Tau can be divided into 4 domains, organised starting with an amino acidic N-terminal domain (45-103aa), followed by the proline-rich domain (PRD) (197-224aa), the microtubule binding repeat domain (MBRD) (224-368aa) and the C-terminal domain (369-441aa) (Goedert et al., 1989) **(Figure 2).**

Each domain has been characterised and evaluated for its physiological function and possible pathological contribution consequent to post-translational modifications (PMTs) during disease. Briefly, the function of each domain is as follows.

The N-terminal domain (also known as the projection domain) is intrinsically disordered and projects away from the microtubules, functioning as a spacer between microtubule units by bridging between tubulin dimers and also interacts with the plasma membrane during cell signalling and transport (Chen et al., 1992, Al-Bassam et al., 2002, Kar et al., 2003). Physiologically, the spatial arrangement of the N-terminal domain extends outward from the surface of microtubules, primarily due to the electrostatic repulsion from its acidic amino terminal, to maintain the proper physiological organisation of Tau and the microtubules (Kar et al., 2003). The N-terminal domain has also been observed to interact with the cell plasma membrane (Brandt et al., 1995) mediated by interactions with Annexin 2, a membrane-linking protein. This association has been proposed to influence Tau localisation due to Annexins key roles in processes like exocytosis and endocytosis (Weissmann et al., 2009, Gauthier-Kemper et al., 2011, Gerke et al., 2005).

Following the acidic N-terminal domain there are two proline-rich domains (PRD) which are heavily involved with cell signalling pathways and protein kinase interactions

(Zabik et al., 2017). The PDR has roles in supporting microtubule binding. By flanking the MBRD, the PDR enhances tubulin binding and polymerisation, facilitating strong microtubule binding (McKibben and Rhoades, 2019). The PRD has multiple phosphorylation sites and proline-rich PPXXP/PXXP motifs involved in cellular signalling, mediating interactions with SH3 domain-containing proteins, including Src-family kinases such as Fyn which has pathological consequences (Lau et al., 2016, Lee et al., 1998, Briner et al., 2020).

The microtubule binding repeat domain (MBRD) contains 3 (3R) or 4 (4R) internal repeats which are highly conserved between nematodes, fruit flies, mice and humans (Goedert et al., 1996, Heidary and Fortini, 2001). The binding and stabilising of Tau to the microtubules occurs at multiple locations along the positively charged repeats, facilitated by electrostatic interactions from the negatively charge of the microtubules (Drechsler et al., 2019). The MBRD functions to bind and stabilise with tubulin units comprising the microtubules. Although the majority of microtubule binding force comes from the MBDR, part of the PRD and the C-terminal also assist microtubule assembly (Abraha et al., 2000). However it is also important to note that the PRD and the C-terminal domains flanking either side of the MBRD are equally important for enhancing tubulin binding and polymerisation capacity both *in vitro* and in cells. Deleting or mutating the PRD leads to significant reduction in the binding and stabilising of the microtubules (McKibben and Rhoades, 2019, Kadavath et al., 2015). The C-terminal region is also subjected to many PTMs and directly contributes towards Tau's solubility and function. Deletion of the C-terminal destabilises Tau and enhances its toxicity *in vivo* (Geng et al., 2015).

### 1.2.3 Tau physiological function

Tau is normally a highly soluble protein which is enriched in axons of neurons (Binder et al., 1985) (de Ancos and Avila, 1993, Kubo et al., 2019). The primary function of

Tau is to bind and promote the polymerisation and stabilisation of microtubules, facilitating axonal transport of vesicles and molecules, and contributing to neuronal stability, growth and health (Parra Bravo et al., 2024).

Microtubules, the major cytoskeletal component of neurons, are important in maintaining neuronal cytoarchitecture and providing long-distance intracellular transport (Brouhard and Rice, 2018). Microtubules are hollow tubes composed of α- and β-tubulin dimers. Microtubule associated proteins (MAPs), including Tau, bind to the surface of microtubules, to promote nucleation, elongation and structural stability **(Figure 3)** (Barbier et al., 2019). Tau also acts as a molecular spacer along the microtubule lattice ensuring strong polymerisation and promoting stability (Barbier et al., 2019). This stability is essential for efficient axonal transport, carried out by motor proteins like kinesin and dynein exporting vital materials along the axonal tracts (Beaudet et al., 2024, Guo et al., 2017). Such cargo include: neurotransmitter vesicles, mitochondria, mRNA and ribosomes, signalling endosomes, lysosomes and other proteins(Guo et al., 2017).

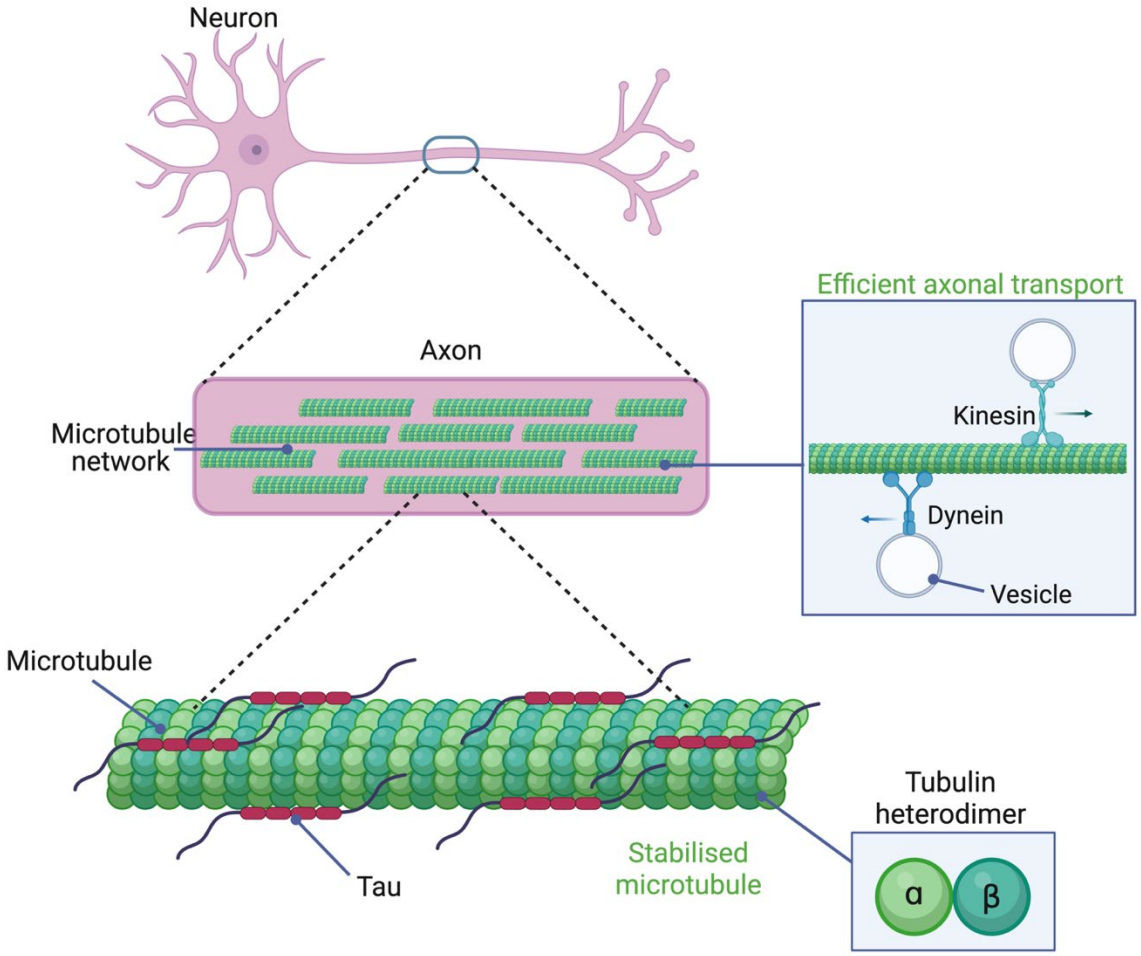


**Figure 3. Physiological Tau functions as a microtubule associated protein.**

Soluble Tau in its physiological state binds and facilitates microtubule assembly by means of nucleation, polymerisation, and stabilisation. In turn this maintains essential axonal trafficking of vesicles via motor proteins kinesin and dynein to maintain neuronal processing and integrity.

The binding of Tau to the neuronal microtubules is dynamically regulated by phosphorylation at multiple sites along the protein (Drechsel et al., 1992). The PDR and MBRD have the highest affinity of interaction with the microtubules (Kadavath et al., 2015). The C-terminal tails of β-tubulin also has affinity for Tau and contributes towards the stability of the Tau-microtubule complex (Brotzakis et al., 2021, Chau et al., 1998, Serrano et al., 1985).

Phosphorylation and de-phosphorylation via kinases and phosphatases, respectively, enable transient and reversible interactions with microtubules. This means that the cytoskeleton can be polymerised and remodelled in a healthy manner. This functional

phosphorylation mostly occurs at the KxGS-motifs (KIGS/KCGS) phosphorylated by the microtubule affinity regulating kinases (MARKs) (Chudobová and Zempel, 2023). Namely, phosphorylation residues S208, S231, S262, S396 and S404 each directly result in changes to microtubule binding affinity and assembly rates (Sengupta et al., 1998, Xia et al., 2020, Fischer et al., 2009). However, there is evidence that it is the multi-site combination of phosphorylation within these sites and others that maintains the dynamic, reversible stability of the microtubule network (Kiris et al., 2011). During disease Tau becomes hyperphosphorylated which impacts the cytoskeletal integrity of the neurons by hindering Tau-microtubule binding (Cowan et al., 2010, Xia et al., 2020) which is further described in **section 1.4.**

Although the primary function of Tau is to regulate microtubule dynamics and facilitate axonal transport, there are several other reported physiological functions of Tau contributing to neuronal health. As small amounts of Tau is found in neuronal nuclei, these include nuclear functions maintaining genomic stability, promoting rRNA transcription, regulate nuclear calcium homeostasis and chromatin dynamics (Violet et al., 2014, Sultan et al., 2011, Ziv et al., 2006).

Tau also plays important roles in neurogenesis and synaptic plasticity where it localises in synapses and dendrites during development to assist neurite growth. The importance of Tau for synaptic function is evident in Tau deficient *Drosophila* and mouse models, which incur synaptic loss and impaired synaptic plasticity (Ahmed et al., 2014, Chen and Mobley, 2019, Voelzmann et al., 2016). Moreover, there is evidence that Tau is involved in neuronal excitability and cell signalling through interactions with several synaptic proteins that control synaptic vesicle clustering, ion channels and neurotransmitter release particularly in a disease state (McInnes et al., 2018, Hall et al., 2015, Holth et al., 2013, Hoover et al., 2010, Gheyara et al., 2014).

Overall, Tau is a central protein involved in many important and dynamic cellular processes.

### 1.2.4 Physiological Tau conformation

Under normal conditions Tau is natively unfolded and a highly soluble protein. As an intrinsically disordered protein (IDP), Tau does not form rigid, tertiary structures under physiological conditions (Mandelkow and Mandelkow, 1998). This flexibility allows Tau to adopt several dynamic conformations enabling it to function as a transient and reversible microtubule-binding protein, amongst other functions.

As an IDP with no stable internal structure, physiological Tau is inherently difficult to crystallize and characterize structurally. Förster resonance energy transfer (FRET)-based spectroscopic methods have been very useful in determining Tau's global structure by measuring local distances between Tau domains and tubulin. FRET studies have shown that soluble Tau adopts a global hairpin fold or "paperclip-like formation" in which intramolecular interactions occur between the N-terminal (residues 17/18), C-terminal (residue 432) and MBRD (residues 291, 310 and 322) (shown later in **Figure 7)** (Jeganathan et al., 2008, Jeganathan et al., 2006, von Bergen et al., 2006).

### 1.2.5 Post-translational modifications

Tau is heavily regulated by post-translational modifications (PTMs) including methylation, acetylation, glycosylation, nitration, sumoylation, truncation, oxidation and most notably phosphorylation and as such can be used as early diagnostic biomarkers (**Table 1**)**.** Under physiological conditions, these PTMs dynamically regulate Tau to alter its protein interactions, subcellular localisation and function. However, dysregulation of these PTMs on Tau contribute to the loss of Tau's physiological function, causing pathological changes which promote conformational misfolding and aggregation (Kavanagh et al., 2022). They

have been identified as early pathological events in disease progression, and as such can be used as early diagnostic biomarkers.

**Table 1. Tau post translational modifications and their modified residue sites.**

Adapted from (Parra Bravo et al., 2024).

| PTM | Description | Number of sites | Modified residues |
|---|---|---|---|
| **Acetylation** | Addition of acetyl groups to lysines | 11 | K163, K174, K180, K259, K274, K280, K281, K290, K321, K353, K369 |
| **Glycation** | Non-enzymatic glycation of lysine residues | 13 | K87, K132, K150, K163, K174, K225, K234, K259, K280, K281, K347, K353, K369 |
| **Glycosylation** | Covalent attachment of oligosaccharide carbohydrates to asparagine residues | 9 | T123, N167, S208, S238, N359, S400, N410, S412, S413 |
| **Methylation** | Addition of methyl groups on lysines, competes with acetylation and ubiquitination | 4 | K174, K180, K254, K267 |
| **Nitration** | Addition of nitro groups typically to tyrosine residues | 4 | Y18, Y29, Y197, Y394 |
| **Phosphorylation** | Addition of phosphate groups to serine, threonine and tyrosine residues | 84 | T17, Y18, Y29, T30, T39, S46, T50, T52, S56, S61, T63, S64, S68, T69, T71, T76, T95, T101, T102, T111, S113, T123, S129, S131, T135, S137, T149, T153, T169, T175, T181, S184, S185, S191, S195, Y197, S198, S199, S202, T205, S208, S210, T212, S214, T217, T220, T231, S235, S237, S238, S241, T245, S258, S262, T263, S285, S289, S293, S305, Y310, S316, T319, S320, S324, S341, S356, T361, T373, T377, T386, Y394, S396, S400, T403, S404, S409, S412, S413, T414, S416, S422, T427, S433, S435 |
| **Polyamination** | Covalent attachment of polyamines | 18 | Q6, Y18, Q88, Q124, K163, K174, K180, K190, K225, K234, K240, Q244, Q276, Q288, Q351, K383, K385, Q424 |
| **Sumoylation** | Covalent attachment of SUMO proteins | 1 | K340 |
| **Ubiquitylation** | Covalent attachment of ubiquitin monomers to lysines | 17 | K180, K240, K254, K257, K259, K267, K274, K281, K290, K298, K311, K317, K321, K343, K353, K369, K395 |
| **O-GlcNAcylation** | Addition of N-acetylglucosamine to | 13 | S199, S202, T205, S208, S214, S237, S238, S400, S409, S412, |

| | | | |
|---|---|---|---|
| | serine/threonine residues, competes with phosphorylation | | S413, T414, S416, S422 (Yuzwa et al., 2012, Liu et al., 2004, Wani et al., 2017) |
| **Truncation** | Shortening of Tau at the N-terminal or C-terminal | n.a. | Tau1-421 (Rissman et al., 2004), TauΔ2-441 (Kovacs, 2015) Tau45-230 (Basurto-Islas et al., 2018)Tau391-Tau441 (Novak et al., 1993)<br>Tau275 and Tau282 (Horie et al., 2022). |

PTMs are also thought to mediate structural heterogeneity between Tauopathies as distinct PTM profiles are observed between each disease. These differences manifest as the modification of disease-specific residues and variations in global frequency of PTMs (Arakhamia et al., 2020, Kametani et al., 2020, Kyalu Ngoie Zola et al., 2023). These unique PTM signatures are thought to produce distinct pathological conformations which underlie the structural diversity of Tau filament cores, recently demonstrated by cryo-EM (Scheres et al., 2020, Shi et al., 2021), as well as the composition of Tau inclusions deposited within the brains of patients(Spillantini et al., 1998). Therefore, PTM patterns represent important pathological events which may underlie distinct mechanisms contributing towards Tau toxicity and neurodegeneration in a disease specific manner.

### 1.2.6 Tau kinases and phosphatases

Phosphorylation is the most common PTM of Tau (**Table 1**,**Table 2),** involved intimately in regulating its physiological function in binding to microtubules in a site-specific manner. Tau phosphorylation is regulated between kinases which add phosphate groups, and phosphatases which remove them. During AD there is an increased shift in kinase activity and downregulation of phosphatase activity, notably protein phosphatase 2A (PP2A) (Sayas and Ávila, 2021, Sontag and Sontag, 2014). This dysregulation contributes to elevated, persistent levels of abnormally hyperphosphorylated Tau.

There are multiple Tau kinases which are classified into three main groups: **1)** Proline-directed kinases eg, glycogen synthase kinase 3 beta(GSK-3β) and cyclin dependent kinase (CDK5), **2)** Non-proline directed kinases eg. Tau-tubulin kinases (TTBK) and microtubule affinity regulating kinases (MARKs)(Chudobová and Zempel, 2023), and **3)** Tyrosine kinases eg. Fyn or Abl kinases (Wu et al., 2025, Xia et al., 2021).

Notably, GSK-3β is one of the most pathologically linked kinases in AD. It targets many of the key phosphorylation sites that are significantly elevated in AD postmortem tissue, and present in Tau aggregates. Furthermore, the kinase itself is found to be elevated during aging (Llorens-Martín et al., 2014), and expression levels are significantly increased in post-mortem tissue comparing AD brains to age-matched controls (Pláteník et al., 2014, Sayas and Ávila, 2021, Jin et al., 2015). More specific roles in how GSK-3β is involved in Tau pathology will be discussed in more detail in **section 1.4.**

## 1.3 Pathological Tau

## 1.4 Tau Hyperphosphorylation

During disease Tau becomes abnormally hyperphosphorylated, being one of the earliest and major pathological hallmarks of AD (Köpke et al., 1993). Direct evidence of this is found in histological staining of AD brain tissue which extensively stains for hyperphosphorylated Tau, progressively increasing in abundance throughout disease progression, according to Braak stages (Braak and Braak, 1991). Moreover, the insoluble Tau filaments extracted from brain tissue are composed of highly phosphorylated Tau species, indicating their contribution towards aggregate formation. In fact, early biochemical assays found global Tau to be phosphorylated around 3-4 times higher in AD than healthy control brains (Köpke et al., 1993). There are several pathogenic consequences of

hyperphosphorylated Tau which has directly toxic consequences within the neuron, which are further explored in **section 1.4.1.**

In the longest Tau isoform (2N4R) there are 84 serine (S), threonine (T) and tyrosine (Y) possible phosphorylation sites along the Tau protein **(Figure 4)** (Xia et al., 2020, Wesseling et al., 2020). Phospho-specific antibody screens, phospho-proteomics and mass spectroscopy studies of postmortem brain tissue have shown that many of these residues are found to be phosphorylated at low levels in healthy brains, indicating that phosphorylation at disease-associated epitopes is not inherently pathological (**Table 2).** However not all sites are equally phosphorylated or pathologically relevant. Despite considerable overlap in phospho-sites detected between AD and controls, there are around 20 common phosphorylation sites including S198, S199, S202, T205, T212, S214, S217, T231, S235, S262, S263, S265, S356, S396, S400, S404, and S422 that are significantly elevated in early-to-late stage AD patients **(Figure 4)** (Mair et al., 2016, Hanger et al., 2007, Wesseling et al., 2020).

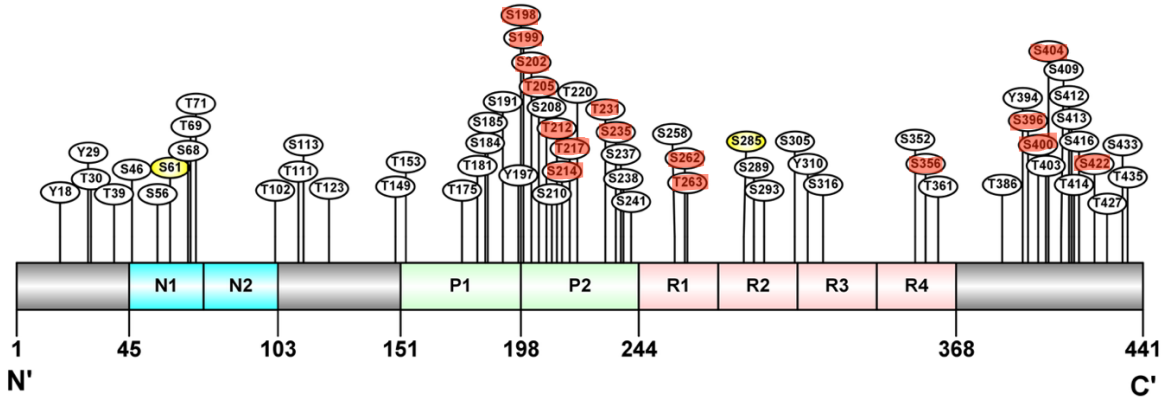


**Figure 4. Schematic showing all phosphorylation sites on full-length 2N4R Tau.**

Tau is heavily regulated by phosphorylation up the entire length of the protein. Phosphorylation occurs in every major domain including the N-terminal domain containing the N1 and N2 inserts, the proline rich domain containing the P1 and P2 domains, the microtubule binding domain containing the R1-R4 inserts, and the C-terminal domain. All identified phosphorylation sites present in AD patient brains are shown. The most frequent phosphorylation sites are clustered in the proline rich domain, and another cluster in the c-

terminal domain. Highlighted red positions shows the commonly elevated epitopes in AD. Two positions highlighted in yellow are absent in AD and control brains.

**Table 2. Tau phosphorylation sites present in AD and control brains, and their acting kinases.**

As reported and summarised, adapted and updated from Xia, Prokop and Giasson 2021, Wesseling 2020 and the Hanger group (most up to date table https://docs.google.com/spreadsheets/d/1hGYs1ZcupmTnbB7n6qs1r_WVTXHt1O7NBLyKBN7EOUQ/edit?gid=0#gid=0 accessed 09/06/2025) and Anthony Aggidis 2019 thesis, Lancaster University. **Kinase abbreviation:** 5' adenosine monophosphate-activated protein kinase (AMPK), Brain-specific kinase 1/2 (BRSK1/2), Calcium-calmodulin kinase II, Casein kinase 1 (CK1), Casein kinase 2 (CK2), Cyclin-dependent kinase-5 (cdk5), Cyclic AMP-dependent protein kinase (PKA), Dual-specificity tyrosine-phosphorylation regulated kinase 1A (DYRK1A), Glycogen synthase kinase-3β (GSK-3β), Microtubule affinity-regulating kinase (MARK), Mitogen and stress activated protein kinase-1 (MSK1), Non-receptor tyrosine-protein kinase (TYK2), p38 mitogen-activated kinase (p38MAPK), p42/p44 mitogen-activated protein kinases (ERKs1/2), Protein kinase C (PKC), Protein kinase N (PKN), Prostate-derived sterile 20-like kinase 1 alpha/beta (PSK1/TAOK2), Prostate-derived sterile 20-like kinase 2 (PSK2/TAOK1), 90 kDa Ribosomal S6 kinase (RSK1/2), Stress-activated protein kinase (SAPK), Tau-tubulin kinase 1/2 (TTBK1/2).

| Phospho-site | AD Brain | Control Brain | Acting Kinase(s) |
|---|---|---|---|
| **Y18** | X | X | Fyn, Syk |
| **Y29** | X | | TYK2 (Kim et al., 2024) |
| **T30** | X | | — |
| **T39** | X | | — |
| **S46** | X | X | GSK-3β, ERK1/2, p38MAPK, SAPK3/2a/2b, CK1 |
| **S56** | X | | — |
| **S61** | – | – | — |
| **S68** | X | | — |
| **T69** | X | | GSK-3β, ERK1/2, p38MAPK |
| **T71** | X | | BRSK1/2 |
| **T102** | X | | — |
| **S111** | X | | — |
| **S113** | X | | CK1 |
| **T123** | X | | PSK1/TAOK2 |
| **T149** | X | | GSK-3β, CK1, LRRK2, PSK2/TAOK1 |
| **T153** | X | | CDK5, GSK-3β, ERK1/2, SAPK2a/2b/3/4, LRRK2 |
| **T175** | X | | GSK-3β, JNK, ERK1/2, SAPK2a/2b/3, LRRK2, p38MAPK, PSK2/TAOK1 |
| **T181** | X | X | CDK5, GSK-3β, JNK, ERK1/2, SAPK2a/2b/3, LRRK2, p38MAPK |
| **S184** | X | X | GSK-3β, SAPK2a/2b/3, CK1, PSK1/TAOK2, PSK2/TAOK1 |
| **S185** | X | | p38MAPK, PSK1/TAOK2, PSK2/TAOK1 |
| **S191** | X | | PSK1/TAOK2, PSK2/TAOK1 |
| **Y197** | X | | Met |

| | | | |
|---|---|---|---|
| **S198** | X | X | GSK-3β, CK1, PKA, PSK1/TAOK2, TTBK1/2 |
| **S199** | X | X | CDK5, GSK-3β, ERK1/2, CK2, PKA, PSK2/TAOK1, TTBK1/2 |
| **S202** | X | X | CDK5, DYRK1A, GSK-3β, JNK, ERK1/2, p38MAPK, SAPK2a/2b/3/4, PKA, TTBK1/2 |
| **T205** | X | | CDK5, GSK-3β, JNK, ERK1/2, p38MAPK, SAPK2a/2b/3/4, PKA, LRRK2, PSK1/TAOK2, PSK2/TAOK1 |
| **S208** | X | | AMPK, CK1, TTBK1/2 |
| **S210** | X | | GSK-3β, CK1, PKA, LRRK2, TTBK1/2 |
| **T212** | X | X | CDK5, DYRK1A, GSK-3β, JNK, ERK1/2, p38MAPK, SAPK2a/2b/3/4, CaMKII, CK1, PKA, LRRK2, PSK1/TAOK2 |
| **S214** | X | X | CDK5, GSK-3β, SRPK2, AMPK, CaMKII, CK1, PKA, MSK1, PKB/AKT, PKC, PKN, PSK1/TAOK2, PSK2/TAOK1, RSK1/2, SGK1 |
| **T217** | X | X | GSK-3β, JNK, ERK1/2, p38MAPK, SAPK2a/2b/3/4, LRRK2, PKA |
| **T220** | X | | — |
| **T231** | X | | CDK5, GSK-3β, JNK, ERK1/2, p38MAPK, SAPK3/4, AMPK, PKA, LRRK2 |
| **S235** | X | X | CDK5, JNK, ERK1/2, p38MAPK, SAPK2a/2b/3/4, AMPK, PKA |
| **S237** | X | | GSK-3β, CK1, LRRK2, Phosphorylase kinase, PSK1/TAOK2, PSK2/TAOK1 |
| **S238** | X | | CK1, PSK2/TAOK1 |
| **S241** | X | | — |
| **S258** | X | | GSK-3β, AMPK, CK1, PKA, LRRK2, PKC, PKN, PSK1/TAOK2, PSK2/TAOK1 |
| **S262** | X | X | GSK-3β, Phosphorylase kinase, AMPK, BRSK, CaMKII, CK1, LRRK2, MARK, MSK1, p45/41, p70S6K, PKC, PSK1/TAOK2, PSK2/TAOK1, Rho kinase |
| **T263** | X | | PAR1 |
| **S265** | X | X | TBK1 |
| **S285** | – | – | — |
| **S289** | X | | GSK-3β, AMPK, CK1, PSK1/TAOK2, PSK2/TAOK1 |
| **S293** | X | | — |
| **S305** | X | | — |
| **Y310** | X | | — |
| **S316** | X | | — |
| **S352** | X | | — |
| **S356** | X | | GSK-3β, JNK, ERK1/2, p38MAPK, SAPK2a/2b/3/4, AMPK, CaMKII, CK1, PKA, LRRK2, MARK, Phosphorylase kinase, PSK1/TAOK2, PSK2/TAOK1 |
| **T361** | X | | — |
| **T386** | X | | — |
| **Y394** | X | | c-Abl, LRRK2 |
| **S396** | X | X | GSK-3β, JNK, ERK1/2, p38MAPK, SAPK2a/2b/3/4, CK1, CK2, PKA |

| | | | |
|---|---|---|---|
| **S400** | X | X | GSK-3β, AMPK, CK2, PSK1/TAOK2, PSK2/TAOK1 |
| **T403** | X | X | AMPK, LRRK2, PSK1/TAOK2, PSK2/TAOK1 |
| **S404** | X | X | CDK5, DYRK1A, GSK-3β, ERK1/2, p38MAPK, CK1, CK2 |
| **S409** | X | | GSK-3β, p38MAPK, SAPK3/4, PKA, p35/41, PSK1/TAOK2, PSK2/TAOK1, Rho kinase |
| **S412** | X | X | CK1, CK2, PKA, PSK2/TAOK1 |
| **S413** | X | X | GSK-3β, CK1, CK2, PKA, PSK1/TAOK2, PSK2/TAOK1 |
| **T414** | X | X | CK1, CK2, PSK1/TAOK2, PSK2/TAOK1 |
| **S416** | X | X | AMPK, CK1, CK2, PKA, PSK1/TAOK2, PSK2/TAOK1 |
| **S422** | X | | CaMKII, CK1, CK2, PKA, PSK1/TAOK2, PSK2/TAOK1, TTBK1/2 |
| **T427** | X | | PSK1/TAOK2, PSK2/TAOK1 |
| **S433** | X | | CK1, PSK1/TAOK2, PSK2/TAOK1 |
| **T435** | X | | CK1, PKA, LRRK2, PSK1/TAOK2, PSK2/TAOK1 |

### 1.4.1 Pathological Consequences of Hyperphosphorylation

Tau hyperphosphorylation is a well-established mechanism of toxicity in AD and has been observed in many experimental models of Tauopathy (Xia et al., 2021). The mechanisms of how hyperphosphorylated Tau is toxic can be divided in two: **1)** the pathogenic loss of function (LOF) consequences and **2)** the pathogenic gain of function(GOF) consequences, like propagation and aggregation, summarised in **Figure 5.**

As discussed, Tau regulates multiple neuronal functions. However, hyperphosphorylation results in less efficient binding to tubulin and microtubules and has multiple pathogenic consequences at the molecular, subcellular and cellular level. *In vitro* studies have demonstrated that expressing phospho-mimicking Tau in neuronal cells has a profound effect on neuronal structure and function, compromising cytoskeletal integrity (Cash et al., 2003, Alonso et al., 1994), suppressing neuronal excitability and impairing synaptic function (Hatch et al., 2017), cellular damage (Esteras and Abramov, 2020), disruption of cellular trafficking and transport (Yu et al., 2019), induction of inflammatory responses (Meng et al., 2022) and inducing significant changes to the normal subcellular

localisation and distribution of Tau (Hatch et al., 2017, Rodríguez-Martín et al., 2013, Hoover et al., 2010).

Similar deficits are reported *in vivo* in *Drosophila* models of Tauopathy where driving hyperphosphorylation, by co-expression of the Tau kinase GSK-3β, or emulating hyperphosphorylation by expressing the phospho-mimicking transgenes disrupted axonal transport (Mudher et al., 2004), reduced microtubule binding (Cowan et al., 2010) and induced significant neuronal and synaptic degeneration (Cash et al., 2003, Mudher et al., 2004, Chee et al., 2005, Chatterjee et al., 2009, Talmat-Amar et al., 2011, Stubbs et al., 2023).

### 1.4.2 Pathologically linked phosphorylation epitopes

Extensive research has been conducted to assess which epitopes are influencers of pathology. Alonso et al., 1996 were the first to document that phosphorylation at specific epitopes were pathologically linked, influencing aggregation. They reported that phosphorylation at S199, S262, T212 and T231 caused a direct association with "normal" Tau *in vitro* using AD brain derived Tau fibrils (Alonso et al., 1996).

Building on these findings, pseudo-phosphorylation by amino acid substitution of Serine/Threonine/Tyrosine to Glutamate (E) or Aspartate (D) has been a particularly effective method for studying the toxic effect of site-specific hyperphosphorylation in Tau-mediated degeneration. The mutation mimics the electrostatic (net negative) charge and weight of a phosphate addition(Limorenko and Lashuel, 2022). Additional studies using phospho-mimetics have shown that phosphorylation of S202, T205, S208, S396, S404 and S422 promotes Tau polymerisation and aggregation in cells (Xia et al., 2020, Abraha et al., 2000, Haase et al., 2004, Alonso Adel et al., 2004, Despres et al., 2017).

More recently, Stefanoska et al., 2022 have identified specific phosphorylation sites that act as crucial contributors to the subsequent hyperphosphorylation of Tau itself. By expressing pseudo-phosphorylated human Tau2N4R in HEK293 cells they found that mimicking phosphorylation at so-called 'master sites' T50, T69, T111, T181, and T205, phosphorylation was induced at other sites. Out of all the master sites identified, T181 promoted the downstream hyperphosphorylation of the most sites that were examined, notably including classical phosphorylation markers frequently observed in the brains of AD patients: S199, S202, T205,(AT8) and T231(AT180) (Stefanoska et al., 2022). Other studies have also implicated T181 as an important phospho-epitope, as it is one of the most abundantly phosphorylated epitopes in brains and biofluids (Barthélemy et al., 2019), and is amongst the earliest sites to be phosphorylated (Luna-Muñoz et al., 2007). Taken together these new reports indicate that some phosphorylation sites have more pathological relevance than others, influencing further phosphorylation and aggregation in distinct ways.

The functional consequences of site-specific hyperphosphorylation have been extensively studied *in vivo* using phospho-mimetic models.

#### 1.4.2.1 Experimental Models Using Phospho-mimetic Tau

Pseudo-phosphorylated Tau impairs neuronal function through multiple mechanisms, including disruption of axonal transport and reduced microtubule binding *in vitro* (Sun and Gamblin, 2009) and *in vivo* (Feuillette et al., 2010, Talmat-Amar et al., 2011). Pseudo-phosphorylated Tau also facilitates self-assembly, aggregation and cell death in CHO cells (Alonso et al., 2010) and induces prion-like propagation (Hallinan et al., 2019), closely recapitulating the behaviour of AD-derived Tau fibrils.

A particularly aggressive pseudo-phosphorylated variant TauE14 has been used as an exacerbated hyperphosphorylated Tau model which mimics phosphorylation at 14 disease relevant sites (Hoover et al., 2010). This mutant recapitulates multiple pathogenic hallmarks

of Tauopathy across diverse experimental systems. In primary neuronal cultures, TauE14 misfolds and aggregates in the absence of exogenous Tau seeds, and demonstrates seed-competency and propagation through distally separated cultured neurons in a microfluidic device (Hallinan et al., 2019). TauE14 expression also induces pathological mis-localisation to dendritic spines, disrupting synaptic dysfunction by supressing AMPAR-mediated synaptic responses (Hoover et al., 2010). The toxic effects of TauE14 are further demonstrated *in vivo Drosophila* models. TauE14 expression induces substantial neuronal degeneration across all *Drosophila* tissue types examined, including PDF neurons (Zhang et al., 2022a), the mushroom bodies (Steinhilb et al., 2007a) and after pan-neuronal expression (Dias-Santagata et al., 2007). Moreover, TauE14 expression in the larval stage significantly reduced microtubule binding activity and altered axonal trafficking of vesicles (Talmat-Amar et al., 2011). Furthermore, when expressed in the *Drosophila* eyes, TauE14 causes aggressive degenerative retinal phenotypes paired with an increased sarkosyl insoluble enriched fraction indicating the presence of aggregated Tau species (Fulga et al., 2007, Katsinelos et al., 2021). Katsinelos et al., also demonstrated that TauE14 significantly contributes to the levels of intracellular Tau available for secretion, providing important insights into how phosphorylated Tau impacts the translocation and transcellular spread of Tau.

There are also many studies which have used more site-specific and smaller phospho-mimicking combination approaches to investigating the impact of hyperphosphorylation. The majority of these studies find significant changes, and induced toxicity even when mimicking phosphorylation at just 1-4 disease relevant epitopes, showing that some epitopes are more pathologically relevant than others. For example, *in vivo, Drosophila* expressing phosphomimicking Tau at just 4 sites: S199E, T212E, T231E and S262E was significantly more toxic than wildtype Tau when expressed pan-neuronally, causing severe degeneration of the mushroom bodies, severe learning deficits and reduced locomotive function (Beharry

et al., 2013). Similarly, in a transgenic rodent model expressing PH-Tau (mimicking phosphorylation at S199E, S262E, T212E and T231E), exacerbated cognitive deficits, axonal fragmentation and loss of synaptic terminal density, when compared to wildtype Tau mice (Alonso et al., 2018). Another *in vitro* study, a phospho-mimicking Tau at 10 residues, TauE10, expressed in differentiated neuronal PC12 cells exerted a significantly cytotoxic degenerative effect when compared to wildtype Tau, inducing cell death, chromatic condensation and DNA fragmentation (Fath et al., 2002). Moreover, Rodriguez-martin et al., showed that phospho-mimetic Tau exacerbated axonal transport and microtubule binding deficits in a dose-dependent manner in CHO cells which were transfected with wildtype-Tau, TauE18 and TauE27 (Rodríguez-Martín et al., 2013). Collectively these show that phosphorylation of disease specific residues can cause significant toxicity in many models. While some epitopes are more pathogenically influential, hyperphosphorylation of Tau does seem to cause toxicity in a concentration dependent manner.

Conversely, if these Serine/Threonine/Tyrosine sites are mutated to non-phosphorylatable Alanine (A) residues, most Tau-mediated toxic effects caused by wildtype Tau are mitigated. TauAP which consists of 14 Alanine substitutions completely prevented the mis-targeting of Tau to dendritic spines in murine neuron culture (Hoover et al., 2010). Similarly, Tau0N4R(AP) did not show any signs of retinal degeneration as wildtype Tau0N4R did when expressed in *Drosophila* retina (Steinhilb et al., 2007b, Bouleau and Tricoire, 2015). Moreover, *Drosophila* studies expressing TauS2A, a variant generated from mutating S262 and S356 to alanine, have shown that toxic phenotypes induced by Tau can be mitigated by inhibiting phosphorylation at these two important residues (Chatterjee et al., 2009, Nishimura et al., 2004, Ramirez-Moreno et al., 2025).

Collectively, these studies demonstrate the profound impact of hyperphosphorylation on inducing misfolding, aggregation and cellular toxicity, affecting microtubule binding,

axonal transport, Tau mis-localisation, propagation, and cell death, summarised below in **Figure 5.**

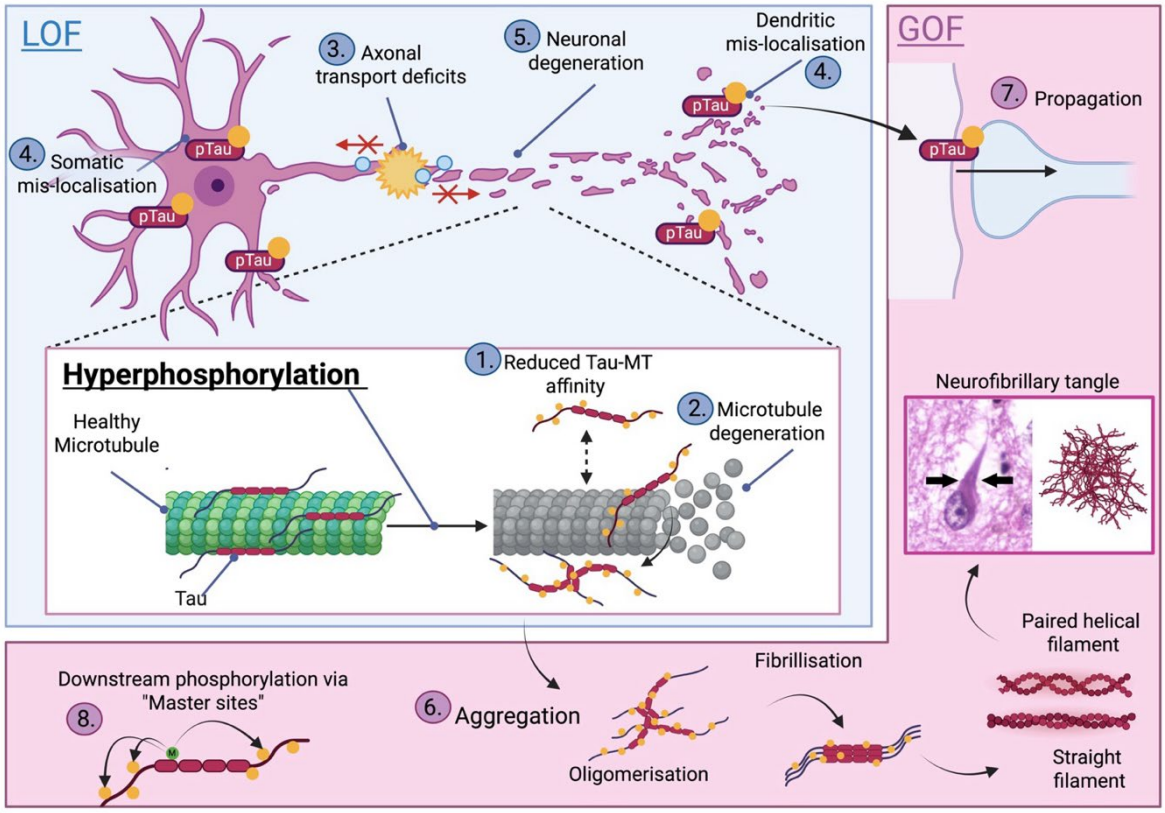


**Figure 5. Schematic diagram of the pathological consequences of Tau hyperphosphorylation.**

These can be split into toxic loss-of-function (LOF) (1-5, blue box) and toxic gain-of-function (GOF) (6-8, red box) which drive Tau pathology in AD. Hyperphosphorylation of Tau reduces its affinity for microtubules (1), causing microtubule destabilisation and degeneration (2), consequential axonal transport deficits (3), Tau mis-localisation away from the axonal compartment to the soma and dendritic compartments (4), ultimately causing cell death and degeneration of the neuron (5). Hyperphosphorylation also increases Tau's propensity for self-aggregation, forming a cascade of oligomers which fibrillise into paired helical and straight filaments, which make up neurofibrillary tangle inclusions. Hyperphosphorylated Tau also increases propensity for trans-synaptic Tau propagation(7). Some phosphorylation "master" sites induce further phosphorylation at secondary sites(8). Image of NFT in the hippocampus of an AD brain, image credit to Mikael Haggstrom, Source: https://commons.wikimedia.org/wiki/File:Histopathology_of_neurofibrillary_tangles_in_Alzheimer%27s_disease.jpg accessed 19/06/2025.

While Glutamate, Aspartate and Alanine mutations are used widely to mimic and inhibit phosphorylation respectively, it is important to note that they do not fully replicate the exact chemical and structural properties of the native phosphorylated residues **(Figure**

**6)** (Limorenko and Lashuel, 2022). Although Glutamate and Aspartate mimics the negative charge and weight of a phosphate group, it will not exactly simulate the stoichiometry and intramolecular interactions (Limorenko and Lashuel, 2022). Consequently, this may alter the native Tau conformation and hinder the interactome activity in its physiological and pathological state.

Nevertheless, phospho-mimetic Tau remains a powerful tool because it replicates many of the toxic effects associated with hyperphosphorylated Tau observed in human AD tissue and *in vivo* models. For example, as discussed, phospho-mimetic Tau disrupts microtubule binding, axonal transport deficits and neuronal degeneration and cell death in cellular and animal models similar to experimental models expressing Tau with upregulated GSK-3β activity (Mudher et al., 2004, Shimura et al., 2004, Talmat-Amar et al., 2011, Katsinelos et al., 2021, Chatterjee et al., 2009). Furthermore, phospho-mimetic Tau promotes Tau aggregation and neurodegenerative phenotypes as also observed in models overexpressing Tau and GSK-3β (Mudher et al., 2004, Povellato et al., 2014, Chatterjee et al., 2009, Chau et al., 2006). Most compellingly, the recently published PAD-12 phospho-mimetic mutant spontaneously forms aggregates *in vitro* and forms *bona fide* ultrastructural cores of those found in AD(Lövestam et al., 2025). This further validates that phospho-mimetic mutants can recapitulate critical aspects of pathological hyperphosphorylation.

Collectively, phospho-mimetic Tau models successfully recapitulate cellular and subcellular toxicity induced by physiological, GSK-3β-mediated phosphorylation. However their structural and biochemical differences between amino acid substitutions and physiological phosphorylation must be considered when interpreting experimental findings.

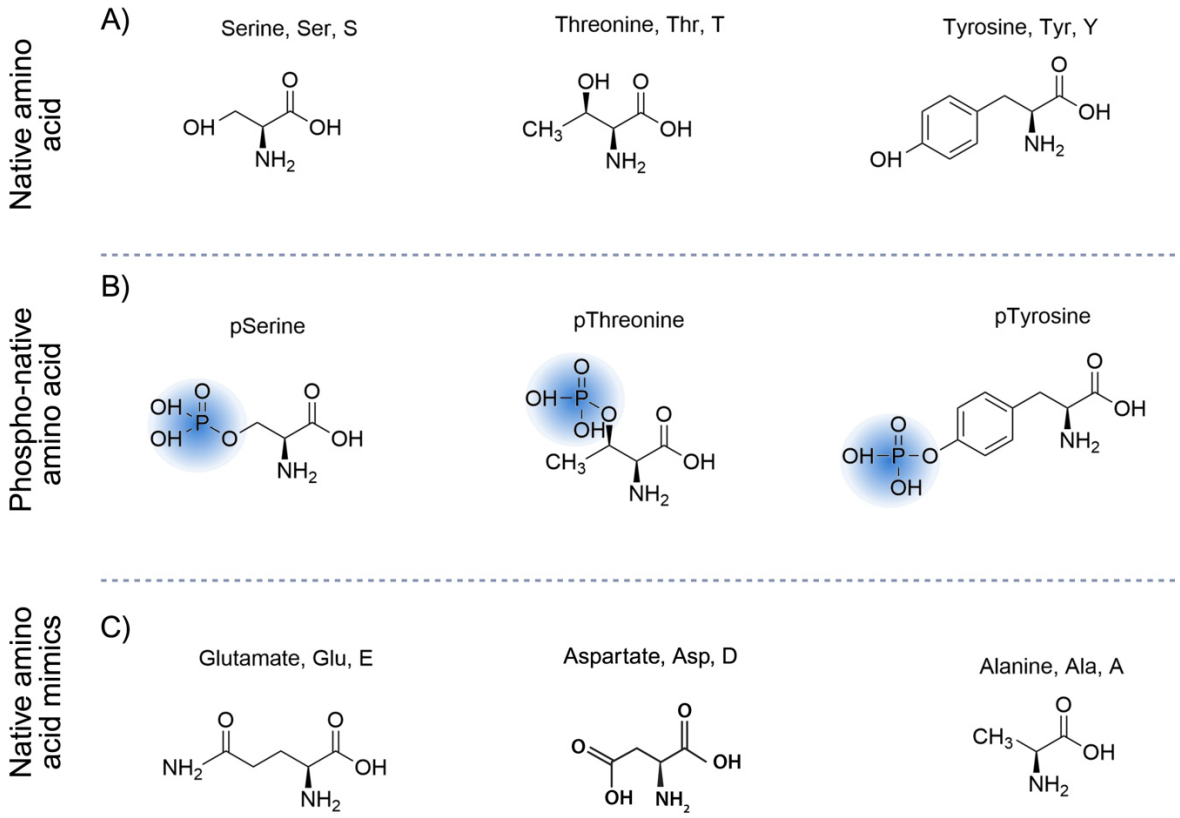


**Figure 6. Amino acid structure comparison of native amino acids, phosphorylated residues and their phospho-mimetic substitutions.**

A) Structures of native Serine, Threonine and Tyrosine which are the targets of phosphorylation in Tau. B) Addition of phosphates highlighted in blue, to the corresponded native residues to make phosphorylated pSer, pThr and pTyr. C) Phospho-mimetic substitutions Glutamate and Aspartate to mimic phosphorylation, and Alanine to inhibit phosphorylation. Adapted from(Limorenko and Lashuel, 2022).

### 1.4.3 Phosphorylation as a biomarker

With such prominence during disease, Tau phosphorylation has become an established biomarker for Tauopathy diagnosis. Phospho-antibodies including AT8 (S199, S202, T205) and AT100 (T212, S213) are used routinely to assess Tau pathology in humans and animal postmortem brain tissue (Braak and Braak, 1991, Strang et al., 2017). Beyond postmortem applications, phosphorylated Tau is becoming increasingly utilised as an *in vivo* diagnostic biomarker. More recently, antibodies targeting T181, T217 and T231 have been

developed as FDA-approved biomarkers in cerebral spinal fluid (CSF) and blood plasma as a diagnostic tool for patients with early AD and mild cognitive impairment (MCI). Elevated phosphorylation of these epitopes is reliably increased precedes decades before other AD-related cognitive symptoms manifest (Janelidze et al., 2020b, Janelidze et al., 2020a, Hirota et al., 2022, O'Connor et al., 2021, Palmqvist et al., 2020).

### 1.4.4 Age-related Tau Phosphorylation:

As dementias are age-associated diseases, several groups have investigated how aging influences the phosphorylation state of Tau. Observational studies have reported elevated Tau phosphorylation in aged human control groups, with resected brain extract tissue staining positive for PHF-1 (S396/S404)(Chatterjee et al., 2023). Similar observations have also been made in non-human primates and rodent controls, showing increased phosphorylation at T235, S396 and T181 epitopes in soluble brain extracts (Leslie et al., 2021, Jung et al., 2013). Although phosphorylation increases at AD-associated epitopes with age, these levels are significantly lower than those observed in patients with AD, demonstrating that disease exacerbates hyperphosphorylation beyond normal aging and contributes to Tau-mediated degeneration.

## 1.5 Aggregation of Tau

Tau aggregates like neurofibrillary tangles (NFTs) are central pathogenic features of AD. Tau aggregates are present in all Tauopathies, each having distinct isoform composition, lesion shape and anatomical region found in **(Table 3).**

**Table 3. Table of neuronal Tau inclusions found in distinct Tauopathy strains.**

Inclusion morphology and Tau isoform composition are heterogenous. Adapted from(Chung et al., 2021)

| Tauopathy | Inclusion Type | Tau Isoform | Image |
|---|---|---|---|
| **Alzheimer's Disease (AD)** | Neurofibrillary Tangles (NFTs) | Mixed 3R/4R | 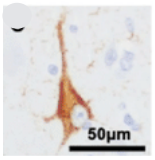 |
| **Pick's Disease (PiD)** | Pick Bodies | Predominantly 3R | 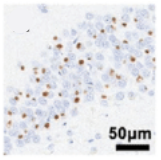 |
| **Progressive Supranuclear Palsy (PSP)** | NFTs and pre-tangles | Predominantly 4R | 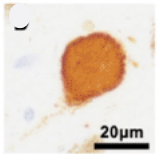 |
| **Corticobasal Degeneration (CBD)** | Pre-tangles and ballooned neurons | Predominantly 4R | 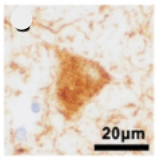 |
| **Chronic Traumatic Encephalopathy (CTE)** | NFTs and pre-tangles | Mixed 3R/4R | 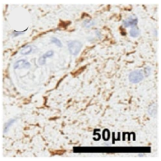 |
| **Argyrophilic Grain Disease (AGD)** | Argyrophilic Grains | Predominantly 4R | 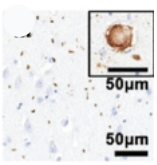 |

### 1.5.1 Phosphorylation promotes aggregation

On its own, native Tau does not aggregate *in vitro* (Goedert et al., 1996, Combs et al., 2017). However, PTMs, particularly phosphorylation, can induce conformational changes that alter both the local and global protein structure, resulting in pathological secondary structures that promote aggregation. Several lines of evidence implicate Tau phosphorylation in promoting aggregation, but the precise patterns and molecular mechanisms underlying this relationship is not fully understood.

Aggregates isolated from AD postmortem is highly composed of hyperphosphorylated Tau (Goedert et al., 1998). Phosphorylation of Tau may influence its aggregation directly by altering Tau conformation or indirectly by priming Tau for additional phosphorylation events (Chatterjee et al., 2009, Haase et al., 2004, Despres et al., 2017, Xia et al., 2020, Stefanoska et al., 2022). Multiple phosphorylation sites including T175, S199, S202, T205, S212, S396, S404, and S422 promote aggregation when pseudo-phosphorylated forming Tau filaments *in vitro* (Gohar et al., 2009, Rankin et al., 2005, Despres et al., 2017). Conversely, pseudo-phosphorylation at certain sites like S214, S262 and S305 appears to suppress further phosphorylation and aggregation (Strang et al., 2018, Schneider et al., 1999, Despres et al., 2017, Haj-Yahya et al., 2020, Keramidis et al., 2020) implying that phosphorylation of some epitopes have protective roles.

*In vivo,* pseudo-phosphorylated mutants, like TauE14 show an increased accumulation of Tau in sarkosyl insoluble fractions and form of *bona fide* Tau aggregates within fly brains (Chatterjee et al., 2009, Katsinelos et al., 2021, Chi et al., 2020). Similarly, rodent models expressing mutant Tau produce misfolded pre-tangle-like conformations, which can be significantly reduced with GSK-3β kinase inhibitor treatment (Lucas et al., 2001, Hernandez et al., 2013, Lauretti and Praticò, 2020, Yokoyama et al., 2022) (Noble et al., 2005, Amaral et al., 2021, Pérez et al., 2003). Collectively, these animal studies offer

mechanistic evidence that phosphorylation is a key driver of pathological misfolding and Tau aggregation.

Despite this evidence, it is still unclear how phosphorylation promotes aggregation at different disease stages, and what the extent of phosphorylation is required for aggregation and neurotoxicity. The dynamic nature of Tau phosphorylation, combined with the high number of phosphorylation combinations events makes these questions challenging to answer. Furthermore, as an intrinsically disordered protein, Tau lacks a well-defined 3D structure, which complicates direct measurements of how phosphorylation influences conformation and aggregation propensity (Pounot et al., 2024). A more comprehensive assessment of phosphorylation patterns across disease stages is needed to fully understand the relationship between hyperphosphorylation, Tau conformation and Tau aggregation propensity.

Nevertheless, the consensus view is that Tau phosphorylation may induce misfolding into seed-competent and aggregation prone conformations (Alonso et al., 2001, Jeganathan et al., 2008). FRET studies have been able useful to measure how the Tau conformation is altered by hyperphosphorylation. Jeganathan et al., demonstrated that pseudo-phosphorylation of full-length Tau at key AD-epitopes, caused conformational tightening or loosening of the native “paperclip” structure (Jeganathan et al., 2008). They report that pseudo-phosphorylation of the AT8 (S199E, S202E, T205E) and PHF1 (S369E, S404E) epitopes independently caused the paperclip structure to open, but in combination with AT100 (T212E, S214E), the paperclip structure adopted a more compacted and compressed conformation (Jeganathan et al., 2008). These mutants also increased immunoreactivity with the MC1 antibody which detects misfolded conformations of Tau prone to aggregation, which also strongly marks aggregates found in AD brains (Jicha et al., 1997).

In addition to conformational changes, phosphorylation promotes aggregation by reducing microtubule binding affinity. In turn this enhances the local cytosolic concentration of free Tau and encourages interaction with other Tau proteins and aggregation-promoting cofactors (Martin et al., 2011, Wang and Mandelkow, 2016, Wegmann et al., 2018). Most recently, Wegmann et al., demonstrated that soluble recombinant Tau and phosphorylated Tau purified from AD brains can spontaneously undergo liquid-liquid phase separation (LLPS) forming Tau-containing droplets *in vitro*(Wegmann et al., 2018). These Tau-rich condensates act as nucleation sites for β-sheet-rich aggregates which are capable of seeding Tau aggregation in live neurons (Wegmann et al., 2018). Overall, multiple lines of evidence demonstrate that Tau phosphorylation is an established prerequisite for Tau aggregation.

### 1.5.2 Biochemical inducers of Tau aggregation

Several factors have been identified as potential triggers of aggregation, however it is still unknown exactly what triggers aggregation in disease. The initiation of Tau aggregation is likely a multifactorial event, involving protein conformational changes as discussed, as well as biochemical changes to the local microenvironment. The addition of cofactors, changes of pH and ionic charges, and high local Tau concentrations have all been described sufficient triggers of Tau fibrillization *in vitro.* For instance, studies using AD brain homogenates report that pH of CSF decreases in the aging brain, and in AD patients (Decker et al., 2021).

Other than PTMs, *in vitro* studies have established that soluble monomeric Tau can nucleate into highly insoluble PHFs with the addition of polyanionic cofactors, altering the intra- and intermolecular interactions of the Tau. These cofactors include polysaccharides like heparin (Goedert et al., 1996), nucleic acids like RNA (Kampers et al., 1996), fatty acids like aracadonic acid (Wilson and Binder, 1997), or peptides like polyglutamates (Friedhoff et al., 1998) (reviewed in (von Bergen et al., 2005)). When full length and truncated variants

of Tau are expressed in cells and incubated with these polyanionic factors, Tau aggregation is accelerated in a concentration dependent manner and will form Tau filaments confirmed by immunoelectron microscopic techniques (Goedert et al., 1996, Kampers et al., 1996).

While these cofactors have proven invaluable tools for studying Tau aggregation *in vitro,* they are artificial inducers that cannot fully recapitulate the true disease microenvironment. Consequently, they may not accurately reflect the downstream effects on Tau conformation or protein interactions that influence Tau toxicity *in vivo*. Understanding how the disease microenvironment impacts pathogenic Tau remains an important and underexplored area of research.

### 1.5.3 Tau species and the aggregation cascade

Several species of aggregated Tau of varying molecular weight and size have been identified in both human brain and animal Tauopathy models. In pathological conditions, hyperphosphorylated, misfolded free-Tau monomers, known as “seeds”, are capable of self-assembly into increasingly larger and more insoluble aggregates(Alonso et al., 2001, Goedert et al., 1996). These seeds can initiate a cascade of Tau aggregation from dimers, trimers and oligomers, to form more mature fibrils like straight filaments (SFs) and paired helical filaments (PHFs) which have highly defined secondary structures(Alonso et al., 2001, Goedert et al., 1996). In AD, SFs and PHFs accumulate within the neuron cell body to form large Tau aggregated tangles called NFTs **(Figure 7).** However, the precise order in which tangles form is unlikely a uniform and linear process (Cowan and Mudher, 2013).

PHFs are the common aggregate species found in the brains of AD patients. They are composed of highly phosphorylated twisted filaments with a β-sheet rich core that forms larger inclusions such as NFTs within neurons. This highly ordered structure has been identified through several techniques including circular dichroism (CD) spectroscopy, Fourier transform infrared (FTIR) spectroscopy and X-ray diffraction (von Bergen et al.,

2005, Dregni et al., 2019). Cryo-EM studies show that Tau's β-sheet rich core domains stack in parallel to form protofilaments (Fitzpatrick et al., 2017). In PHFs, two protofilaments associate asymmetrically to form the twisted fibril core (Fitzpatrick et al., 2017) **(Figure 7).**

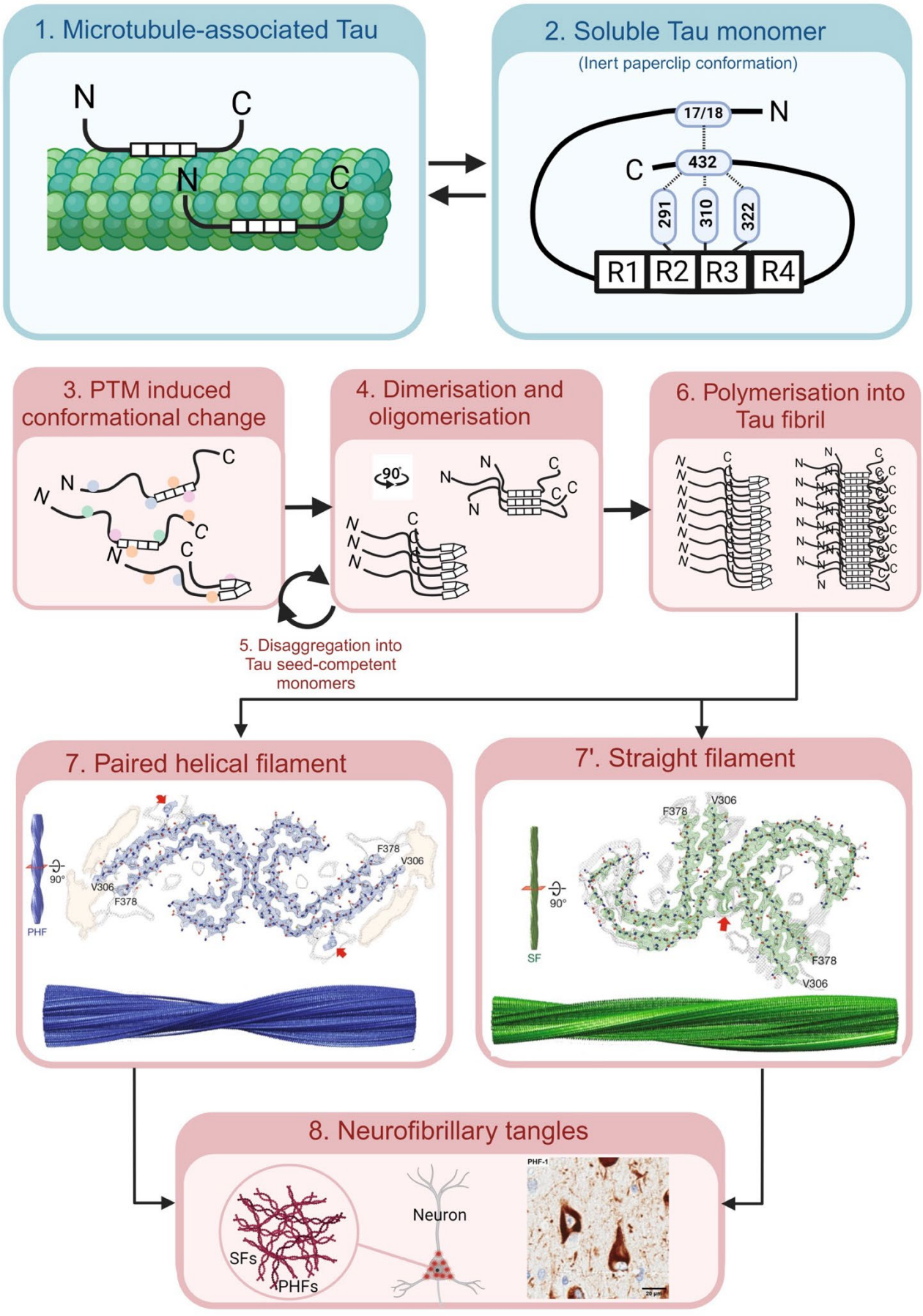


**Figure 7. Schematic of Tau aggregation cascade.**

Physiologically, Tau exists either in its (1) microtubule-bound state or its (2) microtubule-unbound, free soluble state in which Tau adopts an inert "paperclip" conformation with its N-terminal (via position 17/18) and C-terminal (via position 432) folding over the microtubule binding domain at positions 291, 310 and 322 (Jeganathan et al., 2008). (3) Post-translational modifications (PTMs) can cause structural changes to the native structure of Tau, causing misfolding which have increased affinity for aggregation. Misfolded Tau may then start to self-assemble, (4) forming dimers and oligomers which can either (5) be degraded back into seed-competent monomers or (6) polymerise into larger fibrils. Distinct fibrils are formed (7) paired helical filament (PHF) and straight filaments (7') containing rich β-sheet content form and accumulate within neurons to create large insoluble Tau inclusions such as (8) neurofibrillary tangles (NFTs) in AD. Cryo-EM reconstructions and electron density cross-sections of the fibril cores are shown taken from (Fitzpatrick et al., 2017). Image of NFT stained with antibody PHF-1 taken from (Moloney et al., 2021).

### 1.5.4 FTDP-17(*MAPT*) Tau mutations and their consequences.

The discovery of mutations in the *MAPT* gene causing FTDP-17(*MAPT*) established that dysfunctional Tau directly caused neurodegeneration. There are several ways in which Tau mutations can cause disease, however increased aggregation propensity is a common consequence.

Studies have shown that the mechanisms underlying Tau-mediated neurodegeneration are determined by the nature, and loci of the mutation along the *MAPT* gene. For example, *in vitro* assays have demonstrated that mutations within microtubule binding repeats of Tau such as ΔK280, P301L, P301S, and V337M directly weakens the binding ability of Tau to promote polymerisation and assembly of microtubules (Hasegawa et al., 1998, Lee et al., 2001). This impaired microtubule binding increases the concentration of cytoplasmic free-Tau available for self assembly and aggregation.

Analysis of brain tissue extracted from FTDP-17(*MAPT*) patients has also shown that mutations within *MAPT*'s splice sites can change the ratio of 3R:4R Tau isoforms expressed (Spillantini et al., 1998). Although the precise mechanism of this is unknown, altering the ratio of 3R:4R Tau *in vitro* has shown to favour aggregation (Adams et al., 2010). Some research groups have also suggested that equimolar expression of 3R and 4R Tau may

be required for the maintenance of the microtubules, thus preventing cytoskeletal breakdown and an increase of cytoplasmic-free Tau (Adams et al., 2010, Lee et al., 2001). Other missense mutations have been associated to increase Tau phosphorylation (Alonso Adel et al., 2004), which promoted aggregation and filament assembly in human autopsy studies (Crowther and Goedert, 2000, Goedert et al., 1999) and when expressed pan-neuronally in *Drosophila* (Wittmann et al., 2001, Shulman and Feany, 2003).

Overall, while these studies demonstrate that *MAPT* mutations cause neurodegeneration through diverse mechanisms, there are critical questions thar remain unanswered. Due to variability in experimental expression models across studies, it remains difficult to directly compare how each individual mutation directly contributes towards toxicity and neuronal dysfunction, underlying disease heterogeneity.

### 1.5.5 Toxicity of Tau aggregates

Tau aggregates, and the presence of NFTs are highly correlated with neurodegeneration and symptom progression (Bejanin et al., 2017, Höglinger et al., 2017). The pathogenicity of insoluble aggregated Tau species has been extensively investigated with overwhelming evidence demonstrating that Tau aggregates are inherently toxic. Braak and Braak first described the clear development of tangle pathology in AD brains that parallels the progression of disease, neuronal degeneration and cognitive decline, circumstantially suggesting that NFTs were toxic (Braak and Braak, 1991, Gómez-Isla et al., 1997).

However since then substantial evidence has since shown that the larger Tau aggregated species of Tau such as NFTs do not directly induce toxicity and dysfunction. In *Drosophila* and rodent models of Tauopathy, multiple studies demonstrate that degeneration and functional cognitive decline is observed and measured in the absence of NTF formation, suggesting that Tau-induced toxicity is not dependent on NFTs (Wittmann et al., 2001,

Santacruz et al., 2005, Andorfer et al., 2005). One notable study by Santacruz et al., 2005 showed that supressing Tau expression in transgenic mice restored cognitive function and prevented further neuronal loss, despite the persistence of NFTs. Moreover, NFTs have been observed to persist in neurons for decades before symptom onset, further indicating that they are not overtly toxic (Morsch et al., 1999).

Given these findings, it has been proposed that Tau aggregation could be a neuroprotective mechanism which acts to sequester the toxic species of Tau (Cowan and Mudher, 2013). This hypothesis is supported by evidence that smaller hyperphosphorylated oligomeric aggregates mediate the greatest toxicity *in vitro* and *in vivo*(Flach et al., 2012, Tian et al., 2013, Santacruz et al., 2005).

As discussed previously in **section 1.4.1,** there are many examples of soluble monomeric hyperphosphorylated Tau directly inducing toxicity *in vitro* and *in vivo* where hyperphosphorylated Tau induces axonal transport defects, cell death, and is required for Tau propagation (Cash et al., 2003, Alonso et al., 1994, Hatch et al., 2017, Rodríguez-Martín et al., 2013, Hoover et al., 2010, Mudher et al., 2004, Cowan et al., 2010, Chee et al., 2005, Chatterjee et al., 2009, Talmat-Amar et al., 2011, Stubbs et al., 2023). Indeed, more recent *in vitro* studies have shown that the intermediate trimeric and oligomeric Tau species are the most cytotoxic species, leading to decreased cell viability and neuronal death (Tian et al., 2013, Ward et al., 2012, Flach et al., 2012, Marvian et al., 2024). The pathogenic role of oligomeric Tau toxicity is further demonstrated by studies showing that anti-Tau oligomer-specific monoclonal antibodies reverse locomotive and memory deficits in a mouse model of Tauopathy (Castillo-Carranza et al., 2014).

Collectively these findings demonstrate that different Tau species are differentially toxic at distinct disease stages, but not all Tau aggregates are required for Tau-induced toxicity and neuronal dysfunction (summarised in **Table 4**) . Hyperphosphorylated Tau

monomers and small oligomers appear to be the most toxic species of Tau, while larger aggregates like NFTs appear to be non-toxic or even protective in nature. It should noted that oligomeric Tau species are heterogenous and metastable, making them difficult to characterise as they fluctuate between aggregate sizes. A more comprehensive assessment of how smaller Tau aggregates exert toxicity to neurons at different stages of diseases is required to better understand its relative contribution towards Tau-mediated degeneration, however current methods lack sensitivity to study such conformers.

**Table 4. Identified species of Tau within the aggregation cascade.**

Adapted from (Cowan and Mudher, 2013, Mroczko et al., 2019).

| Tau species | Representative icon | Molecular weight/amino acid (aa) size/length | Is the Tau hyperphosphorylated? | Toxicity |
|---|---|---|---|---|
| Monomer |  | 60kDa, 352-441aa | No | No |
| Phosphorylated Tau | 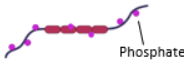 | 67-70kDa | Yes | Yes, when hyper-phosphorylated at AD epitopes |
| Dimer/Trimer | 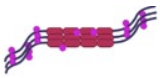 | 120-180kDa, 22-25nm | Yes, sometimes | Yes, some trimers are toxic |
| Small soluble oligomer | 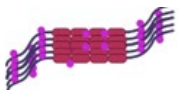 | 300-500kDa | Yes, sometimes | Yes, sometimes |
| Granular Tau oligomer (GTO) | 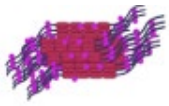 | 1800kDa | Yes, sometimes | Yes, some species |
| Straight filaments (SF) |  | >50nm length | Yes | Probably not toxic |
| Paired helical filament (PHF) |  | >220nm length | Yes | Probably not toxic |
| Neurofibrillary tangle (NFT) |  | <20µm width | Yes | Probably not toxic |

### 1.5.6 $^{306}$VQIVYK$^{311}$ and $^{275}$VQIINK$^{280}$ and the aggregation core

Two important motifs $^{275}$VQIINK$^{280}$ (known as PHF6*) and $^{306}$VQIVYK$^{311}$ (known as PHF6) located within the R2 and R3 of the MBRD respectively, have been identified as critical nucleation sites for aggregation (Mukrasch et al., 2005) **(Figure 8a).** Under pathological conditions, Tau adopts conformations exposing these aggregation domains for increased propensity for self-aggregation(Jeganathan et al., 2008, Jeganathan et al., 2006). The physiological functions and interactions of $^{306}$VQIVYK$^{311}$ and $^{275}$VQIINK$^{280}$ to the microtubules are discussed in **section 1.5.6.2.**

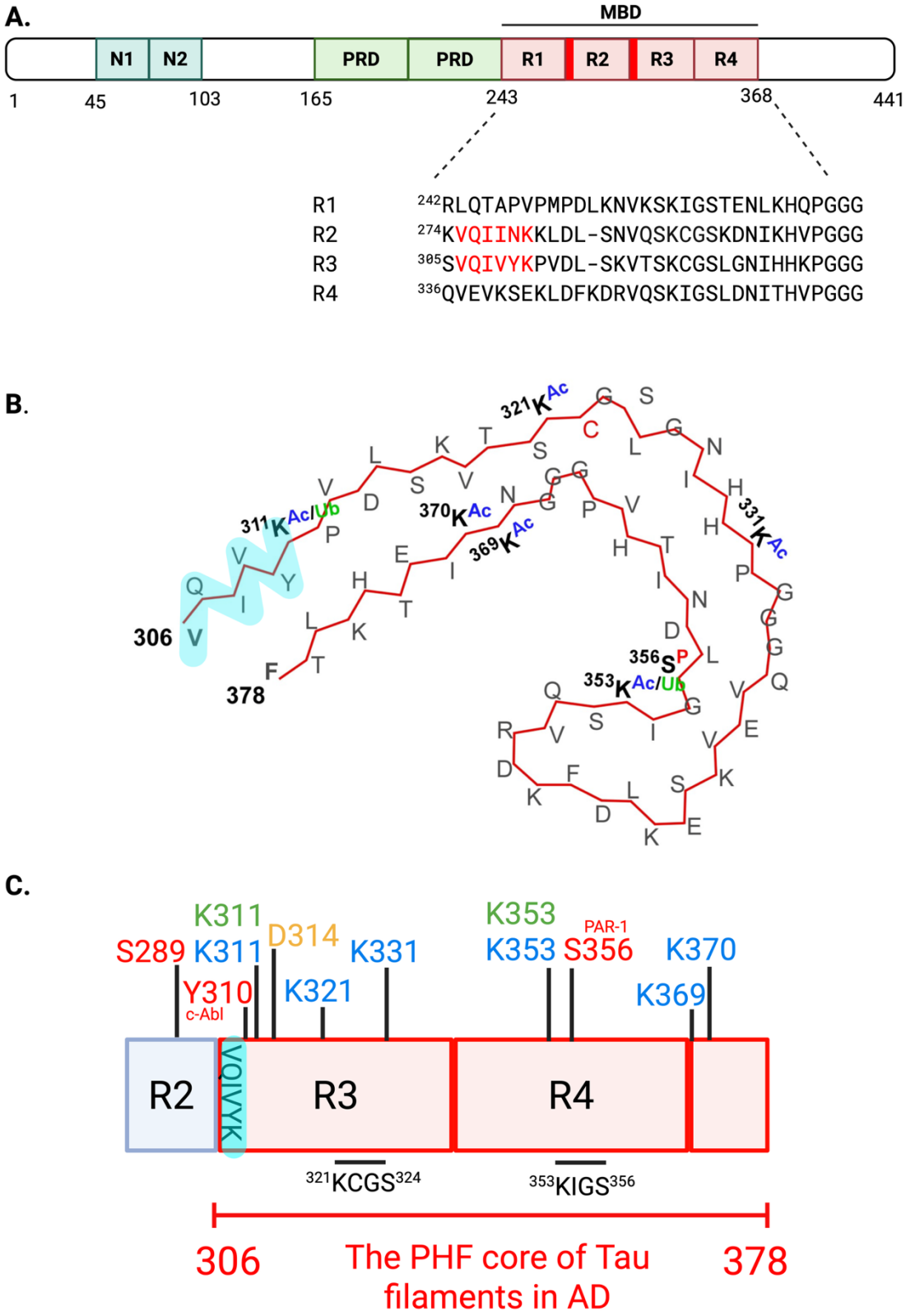


**Figure 8. $^{275}$VQIINK$^{280}$ and $^{306}$VQIVYK$^{311}$ localisation and contribution toward AD-PHF core.**

A) Diagram of full-length Tau and labelled sequence of the microtubule binding domain (MBD). B-C) Adapted from Park et al 2018, B) Protofilament of the aggregation core 306-

378 structure solved using cryo-EM, $^{306}$VQIVYK$^{311}$ involvement highlighted in cyan. C) Shows the PTMs within the protofilament of the PHF core of Tau filaments found in AD. Phosphorylation epitopes and their known acting kinases labelled red, Acetylation epitopes labels blue, Ubiquitination epitopes labelled in green and Truncation labelled in yellow.

Both $^{275}$VQIINK$^{280}$ and $^{306}$VQIVYK$^{311}$ are essential for Tau aggregation. *In vitro*, these motifs are required to drive the assembly of twisted PHFs, promoting the β-sheet-rich amyloid structure of Tau filaments (Barghorn et al., 2000, von Bergen et al., 2001, Sawaya et al., 2007, Daebel et al., 2012, del Mar Farinas Lucas et al., 2025). The $^{306}$VQIVYK$^{311}$ motif in particular is crucial for the Tau-Tau interaction between monomers and assembly into PHFs (von Bergen et al., 2001). Structural analysis of short $^{306}$VQIVYK$^{311}$ peptides using solid state NMR, electron paramagnetic resonance and X-ray crystallography techniques demonstrate that $^{306}$VQIVYK$^{311}$ forms tight parallel β-sheets which stack in an antiparallel, face-to-face arrangements described as steric zipper within the PHF core (Sawaya et al., 2007, Daebel et al., 2012, Zheng et al., 2011). Consequently, these aggregation motifs have become key targets for anti-aggregation strategies. Mutagenic and pharmacological inhibition of these motifs effectively inhibit aggregation *in vitro* and *in vivo* in models expressing 3R and 4R Tau isoforms, discussed later in **section 1.8** (Passarella and Goedert, 2018, Perez et al., 2007, Barghorn et al., 2000, von Bergen et al., 2001).

#### 1.5.6.1 Ultrastructural Characterisation of Tau fibrils.

Recent advances of cryo-EM has significantly improved our understanding about the atomic structure of mature Tau fibrils. Analysis of purified aggregates from AD brains identified that the filament core of Tau spans a short part of the Tau sequence, between amino acid(aa) residues 306-378, spanning R3, R4 and part of C-terminal and containing $^{306}$VQIVYK$^{311}$, *but not* $^{275}$VQIINK$^{280}$ (Fitzpatrick et al., 2017, Wu et al., 2022)(**Figure 8b).** This core region also contains multiple PTM sites which can influence the stability and formation of the AD-PHF core (**Figure 8c).** The remaining sequence forms the disordered

"fuzzy coat" which extends outwards from the filament core and does not have a defined structure (Fitzpatrick et al., 2017).

Most recently, the structures of several brain-derived Tau fibrils from distinct Tauopathies have been solved using cryo-EM, revealing disease specific conformations at the molecular level (Scheres et al., 2020, Shi et al., 2021, Zhang et al., 2020a). The distinct conformational folds be classified morphologically via their inclusion of 3R/4R repeats(Scheres et al., 2020, Shi et al., 2021, Zhang et al., 2020a) and the inclusion of $^{275}$VQIINK$^{280}$ or $^{306}$VQIVYK$^{311}$ as part of the central protofilament core **(Figure 9)** (Wu et al., 2022). Interestingly, despite being 3R/4R Tauopathies, AD, CTE (and PD, a 3R Tauopathy) include only $^{306}$VQIVYK$^{311}$ in their filament core, whereas CBD, PSP, AGD and GGT all have cores containing both $^{275}$VQIINK$^{280}$ and $^{306}$VQIVYK$^{311}$, suggesting presence and combination of aggregation motifs contributes towards fibril diversity (Wu et al., 2022)(**Figure 9).**

Further evidence that $^{275}$VQIINK$^{280}$ and $^{306}$VQIVYK$^{311}$ influence fibril conformation is demonstrated by Lovestam et al., using recombinant Tau fragments of varying lengths containing different combinations of these motifs. They demonstrate that AD-like PHF fibril cores are formed in Tau fragments encompassing 258-391 ($^{275}$VQIINK$^{280}$ and $^{306}$VQIVYK$^{311}$ inclusive), as did Tau297-391 ($^{306}$VQIVYK$^{311}$ only) but not Tau310-391 (neither) (Lövestam et al., 2022). Moreover, a diversity of fibril core morphologies were observed in different Tau fragments. Together these studies demonstrate that the presence and interaction between $^{275}$VQIINK$^{280}$ and $^{306}$VQIVYK$^{311}$ directly influences the molecular conformation and heterogeneity of Tau fibrils present in Tauopathies.

This makes these hexapeptides very attractive targets for therapeutic design against Tau-mediated degeneration. Most designed anti-aggregation peptides work by capping or

blocking intermolecular protein interaction at $^{275}$VQIINK$^{280}$ /$^{306}$VQIVYK$^{311}$ with other Tau monomers, preventing nucleation and fibrilisation, discussed more in **section 1.8.2** (Tomohiro Tsuchida 2020 (Tsuchida et al., 2020, Seidler et al., 2018, Sievers et al., 2011, Zhang et al., 2020b).

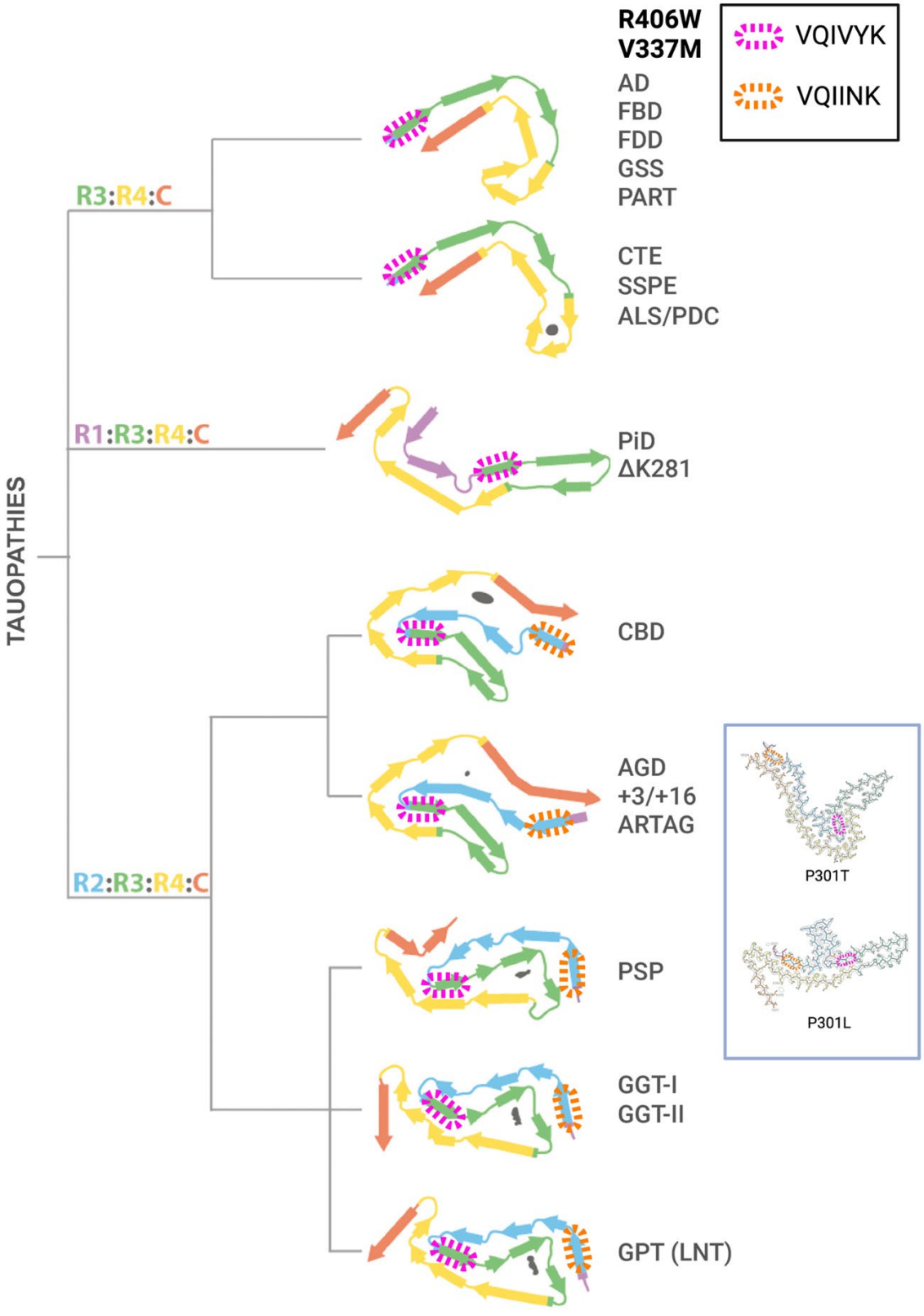


**Figure 9. Heterogeneity of Tau fibril cores in Tauopathies**.

Suggested classification by Shi et al., 2021. Figure is adapted from Shi et al., with my additions highlighting the presence of $^{306}$VQIVYK$^{311}$ (Pink) and $^{275}$VQIINK$^{280}$ (Orange) in diverse structures. Most recent cryo-EM of familial FTDP-17(*MAPT*) mutants V337M and R406W show they adopt the same core as AD (Qi et al., 2025), but P301T and P301L produce distinct, new conformational folds containing both $^{306}$VQIVYK$^{311}$ and $^{275}$VQIINK$^{280}$

(Schweighauser et al., 2025). Fibril cores for Alzheimer's disease(AD), Pick's disease (PiD), chronic traumatic encephalopathy (CTE), corticobasal degeneration (CBD), progressive supranuclear palsy (PSP), argyrophilic grain disease (AGD), primary age-related Tauopathy (PART), familial British dementia (FBD), familial Danish dementia (FDD), globular glial Tauopathy (GGT), and limbic-predominant neuronal inclusion body 4R Tauopathy (LNT) are shown.

#### 1.5.6.2 $^{275}$VQIINK$^{280}$ and $^{306}$VQIVYK$^{311}$ roles in microtubule binding.

As Tau's primary function is to bind and stabilise microtubules, it is important to consider the how $^{275}$VQIINK$^{280}$ and $^{306}$VQIVYK$^{311}$ contribute towards microtubule interactions, and whether therapeutic inhibition of these motifs may affect microtubule binding and assembly. As these motifs lie within the MBRD, their inhibition could have an impact on Tau:microtubule binding affinity.

Early work by Goode et al., using Tau fragments determined how R1-R4 of the MBRD complexes with the tubulin repeats. Interestingly, the R1-R2 (265-279aa) containing $^{275}$VQIINK$^{280}$, has the highest microtubule affinity more than any of the other MBRD repeats(Goode and Feinstein, 1994). Recent advances in structural biology, particularly metaInference cryo-EM microscopy, have enabled detailed mapping of important Tau:microtubule interaction sites *in vitro* (Brotzakis et al., 2021). Importantly, they identify how Tau residues between 202-395 interacts within the microtubule complex, identifying the MBRD containing the strongest, most rigid interactions with tubulin repeats(Brotzakis et al., 2021). These are mostly provided by the strong microtubule binding motifs SK(I/C)GS via α-helix H12 of α-tubulin, and α-helices H11 and H12 of β-tubulin (Brotzakis et al., 2021) **(Figure 10)**.

In contrast to the strong binding motifs, $^{275}$VQIINK$^{280}$ and $^{306}$VQIVYK$^{311}$ contribute towards weaker secondary interactions with tubulin**(Figure 10a)**(Brotzakis et al., 2021). In R2, the $^{275}$VQIINK$^{280}$ domain provides weak microtubule interactions via residues K280 and neighbouring K281 of Tau, forming electrostatic bonds to α-tubulins E416 and β-tubulin

E432 residues **(Figure 10b)** (Brotzakis et al., 2021). In R3, the $^{306}$VQIVYK$^{311}$ domain provides weak microtubule interactions via Y310, K311 and P312 of Tau, forming hydrogen, electrostatic and hydrophobic interactions with α-tubulin R402, E415 and β-tubulin E432, respectively **(Figure 10c)** (Brotzakis et al., 2021).

Collectively, these studies show that while $^{275}$VQIINK$^{280}$ and $^{306}$VQIVYK$^{311}$ contribute to the Tau:microtubule complex stability, their interactions are relatively weak compared to other motifs within the MBRD. Targeted inhibition of these motifs may not have an overall significant impact on microtubule binding as long as the strong binding motifs SK(I/C)GS are conserved. However, as most of the microtubule propensity derives from the R1-R2 anchor, $^{275}$VQIINK$^{280}$ inhibitors could disrupt the proposed zipper-like sequence binding from the proline rich domains to the R' sequences of Tau to the microtubules (Brotzakis et al., 2021). This makes the $^{306}$VQIVYK$^{311}$ domain a more attractive target than $^{275}$VQIINK$^{280}$ to reduce pathogenesis whilst maintaining physiological function.

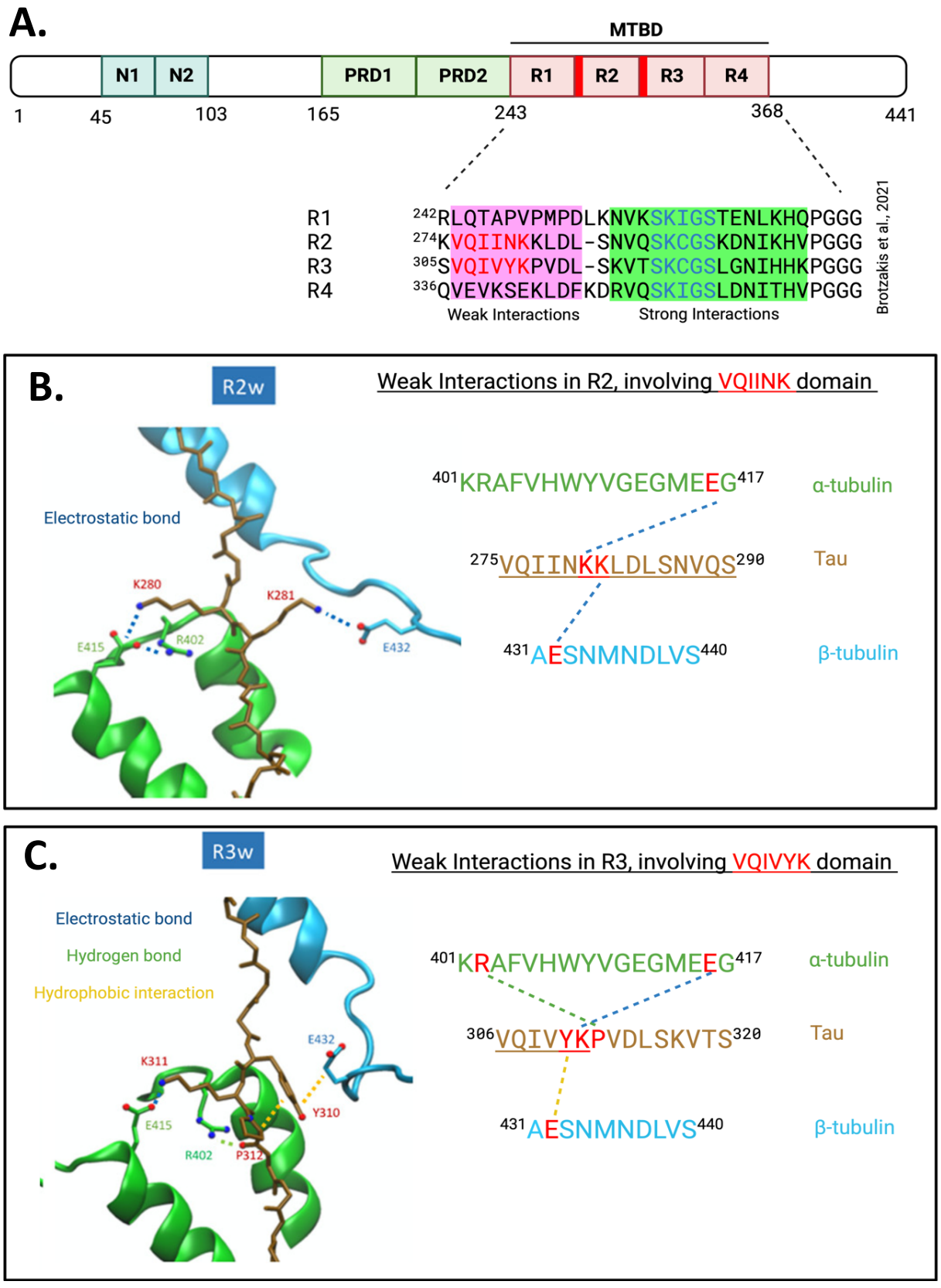


**Figure 10. The contribution of $^{275}$VQIINK$^{280}$ and $^{306}$VQIVYK$^{311}$ towards Tau-microtubule binding.**

A) Diagram of full-length Tau, with all domains labelled, and sequence of the microtubule binding domain (MTBD). Adapted from Brotzakis et al., 2021, the atomic-resolution structural ensemble of the Tau-Microtubule interactions involving the B) $^{275}$VQIINK$^{280}$ and C)

$^{306}$VQIVYK$^{311}$ found within the R2 and R3 of the MTDB respectively. These aggregation domains contribute weak interactions to Tubulin helices through electrostatic bonds (blue) hydrogen bonds(green) and hydrophobic interactions (Brotzakis et al., 2021).

#### 1.5.6.3 Post translational modifications within the $^{275}$VQIINK$^{280}$ and $^{306}$VQIVYK$^{311}$ domains.

As discussed in **section 1.2.5,** Tau is subject to rich PTMs, each which have potential physiological and pathological contributions towards Tau's activity. Namely phosphorylation, acetylation, succylination ubiquitination and truncation each which directly or indirectly can impact Tau's function, conformation and propensity for disease. As nucleating aggregation motifs, PTMs within $^{275}$VQIINK$^{280}$ and $^{306}$VQIVYK$^{311}$ may have direct or indirect contributions towards the initiation and resulting conformation of Tau aggregates that form. Moreover, it is important to consider how inhibiting $^{275}$VQIINK$^{280}$ and $^{306}$VQIVYK$^{311}$ domains by capping inhibitors may impede physiological function of these motifs towards. Several groups have investigated PTMs within the nucleating aggregation motifs $^{275}$VQIINK$^{280}$ and $^{306}$VQIVYK$^{311}$ to evaluate their ramification in the context of disease **(Figure 11).**

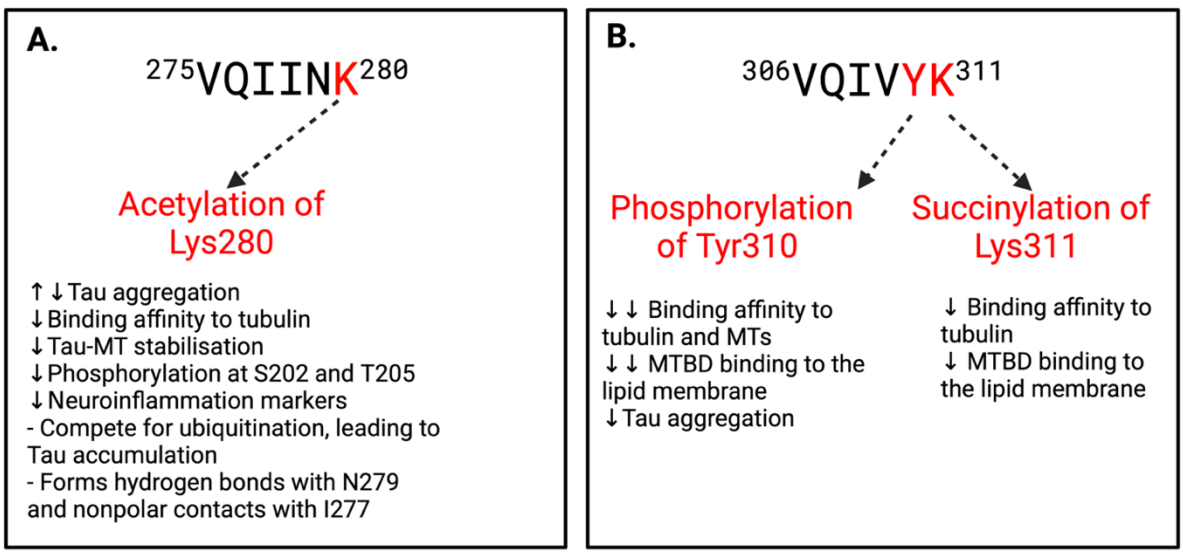


**Figure 11. PTMs consequences within the $^{275}$VQIINK$^{280}$ and $^{306}$VQIVYK$^{311}$.**

Consequences of acetylation, phosphorylation and succinylation within the A) $^{275}$VQIINK$^{280}$ and B) $^{306}$VQIVYK$^{311}$ domains which alter the physiological and pathological functions of

Tau, implicating microtubule binding affinity, lipid binding affinity and Tau misfolding and aggregation (Acosta et al., 2022, Ait-Bouziad et al., 2020, Arakhamia et al., 2020, Cohen et al., 2011, Kumar and Udgaonkar, 2021, Ajit et al., 2019, Tao and Li, 2023, Park et al., 2018).

**Phosphorylation of Tyrosine in $^{306}$VQIVYK$^{311}$:** Tau's primary role is microtubule stabilising protein. Tau achieves a dynamic ability to move freely to support elongating microtubules by phosphorylation via kinases and phosphatases (Drechsel et al., 1992) (Chudobová and Zempel, 2023). Y310 is the only epitope within both aggregation motifs which is available for phosphorylation **(Figure 11).**

The impact of phosphorylation at Y310 is relatively understudied compared to other residues along Tau. The phosphorylation of Y310 is not a prominent epitope elevated in AD patients, nor is Y310 a named "master phosphorylation site" which can influence downstream phosphorylation of other proximal epitopes (Stefanoska et al., 2022). Nevertheless, there is evidence that tyrosine phosphorylation including Y310 may play pathogenic roles in disease. The c-Abl kinase that phosphorylates Y310 and other tyrosine's along Tau (Ait-Bouziad et al., 2020) is upregulated in many Tauopathies (Schlatterer et al., 2011). Furthermore, Tau aggregates extracted from AD patients have an increase in Tau tyrosine phosphorylation (Lebouvier et al., 2009), indicating that the phosphorylation of tyrosine could have pathogenic roles during disease.

A few groups have investigated the impact of phosphorylation at Y310 *in vitro* and how it may impact aggregation, microtubule binding properties and cellular cytotoxicity in light of its proximity in the $^{306}$VQIVYK$^{311}$ domain. Several studies have show that phosphorylation of Y310 in short synthetic PHF6 fragments (310-311aa) alters Tau fibril formation with conflicting results (Santa-María et al., 2006, Hirata et al., 2007, Inoue et al., 2008). In addition, Acosta et al., 2022 using short synthetic Tau mutants (265-290aa) assessing phospho-mimetic Y310E, demonstrated that phosphorylation severely impacted Tau-tubulin binding affinity and decreased binding to lipid vesicles (Acosta et al., 2022). More recently, Ait-Bouzaid et al. 2020 show that site directed phosphorylation of Y310 full

length 2N4R Tau decreases aggregation propensity, reduces microtubule binding affinity and reduces binding affinity to lipid vesicles. Collectively, these groups demonstrate clearly that phosphorylation of Y310 mediates aggregation potential, lipid interactions and microtubule interactions **(Figure 11).** Targeting this domain through inhibitors could result in lower binding affinity but reduce PTMs that could increase aggregation.

**Acetylation of Lysine in $^{275}$VQIINK$^{280}$:** Acetylation, ubiquitination and succinlyation occurs on lysine amino acids, and there are two lysines, K280 and K311, within the $^{275}$VQIINK$^{280}$ and $^{306}$VQIVYK$^{311}$ domains respectively, both of which have been implicated pathogenically.

Similar to phosphorylation, Tau is extensively acetylated in the PD and the MBRD. Acetylation is one of the most common PTMs that occurs within the PHF aggregation core (Park et al., 2018)**(Figure 8).** Acetylation of Tau at K174, K274 and K280 have been detected at elevated levels in Tau aggregates purified from multiple Tauopathies including AD, PD and FTDP-17(*MAPT*) (Min et al., 2015, Irwin et al., 2013), as well as transgenic PS19 mouse models expressing P301S hTau (Arakhamia et al., 2020, Cohen et al., 2011). Collectively, this gives circumstantial evidence that acetylation could have pathological roles in disease.

Several groups have investigated the impact of acetylation at K280 *in vitro* and how it may impact aggregation, microtubule binding properties and cellular cytotoxicity in light of its proximity in the $^{275}$VQIINK$^{280}$ domain. Mimicry of acetylation of K280 Tau fragments *in vitro* decreased tubulin binding affinity, impairing microtubule assembly and stabilisation, and reduced binding to lipid vesicles (Cohen et al., 2011, Acosta et al., 2022). Moreover, some of these groups analysed the impact of acetylation of K280 on aggregation, finding that it directly promoted Tau amyloid fibrillisation faster than wildtype Tau, regulating the monomer-fibril binding affinity, and reducing the lag phase of aggregation (Cohen et al.,

2011, Kumar and Udgaonkar, 2021). Collectively, these groups showed significant pathogenic potential of acetylation of K280 *in vitro*. Conversely, *in vivo* acetylation mimicry of P301S transgenic mice reduced hallmarks of pathology, significantly reducing neuroinflammation markers, abolishing widespread misfolded Tau species detected by MC1 immunoreactivity, and reducing phosphorylation at disease relevant epitopes S202/T205 compared to wildtype PS19 mice by five-fold (Ajit et al., 2019). With the conflicting literature between *in vitro* and *in vivo* experimental models, the relationship between acetylation and pathology is unclear. More *in vivo* research upregulating physiological acetylation, instead of mimicry is needed to evaluate the potential effects of inhibiting acetylation of K280 in the $^{275}$VQIINK$^{280}$ domain.

**Succinylation of Lysine in $^{306}$VQIVYK$^{311}$:** Similar to the other PTMs, Succinylation of Tau at K311 has been investigated due to its loci within the aggregation domain. Interestingly, it has been reported to have elevated presence in AD brains only, whilst absent in all control brains(Yang et al., 2022). Further *in vitro* investigation shows that succinylation mimetic K311E of Tau fragments reduced global binding of tubulin, and lipid vesicles (Yang et al., 2022, Acosta et al., 2022) implying pathogenic contributions that can directly or indirectly alter aggregation and disease progress.

**Ubiquitination of Lysine in $^{275}$VQIINK$^{280}$ and $^{306}$VQIVYK$^{311}$:** There is extensive ubiquitination in the senile plaques and PHFs of Tau aggregates from AD brains, likely contributing directly or indirectly towards Tau fibril formation (David et al., 2002, Perry et al., 1987). 28 Tau ubiquitinoylation sites are detected in human AD brain samples (Abreha et al., 2018) of which K311 is a frequently reported site with elevated ubiquitination (Abreha et al., 2018, Cripps et al., 2006). The primary function of ubiquitination is to facilitate protein degradation. Normal protein degradation could be impacted by the competition between acetylation and ubiquitination for lysine residues at K280 and K311 in $^{275}$VQIINK$^{280}$ and $^{306}$VQIVYK$^{311}$, respectively (Morris et al., 2015). Tau degradation may also be influenced

by Tau aggregation, if the ubiquitination markers are occluded or indirectly cause protein structural changes in favour of aggregation. Collectively, these factors may perpetuate an increase local concentration of aberrant Tau to accumulate and aggregate. Therefore, it is possible that therapeutic targeting of $^{275}$VQIINK$^{280}$ and $^{306}$VQIVYK$^{311}$, could block K280 and K311 ubiquitination interactions which could therefore reduce the potential for Tau degradation.

Overall, there is some evidence that PTMs within the $^{275}$VQIINK$^{280}$ and $^{306}$VQIVYK$^{311}$ sites might perturb normal Tau function, and possibly determine fibril conformation subtypes and influence Tau aggregation and associated toxicity. Therapeutic targeting of these motifs may present some competition against physiological PTMs and microtubule binding affinity. However, the evidence reviewed here indicates that both motifs make excellent therapeutic candidates to inhibit aggregation because they target minimal short sequences that provide overall more pathogenic functions, rather than physiological ones.

## 1.6 Tau propagation

The pathological spread of Tau throughout the brain is described as prion-like. Prions are proteinaceous infectious particles, whereby misfolded proteins have the capacity to induce native proteins to adopt the same conformation as the misfolded protein, like in Creutzfeldt-Jakob disease (Prusiner, 1982). Pathological Tau behaves similarly, with misfolded Tau seeds capable of acting as a template to convert the misfolding of native Tau monomers into the same pathological conformation (Gerson and Kayed, 2013). This enables pathological Tau to amplify in the brain, propagating through neuroanatomically linked regions (de Calignon et al., 2012, Braak and Braak, 1991, Chhatwal et al., 2018) **(Figure 12).**

Tau spreads throughout the brain in consistent patterns during AD progression which has been classified into Braak stages(I-VI) based on the histological detection of NFTs throughout the postmortem brain (Braak and Braak, 1991). In AD, Tau pathology begins to appear in the entorhinal cortex and spread to the limbic regions including the hippocampus, relating to symptom progression and memory loss. In the later stages Tau pathology spreads to the adjacent neocortex (Braak and Braak, 1991, Braak and Del Tredici, 2015) **(Figure 12).** Several groups have recapitulated this spread of Tau through synaptically connected regions in mouse and monkey models by injecting Tau from patient derived tissue (Beckman et al., 2021, Basheer et al., 2024). Although it is unclear why Tau pathology starts from the entorhinal cortex, there is emerging evidence that certain neuronal populations have selective vulnerability to pathological Tau (Mudher et al., 2017, Sivanantharajah et al., 2025).

Across multiple experimental models many groups have demonstrated it is primarily the smaller, highly phosphorylated Tau monomers and low molecular weight oligomers which are able to propagate trans-synaptically from neuron to neuron, perpetuating the spread of pathological Tau in healthy neurons (Hallinan et al., 2019, Hu et al., 2016). In a hippocampal monoculture model isolating neurons showed that only the pseudo-phosphorylated TauE14 species, and not wildtype Tau, were able to spread from a donor and receiver neurons through synaptic contacts (Hallinan et al., 2019). Likewise, *in vivo*, the injection of AD derived phosphorylated, but not de-phosphorylated Tau in the hippocampus of transgenic mice caused propagation to anatomically connected areas (Hu et al., 2016). Another group assessed multiple sizes of Tau species from recombinant and patient derived Tau samples, demonstrating that it was trimers and not larger more mature fibrils which were able to be spontaneously taken up into the cell and seed Tau aggregation(Mirbaha et al., 2015). Collectively, there is lots of evidence to suggest that seed-competent Tau monomers

and small oligomers are required for the propagation of Tau from a diseased to healthy neurons.

Several mechanisms have been proposed for trans-synaptic Tau propagation, broadly categorised into vesicular pathways (exosomal, ectosomal or secretory lysosomal) and non-vesicular pathways (tunnelling nanotubes and passive release following cell damage). Additionally, substantial evidence implicates glial immune cells are involved in Tau propagation(Wang et al., 2022). Despite multiple proposed mechanisms, their relative contributions toward propagation, and the Tau species involved in each pathway are unclear. Preventing the spread of Tau represents a critical therapeutic goal for slowing disease progression, but better models to study propagation are needed to identify possible intervention points.

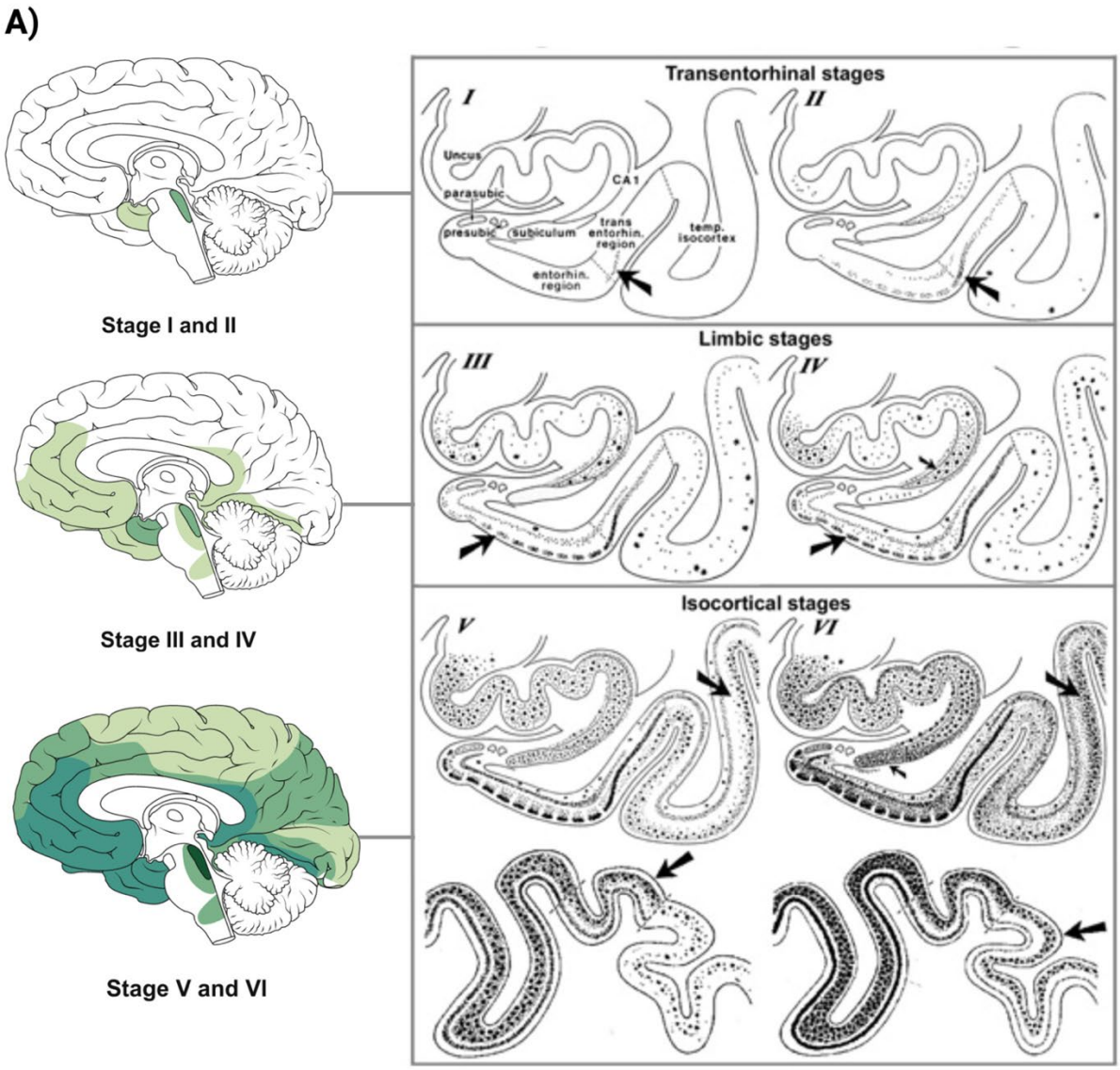


**Figure 12. Spread of Tau pathology in AD.**

Representative images of Tau pathology spread through the trans-entorhinal, limbic and cortical regions in the brain according to Braak staging (I-VI). Coronal sections throughout the medial temporal lobe showing pattern of pathology spread, taken from (Vogel et al., 2020)and (Braak and Braak, 1991).

## 1.7 Tau interactome

As described in **section 1.2.3,** Tau partakes in a diverse range of functions including cytoskeletal regulation, axonal transport and neuronal function. There is a network of interacting proteins and protein complexes which maintain Tau's physiological function, collectively known as the Tau interactome. As this is a relatively new and developing field,

the full mapping of Tau's interactome is incomplete due to several technical challenges. Tau's interactome has been studied through co-immunoprecipitation coupled with mass spectrometry, proximity labelling approaches and more recently, size-exclusion chromatography with quantitative proteomics (Gunawardana et al., 2015) (Kavanagh et al., 2022) (Tracy et al., 2022) (Jiang et al., 2021) (Martinez et al., 2025). However the more traditional approaches using whole brain lysates produce weak and heterogenous signals, and can struggle to isolate one fraction or species of Tau (Martinez et al., 2025). Nonetheless, these studies provide critical insight into pathological changes to Tau's interactome during disease, highlighting different interactome profiles between disease states, where protein interactions of Tau are remodelled in disease which can mediate toxicity (Gunawardana et al., 2015) (Kavanagh et al., 2022).

Under physiological conditions, and in control brains, analysis of Tau's interactome demonstrates many partners beyond the cytoskeleton. A recent systematic review of 12 Tau interactome studies identified 2084 proteins which interact with human tissue with rich interactions between Tau and proteins involved in RNA binding, ribosomes, and proteasome function (Kavanagh et al., 2022)(**Figure 13).** These protein interactions help maintain Tau's homeostasis to support neuronal function, axonal trafficking and synaptic signalling, but are susceptible to change upon post translational modification of Tau. Importantly, interactome studies show that Tau's interactome influenced by cellular location, isoform, presence of PTM, conformation and aggregation state (Gunawardana et al., 2015) (Kavanagh et al., 2022).

### 1.7.1 Protein interactions within the aggregation-promoting motifs.

Interestingly, there are several non-cytoskeletal interacting partners with the aggregation-promoting hexapeptide motifs $^{275}$VQIINK$^{280}$ and $^{306}$VQIVYK$^{311}$, beyond simple microtubule interactions, despite being located within Tau's microtubule-binding

domain. These motifs also appear to serve as important binding sites for RNA-binding proteins and molecular chaperones that contribute to Tau homeostasis.

Tau has rich interactions with RNA binding proteins and heterogenous nuclear ribonucleoproteins (HNRNPs) such as FUS, SFPQ and PTBP1 (Jiang et al., 2021, Wang et al., 2023, Jiang et al., 2023, Zhang et al., 2022b, Baughman et al., 2018). These RNA-binding proteins have broad molecular functions including regulating splicing, mRNA transport, and mediating stress granule dynamics. Notably, the RNA-binding, stress granule protein G3BP2 has been found to interact directly and bind to the MBRD upon its release from microtubules, spanning both $^{275}$VQIINK$^{280}$ and $^{306}$VQIVYK$^{311}$ (**Figure 13)** (Wang et al., 2023). G3BP2-Tau interaction increases with pathology in human AD brains and is proposed to provide protective properties against aggregation. This is supported in studies that show Tau pathology is significantly increased upon loss of G3BP2 in knockout human neurons and brain organoids (Wang et al., 2023). This is particularly relevant as RNA itself is a component of Tau aggregates in AD brains and is a cofactor known to enhance Tau aggregation kinetics (Kampers et al., 1996), and RNA binding proteins are known components of Tau aggregates in Tauopathies (Ginsberg et al., 1997).

The $^{306}$VQIVYK$^{311}$ motif also has direct protein interactions with molecular chaperones including the immunophilin FKBP12 and several heat shock proteins (HSPs). FKBP12 is involved in regulating neuronal resilience and modulating aggregation, binding directly to monomeric Tau at 307QIVYK311 and 391EIVYK395, an interaction which can be disrupted by phosphorylation of Tyrosine at Y310/Y394 residues (Jiang et al., 2023). HSPs involved in Tau's interactome that bind directly to or near the $^{306}$VQIVYK$^{311}$ domain include Hsp27, Hsp70 and Hsp90, each which have significant roles in maintaining protein solubility and preventing protein misfolding (**Figure 13).** Hsp90 binds and interacts more broadly within the MBRD (residues 210-380), whereas Hsp27 contributes chaperone activity by binding directly to $^{306}$VQIVYK$^{311}$ (Zhang et al., 2022b, Baughman et al., 2018).

Interestingly, phosphorylation increases Hsp27 affinity to Tau, providing evidence that conformational changes sensitive to PTMs like hyperphosphorylation may significantly impact chaperone recruitment and protective mechanisms(Zhang et al., 2022b, Baughman et al., 2018).

### 1.7.2 Pathological remodelling of the Tau interactome

Pathological changes to Tau's interactome has been studied in multiple models, in human AD post-mortem brain tissue, human cell culture models and rodent models. Comparison of the interactomes between different FTDP-17(*MAPT*) mutants such as P301S, V337M and wildtype Tau show distinct interactomes of ribosomal units, translation initiation factors and HNRNPs (Kavanagh and Drummond 2022) (Tracy et al., 2022), providing evidence that pathologically distinct Tau species may possess distinct interactomes, consequential to changes in Tau's primary sequence.

Interestingly, proteomic analyses of AD and control brain samples reveal consistent overlaps of interacting partners. However, importantly, they each also contain an additional distinct range of disease-specific interacting partners (**Figure 13)** (Gunawardana et al., 2015, Martinez et al., 2025). Critically, these interactome changes reflect a loss of physiological protein interactions that normally maintain Tau homeostasis, and additional gain of pathological interactions which may drive Tau-mediated toxicity. Therefore interactome studies represent an important method of understanding disease mechanisms that underly Tauopathy.

Recently Martinez et al., describe a novel method of analysing Tau's interactome by isolating defined high molecular weight Tau species using size-exclusion chromatography fractioning and analysing with quantitative proteomic analysis. Comparison of Tau seeds of a defined size in control and AD brain derived Tau revealed important changes to the Tau's interactome between disease states. While there was a considerable overlap between control

and AD Tau interactomes, AD brains showed a loss of 124 control-specific interactors, inclusive of translation factors involved in protein synthesis, representing a loss of physiological function and/or protective mechanisms(Martinez et al., 2025). Additionally, AD Tau gained 819 disease-specific interactors, including proteins upregulating endocytic recycling pathways, suggesting a pathological gain of function (Martinez et al., 2025). Furthermore, enrichment analysis showed than control Tau of the same molecular weight as AD had similar mitochondrial processes and synaptic vesicle transport, however control brains specifically had distinct nuclear protein localisation, calcium signalling and endoplasmic reticulum network organisation (Martinez et al., 2025). Together the loss of these physiological protein interactions represents critical loss of function which disrupts Tau's homeostasis and likely contributes toward neuronal vulnerability and degeneration. Simultaneously, loosing physiological interactors and gaining pathological interactors also likely contribute towards Tau's pathological gain of function mechanisms, promoting pathogenic conformational changes that favour aggregation cytotoxicity.

Further investigations by Martinez et al., provide evidence that high molecular weight species isolated in the same weight fraction between control and AD brains have distinct interactomes due to distinct conformations. With the emerging use of cryo-EM technology, further characterising which conformational features are associated with pathological binding partners may identify common targets for intervention.

Overall, these proteomic studies have revealed extensive remodelling of Tau's interactome during disease, identifying numerous protein interactions which are lost or gained. These studies highlight the complexity of changes of Tau during disease and should be systematically assessed to define the consequence of these changes and how they contribute towards neuronal degeneration and whether they can be potential therapeutic target.

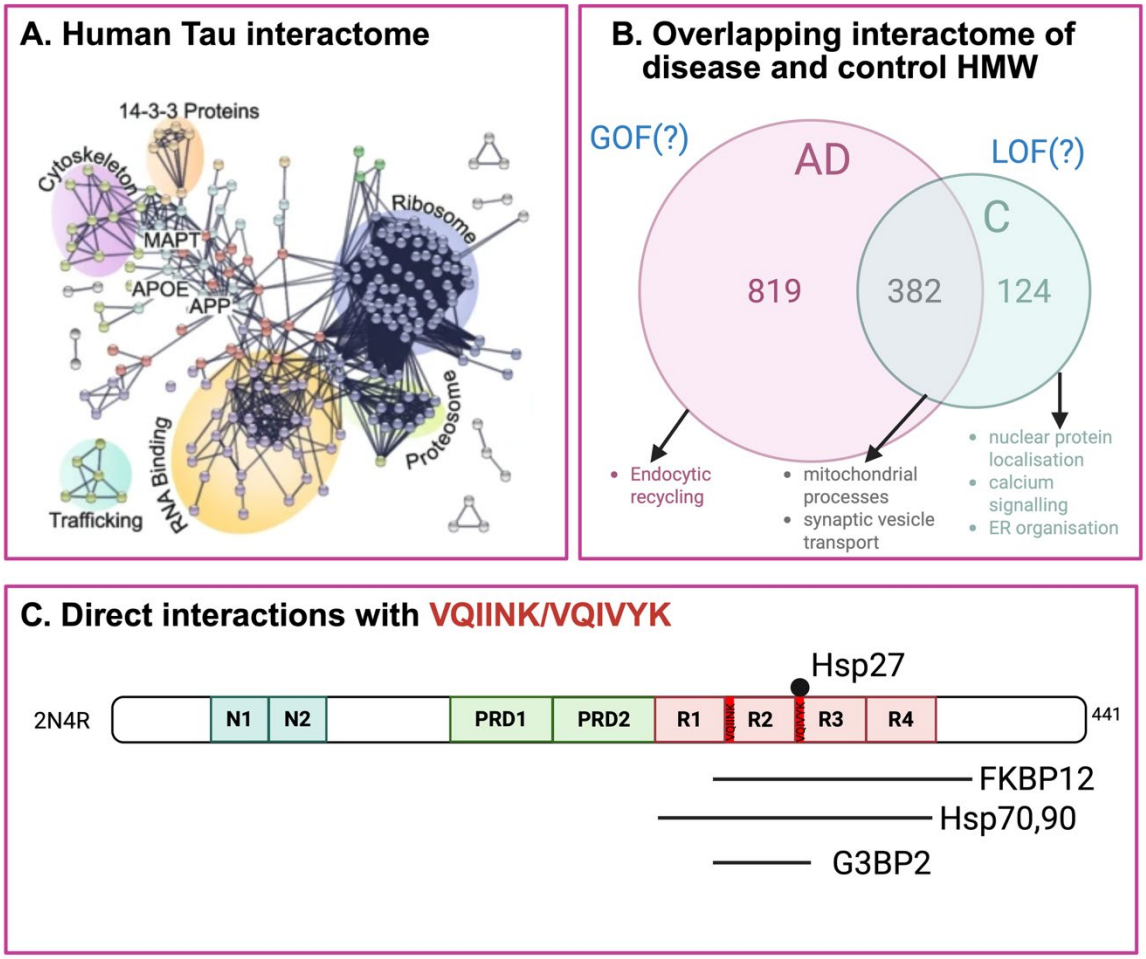


**Figure 13. Schematic diagram of features of Tau's interactome.**

A) Human Tau interactome mapped, taken from (Kavanagh et al., 2022). B) Venn diagram of Tau's interactome in Alzheimer's disease (AD) and control brains (C), showing overlap, loss and gain of interacting proteins which may represent a loss- or gain- of physiological function (LOF/GOF). Adapted from (Martinez et al., 2025). C) Shows identified RNA-binding proteins and molecular chaperones which directly interact with the aggregation-promoting motifs $^{275}$VQIINK$^{280}$ and $^{306}$VQIVYK$^{311}$ (Jiang et al., 2023, Wang et al., 2023, Zhang et al., 2022b, Baughman et al., 2018).

## 1.8 Current Tau-based therapeutic strategies

There are many therapeutic approaches in the pipeline for treating Tauopathies, however thus far none have been FDA approved. Tau strategies are broadly designed to either 1) inhibit Tau aggregation, 2) reduce pathological Tau PTMs like phosphorylation 3) reduce overall Tau levels or 4) restore loss of Tau function summarised in **Figure 14** (Lane-Donovan and Boxer, 2024).

The most direct strategies to reducing Tau pathology is to lower the amount of Tau available in the cell to aggregate. The most successful approach to this has been to prevent translation of Tau mRNA by Antisense oligonucleotides (ASO) such as BIIB080. In mouse and non-human primates Tau ASOs reduce Tau phosphorylation , neurodegeneration and behavioural deficits (DeVos et al., 2017) and has given promising phase I clinical trial results, successfully reducing phosphorylated Tau pTau181 by 50% in the CSF (Mummery et al., 2023).

Other therapies aim to clear extracellular Tau through active or passive immunotherapy. Tau vaccines, such as AADvac1 and ACI-35.030, have been designed to produce antibodies against pathological Tau species like phosphorylated and truncated Tau, aiming to reduce Tau aggregation and propagation (Sol et al., 2025, Novak et al., 2021). Although these vaccines have made it to phase II clinical trials and demonstrate strong immunogenicity and reduced Tau phosphorylation, they have not been effective at improving cognitive function(Sol et al., 2025, Novak et al., 2021). Some groups have postulated that clinical success may be limited by indiscriminately clearing Tau, as this may compromise essential Tau functions and may be inappropriate for early or preventative treatments(Congdon et al., 2023).

### 1.8.1 Tau phosphorylation inhibitors

Other methods of targeting pathological Tau are though small molecules to reduce Tau PTMs, particularly phosphorylation, acetylation and O-GlcNAcylation as they are each strongly implicated in neuronal dysfunction and Tau aggregation. Phosphorylation inhibitors have been a popular avenue for Tau therapies however they have been limited in their preclinical success.

GSK-3β kinase inhibitors have been extensively developed because this kinase phosphorylates the majority of the epitopes implicated in disease. Lithium, a GSK-3β has

shown some clinical promise, slowing disease progression in patients with MCI (Forlenza et al., 2019) and prevented cognitive loss in AD patients treated with a daily microdose (Nunes et al., 2013)). However, more selective GSK-3β inhibitors such as Tideglusib although effective in preclinical rodent models of Tauopathy (Serenó et al., 2009), did not slow progression in MCI, AD or PSP and had negative side effects so was discontinued (Tolosa et al., 2014, Lovestone et al., 2015). Similarly, Saracatinib, a Fyn kinase inhibitor has also shown promising results in preclinical models, improving memory deficits in mouse models yet showed limited efficacy in clinical trials (van Dyck et al., 2019).

Although GSK-3β and other kinase inhibitors have strongly reduced Tau toxicity in preclinical models of Tauopathy (Mudher et al., 2004), failure of the clinical trials may reflect fundamental limitations of targeting phosphorylation. As phosphorylation is ubiquitous to many cellular processes and kinases like GSK-3β regulates many other pathways beyond Tau including cell growth, apoptosis and metabolism (Beurel et al., 2015). Therefore, kinase inhibitor strategies may not be specific enough to reduce Tau pathology, at least not by monotherapy alone. Due to the lack of clinical trial success, kinase inhibitor strategies have mostly lost momentum in favour of other more specific therapeutic approaches.

### 1.8.2 Tau aggregation inhibitors

Complementary to reducing pathological Tau PTM, aggregation inhibitors are a more direct strategy to preventing the formation of toxic, seed competent aggregates. Early studies using broad-spectrum small molecules such as methylene blue and polyhistidine peptides demonstrated inhibition of recombinant Tau polymerisation and reduced Tau toxicity in cell culture (Kondo et al., 2021, Wischik et al., 1996, Mamsa and Meloni, 2021, Taniguchi et al., 2005). Methylene blue disrupts disulfide bond formation in Tau fibrils, and is a good inhibitor Tau aggregation in preclinical transgenic mouse models (Soeda et al.,

2019) but in a recent phase 3 trial with derivative "TauRx" there was no significant clinical improvement in AD patients (Wischik et al., 2022).

There is demand to develop more Tau-specific anti-aggregation drugs. With the increased structural understanding of Tau fibrils, where cryo-EM have identified $^{306}$VQIVYK$^{311}$ and $^{275}$VQIINK$^{280}$ as pivotal motifs to aggregation, several peptide aggregation inhibitors have been designed to target, cap or competitively bind these motifs. These peptides show strong aggregation inhibition and promising results in preclinical studies so far(Aggidis et al., 2024, Zhang et al., 2020b), although none have been taken forward to clinical trials yet **(Table 5).**

**Table 5. Table of experiments investigating $^{306}$VQIVYK$^{311}$ and $^{275}$VQIINK$^{280}$ mutagenesis and small molecule inhibitors.**

| Reference | Model | Method (mutagenic deletion or drug) | Key findings |
|---|---|---|---|
| (Li and Lee, 2006) | *In vitro* recombinant K18 Tau | Mutagenic deletion of $^{275}$VQIINK$^{280}$ or $^{306}$VQIVYK$^{311}$ | Deleting $^{306}$VQIVYK$^{311}$ abolished fibril formation, whereas deleting $^{275}$VQIINK$^{280}$ significantly decreased but did not abolish K18 fibrillisation. Specifically, removal of K311 from $^{306}$VQIVYK$^{311}$ abolished K18 fibrillisation. |
| (Perez et al., 2007) | *In vitro* recombinant Tau3R fragments expressed in COS-F cells. | Mutagenic point mutations in $^{306}$VQIVYK$^{311}$ | Mutations in $^{306}$VQIVYK$^{311}$ prevented fibril formation, and surprisingly led to *increased* phosphorylation of the Tau proteins at sites S396, S404, S422, S262 and S356 |
| (Passarella and Goedert, 2018) | Transgenic Tau0N4R expressing *Drosophila* | Mutagenic deletion of $^{306}$VQIVYK$^{311}$ | Flies expressing Tau0N4RΔVQIVYK prevented β-sheet assembly, rescued rough eye phenotype, climbing and survival deficits, and reduced phosphorylation at AT270, AT8, AT180, AT100 epitopes. |
| (Macdonald et al., 2019) | Transgenic TauP301S expressing mice, *In vitro* recombinant TauP301S | Mutagenic deletion of $^{275}$VQIINK$^{280}$, $^{306}$VQIVYK$^{311}$ or both. | Recombinant TauP301S with single or combination deletions failed to form β-sheet structure filaments with heparin. TauP301S mice had significantly reduced life span and sarkosyl insoluble fraction. However, TauP301S deletion mice had no significant sarkosyl insoluble Tau, and had same normal lifespan when |

| | | | |
|---|---|---|---|
| | | | comparing ΔVQIINK, ΔVQIVYK and both double deletion. |
| (Sievers et al., 2011) | *In vitro* Tau3R K12 and K19 fragments | Computational structure-based design of peptide $^{306}$VQIVYK$^{311}$ capping inhibitor (D-TLKIVW) | D-TLKIVW caps β-strands of the $^{306}$VQIVYK$^{311}$ steric zipper. D-TLKIVW prevented seeded fibril formation of Tau3R K12 for days. However, it had a moderately weak inhibition profile of Tau2N4R compared to Seidler et al., 2018. |
| (Seidler et al., 2018) | Full length Tau2N4R in HEK293 biosensor cells | Computational structure-based design of Peptide inhibitors designed to cap $^{275}$VQIINK$^{280}$ (W-MINK) | Show that $^{306}$VQIVYK$^{311}$ inhibition are ineffective at inhibiting full-length Tau2N4R proteins. Instead $^{275}$VQIINK$^{280}$ capping peptide prevented Tau2N4R growth *in vitro* and reduced the ability for exogenous AD-derived fibril to seed intracellular Tau in biosensor cells. |
| (Mohamed et al., 2013) | *In vitro* AcVQIVYK peptide fragments | Small molecule drugs Nitrocatechol derivatives of tolcapone and entacapone | Nitrocatechol interacts with the $^{306}$VQIVYK$^{311}$ steric zipper interface and significantly reduced aggregation and fibril formation of AcVQIVYK Tau fragments. |
| (Frenkel-Pinter et al., 2016, Frenkel-Pinter et al., 2017) | *In vitro* $^{306}$VQIVYK$^{311}$ fragments, and transgenic R406W Tau expressing *Drosophila* | Small molecule hybrid compound Cl-NOTrp | Cl-NOTrp prevents fibril growth in a dose dependent manner and disassembles pre-formed fibrils *in vitro*. When Tau expressing flies were fed the drug, rough eye phenotype, reduced the accumulation of Tau in larval eye tissue by 70%, reduces Tau hyperphosphorylation and increased climbing ability and improved lifespan |
| Zhang 2020 (Zhang et al., 2020b) | *In vitro*, N2a neuroblastoma cell culture, TauP301S transgenic mice | Peptide inhibitor targeting $^{306}$VQIVYK$^{311}$ mediated aggregation called D-nitmnsrrrrnh (p-NH) | D-nitmnsrrrrnh inhibits fibril formation *in vitro* and reduced Tau aggregation and phosphorylation in N2a tangle formation and increased cognitive scores from intranasally dosed TauP301S transgenic mice. Reduction of phosphorylated Tau was tissue specific in cortex and hippocampal tissue tested. |
| (Dammers et al., 2016) | *In vitro* K19 (Tau3RD) and TauFL, and in N2a cells | Using Mirror image phage display on $^{306}$VQIVYK$^{311}$ fibrils generated D-peptides: APT, KNT, TL28, TD28, TD28rev | These each inhibited Tau aggregation *in vitro* (TD28 the fastest) and in N2a cell culture. Each had good cell penetrance and but indicated cell toxicity from loss of nuclei. |
| (Malhis et al., 2021) | *In vitro* $^{306}$VQIVYK$^{311}$ fragments and Tau2N4R | Using Mirror image phage display on $^{306}$VQIVYK$^{311}$ fibrils generated D-peptides: MMD3 and MMD3rev | Inhibit the formation of Tau fibrils *in vitro,* diverting Tau into amorphous aggregates with no β-sheet content. |

| | | | |
|---|---|---|---|
| (Wang et al., 2016) | *In vitro* Ac-$^{306}$VQIVYK$^{311}$ fragments | Molecular grafting of naturally occurring Disulfide-rich cyclic peptides: SFTI-1 and kB1 | Inhibits $^{306}$VQIVYK$^{311}$ fibril formation |
| (Aillaud et al., 2022) | *In vitro* TauRDΔK fragment, Tau2N4R, and FTDP-17(*MAPT*) mutants Tau2N4RΔK, TauFL-A152T and TauFL-P301L, and in N2a cell culture | Using Mirror image phage display on Tau2N4R: generated peptides ISAD1 and ISAD1rev | Inhibits aggregation of Tau2N4R and FTDP-17(*MAPT*) mutants *in vitro* and in cell culture ISAD can produce large high molecular weight oligomers, but they lack β-sheet content. Is non-toxic to cells and prevents Tau-mediated cytotoxicity. |
| (Kondo et al., 2021) | *In vitro* Tau-R3 fragments and iPS cell-derived neurons carrying Tau or APP mutations | Small molecule hepta histidine (TAT)-7H | TAT-7H inhibited Tau aggregation *in vitro* and supressed Tau phosphorylation in iPS cell derived neurons. |
| (Abskharon et al., 2023) | HEK293 Tau biosensor cells | Nanobody inhibitors of $^{275}$VQIINK$^{280}$ and $^{306}$VQIVYK$^{311}$ capping grafts | Block seeding by Tau fibrils and oligomers in HEK293 biosensor cells expressing Tau-K18 |
| (Aggidis et al., 2024) | *In vitro* $^{275}$VQIINK$^{280}$, $^{306}$VQIVYK$^{311}$, TauΔ1-250 and Tau2N4R, seeding in HEK-239 cells, transgenic *Drosophila* expressing Tau2N4R | Retro inversed peptide aggregation inhibitor designed against $^{306}$VQIVYK$^{311}$: RI-AG03 | RI-AG03 can bind to both $^{306}$VQIVYK$^{311}$ and $^{275}$VQIINK$^{280}$, reduces aggregation in all recombinant Tau species tested, including Tau2N4R in a dose dependent manner. Reduced aggregation of Tau is in its native monomeric state, and during aggregation. But did not cause disaggregation. RI-AG03 was non-toxic to cells <40mM, reduced seeding in HEK-239 cells. RI-AG03 improved retinal degeneration and survival rates incurred by Tau2N4R. |

In addition to strategies aiming to reduce Tau's pathological GOF mechanisms, another major therapeutic strategy is to restore the physiological functions lost due to pathological Tau, such as microtubule stability. There are several microtubule-stabilising agents that have had preclinical success. Davunetide (also called NAP) is a short

neuroprotective peptide which has shown to fortify the cytoskeleton by directly promoting tubulin polymerisation(Gold et al., 2012). In *Drosophila* and rodent models of Tauopathy, NAP treatment improves motor neuron locomotion deficits, microtubule density and axonal transport (Quraishe et al., 2013), reduced the amount of sarkosyl insoluble Tau and cognition based behavioural deficits (Matsuoka et al., 2007). Placlitaxel (also called Taxol) is an alternative microtubule stabiliser which strongly recovered axonal transport deficits, and microtubule density in treated Tau-transgenic mice (Zhang et al., 2005). However, despite impressive results in preclinical models neither drug has produced significant clinical improvements on AD or PSP patients (Boxer et al., 2014).

Whilst there has been significant progress in the development of Tau-centred therapeutics, the clinical translation from bench side to bedside has been challenging, perhaps limited by the experimental models. However, as the mechanism of Tau toxicity is multifactorial it is likely that a combinatorial approach is required. Perhaps a cocktail of Tau-targeted drugs from multiple aspects of these therapies discussed could yield more promising clinical results in the future.

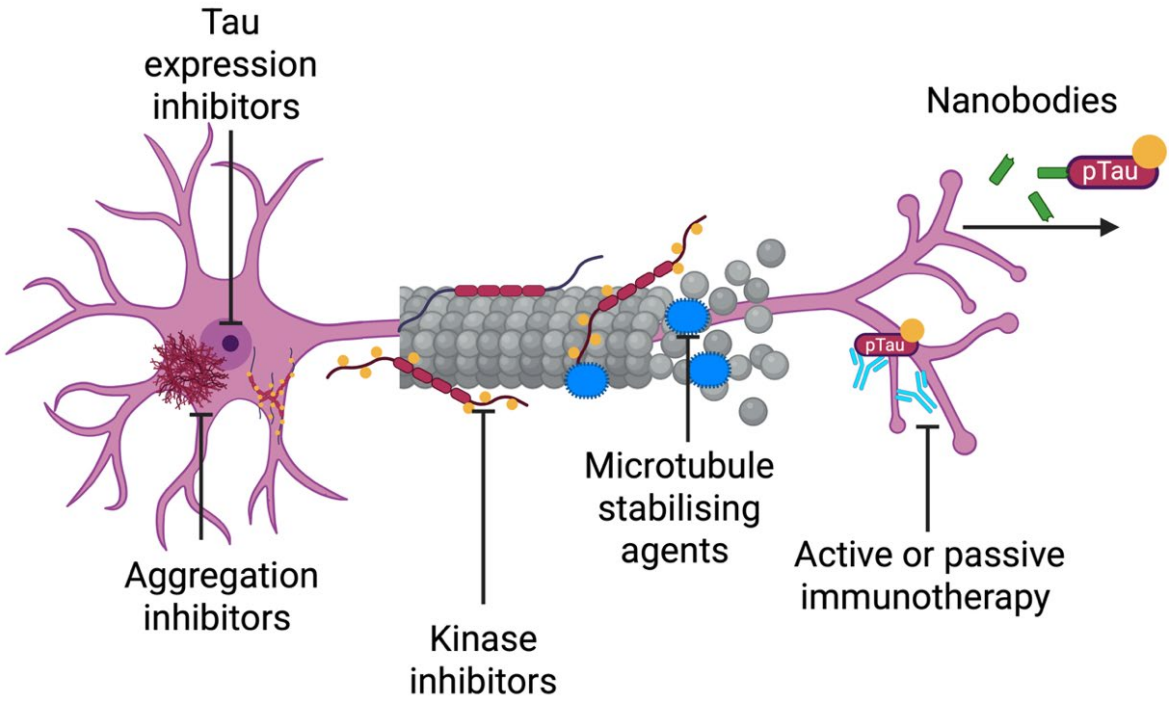


**Figure 14. Current Tau-based therapeutic strategies.**

Schematic representation of the main therapeutic interventions: reducing Tau expression, inhibiting Tau aggregation, modulating kinase activity to prevent hyperphosphorylation, stabilising microtubules, and targeting pathological Tau species through active or passive immunotherapy or nanobody-based clearance.

## 1.9 *Drosophila* as a model of Tauopathy

### 1.9.1 Advantages of *Drosophila*

*Drosophila melanogaster*, the common fruit fly, have proven to be a useful tool to model and study many aspects of neurodegenerative diseases, including AD. There are many practical and economic advantages to using fruit flies which make them superior to vertebrates within the laboratory setting. Primarily, their low maintenance, and large brood generation allows for effective low-cost, large-scale generation, and high-throughput experimental screens of progeny. Their short life cycle (between 30-90 days dependent on environmental temperature) is also a particular advantage in studying age-related diseases

like AD to track consequences of proteinopathies over an entire lifetime in a short period of time, unlike rodent models (lifespan 2-3 years) or non-primate models (25-40 years). This allows for the high throughput investigation of factors which may exacerbate or inhibit Tau pathology.

Nearly 70% of human disease genes have *Drosophila* orthologs(Fortini and Bonini, 2000). Their considerable genetic homology to humans makes *Drosophila* mutants an excellent model of human disease to investigate cellular and molecular processes underlying disease pathogenesis. For instance, *Drosophila* homologs of AD-associated genes such as *Drosophila* Tau (dTau), *Drosophila* amyloid precursor protein-Like (dAPPI) and Shaggy (Sgg; the *Drosophila* ortholog of GSK-3β) have shown remarkable phenotypic and behavioural similarities to the human homologs (Papanikolopoulou et al., 2019, Goguel et al., 2011, Blard et al., 2006). These have been important tools to investigate the structure and function of these proteins in the physiological and pathological state, giving insights as to how they might behave in humans.

Research groups have used *Drosophila* to investigate a broad spectrum of disease characteristics, from behavioural deficits to cellular and molecular degenerative changes. By overexpressing transgenes encoding key pathogenic proteins identified in these diseases, *Drosophila* models can effectively simulate and recapitulate the disease state, providing valuable insights into the pathways and mechanisms underlying neurodegeneration. As such they have been used to identify potential therapeutic targets, and offer a practical platform for drug discovery, with their use in high-throughput screening of novel therapeutics.

One of the greatest technical strengths popularising the use of flies is the ease of transgenic mutant generation with few ethical restraints. Transgenic flies can be used to model disease and recapitulate pathology in several ways, for example by expressing, inserting (or knocking out) human disease alleles or engineering the overexpression of their

*Drosophila* orthologs. The GAL4-UAS binary expression system is one of the most useful and commonly used genetic tools to drive targeted expression of a gene of interest **(Figure 15a)** (Brand and Perrimon, 1993). This well-established system has been responsible for the majority of transgenic *Drosophila* mutants modelling neurodegenerative diseases, allowing for the restricted gene expression and investigation of pathologically relevant genes within targeted tissues. These can further be temporally controlled using gene switch activators like GAL80ts which can be activated through temperature or drugs (eg. Methapristone)**(Figure 15b).** Thanks to the complete genetic mapping and commercialisation of *Drosophila* stock centres, there is wide accessibility to hundreds of transgenic *Drosophila* strains expressing the GAL4 driver in a vast range of tissues, encompassing developmental tissues, organ systems, and specific neuronal circuits(Cook et al., 2010). This has made it possible to characterise the behaviour and mechanism of pathological proteins in many different disease-relevant vulnerable tissues.

Transgenic *Drosophila* offers many practical advantages over mice as a powerful genetic tool that has the capability for larger scale studies of *MAPT* mutants. Typically, such large-scale experiments are not feasible in mice due to ethical, economical, and time restraints. Prior rodent studies have been limited to analysis of one Tauopathy strain to wildtype or control which makes it difficult to compare and cross-examine results to independent studies expressing other variants (Götz et al., 2001, Götz, 2001). Meanwhile, within one *Drosophila* study, controlled equal expression of multiple mutants can be achieved by using the same insertion cassette for Tau expression. This ensures that phenotypic and behavioural responses are attributed to the mutation only, as opposed to the expression of Tau itself. This is important because Tau assembly is concentration dependent, hence why increasing Tau expression in transgenic animals accelerates degenerative phenotypes we observe and measure (Wittmann et al., 2001, Beharry et al., 2013, von Bergen et al., 2000). Another practical advantage of using *Drosophila* is the unrestricted genetic

potential. The accessibility of powerful genetic tools have enabled the generation of designer mutants. By targeting known ways to Tau-mediated pathogenesis, the fly has contributed important insights into the pathogenic mechanisms underlying Tau mediated degeneration, such as phosphorylation and aggregation (Passarella and Goedert, 2018, Chatterjee et al., 2009, Khurana et al., 2006, Sivanantharajah et al., 2019).

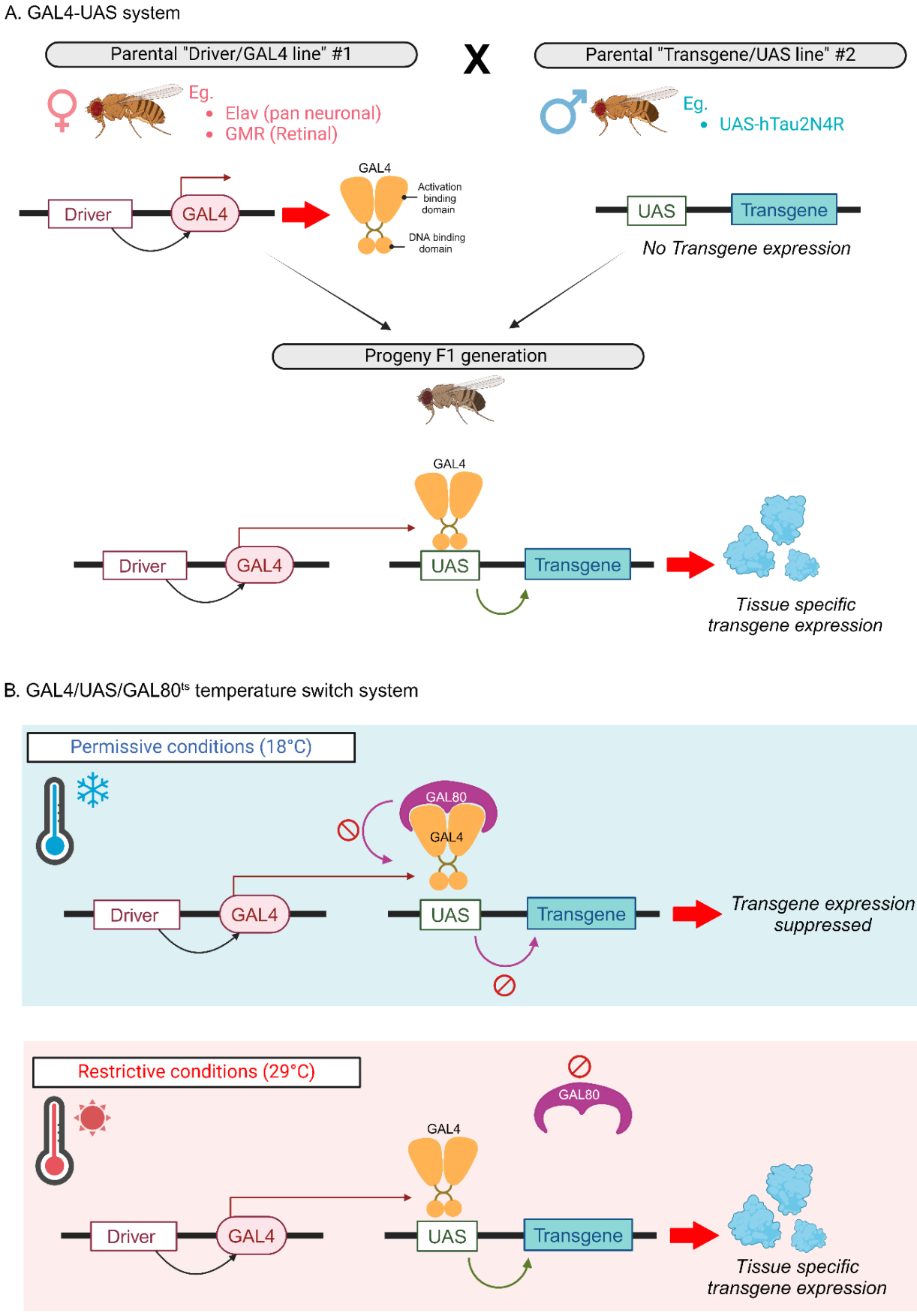


**Figure 15. GAL-UAS binary expression system.**

A)The GAL4-UAS system is a two-part system which allows for tissue specific expression of a reporter transgene. One parental line will carry the transcriptional regulator GAL4 downstream of the tissue of choice. The second parental line contains the upstream activating sequence (UAS) which is an enhancer next to a gene of interest. When the lines cross, the experimental progeny inherits the GAL4 driver with the promotor sequence of a gene of interest in the same genome, and the GAL4 will bind to the UAS elements of the promotor line, and therefore express the transgene of interest, only in the specified tissue of choice. (Brand and Perrimon, 1993). B) The GAL4-UAS/GAL80ts Temperature sensitive switch system is an enhancement of the GAL4-UAS system that allows for temperature dependent "switch" or activation. At permissive, lower temperatures (18°C), the GAL80 molecule binds and represses GAL4 activity. Whereas at restrictive, higher temperatures (29°C), repress GAL80 activity, and allow the GAL4-UAS to function (McGuire et al., 2003).

### 1.9.2 Insights of Tau pathology from *Drosophila*

*Drosophila* models of Tauopathy have provided many novel insights to Tau-mediated neurodegeneration through the transgenic expression of hTau proteins which mimic the molecular pathology and cause tissue degeneration and robust loss of neuronal function reminiscent of observations within human patients (Wittmann et al., 2001, Jackson et al., 2002, Plascencia-Villa and Perry, 2022, Crowther et al., 2006). Key findings from these fly models include characterising how Tau dysfunction is initiated by hyperphosphorylation and resulting loss of physiological function through reduced microtubule binding(Cowan et al., 2010) axonal transport (Cowan et al., 2010, Mudher et al., 2004) and synaptic dysfunction (Hoover et al., 2010). Furthermore, contributing toward our understanding of which pathogenic Tau species can misfold and aggregate (Passarella and Goedert, 2018, Katsinelos et al., 2021) and more importantly, which Tau species functionally contribute towards toxicity (Chatterjee et al., 2009, Nishimura et al., 2004) without tangle pathology formation (Wittmann et al., 2001).

These key findings are particularly relevant and highly translatable to human disease due to the fundamental similarities between *Drosophila* and mammalian cell biology. Comprised of the same molecular components, cellular machinery and neurotransmitters (Monastirioti, 1999) there are many useful homologies between fly and humans neurons,

including their structure (microtubule network and cytoskeleton, axonal transport components, synaptic transmission, neuron excitability, plasticity, signal transduction (Lamprecht and LeDoux, 2004, Ojelade et al., 2013) and mechanisms of degeneration in disease. This makes *Drosophila* a robust model for studying neurodegeneration in application of human diseases.

More holistically, flies can be used for many simple behavioural assays which reflect the toxicity incurred by these degenerative proteins. In particular, pan-neuronal expression of Tau have induced widespread neuronal degeneration which structure and functionality of tissues expressed in. There are multiple assays that can functionally assess the impact of genetic factors being expressed, and these assays are simple to conduct and loosely relevant to the clinical features of neurodegenerative diseases. For example, research has shown that flies expressing human Tau pan-neuronally exhibit a robust decline of longevity, locomotive ability which are progressive with age (Wittmann et al., 2001). More importantly there are several structures within the mushroom bodies and the lateral horn which have roles in associative olfactory learning and memory recall (Papanikolopoulou et al., 2019, Akalal et al., 2006)which when burdened with Tau expression result in behavioural deficits (Vourkou et al., 2022, Keramidis et al., 2020). It is incredibly advantageous to have complex and conserved behaviours to model and recapitulate disease pathogenesis in order to assess Tau toxicity.

There is also great sensitivity of *Drosophila* models when it comes to modelling other forms of Tauopathies, recapitulating disease severity between different familial forms of dementia. For example, flies expressing the P301L and R406W mutations, produce a more severe phenotype (reduced lifespan, locomotive activity and increased neuronal degeneration) than wildtype flies, successfully recapitulating the more aggressive and earlier onset of dementia that is observed clinically (Wittmann et al., 2001, Bardai et al., 2018).

Overall, *Drosophila* serve as an excellent robust model to better elucidate molecular basis of neuronal degeneration in the context of neurogenerative diseases. With their broad applications in the discovery of degenerative mechanisms and drug designs, their potential is only limited by the scope and creativity of the user.

### 1.9.3 *Drosophila* Tau vs human Tau

Many of the popular *Drosophila* models of Tauopathy involve transgenic overexpression of human Tau (hTau) without altering or removing the endogenous *Drosophila* Ta (dTau). There is significant sequence homology between human and *Drosophila* Tau. dTau is shorter (full length dTau is 370aa) and has less isoforms than hTau but executes the same function to bind and stabilise the microtubules (Feuillette et al., 2010). Unlike humans and some mammals, *Drosophila* and other invertebrates do not develop Tau-related disorders. This is in part to their short life cycle and lack of aggregation domains $^{275}$VQIINK$^{280}$ and $^{306}$VQIVYK$^{311}$. Nonetheless, overexpressing dTau does produce toxic effects in the fly, including disrupted axonal transport, neuronal degeneration and locomotor impairments, demonstrating that non-aggregating forms of Tau can be pathogenic (Ubhi et al., 2007).

Previous studies have demonstrated that in hTau-expressing flies most of the hTau remains cytosolic rather than microtubule-bound (Feuillette et al., 2010, Burnouf et al., 2016, Hanger et al., 2009). This would indicate that most of the toxic phenotypes observed in these overexpression models reflect Tau's toxic GOF mechanism triggered from an abundance of free-Tau. However, there is some conflicting literature suggesting phosphorylated hTau can disrupt dTau function. Previously the Mudher lab has shown that the expression of highly phosphorylated Tau0N3R in *Drosophila* larvae motor neurons reduces the dTaus microtubule-binding ability, disrupting axonal transport and synaptic functions (Cowan et

al., 2010). Moreover, they demonstrated that hTau expression did not affect the distribution of dTau which was homogenously distributed throughout the axons like in control experiments (Cowan et al., 2010). This infers that *Drosophila* Tauopathy models of hTau overexpression may compete for dTau-microtubule binding and therefore reflect Tau toxicity from GOF and LOF mechanisms.

### 1.9.4 Using the *Drosophila* olfactory circuit to study Tau-mediated toxicity and neuronal degeneration

The *Drosophila* olfactory system is a large group of highly characterised sensory tissues used to detect and relay odorant information **(Figure 16).** There are 62 olfactory receptor neurons (ORNs) which are expressed in the antennae and maxillary palps (Robertson et al., 2003). Each receptors axons project and converge into the olfactory centre, called the antennal lobe (AL) located at the anterior surface of the *Drosophila* midbrain. The AL contains around 60 glomeruli units, mostly containing one receptor type to one glomerulus, each with their own specific odour stimuli response, for example avoidant, attractive, hormonal, courtship odours (Vosshall and Stocker, 2007). Each glomeruli unit is discretely shaped and positioned throughout the AL. From the AL synapses, local interneurons connect between the glomeruli units, and projection neurons will relay information to higher order processing centres in the brain like the mushroom bodies(MB) and lateral horn(LH) which initiate sensory associated learning, memory and behavioural responses (**Figure 16)** (Barish and Volkan, 2015)**.**

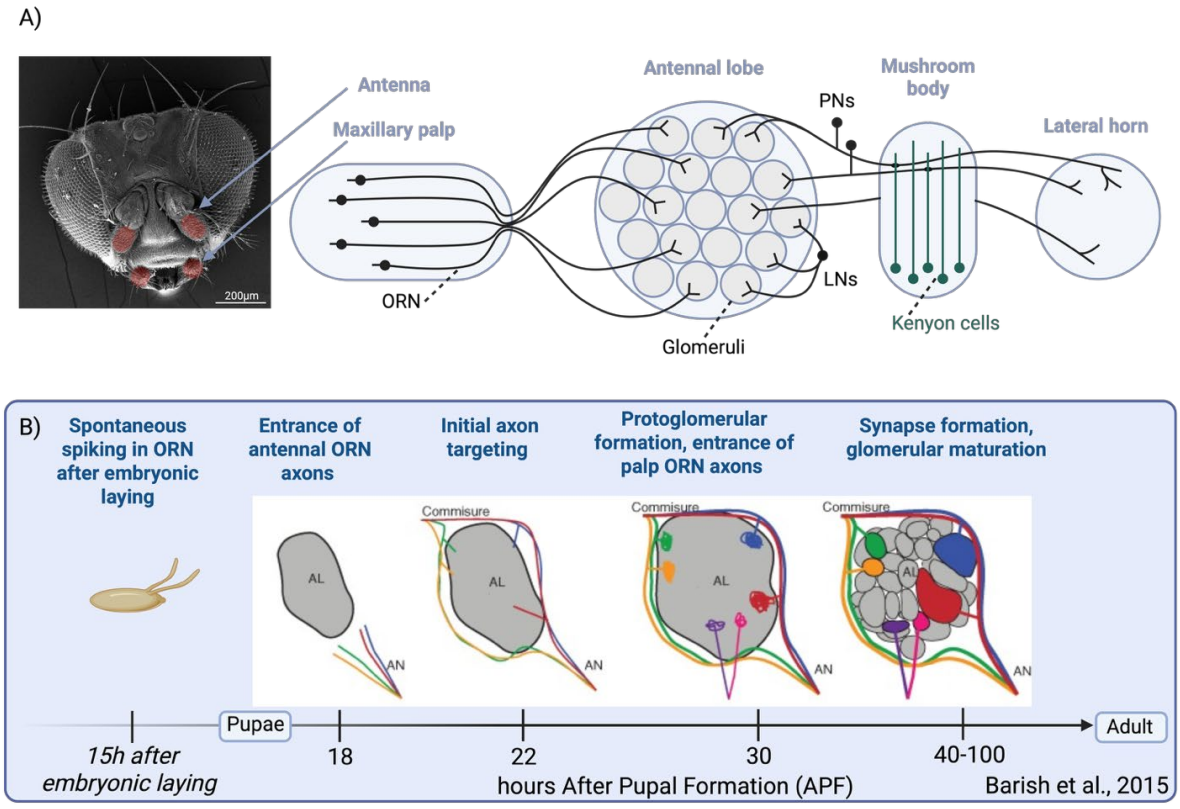


**Figure 16. Drosophila olfactory centre organisation and expression during development.**

A) SEM image of *Drosophila* head with the peripheral receptive organs antenna and maxillary palp highlighted in red (Arrows). These contain the olfactory receptor neurons (ORNs) which project through the antennal segments up into the midbrain, converging onto a single glomerulus within the antennal lobe (AL). ORNs synapse with local interneurons (LNs) and projection neurons (PNs). PNs mostly innervate one glomeruli, but can be multi-glomerular, and project their axons to the higher brain centres: the mushroom bodies (MB) and their Kenyon cells, and the lateral horn (LH). B) ORN development is as follows: 15 hours after embryonic laying there is spontaneous spiking in the ORNs (Prieto-Godino et al., 2012)18-20 hours after puparium formation(APF) the ORN axons enter the AL and start to project and target their respective glomeruli around hour 22 (Barish and Volkan, 2015). 30 hours APF the maxillary palp ORN axons enter the AL, and by hour 40 the glomeruli segregate and form distinct units (Barish and Volkan, 2015). Adapted from (Barish and Volkan, 2015).

For the purpose of my experiments investigating Tau-mediated neuronal degeneration, I harnessed the genetic and molecular tools available in the *Drosophila* olfactory circuit to visualise the toxic effect of each Tau mutant by using immunohistochemistry and confocal microscopy to label and track neurodegeneration and visualise Tau pathology. There are many advantages to using the *Drosophila* olfactory neurons to visualise Tau-mediated neurodegeneration. Practically, the AL is located on the

surface of the midbrain, which meant that after brain dissections I could mount the brains and clearly image the olfactory bulb that has an approximate depth of 150μm.

Secondly, by selecting one of the AL glomeruli units, I was able to assess degeneration and pathophysiology in great detail in a small identified neuronal subset of neurons. For this I chose the Or47b neurons, which innervate the VA1v glomeruli (Jefferis et al., 2004, Dweck et al., 2015)) positioned on the most dorsal surface of the AL. Composed of approximately 60 neurons, they are cholinergic and are responsible for pheromone detection and courtship behaviours (Hueston et al., 2016, Deanhardt et al., 2023). Despite numerical simplicity, there are striking similarities with mammalian olfactory neuron cytoarchitecture and signalling, and also have similar organisation of ORN convergence to one glomeruli (Vosshall and Stocker, 2007). Unlike mammalian ORNs which are continuously renewed throughout adulthood, flies have a defined window of ORN expression in development (**Figure 16**) which will be the finite number of ORNs present during its lifespan, making them an attractive circuit to model degeneration and the effects of Tau on aging neurons. Furthermore, these well-defined olfactory neurons offer segregation of neuronal compartments to facilitate assessment of Tau sub-cellular localisation and toxic effects in the soma, dendrites, axons and synaptic fields **(Figure 22).**

## 1.10 Overview and objectives:

The significant clinical, cellular and molecular heterogeneity between the diverse family of Tauopathies continues to challenge diagnosis and therapeutic development. The hyperphosphorylation and aggregation of Tau are two early and prominent hallmarks of disease in all Tauopathies. However, the extent to which these mechanisms contribute independently towards Tau-mediated toxicity and disease progression is not fully understood. Transgenic models of Tauopathy have been a powerful tool in gaining insights to how *MAPT* mutations influence toxicity, closely recapitulating key behavioural and cellular features of Tauopathy. However it is still unknown how these mechanisms comprehensively induce compartment specific neuronal degeneration and influence the pathological behaviour of Tau.

**The overarching aim of this thesis has been to determine how Tau phosphorylation and aggregation influence neuronal dysfunction and degeneration *in vivo*, to investigate the molecular mechanisms that underpin their toxic effects, and to evaluate the aggregation domain $^{306}$VQIVYK$^{311}$ as a therapeutic target for the treatment of Tauopathies.**

**Hypothesis:** That disease mechanisms such as phosphorylation and aggregation contribute differentially towards Tau pathology, neuronal dysfunctional and degeneration which underlie cell-specific selective vulnerability and heterogeneity observed in Tauopathies.

**Aim 1:** To determine the independent contributions of Tau hyperphosphorylation and aggregation towards Tau-mediated toxicity in *Drosophila* **(Chapter 3)**

- **Objective 1.** Design and develop a genetic model to assess phosphorylation and aggregation independently by characterising phospho-mimicking (TauE14) and aggregation-resistant (TauΔVQIVYK) mutants.

- **Objective 2.** Visualise and quantify phosphorylation- and aggregation-specific axonal and somato-dendritic degeneration of *Drosophila* olfactory and retinal neurons.
- **Objective 3:** Assess phosphorylation- and aggregation-specific Tau accumulation and mis-localisation in axonal and somato-dendritic compartments of *Drosophila* olfactory neurons.

**Aim 2**: To characterise the physiological and pathological properties of phospho-mimicking and aggregation-resistant Tau mutants to investigate the molecular mechanisms underlying toxicity **(Chapter 4).**

- **Objective 1:** Assess phosphorylation profiles of aggregation-resistant Tau.
- **Objective 2:** Assessing aggregation propensity of phospho-mimicking and aggregation-resistant Tau mutants.
- **Objective 3:** Assess the microtubule binding ability of each mutant.
- **Objective 4:** Assess pathogenic conformations formed by phospho-mimicking and aggregation-resistant Tau mutants.

**Aim 3**: To evaluate the functional consequences of degeneration caused by phospho-mimicking and aggregation-resistant Tau mutants using behavioural assays **(Chapter 5).**

- **Objective 1.** Determine functional consequences of expressing phospho-mimicking and aggregation-resistant mutants using cognitive tests.
- **Objective 2**. Determine how the phospho-mimicking and aggregation-resistant mutants affect locomotive function.
- **Objective 3**. Determine how the phospho-mimicking and aggregation-resistant mutants affect longevity of *Drosophila.*

**Aim 4**: Investigate the therapeutic potential of the $^{306}$VQIVYK$^{311}$-targeting Tau aggregation inhibitor RI-AG03 in reducing Tau-mediated neurotoxicity **(Chapter 6).**

- **Objective 1.** Determine if RI-AG03 rescues axonal degeneration and Tau accumulation.
- **Objective 2.** Assess if RI-AG03 can rescue phosphorylation-mediated neurotoxicity of TauE14 and recapitulate mutagenic deletion of hTau2N4R-E14,ΔVQIVYK *in vivo*.

**Aim 5:** To investigate the mechanisms by which frontotemporal dementia-linked *MAPT* mutations influence Tau accumulation and neuronal degeneration (Chapter 7).

- **Objective 1:** Characterise FTDP-17(*MAPT*) associated Tau mutations P301S and R406W mediated neuronal degeneration and Tau accumulation.
- **Objective 2:** Unpick the mechanisms underlying mutant specific degeneration.

# Chapter 2 Methods

## 2.1 Fly husbandry

*Drosophila melanogaster* were grown on standard cornmeal media in a controlled 12/12 hour light/dark cycle at constant humidity. Each genetic cross was set at 18°C, and selected progeny was collected and moved to 29°C to age for 3, 14 or 28 days. The UAS/GAL4 binary expression system was used for human Tau expression (Brand and Perrimon, 1993).

### 2.1.1 Transgenic fly lines.

***GAL4 driver lines.*** Olfactory driver +/+ ;Or47b-GAL4,UAS-mCD8::GFP/Cyo;+/+ for expression of Tau variants in a small bundle of olfactory sensory neurons (Odorant receptor 47b – VA1d glomeruli) was used for confocal and structured illumination microscopy. Retinal driver +/+; GAL4-ninaE.GMR/Cyo; +/+ for strong expression of Tau variants in photoreceptor cells, utilised for western blot immunoassays (total Tau, phospho-Tau, microtubule binding assays and sarkosyl insoluble assays). The pan-neuronal driver Elav-GAL4;+/+;tubulin-GAL80$^{ts}$; +/+ was used in longevity, climbing, and value-based feeding decision assays. **See Table 6.**

***Tau lines.*** All UAS-Tau lines (UAS-mCherry::hTau2N4R, UAS-mCherry::hTau2N4R$^{\Delta VQIVYK}$, UAS-mCherry::hTau2N4R$^{E14}$, UAS-mCherry::hTau2N4R$^{E14/\Delta VQIVYK}$, UAS-mCherry::hTau2N4R$^{P301S}$, UAS-mCherry::hTau2N4R$^{R406W}$, UAS-mCherry::hTau2N4R$^{R406W/S2A}$ and UAS-mCherry::hTau2N4R$^{R406W/\Delta VQIVYK}$ were created by the Allan Lab (University of British Colombia, Canada). Each human Tau transgene was attached to an mCherry fluorophore

which was chosen for imaging purposes. The mCherry tag did not affect Tau accumulation or axonal degeneration in hTau2N4R **(Supplementary Figure 52).**

Tau E14 is generated by mutating 14 AD-relevant epitopes T111, T153, T175, T181, S199, S202, T205, T212, T217, T231, S235, S396, S404 and S422 to glutamate (Hoover et al., 2010). TauS2A is generated by mutating 2 AD relevant epitopes S262 and S356 to alanine(Nishimura et al., 2004). All UAS-Tau variants were integrated into the same attp40 site on the second chromosome, ensuring the same expression of each Tau variant to allow for direct comparison of toxicity. **See Table 6.**

**Table 6. Table of *Drosophila* stocks, genotypes, and source.**

| ***Drosophila* strain** | **Full genotype** | **Source** | **ID** | **Description/use** |
|---|---|---|---|---|
| Or47b-GAL4 | ; Or47b-GAL4,UAS-mCD8::GFP/Cyo; | Professor Liqun Luo (Stanford University, CA, USA). | N/A | For expression of Tau variants in a small bundle of olfactory sensory neurons (Odorant receptor 47b – VA1d glomeruli). |
| GAL4-ninaE.GMR | ;GAL4-ninaE.GMR/Cyo;; | Balanced from Bloomington stock | FBti0002994 BL1104 | Retinal driver +/+; GAL4-ninaE.GMR/Cyo; +/+ for strong expression of Tau variants in photoreceptor cells, used in retinal imaging (SEM and digital microscopy) and used in the western blot immunoassays. |
| Elav-GAL4;;Tub GAL80ts; | Elav-GAL4;+/+;tubulin-GAL80$^{ts}$; +/+ | Skoulakis Lab, Alexander Fleming Research centre, Athens. | N/A | Temperature switch Pan-neuronal driver used in behavioural study of locomotion; climbing assay and value-based feeding decision assay. |
| Tau2N4R | +/+; UAS-mCherry::hTau2N4R/Cyo;+/+ | Allan Lab, UBC | N/A | 10x UAS<br>mCherryTag on N-terminal of Tau<br>Insertion into Attp40 site |
| Tau2N4R$^{\Delta VQIVYK}$ | +/+;UAS-mCherry::hTau2N4R$^{\Delta 306VQIVYK311}$/Cyo;+/+ | Allan Lab, UBC | N/A | 10x UAS<br>mCherryTag on N-terminal of Tau<br>Insertion into Attp40 site |
| Tau2N4R$^{E14}$ | +/+;UAS-mCherry::hTau2N4R$^{E14}$/Cyo;+/+ | Allan Lab, UBC | N/A | 10x UAS<br>mCherryTag on N-terminal of Tau<br>Insertion into Attp40 site |
| Tau2N4R$^{E14-\Delta 306VQIVYK311}$ | +/+;UAS-mCherry::hTau2N4R$^{E14-\Delta 306VQIVYK311}$/Cyo;+/+ | Allan Lab, UBC | N/A | 10x UAS<br>mCherryTag on N-terminal of Tau<br>Insertion into Attp40 site |
| Orco-Gal4 | +/+;Orco-Gal4/Cyo; UAS-mCD8::GFP/Tm6; +/+ | Allan Lab, UBC | N/A | Ordorant receptor co-receptor (Orco): Driver within all olfactory neurons within the antennal lobe within the adult brain |
| Tau2N4R$^{R406W}$ | +/+;UAS-mCherry::hTau | Allan Lab, UBC | N/A | 10x UAS<br>mCherryTag on N-terminal of Tau |

| | | | | |
|---|---|---|---|---|
| | 2N4R$^{R406W}$/Cyo;+/+ | | | Insertion into Attp40 site, FTDP-17(*MAPT*) Familial mutation |
| Tau2N4R$^{P301S}$ | +/+;UAS-mCherry::hTau 2N4R$^{P301S}$/Cyo;+/+ | Allan Lab, UBC | N/A | 10x UAS mCherryTag on N-terminal of Tau<br>Insertion into Attp40 site, FTDP-17(*MAPT*) Familial mutation |
| Tau2N4R$^{R406W/S2A}$ | +/+;UAS-mCherry::hTau 2N4R$^{R406W/S2A}$/Cyo;+/+ | Allan Lab, UBC | N/A | 10x UAS mCherryTag on N-terminal of Tau<br>Insertion into Attp40 site, FTDP-17(*MAPT*) Familial mutation |
| Tau2N4R$^{R406W/\Delta VQIVYK}$ | +/+;UAS-mCherry::hTau 2N4R$^{R406W/\Delta VQIVYK}$/Cyo;+/+ | Allan Lab, UBC | N/A | 10x UAS mCherryTag on N-terminal of Tau<br>Insertion into Attp40 site, FTDP-17(*MAPT*) Familial mutation |

## 2.2 Microscopy

### 2.2.1 Confocal and SIM imaging experimental procedure

***Tissue preparation: Drosophila brains***. This study utilised the *Or47b*-GAL4 driver. Adults were collected 0-1 days after eclosion and moved from 18°C to 29°C to be aged for either 3, 14 or 28 days. Flies were anesthetised with $CO_2$ and the males were selected for dissection. Heads were removed and fixed for 20 minutes in 4% paraformaldehyde (PFA) in phosphate-buffered-saline with 0.2% Triton-X 100 (PBST). The heads were then washed 3 times, for 20 minutes each in PBST, and then dissected under a light microscope in PBST. Brains were then blocked in 3% Normal Goat Serum in PBST (LAMPIRE Biological Laboratories) for 1 hour. Then, primary antibodies were added and incubated overnight. The following day, the primary antibodies were removed and the brains were washed 3 times, for 10 minutes each in PBST. The brains are then left to incubate with the secondary antibodies for 2 hours. Before mounting, the brains are again washed 3 times, for 10 minutes

each in PBST. Primary antibodies used: chicken-Anti-GFP (1:1000)(Abcam ab13970), α-human Tau (1:1000) (rabbit-Anti-human-Tau Dako), MC1(1:200). Secondary antibodies used: Goat-Anti-Rabbit-Alexa-555 (1:500) (Abcam Ab150078), Anti-Mouse-Alexa-488 (1:500) (Invitrogen A11039), Anti-mouse-Alexa-647 (1:300) (Abcam Ab150115).

***For confocal imaging*** the brains are then transferred to a poly-L-Lysine coated slide containing coverslip well, and mounted using Vectashield® hard-set mounting media (H-1400-10). Slides were stored in a dark box in a freezer (-20°C) and imaged within 3 days.

***For structured illumination microscopy (SIM) imaging***, after antibody incubation brains were post-fixed in 4% PFA for 10 minutes, washed and mounted on Superfrost plus adhesion glass slides. Prolong Gold$^{TM}$ is placed on top of the brains and a high-precision thin coverslip (18x18 mm 170± 5μm gently layered on top. Slides left to cure for 24 hours (at room temperature in the dark) before being imaged. *Disclaimer:* Slide preparation, genetic crosses and fly handling was completed myself, and Dr Bradley Richardson kindly performed the SIM acquisition and recording.

***Drosophila antenna.*** The same progeny was used for antennal dissection. Only one antenna was taken from each animal to avoid repeats from the same animal. One antenna was removed from each animal and fixed for 20 minutes in 4% PFA with 0.2% PBST followed by 3 PBST washes and immediate mounting onto a poly-L-Lysine coated slide using Vectashield hard-set mounting media. No antibodies were used because the adult antennal cuticle is too thick and highly auto-fluorescent, instead the endogenous mCherry and CD8::GFP fluorophores were captured during imaging.

***SEM, Drosophila eye.*** 14-day-old flies were euthanised, fixed in 4% formaldehyde 3% glutaraldehyde in 0.1M PIPES buffer. Samples were rinsed in 0.1M PIPES buffer twice, immersed in 2% osmium tetroxide for 1 hour, then dehydrated for 20-minutes at each ethanol concentration: 30%, 50%, 70%, 80%, 90%, 100%, 100%. Samples were critical point dried,

mounted on aluminium stubs before sputter coating with gold/palladium in a Polaron E5100 sputter coater. Samples were examined using a Quanta 250 FEG-SEM at 1600X magnification.

### 2.2.2 Image acquisition

***Confocal Image acquisition.*** Images of the entire *Drosophila* brain and antenna were taken with a Leica SP8 line scanning confocal microscope. Images were taken with 12-bit depth stacks at 63x magnification in glycerol immersion oil, taken at 1024x1024 pixel resolution. 488nm laser was used to detect degeneration of the Or47b neurons and 555nm laser to detect Tau signal. Two sequential excitation steps are used to avoid bleed through between channels. Representative images shown are presented as full Z-stacks, unless otherwise stated. As only structural parameters were evaluated, confocal acquisition settings were adjusted if necessary to capture all structural information **(Supplementary Figure 51).**

***SIM image acquisition.*** Commissure tract of the Or47b axons within the brain were imaged via SIM (DeltaVision OMX Flex super-resolution microscope) with a 63x Immersion oil objective. An immersion oil with a refractive index of 1.510 (Cargille Laboratories USA) was used whilst objective collar settings were adjusted to 013 to provide high-resolution images.

## 2.3 RI-AG03 drug treatment

Crosses were set on standard diet at 18ºC. Male progeny were selected and moved to 29ºC to age on 40mM RI-AG03 [Ac-rrrrrrrG-pkyk(ac)iqv-Gr-NH2] or 40mM Scrambled RI-AG03 [Ac-RG-QPKIK(Ac)YV-GRRRRRRRR] peptide enriched diet. These concentrations were selected after preliminary studies (Aggidis et al., 2024). Due to concerns of drug denaturation and low concentration uptake when mixed directly with food, the flies

were fed on a micronutrient solution 300µl (dd$H_2O$, 5% sucrose, 5/3% peptone, 40mM drug) per day on filter paper, flipping every 24 hours. Flies were anesthetised on $CO_2$ every day for transfer into new micronutrient solution.

## 2.4 Behavioural assays

### 2.4.1 Survival assay

Ten cohorts of 10 male or female flies were collected from each genotype. Crosses were set at 18℃ and switched to 29℃ after eclosion. Flies were flipped into fresh food vials twice a week, and the number of surviving flies was counted 3 times a week. They were housed in rooms with controlled lighting, temperature and humidity. A Kaplan-Meier survival curve was plotted on GraphPad Prism and a Log-rank(mantel cox) test was performed and manual Bonferroni correction was carried out to compensate for multiple comparisons.

### 2.4.2 Climbing assay

Three vials of 10 male flies were collected for each genotype and anesthetised 24 hours prior to the climbing assay. The flies were flipped into 50ml measuring cylinders and left to acclimatise for 30 minutes at 25°C. Flies were tapped down to the bottom of the cylinder with three sharp taps upon a mouse pad and recording the flies climbing up the sides of the measuring cylinder. The distance climbed by the flies was recorded at 10 seconds. They were recorded climbing up the cylinder for 1 minute, followed by a 30 second rest. This was repeated two more times, totalling three trials. The assay was done each week at the same time of day. Climbing ability was quantified by the mean distanced climbed up the cylinder at 10 seconds over the 3 repeats. 2-way ANOVA was used for Statistical Analysis via GraphPad Prism Software.

### 2.4.3 Odorant assays

Three different odorant assays were developed odour assay **1)** was an Attractive choice assay between 2 cups, agar (control) and food. Cups a one-way entry chamber were set up in an enclosure and left for 24 hours to make a choice. Odour assay **2)** was an Attractive choice assay between food (yeast) and no food using a one-way entry Eppendorf in a petri dish. Setup was a reduced enclosure size, and in a dark box for 24hours to control flying and visual variables. Odour assay **3)** Aversive choice assay between water (control) or 1% benzaldehyde were tracked for 1 minute, assessed using the automated behavioural system Zantiks **(Figure 17).**

#### 2.4.3.1 Odour assay 1) Attractive, Two cups choice

Twenty 14-day-old male progeny (18ºC>29ºC) were placed into a netted enclosure containing two cups, one containing a thin layer of normal diet and the other 1% Agar. These cups had entry points to the cups using cut 1ml pipette tips. The arenas were left in 29ºC for 24hours, and then number of flies trapped in each cup was measured. Performance index was calculated = number of flies in food- number of flies in agar/total number of flies. A one-way ANOVA with Tukeys multiple comparison was performed for statistical analysis using Graphpad prism.

#### 2.4.3.2 Odour assay 2) Attractive, Petri dish arena

To reduce variables such as locomotion, and visual perception of animals being able to fly or find the food cups using other senses, the second iteration was improved by using a single-choice assay with a yeast-trap in a dark box. Ten 14-day-old male progeny (18ºC>29ºC) were anesthetised and placed into a closed 150mmx15mm petri dish arena to prevent flying and reducing choice field. Inside the petri dish contained a 1.5ml Eppendorf

with enough yeast paste to fill the lid cap. The Eppendorf tip was cut, as was a p200 pipette tip to make a one-way entry to the yeast paste. A sheet of blotting paper was dampened with 1ml dd$H_2O$. The petri was then placed in a dark box for 24 hours and flies were counted. Performance index was calculated = number of flies in Eppendorf- number of flies outside/total number of flies. A one-way ANOVA with Tukey's multiple comparison was performed for statistical analysis using GraphPad prism.

#### 2.4.3.3 Odour assay 3) Aversive, Zantiks

I tried using a more sensitive automated behaviour system "Zantiks", paired with an aversive odour (benzaldehyde) to increase the behavioural response and improve detection of olfactory impairments in odour assay 3. Flies were anesthetised on $CO_2$ and loaded into single circular chambers within a 6-well Zantiks platform chamber. One hemisphere contained a low dose of 1% benzaldehyde diluted in dd$H_2O$ (aversive odour), and the other hemisphere contained dd$H_2O$ only (no odour). The chamber plate was then loaded into the imaging software and immediately tracked for 1 minute. Quantitative analysis was automatic, measuring the time spent in each zone (seconds), and the cumulative distance walked in each zone (mm). A Two-way ANOVA with Tukey's multiple comparison was performed for statistical analysis using GraphPad prism. Manual analysis comparing heatmaps generated from Zantiks was also performed to qualitatively assess the area the fly spent most its time in. Boundary lines were split between control and benzaldehyde and flies were scored a binary pass/fail if they spent considerable time on the control or aversive odour.

**1. Two Choice Cups Odorant Assay**

(Attractive)

n=20 flies

24hr assay

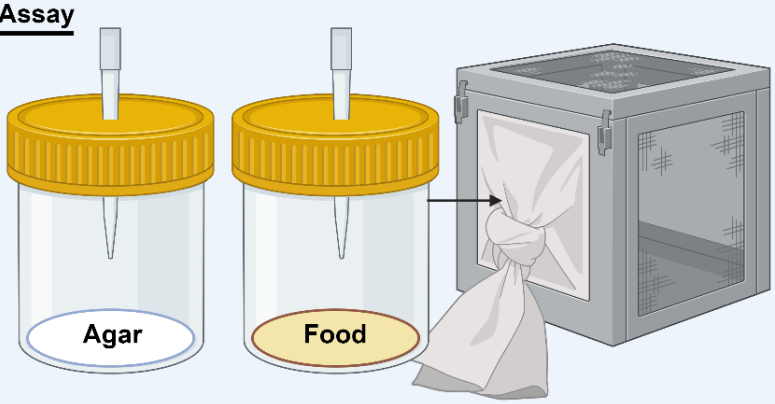


**2. Petri Dish Odorant Assay**

(Attractive)

n=10 flies

24hr assay

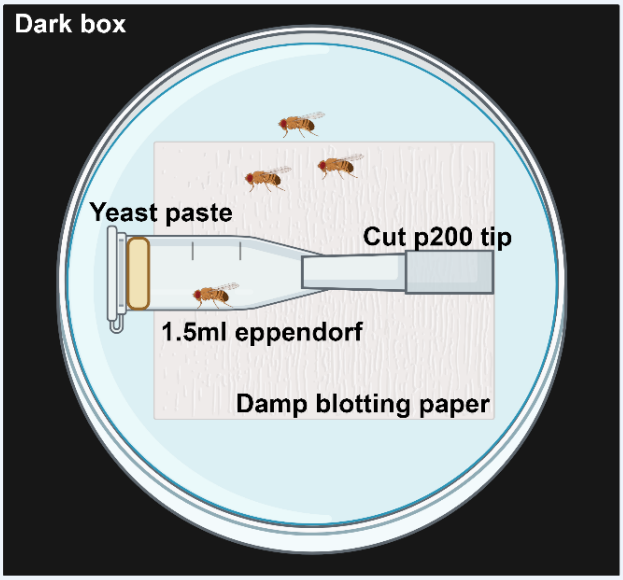


**3. Zantiks Odorant Assay**

(Aversive)

n=12 flies

1min assay

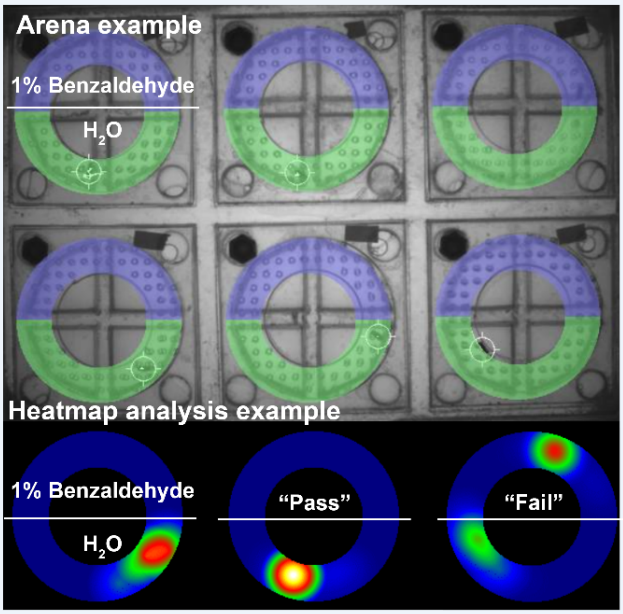


"Pass" = The animal spends a significant time away from aversive odour

"Fail" = The animal spends a significant time in the aversive odour

**Figure 17. Method development for odorant assay.**

Three methods for analysing and quantifying odour perception were trialled. Odour assay **1)** Choice assay between 2 cups, agar (control) and food. Cups a one-way entry chamber were set up in an enclosure and left for 24 hours to make a choice. Odour assay **2)** to reduce enclosure size and remove flying and seeing variables, flies were set up in a dark box within a petri dish with a one-way entry Eppendorf with yeast paste for 24 hours. Odour assay **3)** to improve quantification and to develop a stronger behavioural response the automated behavioural system Zantiks was used assess aversive odour responses. Arenas filled with water (control) or 1% benzaldehyde were tracked for 1 min an assessed the time and distance walked in each arena during the trial. Heatmaps were generated to represent where the majority of the time was spent.

### 2.4.4 Value based feeding decision assay

Flies were anesthetised with $CO_2$ and placed into a vial containing 300 µL distilled water on filter paper and left at 25°C for 12 hours. At 6pm, the flies were anesthetised again and transferred to a 12-well plate (one per well) containing one 5 µL drop of 5% sucrose (Sigma Aldrich S0389) on one hemisphere and a 5 µL drop of 5% arabinose (Sigma Aldrich A3131) on the other. Zantiks was used to record feeding behaviour for 2 hours, producing a time-lapsed video. Feeding behaviour was assessed, under blinded conditions, by manually counting the number of feeds each fly took from either droplet. The performance index was calculated as = (the number of feeds from sucrose-arabinose)/(total feeds), and a ordinary one-way ANOVA with multiple comparisons was performed for statistical analysis.

## 2.5 SDS-PAGE Western blotting procedure

### 2.5.1 Tissue preparation:

These studies utilised the GMR.ninaE-Gal4 driver. Flies were collected at 18°C and moved to 29°C to age for 2 days for total Tau expression and 14 days for measuring total Tau and p-Tau levels. Flies were then snap frozen in liquid nitrogen and decapitated, in preparation for homogenisation. The heads and brains were then homogenised in an Eppendorf using a pestle for 3 minutes in ice-cold fly homogenising buffer (FHB) containing 10mM Tris, 150mM NaCl, 5mM EDTA, 50mM NaF, 1mM $Na_3VOF_3$, 5mM NaPPi, 4mM

Urea, 5mM DDT, Glycerol, Protease inhibitor (1:100) and Phosphatase inhibitor (1:100). 3ul of FHB was used per head. Lysates were then centrifuged at 10,000 x *g* for 5 mins at room temperature. Once centrifuged, the supernatant was collected and boiled with 2X SDS-PAGE sample buffer in a 1:1 ratio at 95°C for 5 minutes in a sterile Eppendorf.

### 2.5.2 Western blotting

Proteins were resolved using vertical electrophoresis on 1.5mm 10% SDS-PAGE acrylamide hand-cast gels at 120V for 90 minutes. ***For total Tau expression:*** 15 male flies were collected for each set of repeats for each sample group. Each well used contained 25µL of the fly homogenate sample buffer mix. Page Ruler Protein Plus ladder (Thermofisher Scientific) was added to each gel. After electrophoresis, the gel containing resolved proteins were electro-transferred onto a nitrocellulose membrane using the electroporator at 60V for 90 minutes, with an icebox to maintain ~4°C. Following electro-transfer, the membranes were immediately placed in blocking buffer containing 5% bovine serum albumin (BSA), 0.1% tween using 1X PBS on a shaker for 60 minutes. Following blocking, the membranes were then incubated with the primary antibodies in a cold room shaker maintaining 4°C overnight. Antibodies listed in table 1 were made up in the blocking buffer at the given concentrations. Actin was the loading control used in all experiments. The membranes were then washed 3 times with 1X PBS 0.5% tween for 5 minutes on a shaker. Lastly, the membrane was incubated in Anti-Rabbit-800 (Licor, #D00804) and Anti-Mouse-680 (Life technologies A21057) (1:20,000), and washed 3 times with 1X PBS 0.5% tween, for 5 minutes. The membranes were then visualised using LiCOR imager, and analysed using ImageJ software. Western blot bands were quantified using ImageJ software. Tau bands were measured at ~100kDa and Actin bands were measured ~40kDa.

**Table 7. Table of antibodies used in immunolabeling for microscopy, and western blot immunodetection.**

Further antibody classification as either rabbit/polyclonal (Rb) or mouse/monoclonal (Ms). Phospho-epitopes detected at serine (Ser) or threonine (Thr) residues.

| Antibody | p-Tau Epitope detected | Vendor and catalogue number | Concentration | Rb/Ms/Chk target |
|---|---|---|---|---|
| Anti-human Tau | Total Tau | Agilent (Dako) A0024 | 1:15000 Western blots<br>1:1000 microscopy | Rb |
| AT180 | pThr231 | Thermo Fisher Scientific MN1040 | 1:250 | Ms |
| AT100 | pThr212<br>pSer214 | Autogen Bioclear UK | 1:250 | Ms |
| AT8 | pSer202<br>pThr205 | Thermo Fisher Scientific MN1020 | 1:800 | Ms |
| AT270 | pThr181 | Thermo Fisher Scientific | 1:800 | Ms |
| pS262 | pSer262 | Thermo Fisher Scientific 44-750G | 1:500 | Rb |
| PHF-1 | pSer396<br>pSer404 | Gifted by Peter Davies (ALZ Forum) | 1:500 | Ms |
| mActin | N/A | Sigma- Aldrich | 1:3000 | Ms |
| rActin | N/A | Cell signalling Technology | 1:3000 | Rb |
| Anti-rabbit 800 | N/A | LiCor | 1:20 000 | Rb |
| Anti-mouse680 | N/A | LifeTechnology | 1:20 000 | Ms |
| anti-chicken Alexa 488 | N/A | Thermo Fisher Scientific | 1:500 | Chk |

| | | | | |
|---|---|---|---|---|
| Anti-rabbit Alexa 555 | N/A | Thermo Fisher Scientific | 1:500 | Rb |
| α-GFP | N/A | Thermo Fisher Scientific | 1:1000 | Chk |

### 2.5.3 Solubility assays

#### 2.5.3.1 SDS solubility assay methods to enrich for NFTs and GTOs.

Briefly, 100 flies (50:50 male:female) reared at 18°C and aged at 29°C for 14 days were collected and snap frozen. Heads were taken and homogenised in 400µl buffer (50mM Tris-HCl, 15mM NaCl, 1M Sucrose, 5mM EDTA;pH 7.4/PI). Samples were then centrifuged for 2 mins at 1000*g*, and debris pellet was discarded. A small amount of the supernatant was saved as the "total Tau, input". The supernatant was centrifuged at 100,000*g* for 30 mins at 4°C. The resulting supernatant (NS1) represents the aqueous soluble Tau fraction, including granular Tau oligomers (GTOs). The pellet was then resuspended and washed in buffer (50mM Tris-HCl, 175mM NaCl, 5% SDS; pH7.4/PI) and centrifuged at 100,000*g* for 30 mins at 25°C. The resulting supernatant was discarded, and the pellet wad resuspended in buffer (50mM Tris-HCl, 175mM NaCl, 8% SDS, 4M Urea; pH 7.4/PI) and then agitated for 12 hours overnight at room temperature. The resulting mixture (NS2) represents SDS insoluble NFT enriched fraction. From NS1, the supernatant was centrifuged at 186,000*g* for 2 hours at 4°C. To further separate the soluble Tau species, the resulting supernatant (S1) was saved and represents the aqueous soluble Tau fraction (monomeric Tau). The pellet was resuspended in buffer (50mM Tris-HCl, 175mM NaCl, 5% SDS; pH7.4/PI) and centrifuged at 186,000g for 2 hours at 25°C. The resulting supernatant (S2) was saved and represents the aqueous insoluble/SDS soluble fraction. The pellet was resuspended and washed in buffer (50mM Tris-HCl, 175mM NaCl, 5% SDS; pH7.4/PI) and centrifuged at 186,000g for 2 hours at 25°C, and the resulting supernatant was discarded. The pellet was resuspended in buffer (50mM Tris-HCl, 175mM NaCl, 8% SDS, 4M Urea;

pH 7.4/PI) and agitated for 12 hours overnight at room temperature. The resulting homogenate is termed S3, representing the SDS insoluble granular Tau oligomer fraction. All samples were diluted in 2 x Laemmli buffer and boiled for 5 mins at 95°C and run on a SDS-polyacrylamide gel. S1 and S2 were loaded equally, and S3 was loaded with double the volume. Each fraction was quantified as a proportion of the sum total of all three fractions. Eg. S1/(S1+S2+S3). Double the amount of NS2 was loaded compared to NS1. The NS2 fraction was then quantified as a proportion of the sum total of the two fractions. Eg. NS2/(NS1+NS2). For each solubility assay the Tau band was quantified in Image Studio Lite. Statistical analysis of each fraction was performed in GraphPad Prism using an ordinary One-way ANOVA with multiple comparisons.

#### 2.5.3.2 Sarkosyl solubility assay methods to enrich for Tau fibrils

Adapted from Colodner et al., 2010 and Goedert et al., 1992. Briefly, 164 heads (50:50 male:female) reared at 25°C and aged at 29°C for 14 days were collected and snap frozen. Heads were taken and homogenised in 200µl of buffer (15mM NaCl 25mM Tris-HCl at pH 7.4, 1mM EGTA, and 1mM EDTA) containing protease cocktail inhibitor. Samples were then centrifuged for 2 mins at 1000*g*, and debris pellet was discarded. The supernatant homogenate was then spun for 1 hour at 100,000g at 25°C, and the resulting supernatant was saved as soluble fraction (SN1). The pellet was resuspended in a salt/sucrose buffer to wash (10% sucrose, 0.8M NaCl, 10mM Tris-HCl at pH 7.4, and 1mM EGTA) containing protease cocktail inhibitor, and centrifuged for 30 mins at 15,000g at 25°C. Sarkosyl was added to the supernatant (to make 1% Sarkosyl) and incubated at 37°C for 1 hour and then centrifuged for 2 hours at 100,000g. The Sarkosyl soluble fraction was saved (SN3), and the pellet was resuspended in 15µl of homogenisation buffer and saved as Sarkosyl insoluble fraction (SN2). All samples were diluted in 2 x Laemmli buffer and boiled for 5 mins at 95°C and run on a SDS-polyacrylamide gel. Equivalent volumes of samples were loaded. For each solubility assay the Tau band was quantified in Image Studio Lite. SN1 Tau band was

normalised to the proportion of protein present in SN2 eg.(SN1*(200/7.5)) and (SN2*2) **(Supplementary Figure 6)**. Statistical analysis of each fraction was performed in GraphPad Prism using an ordinary One-way ANOVA with multiple comparisons.

### 2.5.4 Microtubule binding assay

Briefly, 10 male heads from flies reared at 25°C and aged at 29°C for 14 days were collected and snap frozen. For each condition, heads were homogenised in 50µl microtubule-binding assay buffer containing protease, kinase and phosphatase inhibitors (100 mM MES pH 6.8, 500 µM Mg SO4, 1 mM EGTA, 4 mM DTT, 2 mM dGTP, 20 µM taxol, 0.1% triton-X 100, 30 mM NaF, 20 mM sodium pyrophosphate, 40 mM 2-glycerophosphate, 3.5 mM sodium orthovanadate, 10 µM staurosporine and protease inhibitor cocktail). Samples were then centrifuged for 2 mins at 1000*g*, and debris pellet was discarded. Homogenates were centrifuged at 12,000 *g* for 1 h at 4°C; the pellet representing the fraction enriched for microtubule-bound proteins was resuspended in 35µl of homogenisation buffer. All samples were diluted in 2 x Laemmli buffer and boiled for 5 mins at 95°C and run on a SDS-polyacrylamide gel.

## 2.6 Image analysis

### 2.6.1 3D Image analysis software IMARIS

Quantitative analysis of axonal swelling density, Tau accumulate density, volume of dendritic Tau per cell and total volume of GFP expressing neurons were performed using the IMARIS **(Figure 18)** 3D image analysis software. Quantification of cell body density and cell body widths was performed in ImageJ using the cell counter tool and measuring tool respectively. Only one antenna was imaged from one fly. Both hemispheres of the brain were

analysed, however in some instances where only one hemisphere was available, quantification was doubled.

Quantification was always carried out using defined parameters. To quantify the number of axonal swellings, the IMARIS "spotting" tool was used to discretely measure the number of axonal swelling surfaces of ≥1.2 μm with a surface detail of 0.36 μm. Axonal swelling density was then calculated using the total volume of GFP expressing neurons, which was measured using the "surfacing" tool detecting structures ≥0.5 μm and a surface detail of 0.2 μm. The number of Tau accumulates in the brain were defined using the "spotting" tool for accumulates that had a diameter between 1.5-2.5 μm, with a surface detail of 0.36 μm. The volume of dendritic Tau accumulates was measured using the "surfacing" tool detecting accumulates ≥1.0 μm defined by surface detail of 0.36 μm. Thresholding was achieved with local contrast background subtraction with the diameter of the largest sphere which fits into the object. Thresholding was manually adjusted for each animal to capture true structures. Analysis of each cohort was completed under blinded conditions. Statistical analysis was performed using a Two-way ANOVA and a multiple comparisons test.

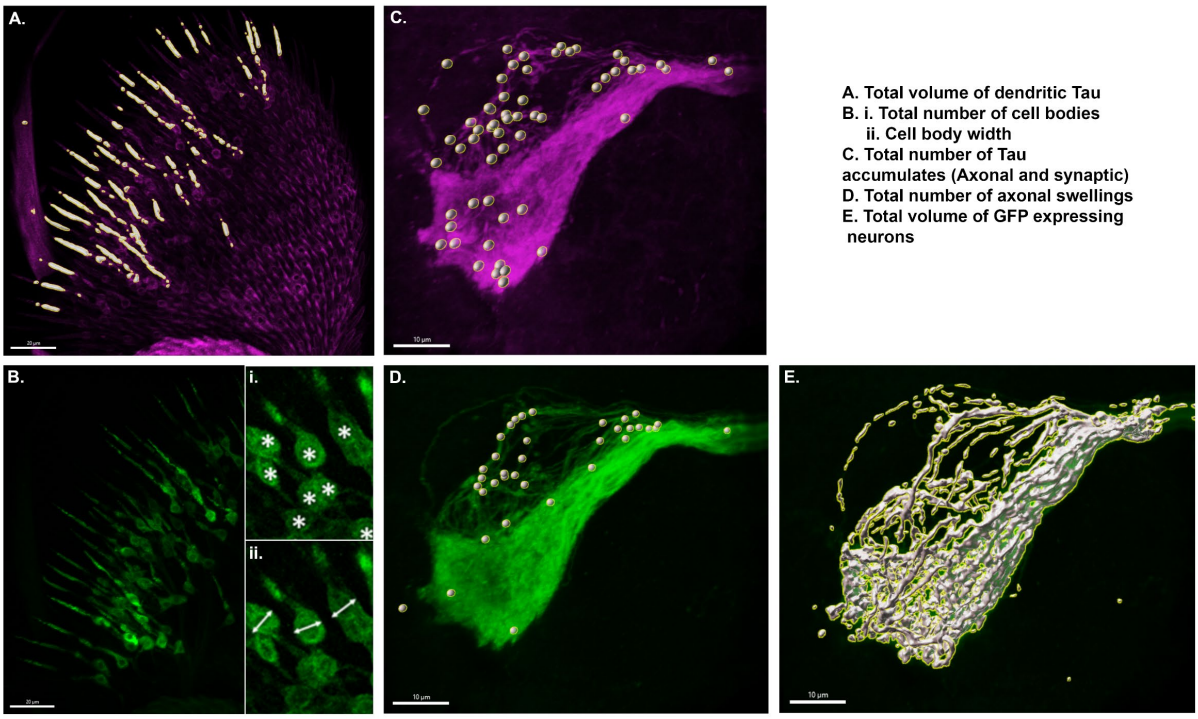


**Figure 18. Using IMARIS software for quantification of Tau accumulation and neuronal degeneration using "spots" and "surfaces" masking tools.**

### 2.6.2 Rough eye phenotype

Quantitative analysis of retinal degeneration was achieved using digital microscope images (at 600x magnification) with established ImageJ plugin tool Flynotyper using light microscope settings (Iyer et al., 2016).

### 2.6.3 Image J fluorescence for MC1

Two methods for quantifying MC1 immunoreactivity was implemented. Both used the same z-stacked confocal images of the antennal lobe **(Figure 19).** Because fluorescence intensity was the parameter of interest, confocal acquisition settings were identical across all samples to allow direct comparison of fluorescence signal levels between genotypes. **Method 1**) Fluorescence was quantified in Image J using manual segmentation of GFP signal using a freehand drawn ROI to separate GFP from background. The ROI was then mapped on to each other channel, and the mean grey value of each slice, corrected to the

average of three background ROIs. **Method 2)** was performed by Dr. Miguel Ramirez-Moreno using MATLAB-based automated segmentation of GFP signal to distinguish neuron-specific (GFP-positive) from background (GFP-negative) pixels. Fluorescence values therefore represent average MC1 signal within GFP-positive pixels minus background signal from GFP-negative pixels.

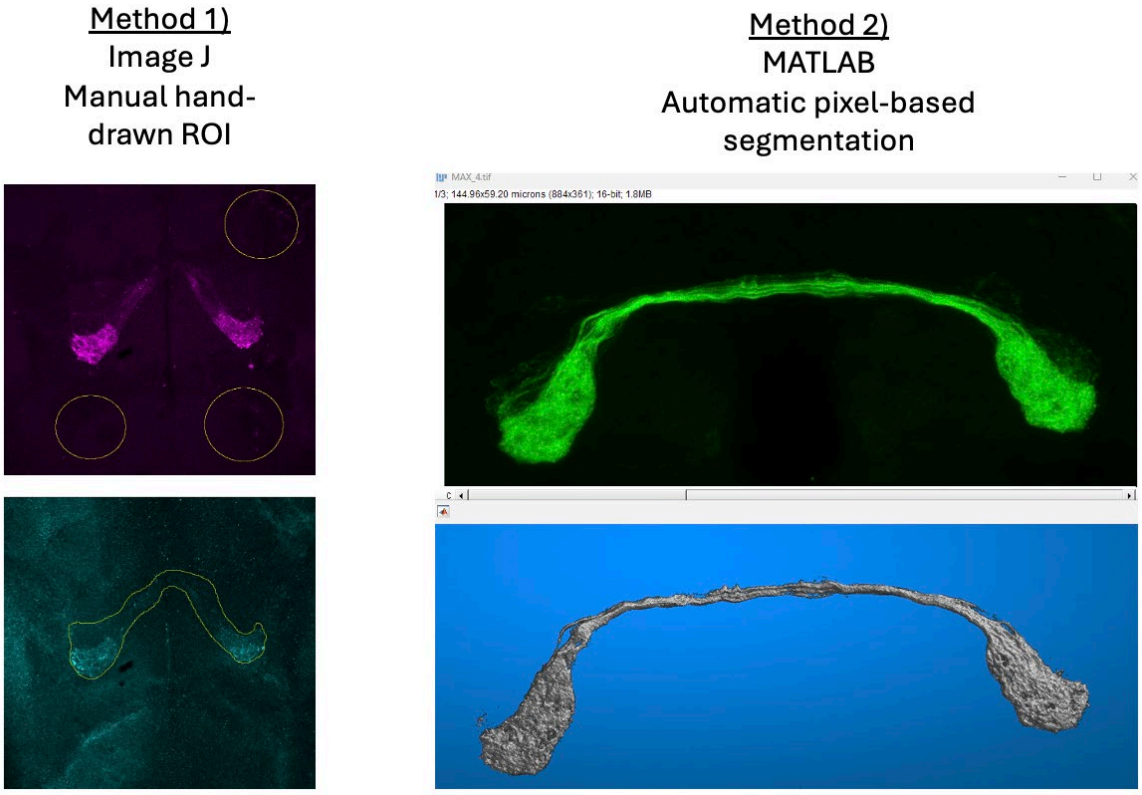


**Figure 19. Quantification of MC1 fluorescence.**

Two methods, manual and automatic as described in the main text.

## 2.7 Statistical analysis

One-way and Two-way ANOVA were calculated using GraphPad prism for most of the data collected in this thesis. The only exception was for survival, in which a Kaplan-Meier survival curve and a Log-rank(mantel cox) test was performed. Statistical analysis are stated in each methods section and under each figure. Results are shown as graphs with standard deviation (SD) unless otherwise stated. Asterisks show the p-value on all graphs where * $p<0.05$, ** $p<0.01$, ***$p<0.001$ and ****$p\leq0.0001$.

# Chapter 3 Aggregation promoting sequences rather than phosphorylation state is essential for Tau-mediated neurotoxicity.

**Disclaimer:** This results chapter contains a significant proportion of work published as a preprint on Bioarchive (**doi:** https://doi.org/10.1101/2024.12.22.629946). Co Authors: Dr Bradley Richardson, Dr Eva Ruiz Ortega, Dr Yongrui Zhang, Dr Ben Batchelor, Dr Aarya Vaikakkara Chithran, Dr Jie Liu, Dr Tianshun Lian, Dr Miguel Ramírez Moreno, Dr Benjamin Boehme, Dr Leila Abtahi, Dr George Devitt, Dr Lovesha Sivanantharajah, Dr Efthimios M. C. Skoulakis, Dr Douglas W. Allan, Dr Amritpal Mudher.

## 3.1 Introduction

The presence of highly phosphorylated, insoluble inclusions of the microtubule associated protein Tau within neurons and/or glia of the CNS is a common pathological hallmark of AD and other Tauopathies (Crowther and Goedert, 2000, Spillantini et al., 1998, Goedert et al., 2017). Tau hyperphosphorylation and aggregation are the two most prominent pathogenic hallmarks that influence Tau-mediated toxicity and have therefore become the primary targets for modern Tau-based diagnostic biomarkers and therapeutics (Janelidze et al., 2022, Hirota et al., 2022). However, the extent of their interdependence or relative contributions to the progression of Tau-mediated toxicity, neuronal degeneration and disease progression remains unclear.

### 3.1.1 Pathological consequences of abnormal Tau phosphorylation

Physiologically, Tau phosphorylation is implicated in the regulation of Tau-microtubule binding, promoting microtubule assembly, stabilisation and spacing of the microtubule network within neurons (Drechsel et al., 1992, Rosenberg et al., 2008). However, a hallmark of the pathogenic process is Tau becoming increasingly hyperphosphorylated, resulting in less efficient binding to microtubules and the induction of toxic consequences at the molecular, subcellular and cellular level (Köpke et al., 1993). *In*

*vitro* studies have demonstrated that expressing phospho-mimicking Tau in neuronal cells has a profound effect on neuronal structure and function, compromising cytoskeletal integrity (Cash et al., 2003, Alonso et al., 1994), suppressing neuronal excitability (Hatch et al., 2017) and inducing significant changes to the normal subcellular localisation and distribution of Tau (Hatch et al., 2017, Rodríguez-Martín et al., 2013, Hoover et al., 2010). Similar deficits are reported *in vivo* in *Drosophila* models of Tauopathy where driving hyperphosphorylation, by co-expression of the Tau kinase GSK-3β, or emulating hyperphosphorylation by expressing the phospho-mimicking TauE14 transgene disrupted axonal transport (Mudher et al., 2004), reduced microtubule binding (Cowan et al., 2010) and induced significant neuronal and synaptic degeneration (Cash et al., 2003, Mudher et al., 2004, Chee et al., 2005, Chatterjee et al., 2009, Talmat-Amar et al., 2011, Stubbs et al., 2023).

In the TauE14 transgene, 14 key disease-associated serines and threonines have been substituted with glutamate, to mimic the charge of phosphorylation. These mutations have a profoundly toxic impact on the pathological behaviour of Tau and consequently impair neuronal function in multiple ways, disrupting axonal transport reducing microtubule binding and inducing significant neuronal degeneration (Dias-Santagata et al., 2007), (Steinhilb et al., 2007b, Beharry et al., 2013, Katsinelos et al., 2021). Moreover, expression of TauE14 resulted in greater accumulation of Tau in sarkosyl insoluble cellular fractions and the formation of *bona fide* Tau aggregates within fly brain (Katsinelos et al., 2021). Furthermore, in FTDP-17(*MAPT*) mouse models, transgenic Tau variants can misfold and form pre-tangle-like fibrils, which can be significantly reduced with GSK-3β inhibitor treatment (Lucas et al., 2001, Hernandez et al., 2013, Lauretti and Praticò, 2020, Yokoyama et al., 2022, Noble et al., 2005, Pérez et al., 2003, Amaral et al., 2021).

While the neurotoxic consequences of phosphorylation are extensively described in the literature, the mechanisms by which it contributes towards misfolding and aggregation in different disease contexts is less clear.

### 3.1.2 Aggregated Tau species drive neurodegeneration

Several species of aggregated Tau have been identified in both human brain and animal Tauopathy models. However, the smaller hyperphosphorylated oligomeric aggregates are thought to mediate toxicity (Flach et al., 2012, Tian et al., 2013). The hypothesis that aggregation of these smaller Tau oligomers mediates Tau toxicity is well-supported in cell culture models, presenting with impaired synaptic function (Hoover et al., 2010), cellular damage (Esteras and Abramov, 2020), disrupted cellular trafficking including axonal transport (Yu et al., 2019), and induction of inflammatory responses (Meng et al., 2022). In addition, transgenic animals over-expressing aggregation-prone Tau mutants and isoforms incur significant neuronal degeneration paired with cognitive and locomotor deficits (Cowan et al., 2010, Wittmann et al., 2001, Santacruz et al., 2005, Andorfer et al., 2005). Such aggregation-induced toxicity has been attributed to two hexapeptide motifs on the Tau protein, denoted PHF6* ($^{275}$VQIINK$^{280}$) and PHF6 ($^{306}$VQIVYK$^{311}$) (von Bergen et al., 2001). When these hexapeptides are deleted, or blocked by site-specific peptide-based drugs, cognitive deficits and reduced lifespan are largely ameliorated in transgenic animals (Passarella and Goedert, 2018, Zhang et al., 2020b, Aggidis et al., 2024).

### 3.1.3 The relationship between phosphorylation and aggregation

Several lines of evidence implicate Tau phosphorylation in promoting aggregation, but the precise molecular mechanism underlying this interplay is not clear. Nonetheless, phospho-epitopes of Tau influence its aggregation, either directly or by promoting phosphorylation at additional sites (Chatterjee et al., 2009, Stefanoska et al., 2022, Alonso et al., 1997, Alonso Adel et al., 2004, Haase et al., 2004, Despres et al., 2017, Xia et al.,

2020). The consensus view is that phosphorylation at residues that reduce microtubule binding can encourage aggregation by enhancing the local cytosolic concentration of free Tau, thus encouraging interaction with aggregation-promoting cofactors (Wegmann et al., 2018). Alternatively, Tau phosphorylation may induce misfolding into seed-competent and aggregation prone conformations (Wegmann et al., 2018, Jeganathan et al., 2008).

Beyond the causal relationship between Tau aggregation and phosphorylation, interpreting the relative contribution of each pathological modification towards Tau-mediated toxicity is challenging. This is because it is difficult, in a single model, to independently and combinatorially manipulate phosphorylation, aggregation, Tau expression levels and neuronal age, all of which contribute to degenerative phenotypes (Wittmann et al., 2001, Barghorn et al., 2000, Beharry et al., 2013). To resolve this conundrum, a systematic assessment of the aggregation-phosphorylation interplay in a well-controlled *in vivo* experimental model is needed.

To address this problem, I assessed the relative contributions of phosphorylation and aggregation on Tau-mediated degeneration using several novel transgenic *Drosophila*. A number of novel human Tau (hTau) mutants were generated to determine toxicity of wildtype and phospho-mimicking Tau, and mutants with deletion of the aggregation-promoting $^{306}$VQIVYK$^{311}$ sequence in both wildtype Tau and phospho-mimicking Tau to enable the assessment of the toxicity of phosphorylated Tau which cannot aggregate.

**Aim: To determine the independent contributions of Tau hyperphosphorylation and aggregation towards Tau-mediated toxicity in *Drosophila***

- **Objective 1.** Design and develop a genetic model to assess phosphorylation and aggregation independently by characterising phospho-mimicking (TauE14) and aggregation-resistant (TauΔVQIVYK) mutants

- **Objective 2.** Visualise and quantify phosphorylation- and aggregation-specific axonal and somato-dendritic degeneration of *Drosophila* olfactory and retinal neurons.
- **Objective 3:** Assess phosphorylation- and aggregation-specific Tau accumulation and mis-localisation in axonal and somato-dendritic compartments of *Drosophila* olfactory neurons.

## 3.2 Materials and methods

See methods **section 2.2** for confocal, SIM, SEM methods and image acquisition. See methods **section 2.5** for western blotting methods and analysis. See methods **section 2.6** for IMARIS 3D image analysis.

## 3.3 Results

### 3.3.1 Generating a model to study the contribution of Tau phosphorylation and aggregation

To investigate the relative contributions of hyperphosphorylation and aggregation to neuronal degeneration, I designed a panel of 10xUAS-hTau2N4R transgenes with mutations that either exacerbated or inhibited phosphorylation and aggregation. The mutant Tau strains were generated into a plasmid downstream of a 10xUAS-Gypsy insulator, which drives the expression of the reporter gene ten times the amount of traditional UAS-Tau lines (Wittman 2001) to ensure robust protein expression. Using snap gene I manipulated the Tau codon sequence to express several Tau mutant transgenic strains: *UAS-mCherry::hTau2N4R*, the phospho-mimicking mutant *UAS-mCherry::hTau2N4R-E14* in which phosphorylation at 14 disease-associated sites is physiochemically mimicked using glutamate (T111E, T153E, T175E, T181E, S199E, S202E, T205E, T212E, T217E, T231E, S235E, S396E, S404E and S422E) (Hoover 2010), the aggregation resistant mutant *UAS-mCherry::hTau2N4R-ΔVQIVYK* in which the aggregation-promoting $^{306}$VQIVYK$^{311}$ motif is deleted (termed

hTau2N4R-DEL), and also a phospho-mimicking but aggregation resistant mutant *UAS-mCherry::hTau2N4R-E14/ΔVQIVYK* **(Figure 20).**

After design, these lines were generated by collaborators from the Allan Lab at the University of British Columbia by targeted integration of an exogenous plasmid into the *Drosophila* genome. A single copy of the transgene was integrated into the *attP40* locus of the fly genome, to ensure equivalent expression of the mutants. Equivalent Tau expression across the genotypes was essential for directly comparing the contributions of hyperphosphorylation and aggregation towards Tau-mediated pathology.

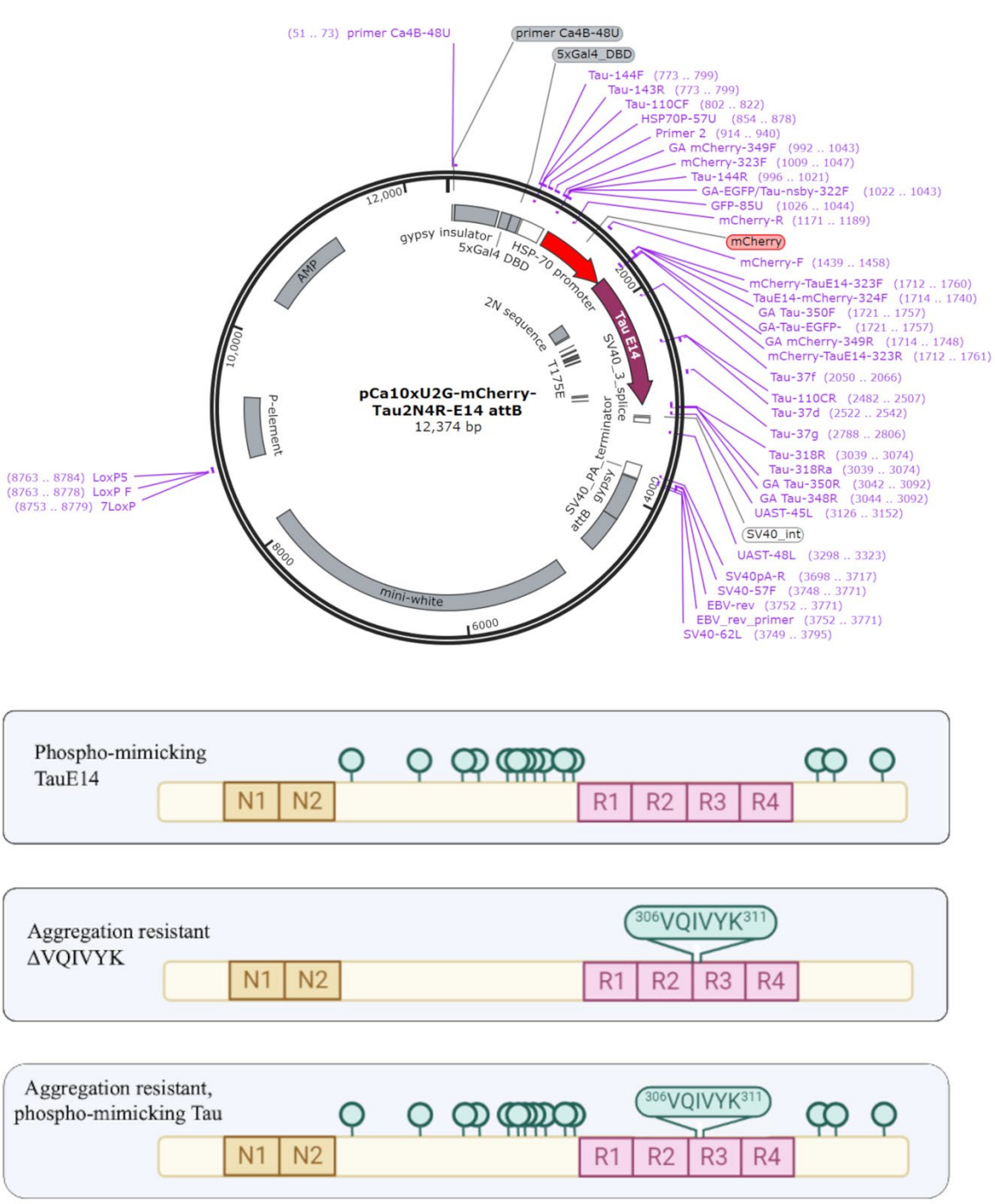


**Figure 20. Design of phospho-mimicking and aggregation-resistant Tau mutants.**

Example Snapgene plasmid map showing transgene construct inserted into the *Drosophila* genome, with a 10xGyspy insulator sequence for high-level protein expression. Each Tau mutant was designed on the longest human Tau isoform hTau2N4R: **A)** Phospho-mimicking *UAS-mCherry::hTau2N4R-E14* in which phosphorylation at 14 disease-associated sites is mimicked, the aggregation resistant mutant **B)** *UAS-mCherry::hTau2N4R-ΔVQIVYK* in which the aggregation-promoting $^{306}$VQIVYK$^{311}$ motif is deleted (termed hTau2N4R-DEL), and C) a combined phospho-mimicking but aggregation resistant mutant: *UAS-mCherry::hTau2N4R-E14/ΔVQIVYK* (termed hTau2N4R-E14/DEL).

### 3.3.2 Tau is equally expressed by all mutants.

First, I needed to validate that any observed differences in toxicity were a direct result of the intended mutations, rather than differential protein expression. This is because Tau expression levels directly influence degenerative phenotypes (Wittmann et al., 2001), meaning that the protein expression could mask or enhance pathological effects independently of phosphorylation or aggregation mechanisms.

Western blot quantification showed equivalent total Tau expression across all mutants at 2 days post-eclosion **(Figure 21 A),** demonstrating that protein levels during development and early adulthood were similar before pathological age-related changes could occur. Likewise, after 14 days of aging total Tau levels remained similar across all mutants, however ΔVQIVYK mutants (hTau2N4R-DEL and hTau2N4R-E14/DEL) had slightly lower average Tau levels compared to hTau2N4R and hTau2N4R-E14 respectively, although differences were not significant **(Figure 21 B).**

With equivalent expression levels validated, I next sought an appropriate system to assess the degenerative contributions of phosphorylation and aggregation with confidence that differences in neurotoxicity would be attributed to the mutations themselves rather than differential transgene expression.

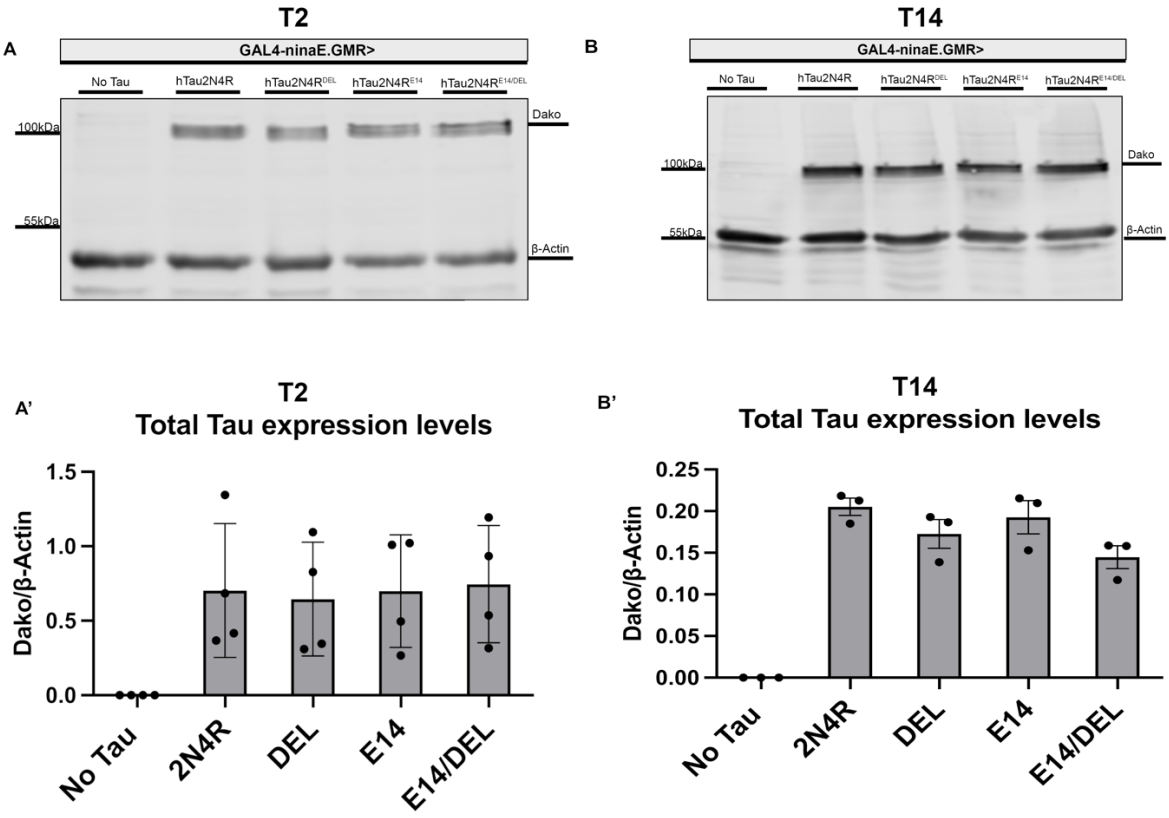


**Figure 21. Tau expression levels are equivalent across all mutants.**

Western blot analysis of total Tau probed with α-hTau Dako, from homogenised fly heads (N=15 males per sample) expressing mCh::hTau2N4R, mCh::hTau2N4R-DEL, mCh::hTau2N4R-E14, and mCh::hTau2N4R-E14/DEL driven by GMR.ninaE-GAL4 at A) 2 days and B)14 days post eclosion. Representative blots are shown (A,B) and quantified (A', B'). Graphs present means ± SD (N=3-4 biological repeats). An ordinary One-way ANOVA showed no statistical difference at T2 or T14. β-actin was used as the loading control. mCherry::hTau2N4R constructs migrate to ~100kDa due to the extra weight of the fluorescent tag (untagged hTau2N4R usually runs at ~70kDa) and Actin at ~45kDa.

### 3.3.3 The Or47b expressing olfactory sensory neurons.

Having validated equivalent expression of the Tau mutants, I next needed to select a neuronal group to assess their differential pathophysiological effects. I required a small, accessible neuronal population to allow detailed analysis of the pathogenic behaviour of Tau and its toxic effect on the neuron.

I chose the Or47b olfactory neurons, composed of ~60 cholinergic neurons which innervate the VA1v glomeruli positioned on the most dorsal surface of the brain (Hueston et al., 2016, Deanhardt et al., 2023, Jefferis et al., 2004, Dweck et al., 2015). There are multiple advantages for choosing the Or47b neurons 1) numerical simplicity allowed for detailed

analysis for Tau-mediated neurodegeneration 2) anatomically, there is excellent segregation of neuronal compartments to enable the individual assessment of Tau in different neuronal compartments **(Figure 22)** and 3) the neurons to not renew after development **(Figure 16)** making them an attractive circuit to model degeneration and the effects of Tau on aging neurons. To visualise Or47b neuronal morphology and Tau localisation, I used *Or47b*-GAL4 combined with *UAS-CD8::EGFP* (membrane-bound GFP marker) and mCherry::hTau mutants, respectively.

Using confocal microscopy with this experimental system allowed me to detect phosphorylation and aggregation-specific effects on Tau pathology and neurodegeneration across different neuronal compartments.

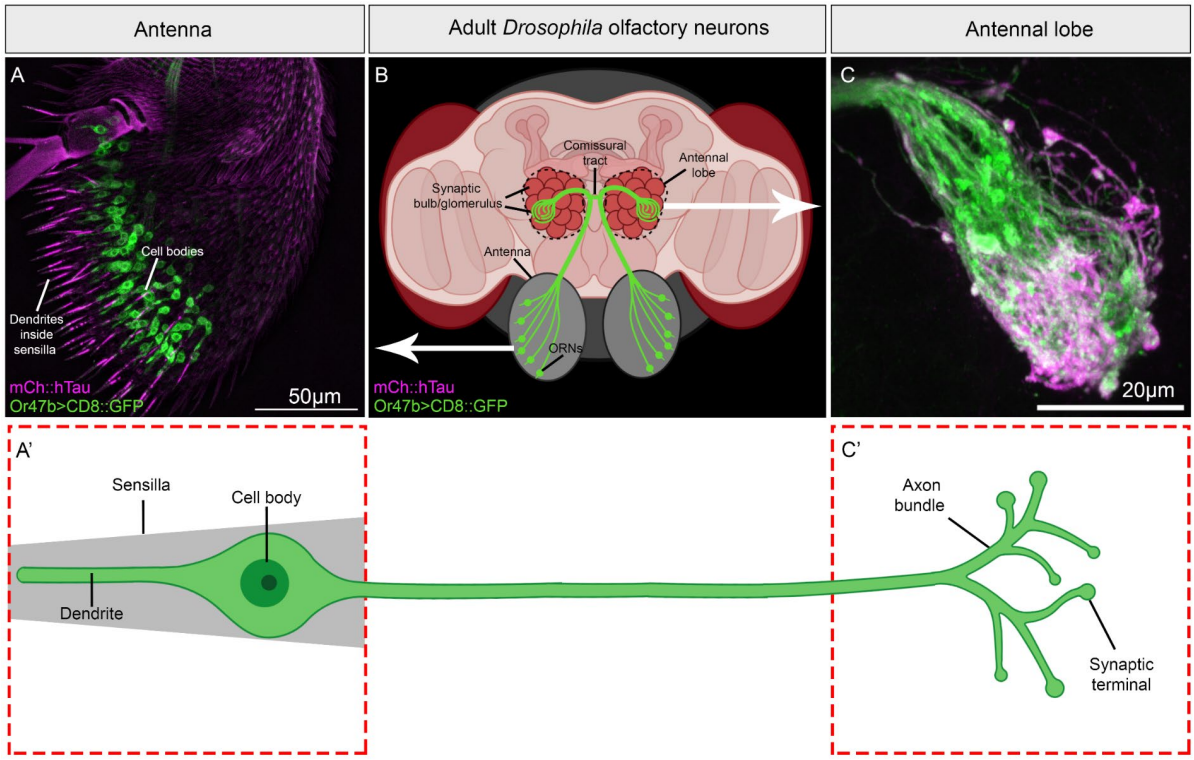


**Figure 22. The Or47b expressing olfactory sensory neurons.**

Schematic panel orientation of the adult *Drosophila* brain, showing the location of the olfactory receptor 47b (Or47b) neurons expressing membrane bound GFP (green), co-expressing mCherry tagged human Tau2N4R (mCh::hTau) (magenta). Representative confocal images of whole mount (**A**) Antenna and (**C**) the Antennal lobe (AL) is shown. (**B**) Schematic diagram of the Or47b olfactory neurons. The AL is outlined in dashed black, containing multiple olfactory glomeruli, including Or47b (green) containing a bundle of ~60 olfactory receptor neurons (ORNs). ORN cell bodies are contained within the 3rd antennal

segment of the Antenna (**A, A'**) and its dendrite projects into the sensilla hairs of the antenna. The axons project from the antenna connecting into the (**C**) AL of the brain, containing the (**C'**) axonal bundles and synaptic terminals of the Or47b neuron. For simplicity, only a few of the 60 ORNs are shown.

### 3.3.4 Phosphorylation-dependent somato-dendritic and axonal degeneration requires the $^{306}$VQIVYK$^{311}$ domain

First, I investigated how hyperphosphorylation and the $^{306}$VQIVYK$^{311}$-aggregation domain influence Tau-mediated somato-dendritic degeneration. Since Tau mis-localises to the soma during AD and the somatic compartments show early phenotypes associated with Tau-mediated damage, the somato-dendritic compartment provides a useful site for assessing the degenerative effects of phosphorylation.

Consistent with previous studies, expression of hTau2N4R led to progressive and quantifiable reduction in soma width that was significantly different from controls by day 14 (T14) (**Figure 23 A6** *versus* **Figure 23 A7**, quantified in **Figure 23 C**). These somato-dendritic defects were exacerbated in animals expressing the phospho-mimicking hTau2N4R-E14 in which neurodegeneration was significantly enhanced such that there was 23% soma loss by day 3 (T3) which increased to 36% by T14 (**Figure 23 A4** and **A9**, quantified in **Figure 23 B**). Moreover, the width of the soma in hTau2N4R-E14-expressing neurons was also significantly reduced by T3 and remained at this level at T14 compared to no Tau and hTau2N4R controls (**Figure 23 A9** quantified in **Figure 23 C**).

These results confirm that hyperphosphorylation significantly accelerates somato-dendritic degeneration and is highly toxic to neuronal cell bodies. Given that neuronal compartments have distinct cellular compositions and functions (Kandel, 2021), I next examined whether hyperphosphorylation has similar degenerative effects in other compartments such as the axon.

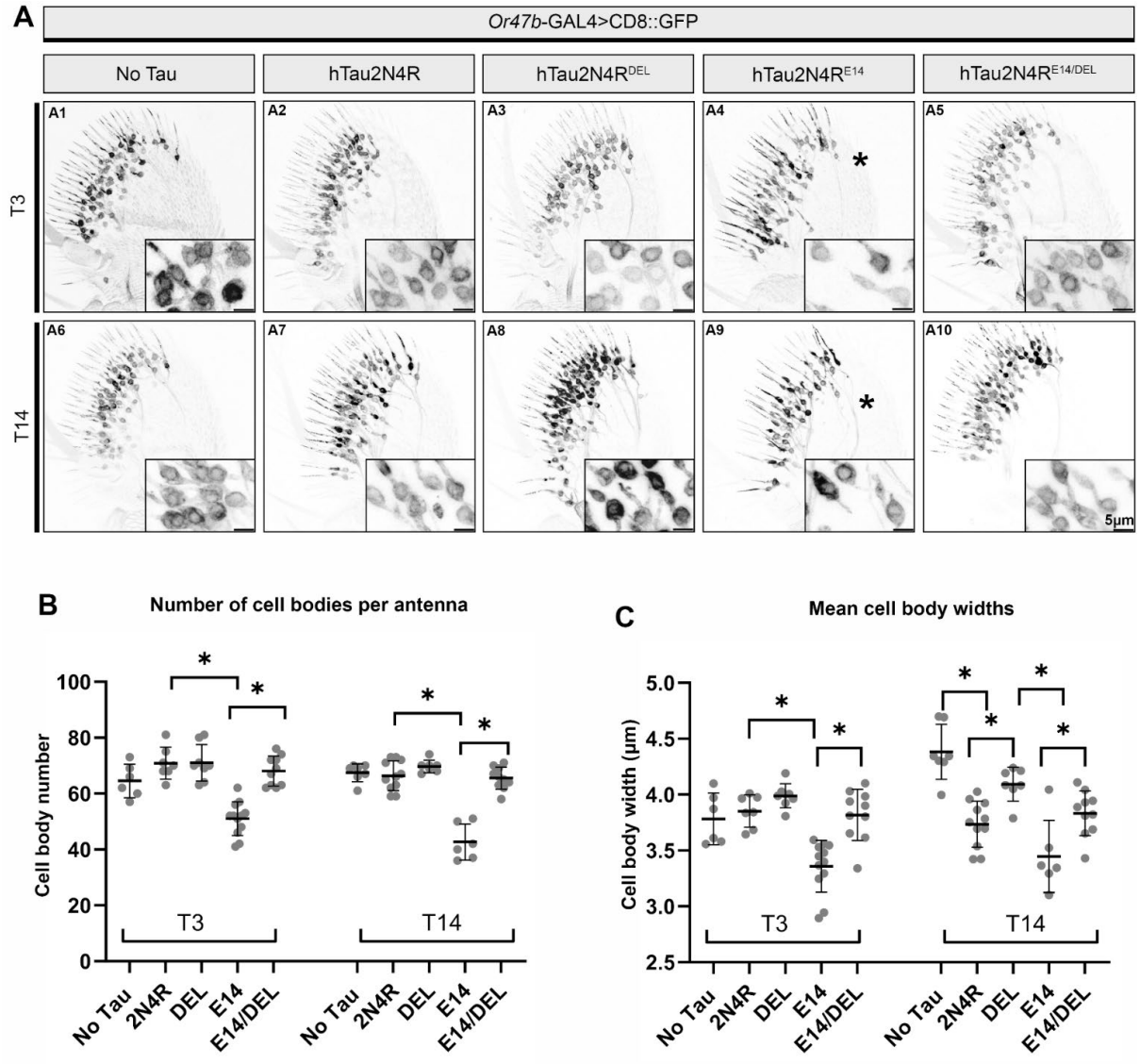


**Figure 23. Phosphorylation dependent somato-dendritic degeneration requires the $^{306}$VQIVYK$^{311}$ domain.**

(A) Maximum projection confocal images of the adult antenna of flies expressing membrane bound GFP (CD8::GFP) at the Or47b neurons. Columns represent genotypes expressing different mCherry-tagged hTau2N4R variants plus the driver alone expressing GFP only as a control (left most column). Rows represent post-developmental age (3 or 14 days). Magnified projections (30 slice depth) of the soma region are included. Asterisk shows the reduced soma density induced by hTau2N4R-E14 expression (A9), which is rescued in hTau2N4R-E14/DEL (A10). (B-C) Quantification of cell bodies per antenna (B) and mean cell body width (C) for the indicated genotypes and time points. Cell bodies were manually counted and measured using ImageJ. Graphs represent mean ±SD, and dots represent averages per antenna. * $p<0.05$ (2-way ANOVA with Tukey's multiple comparisons). N= 6-12 antennas collected from two biological repeats per genotype.

In the axonal compartment, Tau accumulation is reported to impair transport (Mudher et al., 2004, Talmat-Amar et al., 2011) resulting in axonal swellings leading to fragmentation and neuronal loss in mammalian Tauopathy models (Lin et al., 2003, Sahara et al., 2014, Probst et al., 2000). These morphological characteristics were also examined in hTau-expressing Or47b axons.

Control Or47b neurons present with the typical compact highly fasciculated axon bundles with some age-dependent swellings and defasciculation evident in aged animals (**Figure 24 A1, A6**). The number, size and total volume of axonal swellings were greatly increased upon hTau2N4R expression at all ages assayed (**Figure 24 A2, A7**). As was seen in the somato-dendritic compartment, these aberrant axonal phenotypes were greatly exacerbated by hTau2N4R-E14 expression at all time points. This was characterised by the appearance of prominent axonal swellings, fragmentation and dystrophic processes in hTau2N4R-E14-expressing neurons (arrow heads in **Figure 24 A9**), indicative of substantial axonal and synaptic loss. This is also evident in a reduction of the total volume of the axonal bundle (**Figure 25**).

These findings demonstrate that Tau hyperphosphorylation is critically toxic across multiple neuron compartments. This is consistent with other studies showing that neurodegeneration is driven by phosphorylation at sites known to be hyperphosphorylated in Tauopathies validating this experimental system (Hoover et al., 2010, Hallinan et al., 2019, Talmat-Amar et al., 2011). Next, I wanted to assess whether phosphorylation-mediated toxicity required the $^{306}$VQIVYK$^{311}$ aggregation motif, and whether this domain represented a therapeutic target against this highly toxic phospho-mimicking Tau species.

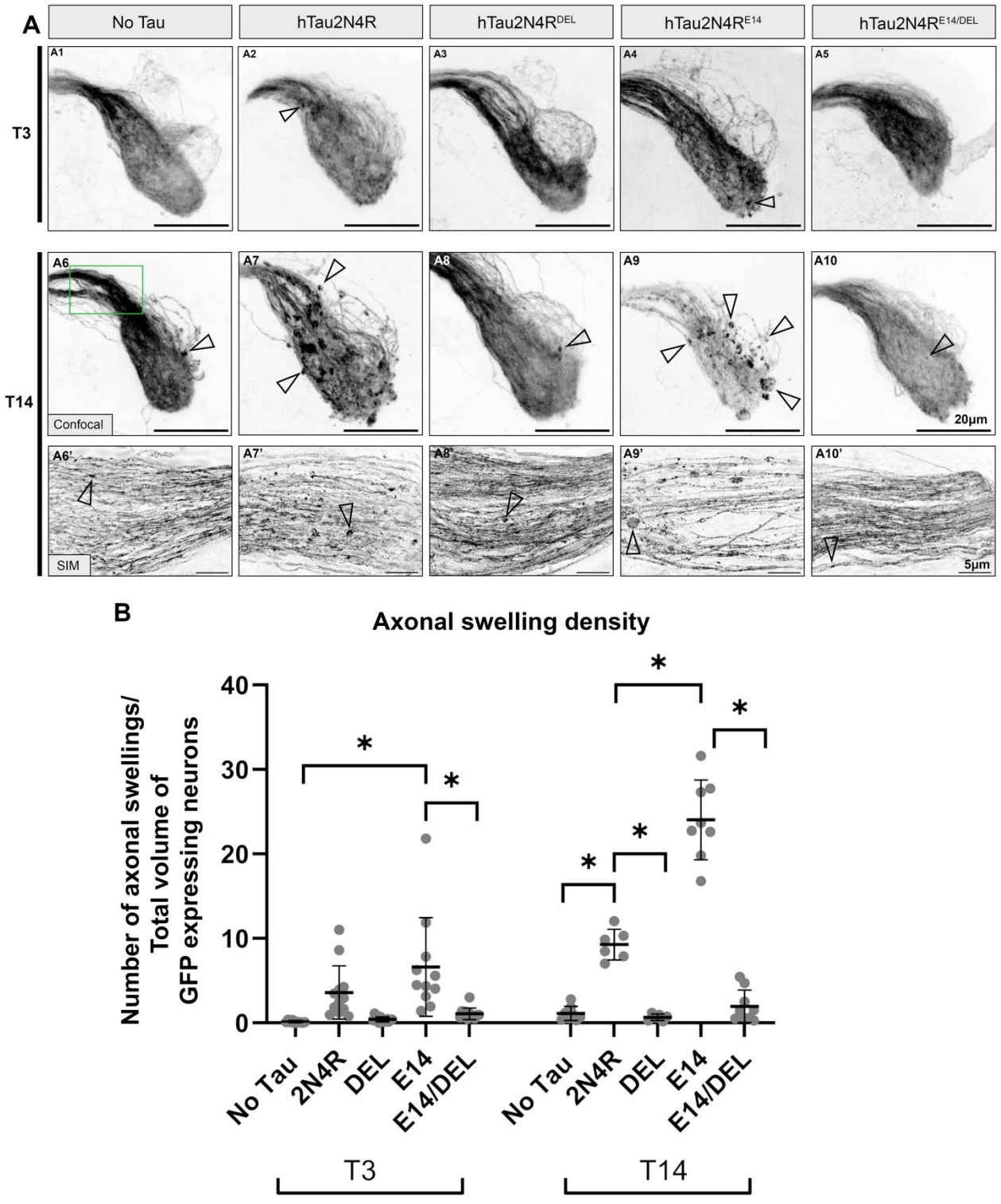


**Figure 24. Phosphorylation dependent axonal and synaptic degeneration requires the $^{306}$VQIVYK$^{311}$ domain.**

(A) Maximum projection confocal (A1-10) or SIM (A6'-10') images of the brain and antennal lobe of flies expressing membrane bound GFP (CD8::GFP) at the Or47b neurons enhanced with α-GFP. Columns represent genotypes expressing different mCherry-tagged hTau2N4R variants plus the driver expressing GFP only as a control (left most column). Rows represent

post-developmental age 3 or 14 days. Normal structure of the neurons shows some axonal swellings (Arrows) that occur with age and are increased in wildtype hTau2N4R flies (A2) and exacerbated in hTau2N4R-E14 expressing flies (A4). Green inset box on A6 highlights the Or47b glomeruli commissure, imaged with SIM at T14(A6'-10') in the middle row. (B) Quantification of axonal swellings were automatically quantified using 3D images with IMARIS (see methods). Graphs represent mean ±SD, and dots represent individual values. * $p<0.05$ (2-way ANOVA with Tukey's multiple comparisons). N= 6-14 brains collected from two biological repeats per genotype.

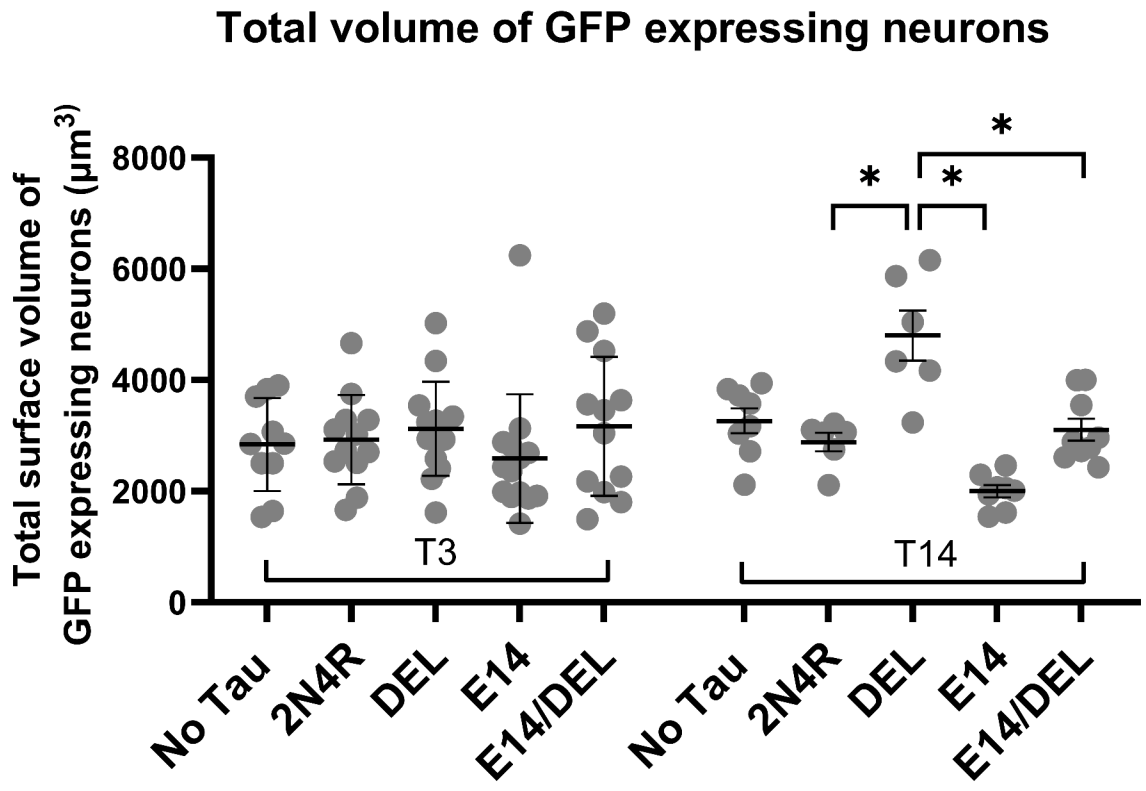


**Figure 25. Total volume of GFP expressing neurons.**

Quantification of neuron volume was automatically quantified using 3D images with IMARIS (see methods). Graphs represent mean ±SD, and dots represent individual values. * $p<0.05$, (2-way ANOVA with Tukey's multiple comparisons). N= 6-14 brains collected from two biological repeats per genotype.

### 3.3.5 Deletion of $^{306}$VQIVYK$^{311}$ rescues Tau mediated somato-dendritic and axonal degeneration

As aggregation is also implicated in Tau-mediated degeneration and is believed to be triggered by misfolding induced by Tau hyperphosphorylation, I next sought to investigate the impact of reducing the aggregation propensity of hTau2N4R and of

hTau2N4R-E14. This was achieved by deleting(Δ) the $^{306}$VQIVYK$^{311}$ domain in both Tau transgenics which are referred to as hTau2N4R-DEL and hTau2N4R-E14/DEL respectively from here on.

Results showed both hTau2N4R-mediated shrinkage of cell body width (**Figure 23 A7, C**) and axonal swellings (**Figure 24 A7**) were completely absent upon $^{306}$VQIVYK$^{311}$ deletion both in hTau2N4R-DEL, and hTau2N4R-E14/DEL-expressing animals at all ages tested (**Figure 23 A8, A10** and **Figure 24 A8, A10**). The cell body widths and axonal profiles of both these $^{306}$VQIVYK$^{311}$ deletion mutants were virtually indistinguishable from age-matched controls (**Figure 23 C**). Quantification of axonal swellings and neuronal loss further supports these conclusions (**Figure 24 B, Figure 25**).

Additional confirmation of these findings was afforded by Structured Illumination Microscopy (SIM) which provides much greater subcellular resolution to visualise Tau-mediated axonal degeneration. SIM imaging of the commissural tract located at the top of the olfactory glomeruli at T14 clearly shows large axonal swellings and profound axonal loss in the hTau2N4R-E14 animals (**Figure 24 A9'**), which are completely attenuated upon $^{306}$VQIVYK$^{311}$ deletion in hTau2N4R-E14/DEL animals (**Figure 24 A10'**).

This shows that deletion of the $^{306}$VQIVYK$^{311}$ motif renders the toxic hTau2N4R protein benign, even in animals mimicking hyperphosphorylation at established disease-associated sites. This implies that the toxicity of hyperphosphorylated hTau2N4R is mediated by the $^{306}$VQIVYK$^{311}$ aggregation promoting motif.

### 3.3.6 Targeting $^{306}$VQIVYK$^{311}$ rescues degeneration across multiple neuronal populations

Next, I wanted to determine whether the rescue of phosphorylation-mediated degeneration by deleting $^{306}$VQIVYK$^{311}$ was specific to olfactory neurons or was more generally neuroprotective. Given that distinct neuronal populations exhibit different

vulnerabilities to Tau-mediated toxicity (Sivanantharajah et al., 2025), it was essential to test if $^{306}$VQIVYK$^{311}$ deletion would rescue phosphorylation-enhanced pathology across diverse neuronal types. Therefore, I examined the same Tau variants in developing photoreceptors, using a *GMR-GAL4* driver, where Tau toxicity manifests as fusion, loss and disorganisation of ommatidia and sensory bristles (**Figure 26**), which can be quantified using a phenotypic score using Flynotyper (Iyer et al., 2016) .

Expression of hTau2N4R led to a subtle eye disorganisation (**Figure 27 A2, B2**) which was significantly exacerbated in the hTau2N4R-E14 animals (**Figure 27 A4, B4**). The phospho-mimicking mutant produced severely misshapen ommatidia that were a mixture of shrunken, swollen and fused cells, along with deep holes of tissue degeneration and complete loss of sensory hairs (**Figure 27 B4**). Reminiscent of the rescue seen in the Or47b neurons, these eye phenotypes were also totally eliminated upon expression of either hTau2N4R-DEL or hTau2N4R-E14/DEL, restoring normal ommatidia phenotypes back to controls (**Figure 27 A3, A5, B3** and **B5**). Quantitative analysis supports this showing that ΔVQIVYK significantly reduced disorganisation phenotypes of hTau2N4R-E14 (**Figure 27 C**).

Collectively, these findings demonstrate that ΔVQIVYK-mediated rescue is not specific to olfactory neurons but is neuroprotective across multiple neuronal populations. The consistent rescue of degenerative phenotypes even in severely toxic phospho-mimicking Tau demonstrates that hyperphosphorylation-mediated neurodegeneration is gated through the aggregation-promoting $^{306}$VQIVYK$^{311}$ motif, representing a viable target for Tau-centred therapeutics. Given such effective neuroprotection, I next sought to assess how ΔVQIVYK would affect the pathological behaviour of Tau localisation and accumulation.

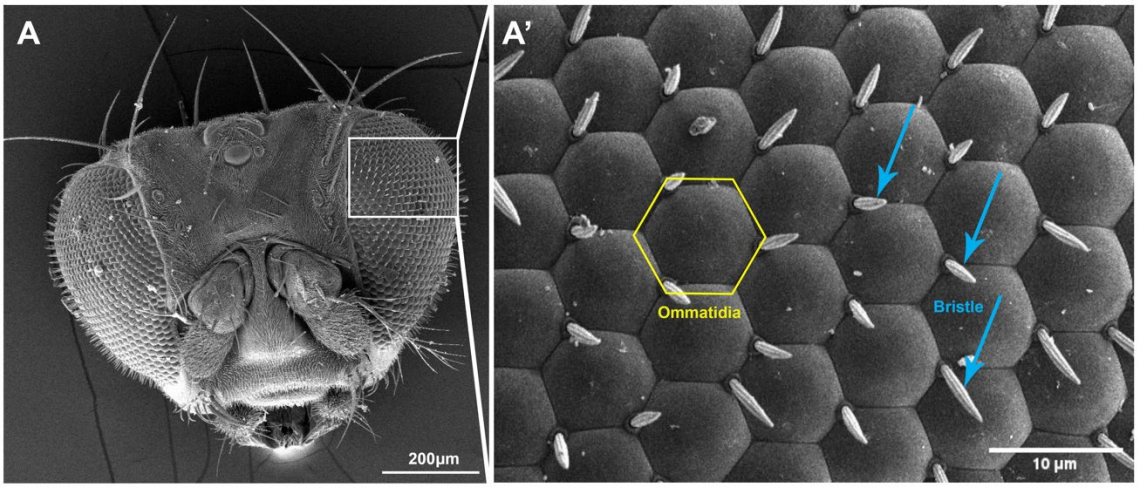


**Figure 26. *Drosophila* eye diagram.**

(A) SEM micrograph of whole *Drosophila* head. White insert shows the posterior region of interest where Tau-mediated retinal degeneration occurs using the GAL4-ninaE.GMR driver. (A') The *Drosophila* eye comprises of ~800 single ommatidia units (highlighted in yellow) which are morphologically sensitive to toxic proteins like Tau. Loss of sensory bristles (blue arrows) are also markers of retinal health.

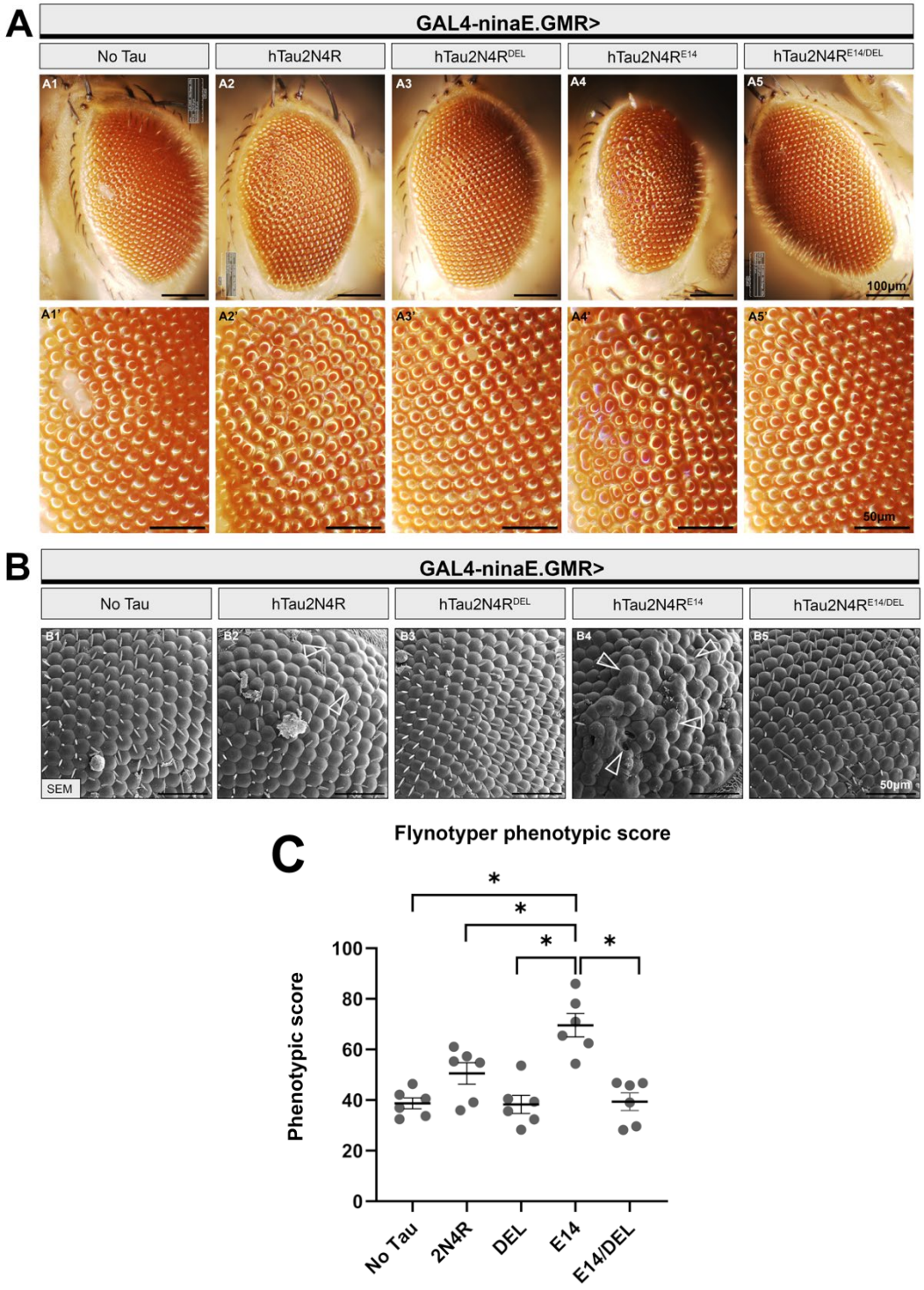


**Figure 27. Phosphorylation dependent retinal degeneration requires the $^{306}$VQIVYK$^{311}$ domain.**

A1-A5') Digital microscope images (600x) and B1-B5) SEM micrographs (1600x) of 14-day-old *Drosophila* eyes expressing each hTau2N4R mutant using the GAL4-ninaE.GMR driver. A rough appearance of the posterior half of the eye appears after hTau2N4R expression and is exacerbated by the TauE14 mutations. Abnormal retina and degenerated cells are labelled with arrowheads. (C) Quantification of retinal degeneration using a phenotypic scoring system Flynotyper plugin. Graphs represent mean ±SD, and dots represent individual values. * $p<0.05$ (one-way ANOVA with Tukey's multiple comparisons). N=6 per genotype.

### 3.3.7 Dendritic mis-localisation and axonal accumulation of Tau require the $^{306}$VQIVYK$^{311}$ domain

Two central features of AD pathology is neurodegeneration and abnormal Tau behaviour. Having demonstrated that neurodegeneration can be rescued by deleting the aggregation-promoting $^{306}$VQIVYK$^{311}$ motif, I next investigated how its deletion affects the underlying pathological behaviour of Tau. Firstly, I assessed the intracellular Tau localisation and accumulation, as others have shown that Tau mis-localises from axonal to the somato-dendritic compartments during disease (Kubo et al., 2019, Binder et al., 1985), where it accumulates in large insoluble cytoplasmic hyperphosphorylated inclusions (Hoover et al., 2010, Kubo et al., 2019, Binder et al., 1985, Zempel and Mandelkow, 2014).

My results show that in the Or47b neurons, Tau is expressed throughout the soma, axons and dendrites (**Figure 28 B**, **Figure 29** and **Figure 30**). However, in the somato-dendritic compartment, Tau appears to be more highly concentrated within the dendrites that lie within the antennal sensilla(hairs) (**Figure 28 B, A1-A10**), indicating mis-localisation to this compartment. Within the dendrites hTau2N4R distribution became uneven and fragmented from T3 to T14 (**Figure 28 A2, A7** and **Figure 29 A2, A7**). By comparison, dendritic mis-localisation was greatly exacerbated in an age-dependent manner in hTau2N4R-E14-expressing neurons (**Figure 28 A4** and **Figure 29 A4, A9**). However, deletion of the $^{306}$VQIVYK$^{311}$ domain either in hTau2N4R or hTau2N4R-E14 led to a profound reduction of this mis-localisation, as smaller and sparser Tau accumulates were observed within dendrites (**Figure 28 A3, A5, A8** and **A10**). This is supported by quantification of the volume of hTau in the dendritic compartment showing significantly greater dendritic accumulation in hTau2N4R-E14 compared to hTau2N4R, which was significantly reduced in hTau2N4R-E14/DEL (**Figure 28 C**).

These results confirm that hyperphosphorylation significantly increases Tau mis-localisation in the somato-dendritic compartment, dependent on the $^{306}$VQIVYK$^{311}$ domain.

Given that neuronal compartments have distinct cellular compositions and functions, I next investigated the behaviour of Tau in the axonal compartment.

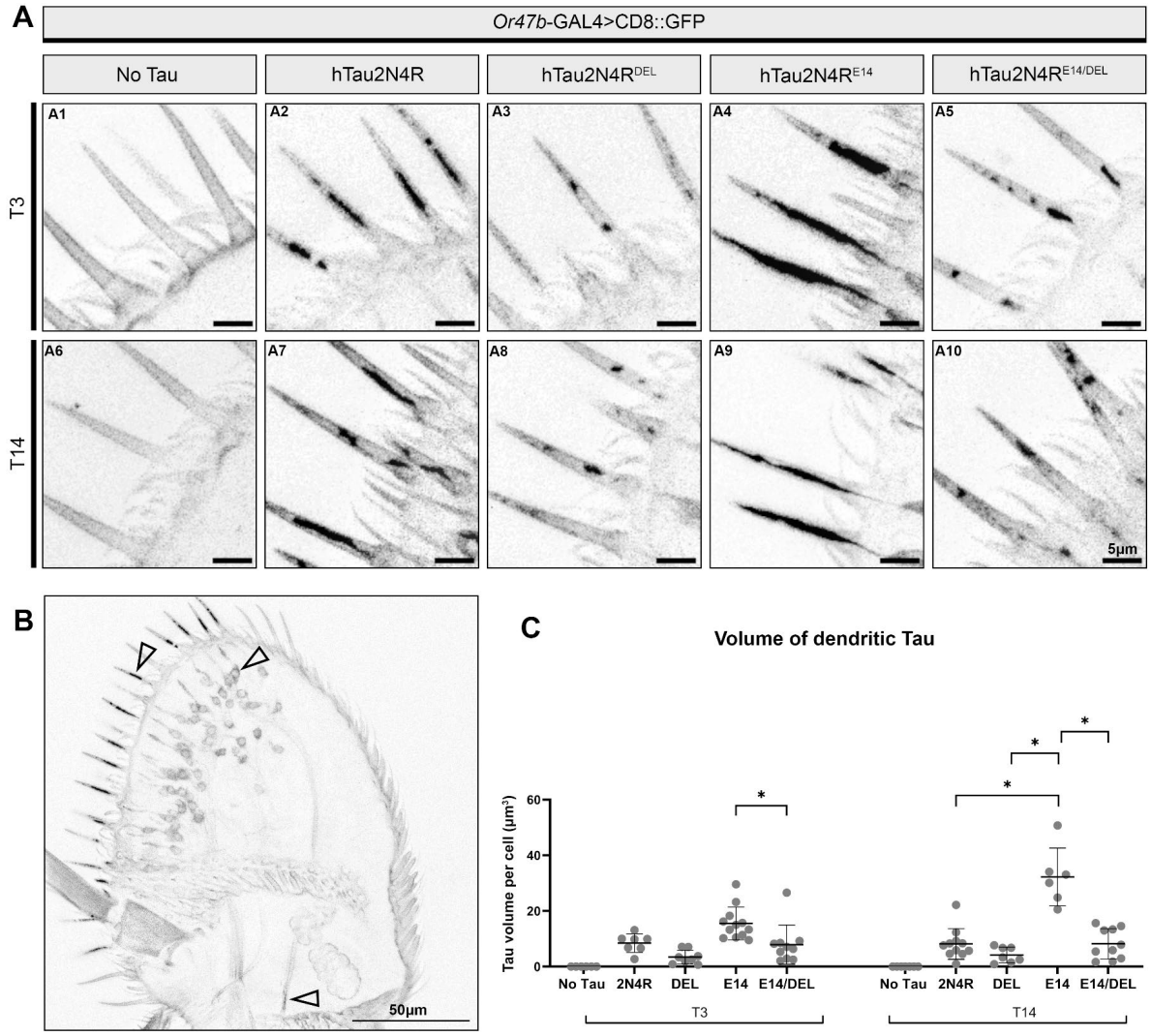


**Figure 28. Phosphorylation dependent dendritic Tau accumulation requires the $^{306}$VQIVYK$^{311}$ domain.**

(A) Midline 30 slice stacked confocal images of the adult antenna of flies labelled by the mCherryTau signal from expressed mutants in the Or47b neurons. Columns represent genotypes expressing different mCherry-tagged hTau2N4R variants plus the driver expressing GFP only as a control (left most column). Rows represent post-developmental age (3 or 14 days). Magnified regions of interest over the dendrites are presented (A1-A10). (B) Example image of whole mount antenna, of A2. Arrows point towards Tau expression present within the dendrites, somas and axons. Other whole mounts can be viewed in **Figure 29**. (C) Quantification of the volume of dendritic Tau in the antenna was quantified using 3D projection images with IMARIS with a surfacing tool using N=6-12 from two biological

repeats. Graphs represent Mean ±SD. * = p<0.05 (2-way ANOVA with Tukey's multiple comparisons).

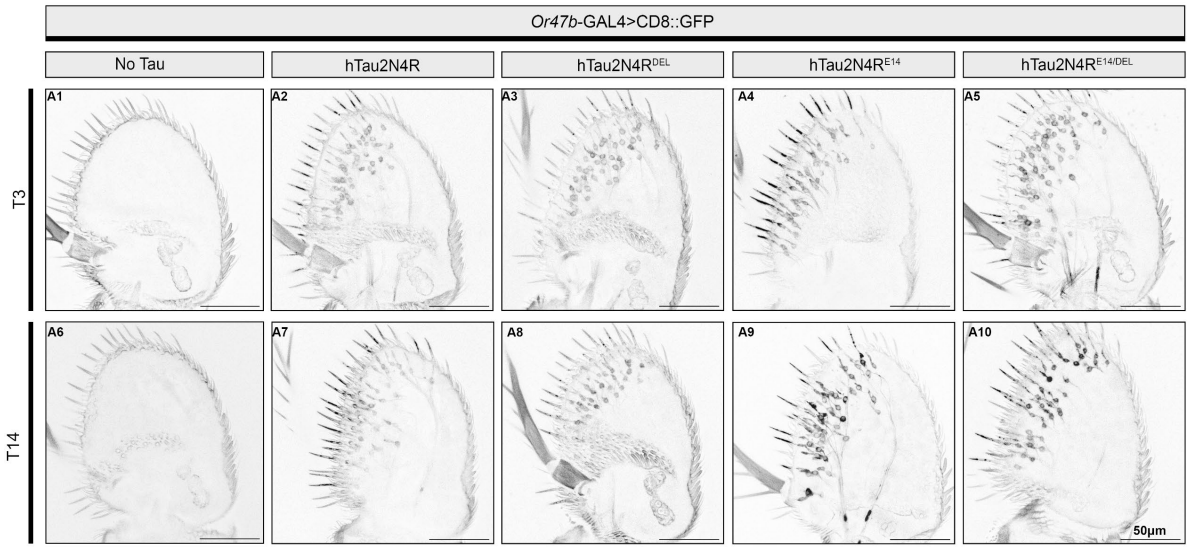


**Figure 29. T3 and T14 somato-dendritic Tau accumulation in whole mount antenna.**

Midline 30 slice stacked confocal images of the adult antenna of flies labelled by the mCherryTau signal from expressed mutants in the Or47b neurons. Columns represent genotypes expressing different mCherry-tagged hTau2N4R variants plus the driver GFP only control (left most column). Rows represent post-developmental age 3 or 14 days.

In the axonal compartment, all Tau mutants were uniformly distributed in Or47b expressing axons and synapses at T3 (**Figure 30 A2-A5**). However, by T14 the frequency and size of Tau accumulates increased in hTau2N4R-expressing flies consistent with the excessive axonal swellings displayed by these axons (arrowheads **Figure 30 A7**). These accumulates almost doubled in Tau2N4R-E14-expressing animals (arrowheads **Figure 30 A9**), relative to those accumulating hTau2N4R (**Figure 30 B**). These pathological Tau accumulates were suppressed by $^{306}$VQIVYK$^{311}$ deletion such that by T14, axons were almost devoid of them in hTau2N4R-E14/DEL animals and the axonal profiles looked smooth and completely normal (arrowheads in **Figure 30 A10** *versus* **A9**). Scrutiny of the axonal bundle using SIM imaging confirms the denser and more prominent intracellular Tau accumulations observed in hTau2N4R-E14-expressing flies (**Figure 30 A9'** *versus* **A7'**) and complete suppression of Tau accumulation in the hTau2N4R-E14/DEL-expressing neurons (**Figure 30 A10'** *versus* **A9'**).

Collectively these results demonstrate that the aggregation promoting $^{306}$VQIVYK$^{311}$ domain is essential for Tau mis-localisation and pathological accumulation in both somato-dendritic and axonal compartments. Together with the prevention of neurodegeneration by ΔVQIVYK these results implicate $^{306}$VQIVYK$^{311}$ as an excellent target to reduce Tau mediated neuropathology.

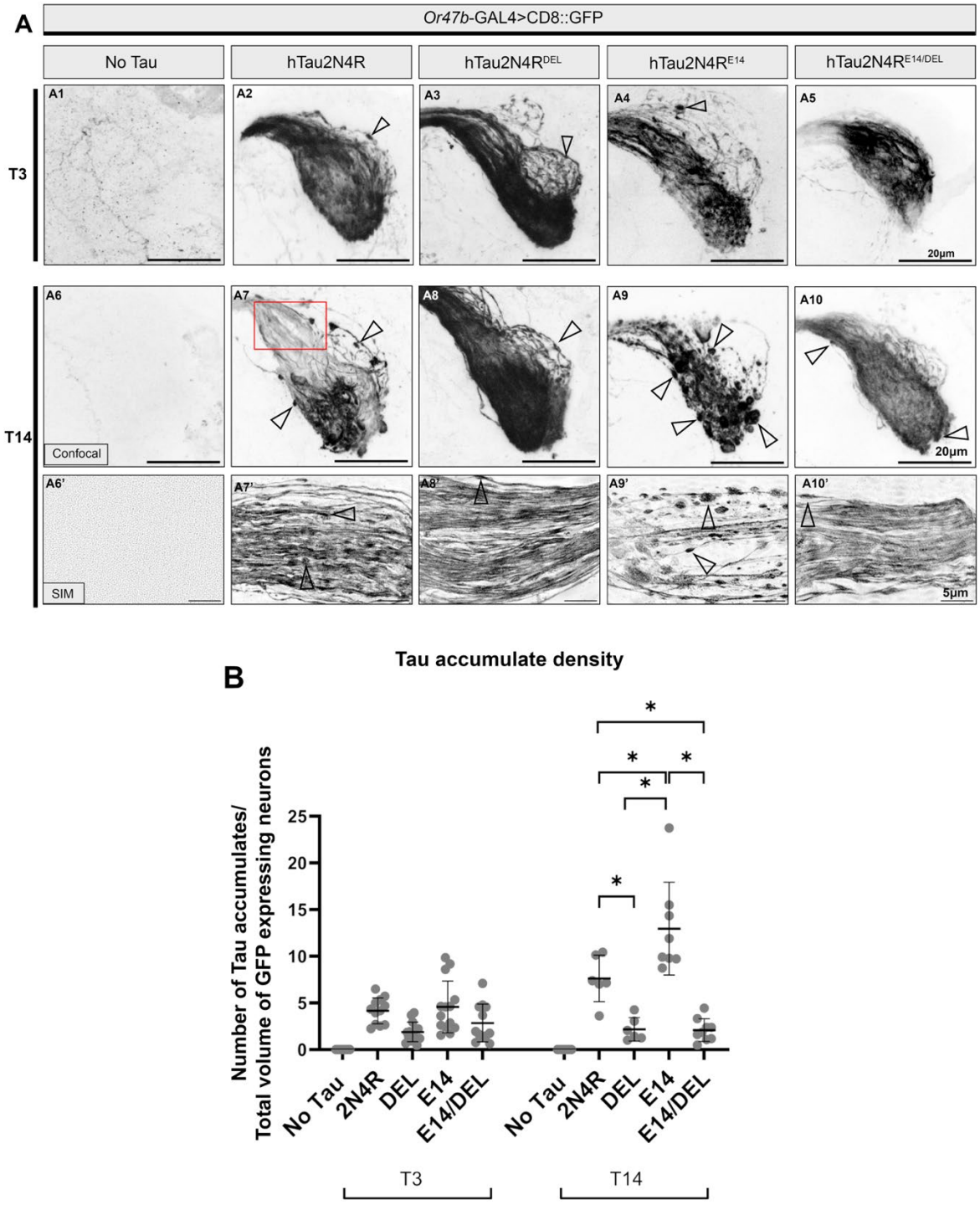


**Figure 30. Phosphorylation dependent axonal and synaptic Tau accumulation requires the $^{306}$VQIVYK$^{311}$ domain.**

A) Maximum projection confocal (A1-10) or SIM (A6'-10') images of the antennal lobe in the brain of day 14 old flies expressing mCherry::Tau mutants in the Or47b neurons (enhanced with α-hTau Dako). Arrows point toward beaded Tau accumulates within expressing neurons which increase in frequency and size with age and are exacerbated in hTau2N4R-E14 expressing flies (A9), but are significantly supressed in hTau2N4R-DEL (A8) and hTau2N4R-E14/DEL (A10). Red inset box on A7 highlights the Or47b glomeruli commissure, imaged with SIM (A6'-A10') at T14 on the bottom row. (B) Quantification of the Tau accumulate density were quantified using 3D images with IMARIS with a spotting tool (see methods)

N=6-14 from two biological repeats. Graphs represent mean ±SD. *p<0.05 (2-way ANOVA with Tukey's multiple comparisons).

## 3.4 Discussion

Phosphorylation and aggregation are both established pathogenic post translational modifications of Tau thought to play a central role in mediating Tau-toxicity. They therefore represent significant disease-modifying therapeutic targets for the treatment of Tauopathies. Yet the causal relationship between these distinct post-translational modifications and their relative contribution towards Tau toxicity is not clear. In this Chapter I determined the relative contribution of hyperphosphorylation and aggregation in Tau-mediated neurodegeneration in aging *Drosophila* olfactory neurons. I have shown that $^{306}$VQIVYK$^{311}$ is an excellent candidate for therapeutic intervention *in vivo*, and provide novel data which shows that its targeting can render even highly phosphorylated Tau species inert.

### 3.4.1 Phosphorylation as a key driver of Tau-mediated toxicity

I have demonstrated that the pseudo-phosphorylated hTau2N4R-E14 mutant significantly exacerbates neurodegenerative phenotypes compared to hTau2N4R in various neuronal compartments in a novel experimental system. This finding aligns with previous research using TauE14 and other phospho-mimicking mutants which have consistently shown increased neuronal loss and organisational defects when expressed in alternative *Drosophila* neuron subtypes including the mushroom bodies (Kosmidis et al., 2010), retinal neurons (Fulga et al., 2007, Katsinelos et al., 2021), and circadian clock neurons (Zhang et al., 2022a). However, focusing on Or47b neurons revealed not only severe morphological deficits, such as profound loss of somatic and axonal tissue, but also subtler hallmark

manifestations more difficult to document *in situ* such as the marked increase in axonal swelling size and frequency, and spaciotemporal changes to Tau localisation.

While TauE14 is an aggressive mutant mimicking extensive hyperphosphorylation akin to that seen in AD, it effectively recapitulates the pathogenesis associated with pathological Tau hyperphosphorylation. This underscores the causal role of the 14 GSK-3β phosphorylation sites mutated in TauE14, in Tau-mediated toxicity and validates the focus on reducing phosphorylation as a therapeutic strategy. Adding to this I now show, for the first time, that the pathogenic potential of these sites requires the aggregation promoting $^{306}$VQIVYK$^{311}$ domain.

### 3.4.2 The critical role of the $^{306}$VQIVYK$^{311}$ motif in Tau toxicity

There is significant evidence suggesting that phosphorylation is a precursor for aggregation. Using pseudo-phosphorylated Tau mutants, like TauE14, multiple groups have identified a number of phosphorylation sites that act in concert to promote polymerisation of monomeric Tau (Haase et al., 2004, Despres et al., 2017, Xia et al., 2020, Strang et al., 2019b, Abraha et al., 2000, Rankin et al., 2005, Chang et al., 2011). Other studies using TauE14 have shown increased levels of Tau in sarkosyl-insoluble fraction in *Drosophila* suggestive of increased hTau aggregation in these pseudo-mutants (Fulga et al., 2007, Katsinelos et al., 2021).

Importantly, my results reveal that the toxicity driven by hyperphosphorylation is fundamentally dependent on the aggregation-promoting $^{306}$VQIVYK$^{311}$ domain. Remarkably, deletion of this domain in both hTau2N4R and hTau2N4R-E14 almost completely eliminated toxicity, despite persistent presence of phospho-mimicking epitopes at disease-associated sites. Consistent with these findings, a previous study similarly showed

that deleting the $^{306}$VQIVYK$^{311}$ motif in a *Drosophila* model expressing hTau0N4R attenuated Tau toxicity, rescuing retinal degeneration and shortened lifespan (Passarella and Goedert, 2018).

Collectively this highlights the therapeutic potential of targeting this domain *in vivo*. Building on this, I provide novel insight into its critical role in the context of disease-related hyperphosphorylation, suggesting that the gain-of-function toxicity driven by $^{306}$VQIVYK$^{311}$-dependent mechanisms surpasses any phosphorylation-mediated contributions to overall Tau toxicity.

### 3.4.3 The interplay between phosphorylation and aggregation

My data provides compelling evidence that Tau aggregation is downstream of and gates the toxicity of hyperphosphorylated Tau. I show that hTau2N4R-E14 significantly increases both the number and size of Tau accumulates within axons, consistent with findings in murine hippocampal neurons (Hallinan et al., 2019) and other *Drosophila* models expressing Tau0N4R-E14 (Chi et al., 2020). Several mechanisms may explain how Tau phosphorylation promotes aggregation, including changes in electrostatic charges that create seed-competent species (Hallinan et al., 2019, Hu et al., 2016) and reduced microtubule binding, both of which can shift the micro-environmental equilibrium towards aggregation (Alonso Adel et al., 2004, Hernández-Vega et al., 2017, Kanaan et al., 2020).

Importantly, my results demonstrate that the $^{306}$VQIVYK$^{311}$ domain is crucial for facilitating Tau accumulation and subsequent neuronal degeneration, regardless of the specific mechanism by which phosphorylation enhances Tau aggregation. This is corroborated by previous studies showing that deletion of this motif significantly impedes aggregation and β-sheet assembly of both 3R and 4R Tau proteins *in vitro* and *in vivo* (Passarella and Goedert, 2018, Perez et al., 2007, von Bergen et al., 2001).

### 3.4.4 Impact on Tau mis-localisation and accumulation

The mis-localisation of Tau away from the axonal compartment is well documented in patients with primary Tauopathies (Wang et al., 2013). It is well established that hyperphosphorylated Tau is associated with mis-localisation and accumulation in the somato-dendritic compartment (Zempel and Mandelkow, 2014, Binder et al., 1985, Kubo et al., 2019). Mis-localisation has directly been demonstrated using TauE14 in transgenic mouse primary neuron cultures, where TauE14 induced rapid translocation to the dendritic spines, and resulted in direct dysfunction of AMPAR-mediated synaptic responses (Hoover et al., 2010). The presence of phosphorylated Tau in this compartment can lead to multiple pathogenic consequences, as demonstrated in various models using TauE14. These consequences include Tau aggregation (Fulga et al., 2007, Katsinelos et al., 2021), propagation (Hallinan et al., 2019), and cellular dysfunction, such as altered axonal trafficking of vesicles (Talmat-Amar et al., 2011) which contribute to the disruption of retrograde transport, defective protein degradation, and ultimately, cell death.

I demonstrate that mimicking hyperphosphorylation leads to greater dendritic mis-localisation and accumulation of Tau, while deletion of the aggregation-promoting domain reduces and delays this effect. The increased mis-localisation of phosphorylated Tau may be due to its detachment from microtubules and subsequent transport to the somato-dendritic compartment. Previous studies have also shown phospho-mimicking TauE14 increases molecular motility, possibly contributing to its strong somato-dendritic localisation (Padmanabhan et al., 2024). The increased motility of TauE14 likely advances accumulation of mis-localised Tau into the soma to accelerating somato-dendritic degeneration much faster than wildtype Tau. The fact that deletion of the $^{306}$VQIVYK$^{311}$ domain of Tau reduced its dendritic mis-localisation suggests that this domain, perhaps through aggregation, plays a role in sequestering Tau within the somato-dendritic compartment.

### 3.4.5 Implications for therapeutic strategies

Disease-modifying treatments for Tauopathies aim to reduce pathogenic Tau species, whether that is through anti-sense oligonucleotide (Mummery et al., 2023) or vaccination (Tan et al., 2024) mediated clearance, reduction of Tau phosphorylation through kinase inhibition (Serenó et al., 2009, Lovestone et al., 2015, Melchior et al., 2019), or suppression of Tau aggregation using aggregation inhibitors (Zhang et al., 2020b, Kondo et al., 2021, Aggidis et al., 2024, Hochgräfe et al., 2015, Aillaud et al., 2022).

My findings have significant implications for the design of Tau-centred disease-modifying therapeutics. While reducing phosphorylation remains a valid approach, my results suggest that targeting the $^{306}$VQIVYK$^{311}$ domain may be a more effective strategy to suppress the toxicity of multiple pathogenic forms of Tau. This domain appears to be crucial for pathogenic mechanisms, including those downstream of hyperphosphorylation, in mediating the toxic effects of Tau. Indeed, several studies have reported promising findings showing the neuroprotective effect of peptides targeting both the $^{306}$VQIVYK$^{311}$ and the $^{275}$VQIINK$^{280}$ domain (Zhang et al., 2020b, Kondo et al., 2021, Aggidis et al., 2024, Aillaud et al., 2022).

## 3.5 Conclusion

In summary, much of the current research has independently assessed the pathological contributions of phosphorylated or aggregated Tau species to Tau-mediated toxicity and neuronal degeneration in different experimental systems. Using one experimental paradigm assessing two distinct neuronal compartments I was able to provide important insights into the compartment-specific mechanisms of Tau-mediated degeneration. Importantly, this chapter provides compelling evidence that while Tau phosphorylation is a key driver of toxicity, its pathogenic effects are primarily mediated through the aggregation promoting $^{306}$VQIVYK$^{311}$ domain. This insight offers a novel

perspective on the hierarchy of pathogenic events in Tauopathies and that regardless of the level of Tau phosphorylation, if aggregation is inhibited early enough, the toxicity of Tau can be reduced.

## 3.6 Future directions

Although there is strength in targeting $^{306}$VQIVYK$^{311}$ as it is present in all 6 Tau isoforms, there is also merit in investigating phosphorylation-dependent $^{275}$VQIINK$^{280}$ mediated Tau toxicity. As $^{275}$VQIINK$^{280}$ is restricted to 4R Tau isoforms, comparing its contribution towards Tau mediated toxicity relative to $^{306}$VQIVYK$^{311}$ may inform the development of aggregation inhibitors.

Although Tauopathies are classified by the inclusion of 3R, 4R, or 3R and 4R Tau, factors like local isoform concentration, isoform specific selective neuron vulnerability, and changing expression profiles throughout disease progression may require a more personalised approach to targeting $^{275}$VQIINK$^{280}$ and $^{306}$VQIVYK$^{311}$. Creating a transgenic fly such as hTau2N4R-E14/ΔVQIINK and comparing to the hTau2N4R-E14/ΔVQIVYK expressing flies using experiments I have used in this Chapter could provide further insight to the differential contributions of these aggregation domains during aggregation and neurotoxicity.

Additionally, expanding the investigation of phospho-mimicking and aggregation resistant Tau mutants across other Tau isoforms may further inform how isoform-specific contributions of phosphorylation and aggregation drive neurotoxicity. This would give insight into how these mechanisms relate to the distinct clinical and pathological profiles observed across isoform-specific Tauopathies.

Further definition of the mechanisms underlying how deleting $^{306}$VQIVYK$^{311}$ rescues TauE14 mediated toxicity is needed. Understanding how $^{306}$VQIVYK$^{311}$ contributes towards

microtubule binding, Tau phosphorylation and formation of pathological conformers will form the basis for my next results chapter.

# Chapter 4 Investigating the molecular mechanisms by which the $^{306}$VQIVYK$^{311}$ domain mediates toxicity

## 4.1 Introduction

The aim of this thesis is to investigate how phosphorylation and aggregation contribute towards Tau toxicity and neuronal degeneration. In **Chapter 3,** I demonstrated that mimicking Tau phosphorylation greatly exacerbates axonal and somato-dendritic degeneration and Tau accumulation in aging *Drosophila* OR47b olfactory sensory neurons. Remarkably, the mutagenic targeted deletion of $^{306}$VQIVYK$^{311}$ almost completely abolished degeneration even in extremely toxic, phospho-mimicking TauE14 mutants. As one of two important aggregation domains required for β-sheet assembly and formation of fibrillar aggregate cores (von Bergen et al., 2000, von Bergen et al., 2001), the mode of action by which ΔVQIVYK reduces toxicity in wildtype and phospho-mimicking contexts is most likely by inhibiting aggregation. However, there other well documented loss-of-function (LOF) and gain-of-function(GOF) mechanisms of Tau toxicity, which $^{306}$VQIVYK$^{311}$ could be promoting or restricting. The precise mechanisms by which deleting $^{306}$VQIVYK$^{311}$ reduces toxicity remains unclear, whether through preventing pathological misfolding and aggregation, producing non-toxic intermediates, or enhancing physiological functions like microtubule binding. Within this Chapter, I investigated the molecular mechanisms by which $^{306}$VQIVYK$^{311}$ deletion confers neuroprotection, focusing on microtubule binding ability, phosphorylation, conformation and aggregation.

### 4.1.1 Tau aggregation and oligomeric intermediates

Tau aggregation increases with age and disease progression (Haroutunian et al., 2007, Schöll et al., 2016), characterised by the accumulation of increasingly insoluble,

hyperphosphorylated aggregates in human, mammalian and *Drosophila* Tauopathy models (Levy 2022 (Levy et al., 2022, Cowan et al., 2015, Colodner and Feany, 2010, Ercan-Herbst et al., 2019, Ramsden et al., 2005, Sahara et al., 2002, Katsuno et al., 2005).

Although a spectrum of intermediate Tau conformers appear during paired helical filament (PHF) core formation (Lövestam et al., 2022, Lövestam et al., 2024), low molecular weight species are often considered the most seed-competent and neurotoxic (Flach et al., 2012, Tian et al., 2013). However, emerging evidence from brain-derived Tau oligomers has revealed structural, morphological, and interactome diversity among oligomeric species, each potentially contributing differently to disease pathology (Lo Cascio et al., 2025, Martinez et al., 2025). Notably, not all brain-derived Tau oligomers appear to be seed-competent or overtly toxic. For instance, high molecular weight (HMW) Tau oligomers isolated from individuals with asymptomatic AD pathology exhibit structural and biochemical properties distinct from those found in symptomatic patients, suggesting that certain oligomeric conformations may be non-toxic (Jury-Garfe et al., 2024). It remains unclear how phosphorylation and aggregation contribute towards the generation of these oligomeric intermediates.

### 4.1.2 The reciprocal relationship of Tau phosphorylation and aggregation.

The consensus view is that phosphorylation at pathologically linked epitopes encourages misfolding into seed-competent and aggregation-prone conformations which may stabilise conformations that expose the aggregation motifs $^{275}$VQIINK$^{280}$ and $^{306}$VQIVYK$^{311}$ which triggers self-assembly (Alonso et al., 2001, Jeganathan et al., 2008). There are several Tau antibodies like MC1 and Alz50 which detect misfolded Tau, and mark pre-fibrillar aggregates observed in both animal models and human brains (Jicha et al., 1997). These conformation-specific markers provide insight into early, toxic Tau species

before overt aggregation occurs, and have shown to increase immunoreactivity when tested with phospho-mimicking Tau mutants (Jicha et al., 1997, Jeganathan et al., 2008).

There is also evidence to suggest that phosphorylation inducing aggregation is not a linear process (Cowan and Mudher, 2013). Current literature investigating the reciprocal relationship of phosphorylation downstream of aggregation is sparse. However, $^{306}$VQIVYK$^{311}$ ablation and peptide-based aggregation inhibitor studies have demonstrated that inhibiting $^{306}$VQIVYK$^{311}$ reduces but sometimes increases phosphorylation within *in vitro* and *in vivo* models of Tauopathy (Passarella and Goedert, 2018, Zhang et al., 2020b, Perez et al., 2007, Kondo et al., 2021), suggesting that aggregation may in fact promote phosphorylation. With the limited and conflicting literature, it is unclear if phosphorylation lies strictly upstream of aggregation, and whether Tau2N4R-DEL attenuates Tau-mediated neurotoxicity seen in **Chapter 3** by preventing downstream phosphorylation at AD-pathologically linked sites.

### 4.1.3 $^{306}$VQIVYK$^{311}$ roles in physiological and pathological function

As $^{306}$VQIVYK$^{311}$ resides within the microtubule-binding domain, its deletion could potentially affect Tau's primary physiological function of binding and stabilising microtubules. Tau-microtubule interactions are tightly regulated by phosphorylation, with hyperphosphorylation at specific residues reducing binding affinity in disease states. Phospho-mimetic mutations at sites S214E, T231E, S262E, S356E, S396E, and S404E directly impair microtubule binding (Abraha et al., 2000, Sengupta et al., 1998, Biernat et al., 1993, Fischer et al., 2009), with four of these sites present in the hTau2N4R-E14 construct. Notably, S262 and S356 reside within the microtubule-binding domain alongside $^{275}$VQIINK$^{280}$ and $^{306}$VQIVYK$^{311}$.

While $^{275}$VQIINK$^{280}$ and $^{306}$VQIVYK$^{311}$ contribute weaker hydrogen, electrostatic, and hydrophobic interactions with α-tubulin compared to high-affinity regions like

SK(I/C)GS, structural studies suggest they support the zipper-like progression of Tau-microtubule binding initiated by the R1-R2 anchor (Brotzakis et al., 2021, Goode and Feinstein, 1994). Therefore, $^{306}$VQIVYK$^{311}$ deletion could alter physiological function.

Alongside driving β-sheet aggregation (von Bergen et al., 2001), $^{306}$VQIVYK$^{311}$ may also contribute towards neurotoxicity via alternative mechanisms. The $^{306}$VQIVYK$^{311}$ motif contains tyrosine and lysine residues (Tyr310, Lys311) susceptible to pathological post-translational modifications including phosphorylation and succinylation, both of which impair tubulin binding and promote aggregation *in vitro* (Acosta et al., 2022, Ait-Bouziad et al., 2020). Consequently, $^{306}$VQIVYK$^{311}$ deletion may confer protection through multiple mechanisms: blocking aggregation, improving microtubule interactions, and eliminating sites for pathological modifications. The relative contributions of these are unknown.

### 4.1.4 Chapter aims and objectives

In the previous **Chapter 3**, I demonstrated that deletion of $^{306}$VQIVYK$^{311}$ in TauE14 rescues phosphorylation-mediated toxicity. However, it remains unclear whether this rescue is due to reduced aggregation or alternative mechanisms of Tau mediated toxicity. In this chapter, I aim to further characterise the molecular behaviour of phospho-mimicking and aggregation-resistant Tau mutants using a series of biochemical assays and conformational analysis of the Tau expressed, assessing (1) the phosphorylation profiles of aggregation-resistant Tau, (2) the aggregation propensity of phospho-mimicking and aggregation-resistant mutants using detergent-based insolubility assays, (3) the microtubule-binding ability of each mutant and (4) the presence and relative abundance of pathogenic, misfolded Tau conformations within aging Or47b neurons. These studies will give insight to the interdependent relationship of phosphorylation and aggregation towards Tau-mediated toxicity, and identify the mechanism by which targeting $^{306}$VQIVYK$^{311}$ confers its protective effects.

**Aim**: To characterise the physiological and pathological properties of phospho-mimicking and aggregation-resistant Tau mutants to investigate the molecular mechanisms underlying toxicity.

- **Objective 1:** Assess phosphorylation profiles of aggregation-resistant Tau.
- **Objective 2:** Assessing aggregation propensity of phospho-mimicking and aggregation-resistant Tau mutants.
- **Objective 3:** Assess the microtubule binding ability of each mutant.
- **Objective 4:** Assess pathogenic conformations acquired by phospho-mimicking and aggregation-resistant Tau mutants.

## 4.2 Materials and methods

See methods **section 2.5** western blotting methods for phosphorylation detection, insolubility analysis and microtubule-binding analysis. See methods **section 2.2** for confocal methods and image acquisition. See methods **section 2.6.3** for fluorescence analysis.

## 4.3 Results

### 4.3.1 Optimising the driver line for biochemical analyses of Tau

Biochemical analyses require a high-level of Tau expression to achieve sufficient protein yields for detection and quantification. To identify a sufficient driver, I tested several GAL4 lines targeting tissues in varying sizes including the small subset of Or47b olfactory neurons used in **Chapter 3** (Or47b-Gal4), the whole olfactory bulb (Orco-Gal4), all retinal neurons (GMR-Gal4 and GMR.ninaE-Gal4) and a pan-neuronal driver Elav-Gal4.

Western blot analysis revealed that GMR.ninaE, GMR and Elav drivers produced the highest level of total Tau expression (**Figure 31**). While Elav-Gal4 is a traditional driver used for biochemical analysis due to its broad neuronal expression, when trying to generate hTau2N4R-E14 progeny, there was significant pupal lethality, making this driver non-viable for comparative analysis of all phospho-mimicking and aggregation resistant mutants.

Nevertheless, the expression of hTau2N4R using GMR drivers was similar to Elav (**Figure 31**) with the additional advantage of using the phenotypic rough-eye phenotype (**Figure 27**) to be able to confirm Tau expression. Therefore, the GMR.ninaE-Gal4 driver was selected as the driver of choice as it provided me with the high Tau expression without pupal lethality for subsequent biochemical analyses, including total Tau quantification (**Figure 21)**, phosphorylated Tau quantification (**Figure 33**) and insoluble Tau quantification (**Figure 34**, **Figure 35**).

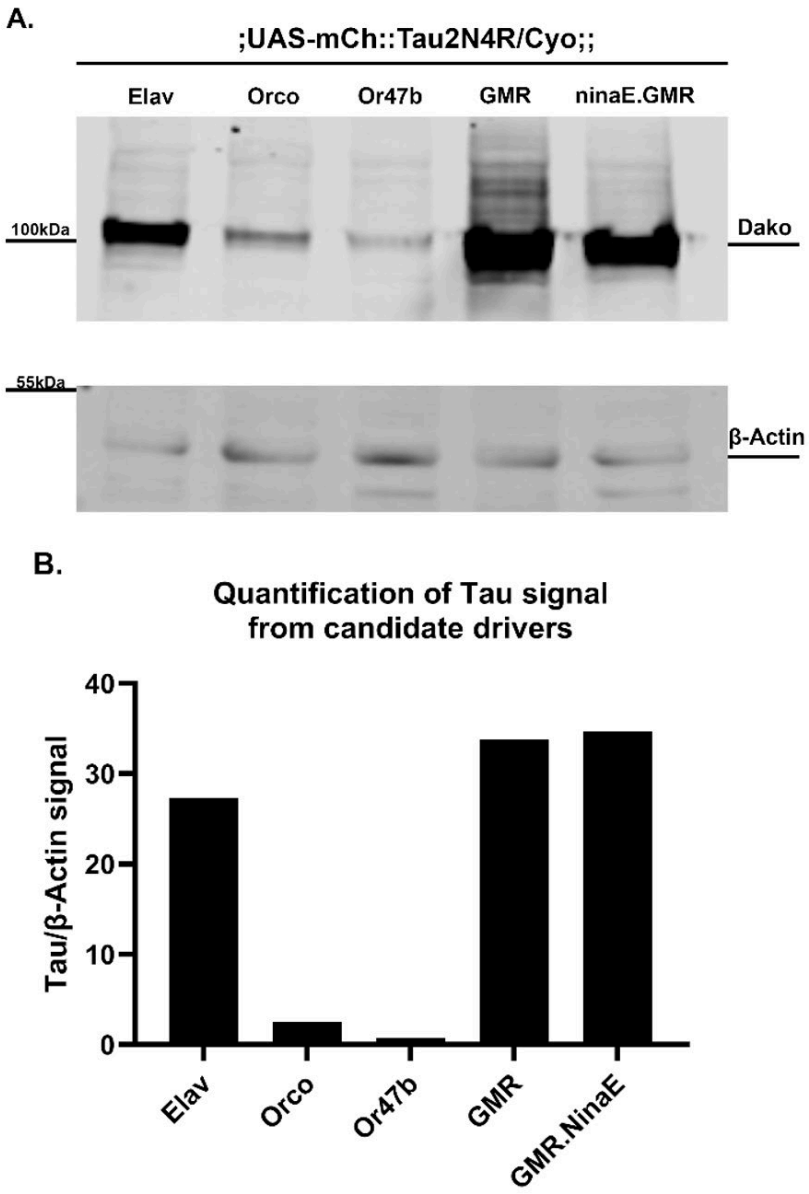


**Figure 31. Assessing candidate drivers appropriate for western blot analysis.**

A) Western blot and B) band quantification of Tau protein levels in 3-day-old male flies expressing UAS-mCh::Tau2N4R (Attp40) driven by different GAL4 drivers. Drivers tested include pan-neuronal (Elav-GAL4), olfactory neuron-specific (Orco-GAL4 and Or47b-GAL4), and retinal neuron-specific (GMR-GAL4 and GMR.NinaE-GAL4). Brain homogenates were prepared from 15 fly heads per sample. Flies were maintained at 25°C throughout development. Elav-GAL4 and both GMR drivers showed the highest Tau expression levels. Furthermore GMR.NinaE-GAL4 did not incur significant pupal lethality when crossed in with hTau2N4R-E14. N=1 biological replicate. Full blot shown in **Supplementary Figure 1.**

### 4.3.2 Could the transgenes be differentially expressed?

To confirm that $^{306}$VQIVYK$^{311}$ mediates toxicity in hTau2N4R and hTau2N4R-E14 mutants, I first needed to exclude the possibility that the observed neuroprotection in hTau2N4R-DEL and hTau2N4R-E14/DEL flies resulted from reduced transgene expression. Since Tau expression levels directly correlate with neurodegeneration severity (Wittman 2001), differential Tau protein levels could provide an alternative explanation for the protective phenotype. However, as previously shown, quantitative analysis revealed all designer mutants had equivalent expression levels in 2-day-old flies **(Figure 21).** Therefore, the neuroprotection conferred in ΔVQIVYK Tau mutants (hTau2N4R and hTau2N4R-DEL) must be attributed to the absence of the motif itself, rather than differential transgene expression.

### 4.3.3 Is the mechanism of ΔVQIVYK-mediated protection related to loss of physiological function?

Next, to determine how $^{306}$VQIVYK$^{311}$ and TauE14 mutations contributed to toxicity by loss-of function mechanisms, I assessed the microtubule binding capacity of each mutant. While deletion of the $^{306}$VQIVYK$^{311}$ motif is unlikely to significantly impair microtubule binding, given its short sequence and the presence of other high-affinity binding regions such as SK(I/C)GS (Brotzakis et al., 2021), its location within the microtubule-binding domain could potentially influence Tau-tubulin interactions. Counterintuitively, removing part of the microtubule-binding domain might be expected to reduce rather than improve microtubule

affinity. However, extensive evidence demonstrates that hyperphosphorylated Tau exhibits reduced microtubule binding, suggesting that hTau2N4R-E14 might confer neurotoxicity through diminished microtubule affinity, which could be rescued by $^{306}$VQIVYK$^{311}$ deletion in the hTau2N4R-E14/DEL mutant.

Therefore, I assessed the ability of each Tau construct (hTau2N4R, hTau2N4R-DEL, hTau2N4R-E14, and hTau2N4R-E14/DEL) to bind to the endogenous *Drosophila* microtubules using a homogenisation buffer containing pacitaxel (Taxol) which binds and stabilises microtubules.

My results showed that each Tau mutant produced a Tau-microtubule bound fraction **(Figure 32)** indicating that each mutant retained microtubule-binding capacity, behaving as true physiological Tau proteins despite their designer manipulations. No obvious differences in microtubule-binding ability were observed between hTau2N4R *versus* hTau2N4R-DEL or hTau2N4R-E14 *versus* hTau2N4R-E14/DEL. Although western blot quantification revealed a trending reduction in the microtubule-bound Tau fraction for hTau2N4R and hTau2N4R-E14 *versus* hTau2N4R-DEL and hTau2N4R-E14/DEL respectively, these differences were not statistically significant **(Figure 32 B).**

Western blot quantification should be interpreted with caution, due to the nature of the protocol. Due to homogenising the whole *Drosophila* head from GMR-driven Tau expressing flies, the resulting microtubule-Tau pellet contained an excess of endogenous tubulin which could inflate the microtubule-bound Tau fraction. More robust quantification for microtubule-Tau binding affinity, would require exogenously added microtubules at known concentrations.

Nonetheless these results demonstrate that all Tau mutants maintain their physiological ability to bind to microtubules. More importantly, these results indicate that

the mechanism of $^{306}$VQIVYK$^{311}$-mediated toxicity is most likely through a toxic gain-of-function mechanism rather than a loss of physiological function as tested here.

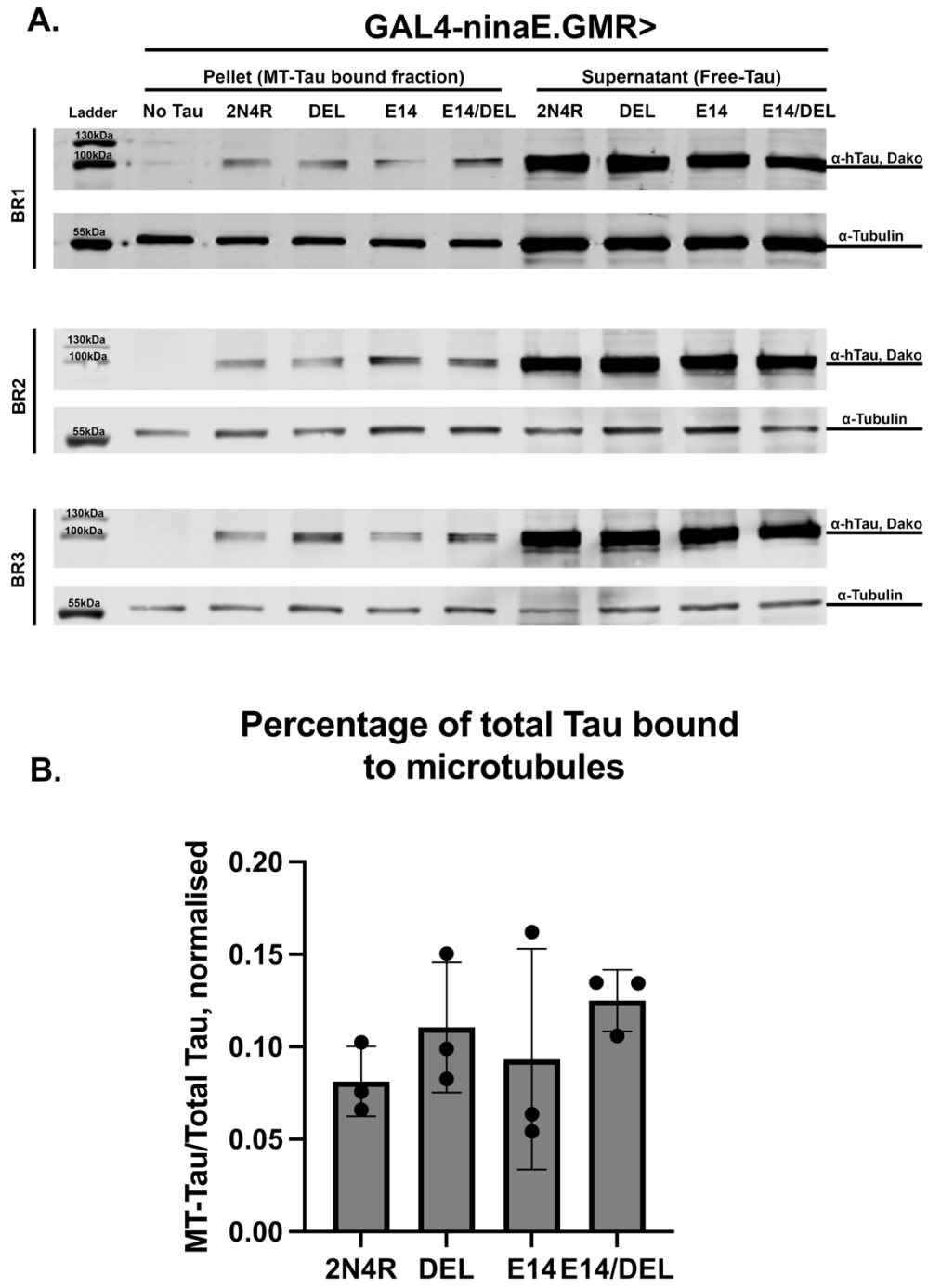


**Figure 32. Microtubule binding ability of Tau mutants.**

A) Western blot and B) quantitative analysis of microtubule (MT)-bound Tau in 14-day-old male flies expressing hTau2N4R, hTau2N4R-DEL(DEL), hTau2N4R-E14, and hTau2N4R-E14/DEL in adult retinal neurons using the GAL4-ninaE.GMR driver. Control "no Tau" flies contain the GAL4 driver only. Brain homogenates were fractioned into microtubule-bound (pellet) and unbound, free Tau (supernatant). mCherry::Tau constructs migrate to ~100kDa and α-Tubulin (loading control) migrates to ~50kDa. Error bars are plotted ±SD (N=3 biological repeats.). Statistical analysis was performed using a one-way ANOVA, and no

statistical significance was reported between genotypes when *p<0.05. Full blots can be found in **Supplementary Figure 2.**

### 4.3.4 Deletion of the $^{306}$VQIVYK$^{311}$ motif does not alter the ability of Tau to be phosphorylated

One potential gain-of-function mechanism by which ΔVQIVYK could be influencing toxicity is by altered Tau phosphorylation activity. Given that many studies have reported a bi-directional relationship between phosphorylation and aggregation (Passarella and Goedert, 2018, Zhang et al., 2020b, Perez et al., 2007), I investigated whether deleting the $^{306}$VQIVYK$^{311}$ domain affects downstream Tau phosphorylation patterns.

I used western blot analysis to examine the extent of Tau phosphorylation using established phospho-Tau antibodies AT8, AT180, AT270, PHF-1, and S262, which detect phosphorylated Tau (p-Tau) at AD-relevant epitopes (S202, T205, T231, T181, S396, S404 and S262). Since hTau2N4R-E14 is mutated at most of these sites preventing antibody recognition, I conducted the analysis only in non-phospho-mimicking Tau mutants hTau2N4R *versus* hTau2N4R-DEL.

Results showed that after 14 days of expression, the amount of total Tau and Tau phosphorylated at all epitopes tested were unchanged by the deletion of the $^{306}$VQIVYK$^{311}$ motif (**Figure 33**). This implies that deletion of the aggregation-promoting $^{306}$VQIVYK$^{311}$ domain does not change the ability of Tau to be phosphorylated. This means two things **1)** $^{306}$VQIVYK$^{311}$ does not mediate toxicity via pathological phosphorylation and **2)** that deleting $^{306}$VQIVYK$^{311}$ does not alter the ability for Tau to be recognised by endogenous kinases.

Therefore, these findings demonstrate that ΔVQIVYK-mediated neuroprotection is not through altered phosphorylation propensity, supporting the current hypothesis that $^{306}$VQIVYK$^{311}$ confers toxicity through alternative toxic gain-of-function mechanisms such as Tau aggregation.

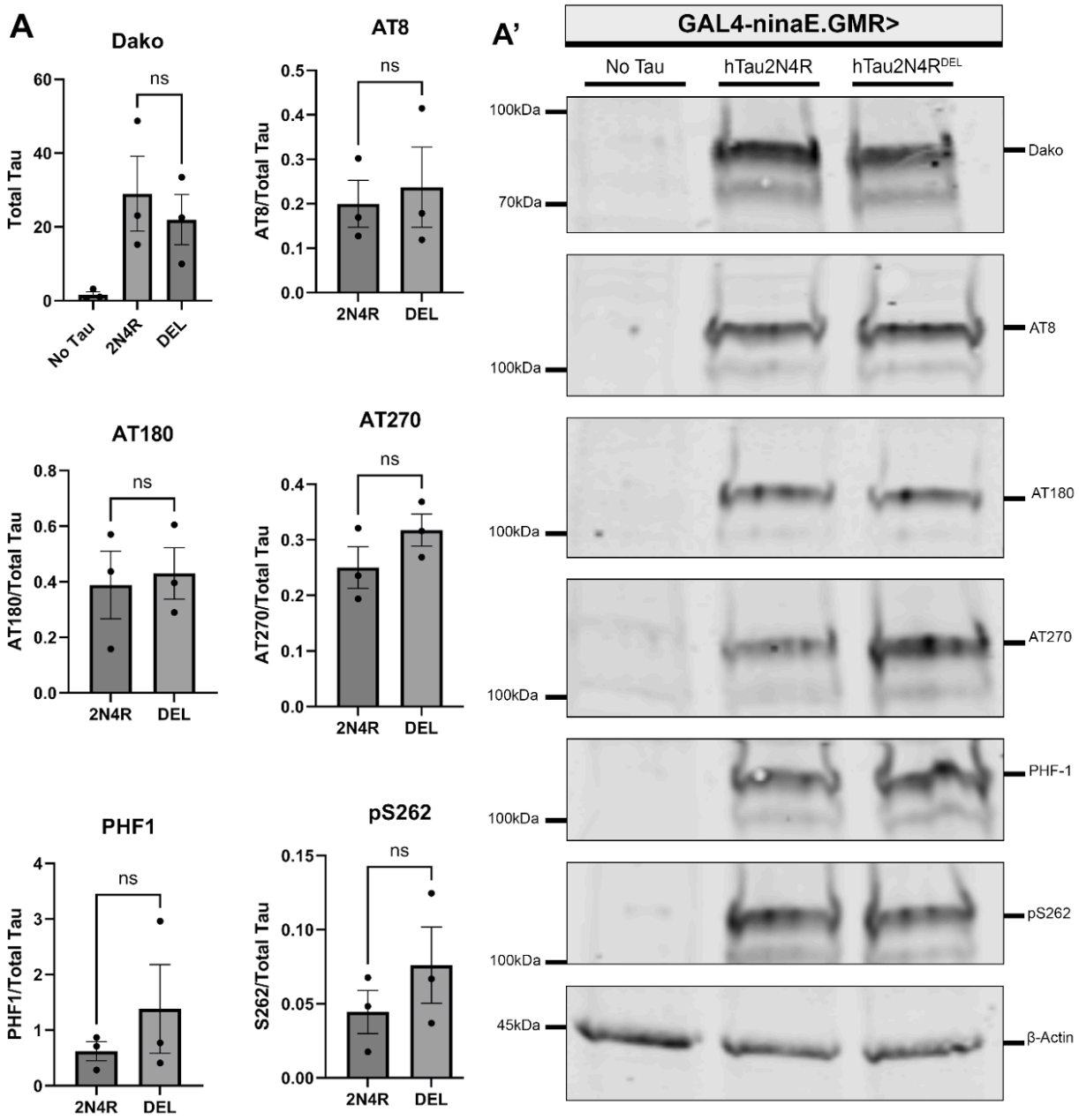


**Figure 33. Deletion of the $^{306}$VQIVYK$^{311}$ domain does not alter Tau phosphorylation at multiple AD relevant epitopes.**

(A) Quantitative analysis and (A') representative western blot of total Tau and phospho-Tau levels in 14-day-old transgenic flies expressing hTau2N4R versus hTau2N4R-DEL using the GMR.ninaE-Gal4 driver. Phosphorylation was assessed using antibodies: AT8 (S202,T205), AT180 (T231), AT270 (T181), PHF-1(S396, S404) and S262. Total Tau was detected using anti-hTau(Dako). No significant differences were observed between genotypes for total Tau or any phospho-epitope tested. mCherry-tagged hTau2N4R constructs migrate at ~100 kDa; β-actin (loading control) migrates at ~45 kDa. Data presented as mean ±SD. Statistical analysis: One-way ANOVA with significance set at *p< 0.05. N = 3 biological repeats of 15 male fly heads.

### 4.3.5 Reduced aggregation contributes to but is not the only factor by which ΔVQIVYK confers neuroprotection.

Since $^{306}$VQIVYK$^{311}$ does not mediate toxicity through altered phosphorylation, I investigated whether it could be mediating toxicity via aggregation. Several studies have shown that mimicking phosphorylation promotes Tau aggregation, which is associated with toxicity (Katsinelos et al., 2021, Zhang et al., 2022a, Padmanabhan et al., 2024, Beharry et al., 2013, Keramidis et al., 2020, Talmat-Amar et al., 2011). Therefore, I hypothesized that hTau2N4R-E14 confers toxicity through enhanced aggregation, while $^{306}$VQIVYK$^{311}$ deletion reduces aggregation as a key domain traditionally associated with aggregation (von Bergen et al., 2001, von Bergen et al., 2000).

I assessed Tau protein solubility, which is an established method of quantifying Tau aggregates, because Tau becomes progressively less soluble as it aggregates during disease progression (Haroutunian et al., 2007, Schöll et al., 2016, Levy et al., 2022, Cowan et al., 2015, Colodner and Feany, 2010, Ramsden et al., 2005, Sahara et al., 2002, Katsuno et al., 2005, Ercan-Herbst et al., 2019)). Given that TauE14 promotes Tau aggregation and reduces solubility in *Drosophila* (Katsinelos et al., 2021), and that $^{306}$VQIVYK$^{311}$ is a key aggregation domain involved in β-sheet formation and Tau fibrillisation (von Bergen et al., 2001, von Bergen et al., 2000), I quantified the relative amounts of insoluble Tau fractions in each mutant to assesses $^{306}$VQIVYK$^{311}$-mediated aggregation.

Two distinct solubility assays were performed using two detergents to fractionate different Tau species by aggregation state (**Table 8**): sodium dodecyl sulfate (SDS) for isolating highly resistant insoluble aggregates, and N-lauroylsarcosine (sarkosyl) for moderately insoluble aggregates. The SDS-based fractionation protocol enriched for insoluble Tau aggregates as previously described (Cowan et al., 2015, Sealey et al., 2017, Mancuso et al., 2019), yielding multiple fractions: pre-fibrillar species (S1: aqueous soluble, S2: aqueous insoluble/SDS soluble, NS1: aqueous and SDS soluble Tau + granular Tau

oligomers) and fibrillar species (S3: SDS insoluble granular Tau oligomers, NS2: insoluble NFT-enriched fraction) (**Table 8, Supplementary Figure 3**).

**Table 8. Contents guide of the Tau species separated in each Tau-enriched fraction from the Sarkosyl solubility protocol (green rows) or the SDS solubility protocol (pink rows).**

| Fraction | Tau species | Centrifuge protocol |
|---|---|---|
| Aqueous soluble Tau (SN1) | Contains soluble, mostly cytosolic, Tau monomers which have normal physiological functions. There will also be pathological P-Tau and small pathological oligomers. | Sarkosyl; 1h x 100,000*g* |
| Sarkosyl soluble Tau (SN3) | Contains pre-fibrillar Tau species which are any intermediate sized Tau aggregates. This includes misfolded and oligomeric Tau species, all which dissolve in Sarkosyl. | Sarkosyl; Supernatant of 2h x 100,000*g* + 1% Sarkosyl |
| Sarkosyl insoluble Tau (SN2) | Contains aggregated Tau species, including fibrils eg. SFs and PHFs. | Sarkosyl; Pellet of 2h x 100,000*g* + 1% Sarkosyl |
| Aqueous soluble Tau (NS1) | Contains soluble, mostly cytosolic, Tau monomers which have normal physiological functions. There will also be pathological P-Tau and small pathological oligomers. | SDS; 30min x 100,000*g* |
| NFT-enriched Tau (NS2) | Contains highly aggregated Tau species resistant to SDS, including fibrillar Tau such as PHFs and NFTs which are solubilised by urea. | SDS; Pellet washed, 30min x 100,000*g* + 5% SDS, 12hr agitation |
| Monomeric Tau (S1) | Contains monomeric, aqueous soluble Tau | SDS; 2h x 186,*000g* |
| SDS-soluble Tau (S2) | Contains aqueous insoluble, SDS-soluble pre-fibrillar Tau species which are any intermediate sized Tau aggregates. This includes misfolded and oligomeric Tau species, all which dissolve in SDS. | SDS; 2h x 186,000*g* + 5% SDS |

| | | |
|---|---|---|
| Granular Tau oligomers (S3) | Contains pre-fibrillar granular Tau oligomers, considered to be an intermediate form of Tau fibril | SDS; Pellet washed, 2h x 186,000*g* + 8% SDS, 12h agitation |

Starting with the SDS-solubility assay, which fractionates more robust fibrillar species, results revealed no significant differences in Tau solubility between genotypes across all fractions examined (**Figure 34 B-F**). While the majority of Tau in all mutants was detected in the monomeric, aqueous soluble fractions (S1 and NS1) with smaller amounts in SDS-insoluble fibrillar and oligomeric fractions (NS2 and S3), the distribution patterns were remarkably similar between hTau2N4R, hTau2N4R-DEL, hTau2N4R-E14, and hTau2N4R-E14/DEL variants **(Figure 34).** This indicates that $^{306}$VQIVYK$^{311}$ deletion does not alter Tau aggregation propensity only.

This suggests that toxicity conferred by hTau2N4R and hTau2N4R-E14 is mostly by monomeric and oligomeric Tau species. More importantly, ΔVQIVYK does not confer protection by reducing the ability for fibrillar Tau species to form.

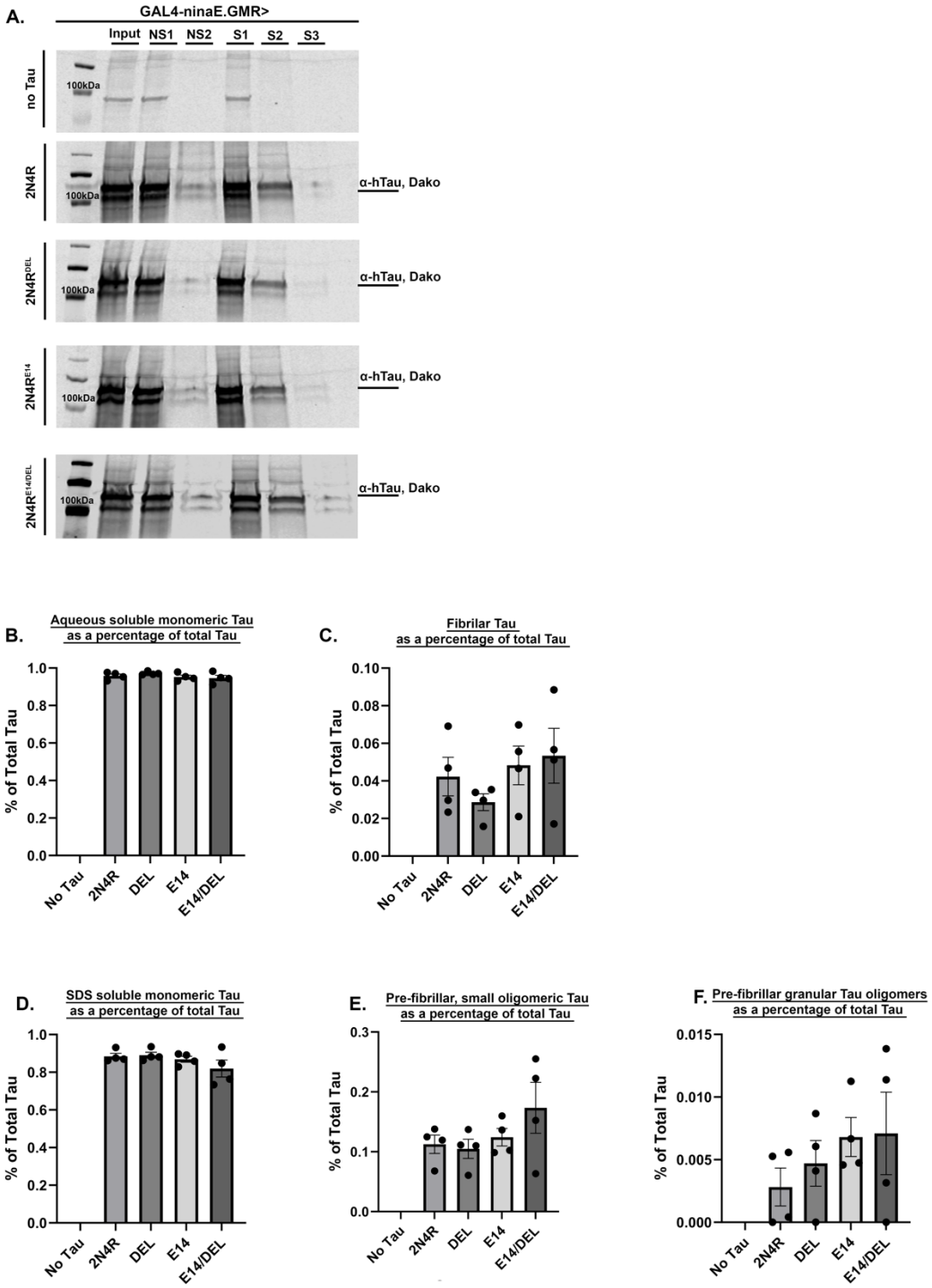


**Figure 34. Tau solubility does not differ between phospho-mimicking and ΔVQIVYK mutants using SDS detergent.**

A) Representative Western blots of sequential detergent fractionation showing input (total Tau) and extracted NFT(NS1, NS2) and GTO(S1, S2, S3) enriched fractions from 14-day-old transgenic flies expressing hTau2N4R, hTau2N4R-DEL(DEL), hTau2N4R-E14, and hTau2N4R-E14/DEL driven by GMR-NinaE-GAL4. mCherry-tagged Tau constructs migrate at ~100 kDa. B-F) Quantification of each fraction as percentage of total Tau input: B)NS1, C)NS2, D)S1, E)S2 and F)S3. No significant differences were observed between genotypes across any fraction. Genetic crosses set at 18°C and progeny collected and aged at 29°C. Data

represent mean ±SD (N=4 biological replicates, 100 male heads each). *p<0.05. Statistical analysis was a one-way ANOVA. Full blots shown in **Supplementary Figure 4.**

### 4.3.6 Deletion of $^{306}$VQIVYK$^{311}$ does not eliminate insoluble Tau species.

As most of the Tau species produced by these mutants were found in the monomeric and oligomeric fractions, I next sought out to increase protein load and use a milder detergent for more robust separation of soluble *versus* insoluble Tau species. This was achieved using an established sarkosyl-based solubility protocol (Colodner and Feany, 2010), (**Supplementary Figure 6**) which produced three distinct fractions containing aqueous soluble (SN1), sarkosyl soluble (SN3), and sarkosyl insoluble (SN2) Tau species (**Table 8, Figure 35).** To enhance detection of insoluble Tau species, I increased total Tau protein yield by increasing the temperature at which genetic crosses were set from 18ºC to 25ºC and increasing the number of fly heads from 100 to 164 per sample, yielding ~14.6µg Tau **(Supplementary Figure 5).**

Using this new sarkosyl-based insolubility assay, results showed that phospho-mimicking hTau2N4R-E14 produced the highest levels of insoluble Tau species (SN2) compared to other variants (**Figure 35 A, C** and **D**). Importantly, $^{306}$VQIVYK$^{311}$ deletion showed consistent trends in producing increased soluble monomeric Tau and reduced insoluble fibrillar species in both genetic backgrounds ( hTau2N4R *versus* hTau2N4R-DEL and hTau2N4R-E14 *versus* hTau2N4R-E14/DEL) (**Figure 35 C**). While not statistically significant, this trend suggests that mimicking phosphorylation promotes aggregation, while $^{306}$VQIVYK$^{311}$ deletion partially supresses aggregation.

Similar trends are also seen in the quantified proportion of fibrillar: oligomeric Tau species (SN2:SN3) where flies expressing hTau2N4R-E14 produced the highest mean signal of insoluble Tau, while all other mutants showed ~80% lower fibrillar ratios,

including hTau2N4R-E14/DEL (**Figure 35 D**). However, no differences in the amount of fibrillar Tau species were observed between hTau2N4R *versus* hTau2N4R-DEL (**Figure 35 D**).

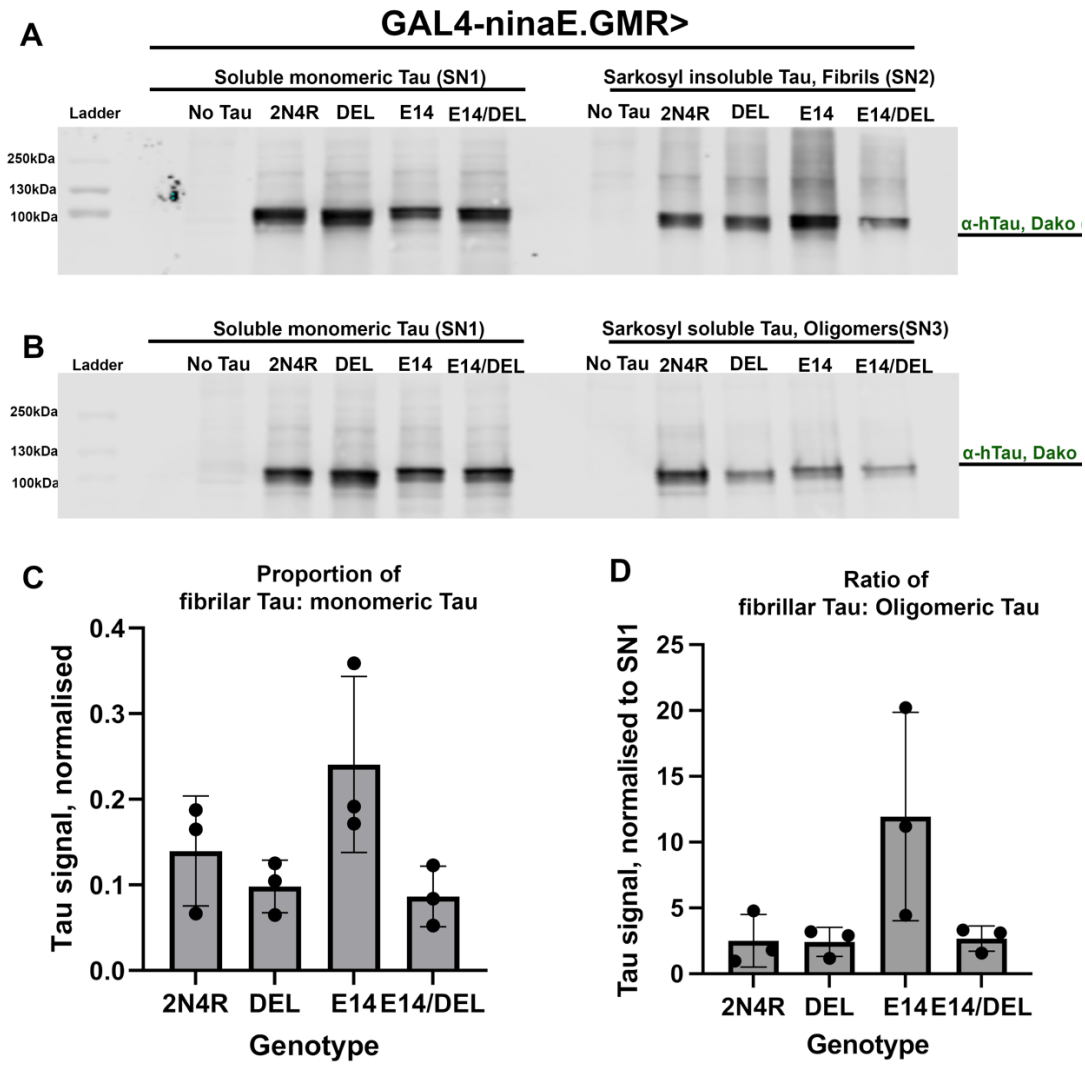


**Figure 35. Aqueous soluble, sarkosyl-soluble and sarkosyl-insoluble fractions isolated from transgenic *Drosophila* brain homogenates.**

Comparison of aqueous soluble monomeric Tau (SN1), sarkosyl insoluble, fibrillar Tau(SN2) and sarkosyl soluble, oligomeric Tau (SN3) enriched fractions between different transgenic flies tested after 14 days of aging (mCherry tagged hTau2N4R, hTau2N4R-DEL, hTau2N4R-E14 and hTau2N4R-E14/DEL). Driver used was GAL4-GMR.ninaE. Genetic crosses set up at 25°C and progeny aged at 29°C (n=164 heads 50:50 male:female). (A-B) Representative Western blots probed with anti-hTau (Dako) comparing aqueous soluble fraction to A) sarkosyl insoluble and B) sarkosyl soluble fractions. mCherry-tagged Tau constructs migrate at ~100 kDa. (C-D) Quantitative analysis of fraction ratios normalised to respective inputs: C) sarkosyl insoluble:aqueous soluble Tau and D) sarkosyl insoluble:sarkosyl soluble Tau. No significant differences were observed between genotypes in any fraction or ratio analysed.

Graphs represent mean ±SD (N=3 biological replicates). Statistical analysis: one-way ANOVA. Full blots shown in **Supplementary Figure 7** and **Supplementary Figure 8**.

These findings suggest that while $^{306}$VQIVYK$^{311}$ contributes to aggregation, it is not essential for high molecular weight species formation. Critically, both hTau2N4R-DEL and hTau2N4R-E14/DEL retain substantial insoluble Tau species yet exhibit no toxicity in olfactory or retinal neurons (**Chapter 3, Figure 24** and **Figure 27**). This indicates that $^{306}$VQIVYK$^{311}$-mediated toxicity likely involves conformational rather than quantitative differences in Tau aggregates. One way to look at conformation is to assess the β-sheet content which I did not do in my experiments. Instead, I chose to assess whether each mutant produced different pathogenic conformations using a conformational sensitive antibody *in vivo.*

### 4.3.7 $^{306}$VQIVYK$^{311}$ mediates the production of pathogenic Tau conformers.

Tau is an intrinsically disordered protein lacking a secondary structure in physiological conditions (Schweers et al., 1994). In AD, Tau misfolds to adopt pathological conformations, which can be recognised by conformation-specific antibodies such as MC1, Alz-50, Tau-66 and MN423 **(Supplementary Table 1).** I selected MC1 to assess Tau conformation for its availability, widespread use and reliability having been validated thoroughly in human AD postmortem tissue and transgenic Tauopathy models (Jicha 1999 (Jicha et al., 1997, Jicha et al., 1999, Eckermann et al., 2007, Koss et al., 2016, Weaver et al., 2000, Götz et al., 2001, Ramsden et al., 2005)). MC1 is a purely conformational-dependent antibody, binding Tau independently of phosphorylation or other pathological PTMs. As deletion of $^{306}$VQIVYK$^{311}$ still produced insoluble Tau species, I next assessed whether $^{306}$VQIVYK$^{311}$ affects Tau conformation by immunostaining O47b-expressing neurons with MC1, visualised using confocal microscopy.

Results showed that MC1 staining was specific to Tau-expressing flies, with no signal detected in no Tau controls (**Figure 36 A3**). After 14 days of aging, flies expressing hTau2N4R, hTau2N4R-DEL and hTau2N4R-E14/DEL each produced MC1-specific labelling, restricted to small puncta ~0.2-2µm in size within the Or47b neurons (**Figure 36 B3, C3**, and **E3**). MC1 positive accumulates in these animals colocalised strongly with mCherry::Tau and were primarily localised to the axonal terminals at the periphery of the Or47b glomerulus, representing only a minor proportion of the total Tau (**Figure 36 B2** *versus* **B3, C2** *versus* **C3**, and **E2** *versus* **E3**).

In contrast, hTau2N4R-E14 expressing neurons showed a striking increase in the number and size of MC1-positive accumulates, staining misfolded Tau throughout the axons and extending throughout the commissure of the Or47b glomeruli (**Figure 36 D3**). Although the majority of hTau2N4R-E14 Tau expressed was MC1 positive, some accumulations were mCherry positive but MC1-negative (**Supplementary Figure 12**) indicating that not all aggregates formed by phospho-mimicking Tau adopt the MC1 misfolded conformation.

Quantification of MC1 signal confirmed that hTau2N4R-E14-expressing neurons contained a significantly higher proportion of misfolded Tau compared to all other genotypes (**Figure 36 B**). Importantly, these pathological conformers were substantially suppressed by $^{306}$VQIVYK$^{311}$ deletion, with hTau2N4R-E14/DEL showing profoundly reduced MC1 reactivity compared to hTau2N4R-E14 (**Figure 36 D3** *versus* **E3, B**). A similar trend toward reduced misfolded Tau was observed between hTau2N4R and hTau2N4R-DEL, though this did not reach statistical significance (**Figure 36 B3** versus **C3, B**). Collectively, it suggests that mimicking phosphorylation promotes the formation of misfolded Tau conformations, while $^{306}$VQIVYK$^{311}$ deletion supresses pathogenic conformers forming.

Western blot analysis of GMR-driven brain homogenates probed with MC1 confirmed these trends, showing increased MC1 reactivity in hTau2N4R-E14 flies under denaturing conditions, though quantification was not significant (**Supplementary Figure 13**).

Collectively, these findings demonstrate that ΔVQIVYK-mediated neuroprotection is through reducing the production of toxic conformations of Tau species, rather than mechanisms of aggregation, phosphorylation or improving physiological function. While the deletion of $^{306}$VQIVYK$^{311}$ modestly reduced insoluble Tau species from forming, they significantly change the toxic conformational state of Tau.

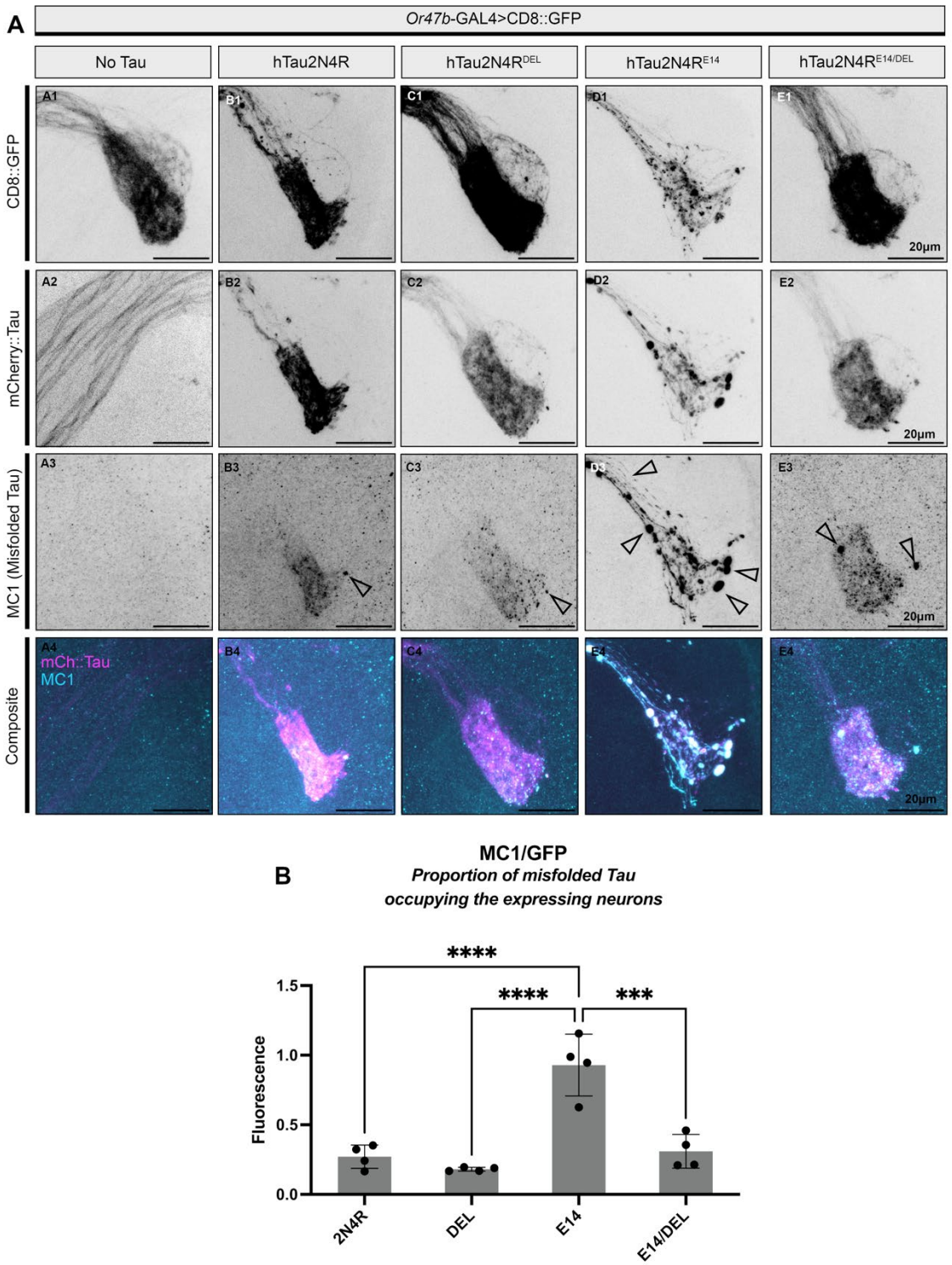


**Figure 36. $^{306}$VQIVYK$^{311}$ deletion rescues phosphorylation dependent production of pathogenic Tau conformations.**

A) Maximum projection confocal images of the antennal lobe in the brain of 14-day-old flies expressing mCherry::Tau mutants in the Or47b neurons. Rows represent isolated channels 1) membrane bound CD8::GFP tagging the neuron morphology, 2) mCherry::Tau and 3)MC1 antibody detecting pathological misfolded conformations of Tau and 4) composite image of mCherry::Tau and MC1 to show the co-localisation of misfolded Tau within the total Tau expressed. Arrows indicate MC1-positive accumulations, which are substantially more abundant and extensive in hTau2N4R-E14 neurons compared to all other genotypes. B) Automated quantification of misfolded Tau proportion within expressing neurons. Analysis

performed by Dr. Miguel Ramirez-Moreno using MATLAB-based automated segmentation of GFP signal to distinguish neuron-specific (GFP-positive) from background (GFP-negative) pixels. Fluorescence values represent average MC1 signal within GFP-positive pixels minus background signal from GFP-negative pixels. hTau2N4R-E14 shows significantly elevated misfolded Tau levels, which are rescued by $^{306}$VQIVYK$^{311}$ deletion in hTau2N4R-E14/DEL. Graphs represent mean ± SD (N=4 from single biological replicate). Statistical analysis: one-way ANOVA with Tukey's multiple comparisons (***p<0.001, ****p<0.0001). Raw fluorescence values and manual quantification comparison shown in **Supplementary Figure 9 and Supplementary Figure 10.**

## 4.4 Discussion

This chapter addressed several potential mechanisms by which phospho-mimicking hTau2N4R-E14 exacerbated neurotoxicity in Or47b neurons and how deletion of $^{306}$VQIVYK$^{311}$ reversed all phosphorylation-mediated toxicity in **Chapter 3**. To better understand the mechanism by which $^{306}$VQIVYK$^{311}$ confers neuroprotection, I investigated its contributions to microtubule binding, downstream phosphorylation, misfolding, and aggregation. In this Chapter I demonstrate that $^{306}$VQIVYK$^{311}$ confers neuroprotection by preventing the formation of pathological, misfolded Tau conformers rather than simply blocking aggregation or hyperphosphorylation.

### 4.4.1 $^{306}$VQIVYK$^{311}$ deletion does not compromise physiological microtubule binding function

A critical concern for any $^{306}$VQIVYK$^{311}$-targeting therapeutic is whether disrupting this domain would impair Tau's normal physiological functions. While FRET studies suggest $^{306}$VQIVYK$^{311}$ forms weak interactions with tubulin (Brotzakis et al., 2021), I show that deletion of $^{306}$VQIVYK$^{311}$ did not eliminate the ability of either hTau2N4R-DEL or hTau2N4R-E14/DEL mutants to bind to *Drosophila* microtubules. This supports the existing evidence that $^{306}$VQIVYK$^{311}$ mostly confers toxicity through gain-of-function mechanisms facilitating Tau misfolding and aggregation (von Bergen et al., 2001, von Bergen et al., 2000) rather than loss of physiological function.

This preservation of microtubule binding capacity has important implications for therapeutic development. $^{306}$VQIVYK$^{311}$-targeted therapies could potentially suppress pathogenic mechanisms of Tau-mediated toxicity while preserving Tau's essential physiological microtubule binding functions.

### 4.4.2 $^{306}$VQIVYK$^{311}$-mediated neuroprotection is independent of phosphorylation status

Results from **Chapter 3** provided compelling evidence that Tau aggregation and toxicity are downstream consequences of hyperphosphorylation, critically dependent on the $^{306}$VQIVYK$^{311}$ motif to mediate Tau accumulation and neurodegeneration. Results from this Chapter show that phosphorylation levels at multiple disease-associated epitopes were unchanged between hTau2N4R and hTau2N4R-DEL animals. This indicates that the suppression of neuronal degeneration and Tau accumulation in **Chapter 3** is not because of reduced phosphorylation capacity at these sites and implies that $^{306}$VQIVYK$^{311}$ does not mediate pathogenic Tau phosphorylation.

However, this finding adds to a conflicting body of literature regarding $^{306}$VQIVYK$^{311}$'s influence on phosphorylation. Several other groups have reported that mutagenic deletion or therapeutic targeting of $^{306}$VQIVYK$^{311}$ alters phosphorylation patterns, while others, like my study, observe no significant changes, summarised below in **Table 9**. For example, a *Drosophila* study reported hTau0N4R-ΔVQIVYK-expressing flies significantly reduced phosphorylation at several overlapping epitopes tested (Passarella and Goedert, 2018). In contrast, my findings align with one study showing an anti-$^{306}$VQIVYK$^{311}$ aggregation inhibitor treated Tau1N4R-P301S mice had no significant changes to phosphorylation levels across multiple tissues (Zhang et al., 2020b). The variability may be due to differences in Tau isoforms, expression systems, aggregation states, or tissue context. This is further highlighted in Zhang et al. 2020, who showed that targeting $^{306}$VQIVYK$^{311}$

with the peptide inhibitor "p-NH" produced different phosphorylation outcomes *in vitro* versus *in vivo,* and even between different brain regions within the same model.

Collectively, these observations suggest that the influence of $^{306}$VQIVYK$^{311}$ on phosphorylation may be Tau conformation and tissue specific. Therefore, it should be considered that $^{306}$VQIVYK$^{311}$-targeted therapeutic approaches may have variable efficacies across different Tauopathies.

**Table 9. Epitope specific phosphorylation changes upon $^{306}$VQIVYK$^{311}$ deletion or inhibition.**

Each row represents a phosphorylation site, while columns represent key studies. Key: ↑= significant increase, ↓= significant decrease, → = no change in phosphorylation. N/A = epitope was not analysed.

| **Tau** | **Tau3R-ΔVQIVYK fragments** | **FL Tau0N4R-ΔVQIVYK** | ***PHF-6 fibrils* + "p-NH", *$^{306}$VQIVYK$^{311}$ inhibitor*** | **"p-NH", *$^{306}$VQIVYK$^{311}$ inhibitor*** | **"p-NH", *$^{306}$VQIVYK$^{311}$ inhibitor*** | **"(TAT)-7H", Tau aggregation inhibitor** | **FL mCh::Tau2N4R-ΔVQIVYK** |
|---|---|---|---|---|---|---|---|
| **Model** | ***In vitro* COS-F cells** | ***Drosophila*** | ***In vitro* TauP301S-*N2a cells*** | **Tau1N4R-P301S mice, cortex** | **Tau1N4R-P301S mice, hippocampus** | ***In vitro* TauP301S-iPS neurons** | ***Drosophila*** |
| **Ref** | **(Perez et al., 2007)** | **(Passarella and Goedert, 2018)** | **(Zhang et al., 2020b)** | **(Zhang et al., 2020b)** | **(Zhang et al., 2020b)** | **(Kondo et al., 2021)** | **This thesis** |
| **T181** | N/A | ↓ | ↓ | → | → | N/A | → |
| **S199** | N/A | N/A | → | → | → | N/A | N/A |
| **S202** | N/A | ↓ | ↓ | → | → | ↓ | → |
| **T205** | N/A | ↓ | N/A | N/A | N/A | ↓ | → |
| **T231** | N/A | ↓ | ↓ | ↓ | → | N/A | → |
| **S262** | ↑ | N/A | N/A | N/A | N/A | N/A | → |
| **S356** | ↑ | N/A | N/A | N/A | N/A | N/A | N/A |
| **S396** | ↑ | N/A | ↓ | → | → | N/A | → |
| **S404** | ↑ | N/A | ↓ | ↓ | → | N/A | → |
| **S422** | ↑ | N/A | N/A | N/A | N/A | N/A | N/A |

### 4.4.3 $^{306}$VQIVYK$^{311}$ influences Tau conformation rather than aggregation

The most important finding in this results Chapter challenges the consensus that $^{306}$VQIVYK$^{311}$ mediates toxicity by promoting Tau aggregation, and that therapeutically targeting it reduces toxicity by reducing total aggregate burden (von Bergen et al., 2001, von Bergen et al., 2000, Passarella and Goedert, 2018). While multiple other studies have shown that removing or inhibiting $^{306}$VQIVYK$^{311}$ abolishes Tau aggregation, unexpectedly I show that deletion of $^{306}$VQIVYK$^{311}$ in phospho-mimicking Tau (hTau2N4R-E14/DEL) did not significantly reduce overall levels of insoluble Tau compared to hTau2N4R-E14. All mutants, including both ΔVQIVYK mutants produced substantial sarkosyl-insoluble fractions consistent with intermediate-stage Tau oligomers and aggregates that precede mature tangle pathology. Notably, none of the mutants produced a strong SDS-insoluble fraction, indicating an absence of highly cross-linked, late-stage fibrils typical of advanced Tauopathy.

The presence of insoluble fibrillar and oligomeric Tau species in ΔVQIVYK mutants implies that insoluble, high molecular weight (HMW) Tau species can form independently of the $^{306}$VQIVYK$^{311}$ motif. For example, via alternative aggregation pathways, perhaps forming partial fibrils or protofibrils through the second aggregation motif $^{275}$VQIINK$^{280}$ (von Bergen et al., 2000). This supports the current consensus that the Tau aggregation cascade is not linear, multi-factorial and may have multiple target points for anti-aggregation therapies (Cowan and Mudher, 2013). More importantly, it shows that $^{306}$VQIVYK$^{311}$ mediates toxicity not solely through aggregation, but through changes in conformational state, structure and pathogenic function of the Tau species formed. Indeed, partial rescue of pathology by Tau aggregation inhibitors in preclinical studies does prove that aggregation contributes towards toxicity. However, my findings suggest that aggregation and conformation collectively determine Tau toxicity, which are both mediated by $^{306}$VQIVYK$^{311}$.

Indeed, conformational analysis of the Tau species formed *in vivo* using the MC1 antibody which recognises pathological misfolded Tau conformers showed that ΔVQIVYK critically reduced the population of phosphorylation induced pathological Tau conformers. Critically, this demonstrates that $^{306}$VQIVYK$^{311}$ deletion doesn't prevent pathological aggregation per se but fundamentally alters the conformation of Tau to favour non-toxic species. Notably, both $^{306}$VQIVYK$^{311}$ deletion mutants hTau2N4R-DEL and hTau2N4R-E14/DEL did not eliminate MC1 immunoreactivity, showing that $^{306}$VQIVYK$^{311}$ mediates a significant proportion, but not all pathological conformations formed.

These findings contrast with previous work showing no MC1 immunoreactivity in Tau0N4R-ΔVQIVYK expressed in *Drosophila* retinal neurons (Passarella and Goedert, 2018). These differences could be explained by isoform-specific effects or selective neuronal vulnerability of different tissues tested (Sivanantharajah et al., 2025). Isoform-specific pathological behaviours are highlighted by a recent cryo-EM study showing that phospho-mimicking Tau at 12 sites (PAD12) forms bona fide PHF filaments in the 0N3R background whereas only protofilaments are formed by 0N4R, demonstrating that identical pathogenic modifications can produce distinct structural conformations depending on the isoform background (Lövestam et al., 2025). Importantly, this suggests that the effectiveness of targeting $^{306}$VQIVYK$^{311}$ may vary across Tauopathy subtypes depending on their isoform composition.

Collectively, these findings demonstrate that $^{306}$VQIVYK$^{311}$ mediates toxicity mostly through controlling pathogenic conformations rather than simply promoting Tau aggregation. My results align with recent evidence that conformation rather than Tau abundance, determines the pathological behaviour of Tau (Martinez et al., 2025, Jury-Garfe et al., 2024).

The consensus view is that small multimeric and oligomeric Tau species principally confer cellular toxicity, contributing towards impaired axonal transport, synaptic dysfunction, Tau aggregation and neurodegeneration in the absence of tangle pathology (Flach et al., 2012, Tian et al., 2013, Andorfer et al., 2005, Santacruz et al., 2005). However that is not to say all aggregated Tau intermediates are toxic. Recently, HMW Tau species including oligomers have been found in brains of individuals with asymptomatic AD with distinct structural and biochemical properties to that of symptomatic AD samples, demonstrating that not all oligomers are pathogenic (Jury-Garfe et al., 2024). Similarly, Martinez et al., demonstrated that HMW Tau species are also isolated in control brains at the same weight as AD brains, yet they lack seeding competency. These findings demonstrate that it is the conformation, rather than aggregate size or abundance which determines Tau's toxicity (Martinez et al., 2025). In line with this, hTau2N4R-DEL and hTau2N4R-E14/DEL mutants produced a substantial HWM sarkosyl insoluble fraction which had significantly less MC1 immunoreactivity, suggesting that the Tau species formed adopted an inert structural conformation, perhaps similar to seeding incompetent, non-toxic species found in control brains (Martinez et al., 2025).

This does not dismiss aggregation as a critical contributor towards pathology, however it emphasises that Tau aggregation is not likely the sole cause of toxicity, and may explain why current aggregation inhibitors only partially reduce the effects of Tau toxicity (Kondo et al., 2021, Zhang et al., 2020b, Soeda et al., 2019).

### 4.4.4 Implications of $^{306}$VQIVYK$^{311}$-mediated conformational changes

The conformational differences I observed within the ΔVQIVYK mutants may have profound implications for Tau's cellular interactions. Tau's interactions with other homeostatic cellular proteins are highly dependent on its PTM state, cellular localisation, conformation, and aggregation state (Kavanagh et al., 2022). Martinez et al., also

demonstrate that the HMW Tau species isolated from AD and control brains form strikingly distinct interactome complexes. AD Tau-seeds had gained over twice as many interacting partners including synaptic, mitochondrial and vesicular proteins, whilst losing a significant population of binding partners only present in control HMW species (Martinez et al., 2025). Likewise, high MC1 immunoreactivity of hTau2N4R-E14 may reflect pathogenic conformations which enable an expanded disease-associated interactome, while ΔVQIVYK promotes conformations that maintain a protective, non-disease interactome. Prevention of pathological interactions could explain why ΔVQIVYK mutants produce HMW insoluble Tau species while functionally being non-toxic.

Interestingly, $^{306}$VQIVYK$^{311}$ itself contains direct binding sites for molecular chaperones and RNA-binding proteins which supress misfolding and aggregation, many of which have *Drosophila* homologs **(Supplementary Table 2).** For example, immunophilin FKBP12 and several heat shock proteins (Hsp's) including Hsp27 all which modulate protein solubility and preventing protein misfolding directly bind to $^{306}$VQIVYK$^{311}$ (Zhang et al., 2022b, Jiang et al., 2023, Baughman et al., 2018). Similarly, RNA-binding stress granule protein G3BP2 which binds to the MBRD spanning both $^{275}$VQIINK$^{280}$ and $^{306}$VQIVYK$^{311}$ also suppresses aggregation (Wang et al., 2023). Targeting $^{306}$VQIVYK$^{311}$ could therefore diminish protective chaperone activity by removing key docking interfaces. While in my model the reduction in Tau-mediated toxicity by deleting $^{306}$VQIVYK$^{311}$ outweighs the loss of possible protective chaperone interactions, it highlights a potential caveat for therapeutic strategies which aim to totally immobilise $^{306}$VQIVYK$^{311}$ or $^{275}$VQIINK$^{280}$ motifs to prevent aggregation-mediated toxicity.

### 4.4.5 Implications for therapeutic design.

The findings from this chapter have several important implications for developing $^{306}$VQIVYK$^{311}$-targeting therapeutics. This study provides mechanistic evidence supporting

$^{306}$VQIVYK$^{311}$ as a viable therapeutic target for suppressing Tau-mediated toxicity and neurodegeneration while preserving Tau's physiological functions, including microtubule binding and phosphorylation. More importantly, these findings validate $^{306}$VQIVYK$^{311}$ as a regulator of conformational-mediated Tau toxicity, providing support for the ongoing developments of therapeutic design against this domain. Tau aggregation inhibitors that target $^{306}$VQIVYK$^{311}$ are discussed in more detail in **Chapter 5.**

## 4.5 Conclusions

Collectively, this results chapter demonstrates that deletion of the $^{306}$VQIVYK$^{311}$ motif confers neuroprotection through multiple mechanisms, most predominantly by reducing the formation of pathological, misfolded Tau conformers, while also reducing aggregation as previously reported. Although insoluble Tau species still form in ΔVQIVYK mutants, they form structurally distinct conformations that produce non-toxic intermediate aggregates rather than highly misfolded MC1-positive species. These findings support $^{306}$VQIVYK$^{311}$ as a key, but not exclusive, modulator of Tau misfolding and aggregation. However, the protective effect of targeting $^{306}$VQIVYK$^{311}$ is contextually dependent. Anti-$^{306}$VQIVYK$^{311}$ therapeutic strategies may therefore need to be tailored according to isoform, disease subtype and disease stage. Future therapies must also strike a balance between aggregation inhibition and preserving Tau interactome which maintains Tau's solubility and function.

## 4.6 Future directions

To improve and build on the findings of this study, future work should aim to more precisely characterise the conformation of insoluble, fibrillar Tau species formed by each Tau mutant. For example, using high resolution ultra-structural analysis using cryo-EM could give more precise insights to the core conformation of aggregates that are associated with toxicity or neuroprotection. A proteomic mapping of each Tau mutants interactome

would also provide critical insights to understanding how conformational changes and interacting partners can confer $^{306}$VQIVYK$^{311}$-mediated protection, to inform the next generation of Tau-centred therapeutics.

# Chapter 5 $^{306}$VQIVYK$^{311}$ deletion prevents Tau-mediated functional deficits.

## 5.1 Introduction

### 5.1.1 The relationship between cellular and functional degeneration

In previous Chapters, I demonstrated that deletion of $^{306}$VQIVYK$^{311}$ rescues cellular neurodegeneration caused by phospho-mimicking Tau in both the olfactory and photoreceptor neurons, providing morphological evidence of neuroprotection across multiple neuron populations. To fully evaluate $^{306}$VQIVYK$^{311}$ as a therapeutic target, I needed to determine whether this cellular rescue translated into functional improvements in larger neuronal populations.

This is crucial as Tau mutants may still disrupt neuronal function without causing overt cell death. As previously discussed, pathological Tau species can accumulate and disrupt neuronal function through microtubule destabilisation, axonal dysfunction and synaptic impairment, leading to functional deficits that precede complete neuronal loss (Mudher et al., 2004, Richardson et al., 2024, Hoover et al., 2010, Talmat-Amar et al., 2011). These cellular pathological mechanisms directly drive neuronal loss.

Tauopathies are clinically characterised by progressive functional decline affecting memory, motor control and survival rather than simply neuronal loss. Therefore, improving behavioural responses as a measure of neuron function would provide more evidence for the therapeutic potential of targeting $^{306}$VQIVYK$^{311}$. Behavioural assays can provide a more holistic and sensitive measure of neuronal integrity and function across larger neuronal populations that reflect clinical profiles of patients.

### 5.1.2 *Drosophila* as a model for functional assessment of neurodegeneration

*Drosophila* are an established model for studying neurodegeneration, offering genetic tractability and a range of robust behavioural assays. Despite having a simpler nervous system (~200,000 neurons vs ~86 billion neurons in humans) (Zars et al., 2000), *Drosophila* share key aspects of mammalian neurobiology, including conserved neurotransmitters (Bellen et al., 2010), some neuronal architecture (Meinertzhagen and Lee, 2012), and the capacity for complex behaviours such as learning and memory (Papanikolopoulou et al., 2019, Mershin et al., 2004).

*Drosophila* also recapitulate many hallmarks of mammalian neuronal aging, including age-dependent behavioural decline, vulnerability to disease-associated proteins like Tau, and cytoskeletal deterioration (Richardson et al., 2024). Expression of human Tau in flies induces cognitive impairment, reduced lifespan, and locomotor deficits, making it a robust *in vivo* model for assessing the functional consequences of Tau pathology (Papanikolopoulou et al., 2019) (Vourkou et al., 2022, Wittmann et al., 2001). Assays such as climbing, longevity, and memory have been widely used in *Drosophila* to distinguish the effects of different Tau isoforms and familial mutations (e.g. V337M, R406W, P301S), successfully recapitulating clinical heterogeneity to give insights to the underlying cause of pathology (Wittmann et al., 2001, Vourkou et al., 2022). Therefore, I employed several behavioural assays to determine how hyperphosphorylation and the $^{306}$VQIVYK$^{311}$ motif independently contribute towards functional toxicity.

### 5.1.3 Chapter aims and objectives

This chapter investigates whether the cellular neuroprotection observed in the Or47b neurons conferred by $^{306}$VQIVYK$^{311}$ deletion translates to functional rescue *in vivo*. I assessed cognitive performance, locomotor ability, and lifespan in flies expressing different phospho-mimicking and aggregation resistant Tau mutants. A range of behavioural assays

were employed to capture both general toxicity and functional impairments across distinct neural circuits. Given that some Tau mutants may exert tissue-specific effects or differentially impair neuronal subtypes, multiple assays were necessary to assess the broader impact of Tau pathology. Olfactory-based cognitive tests were used to evaluate the neuronal function of higher-order brain circuits involved in olfactory learning and memory, climbing assays measured motor coordination and peripheral neuronal function, and lifespan analysis provided a global readout of Tau toxicity. This systematic analysis of neuronal function helped determine how phosphorylation and aggregation independently contribute toward functional decline and evaluate the efficacy of $^{306}$VQIVYK$^{311}$ as a therapeutic target.

**Aim:** To evaluate the functional consequences of degeneration caused by phospho-mimicking and aggregation-resistant Tau mutants using behavioural assays.

- **Objective 1.** Determine functional consequences of expressing phospho-mimicking and aggregation-resistant mutants using cognitive tests.
- **Objective 2**. Determine how the phospho-mimicking and aggregation-resistant mutants affect locomotive function
- **Objective 3**. Determine how the phospho-mimicking and aggregation-resistant mutants affect longevity of *Drosophila.*

## 5.2 Methods

See methods **section 2.4** for all behavioural assays.

## 5.3 Results

### 5.3.1 Odorant perception as a measure of cognitive ability

To investigate whether cellular neuroprotection observed in the ΔVQIVYK mutants could produce a functional rescue associated with Tau-mediated toxicity, I first assessed cognitive function by testing odorant perception. Given that I had previously shown

phospho-mimicking Tau incurred profound degeneration of the Or47b olfactory neurons which was rescued by ΔVQIVYK, I hypothesised that these cellular changes would produce functional phenotypes in odour perception and processing. The Orco-Gal4 driver which encompasses all olfactory receptor neurons was selected to assess the effect of Tau mutants on olfactory function, as degeneration of these neurons should impair the fly's ability to detect, process and respond to attractive and/or aversive odours.

I developed three olfactory perception assays of increasing sensitivity: **1)** an attractive odour 2-choice assay using cups, **2)** an attractive odour 1-choice yeast-trap assay using a petri-dish and **3)** an aversive odour assay using automated tracking software. See methods section **2.4.3, Figure 17** for diagrams of experimental setups.

| | |
|---|---|
| Odour Assay 1) | Attractive choice assay between 2 cups, agar (control) and food. A one-way entry chamber was set up in an enclosure and left for 24 hours to make a choice (**Figure 17, Figure 37).** |
| Odour Assay 2) | Attractive choice assay between food (yeast) and no food using a one-way entry Eppendorf in a petri dish. Setup was a reduced enclosure size, and in a dark box for 24hours to control flying and visual variables **(Figure 17, Figure 37).** |
| Odour Assay 3) | Aversive choice assay between water (control) or 1% benzaldehyde were tracked for 1 minute, assessed using the automated behavioural system Zantiks (**Figure 17, Figure 37).** |

Despite clear cellular degeneration of the olfactory neurons following the same Tau mutant expression in **Chapter 3**, no significant behavioural differences in odour perception emerged between hTau2N4R-muntant expressing flies and no-Tau controls across all assays (**Figure 37 A-C**, **Supplementary Figure 16**). Although there were no significant differences between the genotypes, the performance indices showed that most flies regardless of Tau mutant expressed, favoured the food odour in both attractive assays, and favoured the non-aversive odour in the aversive assay, demonstrating intact odour perception function (**Figure 37 A-C**, **Supplementary Figure 15**).

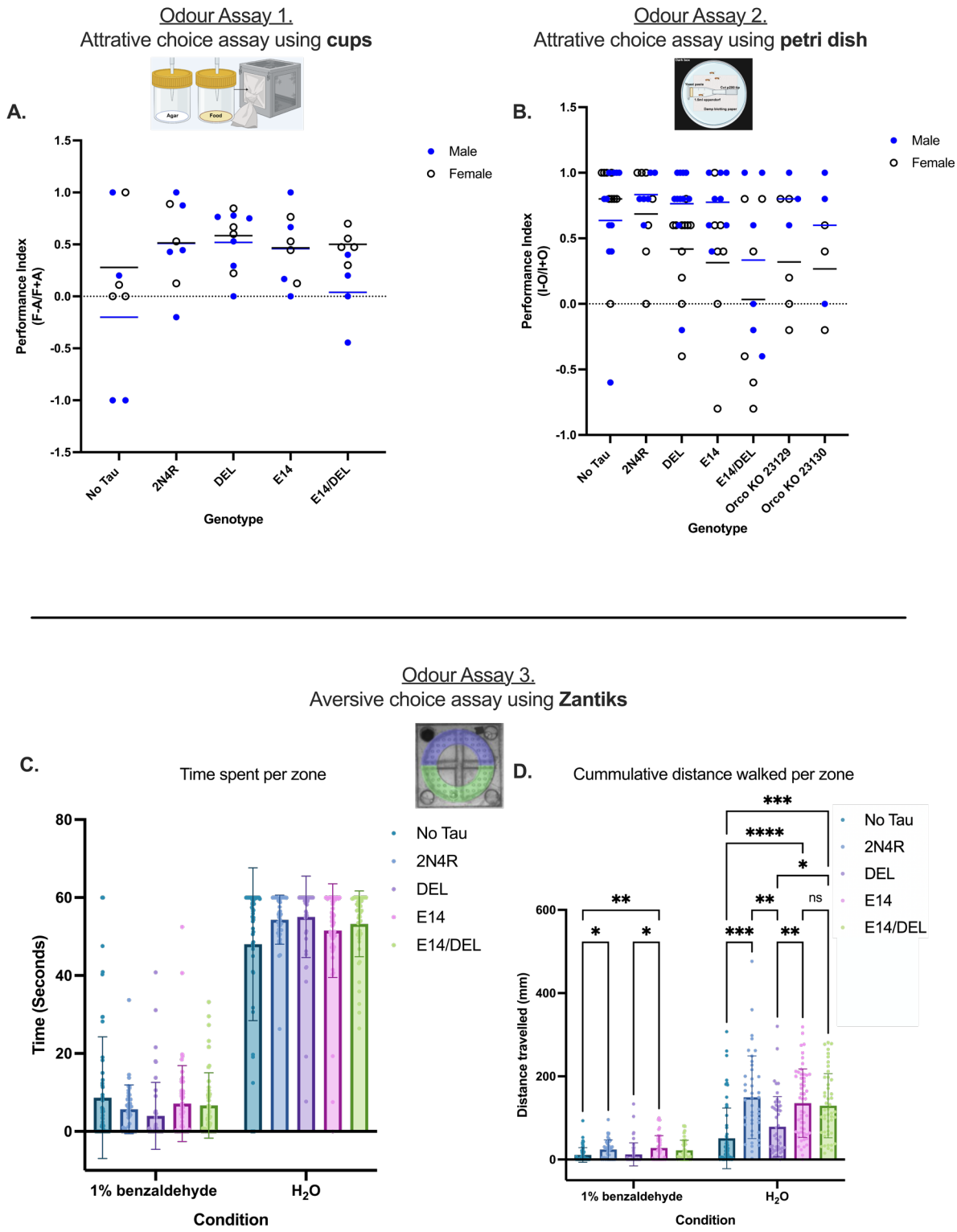


**Figure 37. Quantification of odour assays following Tau mutant expression.**

Three distinct assays were trialled to optimise odour perception in 14-day old aged flies (reared at 18ºC and aged at 29ºC) expressing Tau mutants using the Orco-GAL4 driver. **A)** Odorant assay 1. Attractive 2-choice assay between 1% agar and normal diet over 24 hours. Males(blue) and females(black) were assessed independently. Each data point represents a group of 20 animals with 4-6 biological repeats per genotype. Graph shows mean performance index = (flies in food(F) - flies in agar(A))/(total flies). Two-way ANOVA with Tukey's multiple comparisons test showed no significant differences between genotype or sex. **B)** Odour assay 2. Improved attractive 1-choice assay using a petri dish enclosure and a Eppendorf

yeast-trap. Males(blue) and females(black) were assessed independently. Each data point represents a group of 10 animals assessed for 24 hours. 10 biological repeats were assessed per genotype. Graph shows mean performance index = (flies inside(I) - flies outside(O))/(Total flies). Two-way ANOVA with Tukey's multiple comparisons test showed no significant differences between genotype or sex. **C-D)** Odour assay 3. Aversive choice assay between water and 1% aversive odour benzaldehyde. Only males were used. Each animals cumulative distance walked (mm) and time spent per zone (s) was tracked and quantified automatically using Zantiks. Each data point shows an individual animal N= 42-65 per genotype. **C)** Graphs represent mean ±SD time spent per zone condition. Non-parametric two-way ANOVA with Tukey's multiple comparisons test showed no significant differences between genotype or condition. D) Graph shows the mean ±SD cumulative distance walked per condition. *=P<0.1, **=p<0.01, ***=p<0.001 and ****= p<0.0001 (non-parametric two-way ANOVA, with Tukey's multiple comparisons). All flies spend significantly more time away from aversive odour, regardless of no Tau controls or Tau-mutant genotypes **(Supplementary Figure 15).** All behavioural tests were performed at the same time of day for optimal activity.

However, subtle behavioural differences emerged in the most sensitive assay using the automatic tracker "Zantiks" software which measured 2 variables, distance walked and time spent in aversive/non-aversive areas. Results showed that while there was no apparent difference in olfactory perception between genotypes, that hTau2N4R, hTau2N4R-E14 and hTau2N4R-E14/DEL mutants walked significantly more in the non-aversive areas compared to hTau2N4R-DEL and no Tau controls (**Figure 37 D**). Notably, there was no difference in locomotive activity between phospho-mimicking hTau2N4R-E14 and the aggregation resistant version hTau2N4R-E14/DEL.

The lack of overt olfactory perception deficits indicates that the olfactory system was either not sensitive enough to observe subtle behavioural phenotypes, or that the fly has other sensory organs which can compensate for olfactory deficits. However, the unexpected increase in walking distance in the aversive assay may reflect a broader Tau-mediated stress response as a reflection of underlying neuronal dysfunction, which was rescued when $^{306}$VQIVYK$^{311}$ was targeted in wildtype Tau mutants. These findings prompted me to examine more robust functional readouts using larger neuronal populations to promote a stronger behavioural response to the Tau mutants.

### 5.3.2 Gal80$^{ts}$ temperature switch is required for functional assessment of toxic Tau mutants.

As the olfactory-specific Orco-Gal4 driver was ineffective at producing robust behavioural phenotypes, I needed a driver which could express Tau in a wider population of neurons to generate detectable functional deficits. I switched to using a pan-neuronal Elav-Gal4 driver, which is a well-established tool for assessing Tau-mediated neurodegeneration in flies, often used for assessing functional deficits in *Drosophila* survival and climbing (Wittmann et al., 2001, Passarella and Goedert, 2018). However, initial crosses with a standard Elav-Gal4 (C155) line resulted in extreme pupal lethality when crossed with the toxic hTau2N4R-E14 lines, preventing any functional assessment.

To circumvent the developmental lethality, I used the temperature-sensitive Gal80ts system combined with a Elav-Gal4 driver (ElavGal4;+/+;TubulinGal80ts;+/+). This driver offers precise control of gene expression in *Drosophila* through permissive or restrictive temperature conditions. At 18ºC (permissive condition) Gal80ts blocks Gal4, inhibiting Tau expression, and at 29ºC (restrictive condition) Gal80ts is inactive, allowing Gal4-driven Tau expression **(Figure 15 B).** Using this system, I was able to restrict Tau expression only in newly eclosed adults. I validated that the Gal80ts temperate switch expression system was correctly working at the permissive and restrictive conditions pre- and post-developmentally (**Supplementary Figure 17**).

By restricting Tau expression to adult neurons only, the expression of hTau2N4R-E14 no longer caused pupal lethality. This allowed me to assess the toxicity of all Tau mutants in the entire nervous system, using survival, motor and cognitive assays.

### 5.3.3 Value-based feeding decision assay to assess cognitive ability.

Having established a functional pan-neuronal expression system, next I assessed cognitive ability using a decision-making test. I used an automated value-based feeding

decision assay (VBFDA) adapted from Yu et al., 2021, to assess the higher-order cognitive processing by measuring each animal's ability to make nutritional choices between sucrose and a non-nutritious sweetener arabinose. Using the automated tracking system "Zantiks" I was able to quantify feeding decisions in a more precise and less subjective manner than previously described (Yu et al., 2021).

To maximise behavioural responses, I optimised experimental conditions by conducting all assays at 4pm when flies showed the greatest activity (**Supplementary Figure 18**) following an optimised 12-hour starvation period to increase feeding motivation (**Supplementary Figure 19**). This allowed me to maximise the potential feeding decisions made during the assessment period.

Similar to the odorant perception assays, results from the VBFDA showed no cognitive deficits between control and Tau-expressing flies. All Tau mutants showed an intact decision-making ability, preferring sucrose over arabinose, with no significant differences between genotypes (**Figure 38 A**). However, there were significant differences in the cumulative distance walked. Notably, the phospho-mimicking hTau2N4R-E14 mutant travelled 80% less than wildtype hTau2N4R (**Figure 38 B**). Importantly, locomotive deficits of hTau2N4R-E14 were significantly improved by about 50% upon $^{306}$VQIVYK$^{311}$ deletion in hTau2N4R-E14/DEL mutants, though they still travelled significantly less than hTau2N4R (**Figure 38 B**). Interestingly, there were no significant differences in distance walked between hTau2N4R versus hTau2N4R-DEL (**Figure 38 B**).

The locomotion deficits incurred from pan-neuronal Tau expression likely interfered with the VBFDA performance. This is because reduced movement would limit the number of decisions made during the assessment period, potentially masking the Tau-mediated deficits and making this assay unsuitable for assessing cognitive function. Nonetheless, these findings demonstrate that phospho-mimicking Tau causes significant functional deficits and

that deleting $^{306}$VQIVYK$^{311}$ confers considerable neuroprotection against functional, locomotive decline. These strong phenotypes prompted me to use a more robust assessment of locomotive ability to more directly assess the functional impact of each Tau mutant.

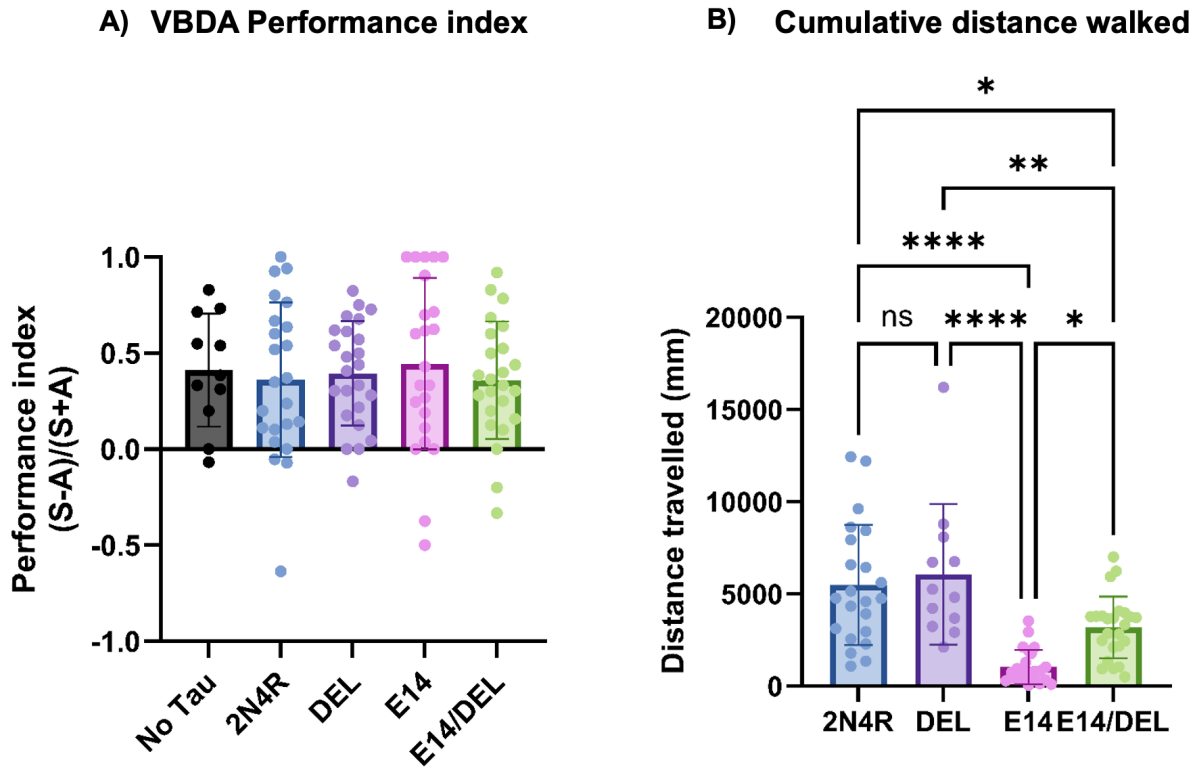


**Figure 38. Deletion of $^{306}$VQIVYK$^{311}$ rescues phosphorylation-induced locomotive deficits in a value-based feeding decision assay.**

Cognitive function assessed using automated tracking of feeding decisions between nutritionally dense 5% sucrose(S) or the sweetener 5% arabinose(A) in 14-day-old flies expressing hTau2N4R mutants driven by Elav-Gal4;;Tubulin-Gal80ts;. A) Performance index shows intact decision-making across all genotypes (n=12 per group from 2 biological repeats). B) Cumulative distance travelled shows hTau2N4R-E14 significantly impairs locomotion, which is rescues by ΔVQIVYK in hTau2N4R-E14/DEL. Graphs represent mean ± SD. **** $p<0.0001$, ** $p<0.01$, * $p<0.05$ (Ordinary one-way ANOVA with multiple comparisons).

### 5.3.4 Deletion of aggregation motif $^{306}$VQIVYK$^{311}$ rescues progressive Tau-mediated phosphorylation-dependent locomotive dysfunction.

To directly assess the locomotive deficits observed in the VBFDA, I used a more robust, dedicated climbing assay using negative geotaxis. This well-established behavioural

test specifically measures motor coordination and strength by measuring the flies ability to climb up vial walls, and has previously demonstrated good recapitulation of Tau-toxicity across familial mutants (Wittmann et al., 2001).

Results showed that expression of hTau2N4R-E14 caused severe behavioural deficits, with significant reductions in climbing ability at all time points assessed (0-3 weeks). hTau2N4R-E14 climbing ability decreased progressively from 25% at week 1, 50% at week 2 and 65% at week 3 compared to hTau2N4R, with no hTau2N4R-E14 expressing flies surviving past 4 weeks (**Figure 39**).

In contrast, both ΔVQIVYK mutants (hTau2N4R-DEL and hTau2N4R-E14/DEL) did not demonstrate any significant toxicity or deficits compared to wildtype hTau2N4R, with hTau2N4R-DEL often outperforming all other genotypes. Importantly, hTau2N4R-E14/DEL significantly improved the severe climbing deficits incurred by hTau2N4R-E14 by around 33% at week 1 and 2, and 240% by week 3 (**Figure 39**).

These results demonstrate that $^{306}$VQIVYK$^{311}$ deletion improves neuronal function and reduces overall toxicity of phospho-mimicking Tau. Critically, this aligns with cellular neuroprotection observed in previous results chapters suggesting that therapeutically targeting $^{306}$VQIVYK$^{311}$ can be neuroprotective molecularly and functionally. Given that hTau2N4R-E14 showed complete lethality by week 4 while ΔVQIVYK mutants survived, I next directly examined how ΔVQIVYK effects overall survival and longevity.

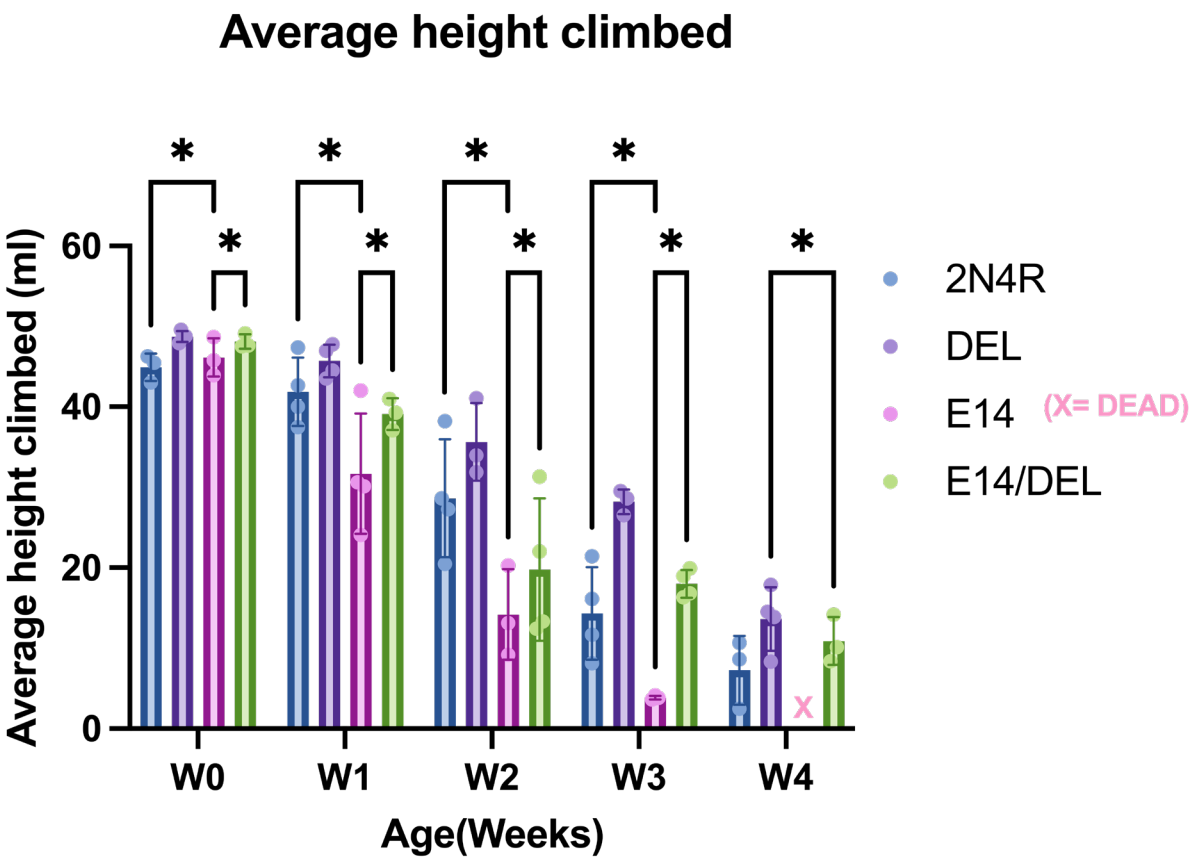


**Figure 39. Deletion of $^{306}$VQIVYK$^{311}$ rescues progressive Tau-mediated phosphorylation-dependent climbing deficits.**

Locomotive function was assessed using a negative geotaxis climbing assay in flies expressing Tau mutants using the Elav-Gal4;;Tubulin-Gal80ts; driver. Graph show the average height climbed after three repetitions, using 3-4 biological repeats of n=10 males per group, over the span of 4 weeks. Graphs represent mean ± SD. *p<0.05 (Ordinary 2-way ANOVA with multiple comparisons). Over the 4-week assessment period each mutant had a robust decline of climbing ability which was significantly enhanced by the expression of hTau2N4R-E14. Climbing ability was improved upon $^{306}$VQIVYK$^{311}$ deletion and enhanced longevity.

### 5.3.5 Deletion of aggregation promoting motif $^{306}$VQIVYK$^{311}$ promotes longevity and rescues premature death caused by phosphorylation.

Having observed significant lethality in hTau2N4R-E14 flies during climbing assays, I next recorded the survival rates of each genotype. Longevity assays provide a robust measure of overall toxic Tau burden and reflect the extent of global neuronal dysfunction.

Results show that compared to controls expressing mCherry (no Tau), pan-neuronal hTau2N4R expression significantly reduced median lifespan, which was exacerbated by

phospho-mimicking hTau2N4R-E14. In fact, hTau2N4R-E14 caused the most severe survival deficits, reducing median survival of wildtype hTau2N4R flies by 18% (from 37 to ~30 days in both female **(Figure 40)** and male **(Figure 41)** populations.

In contrast, both $^{306}$VQIVYK$^{311}$ deletion mutants critically improved survival in both Tau backgrounds (hTau2N4R *versus* hTau2N4R-DEL and hTau2N4R-E14 *versus* hTau2N4R-E14/DEL). The hTau2N4R-E14/DEL flies showed significant recovery from the survival deficits caused by the phospho-mimicking mutations, with median survival returning to levels similar to wildtype hTau2N4R **(Figure 40, Figure 41)**. Remarkably, hTau2N4R-DEL flies showed an enhanced survival compared to hTau2N4R, particularly in the female cohort where median survival increased from 37 to 44 days **(Figure 40).**

Gender can influence physiology, disease risk, behaviour and treatment response, therefore I investigated if there were gender-specific responses to the Tau mutants. Results showed that both genders revealed consistently mirrored trends of toxicity, however females generally showed higher survival rates and stronger rescue effects with the ΔVQIVYK mutation, particularly for hTau2N4R-DEL (**Supplementary Figure 20**). These results demonstrate that gender-specific factors contribute to Tau-mediated toxicity influenced by the $^{306}$VQIVYK$^{311}$ motif.

Collectively, these longevity results demonstrate that $^{306}$VQIVYK$^{311}$ deletion provides comprehensive neuroprotection against both functional and global survival deficits induced by pathological Tau. These findings establish $^{306}$VQIVYK$^{311}$ as an excellent therapeutic target candidate for protection against toxic Tau species.

A.

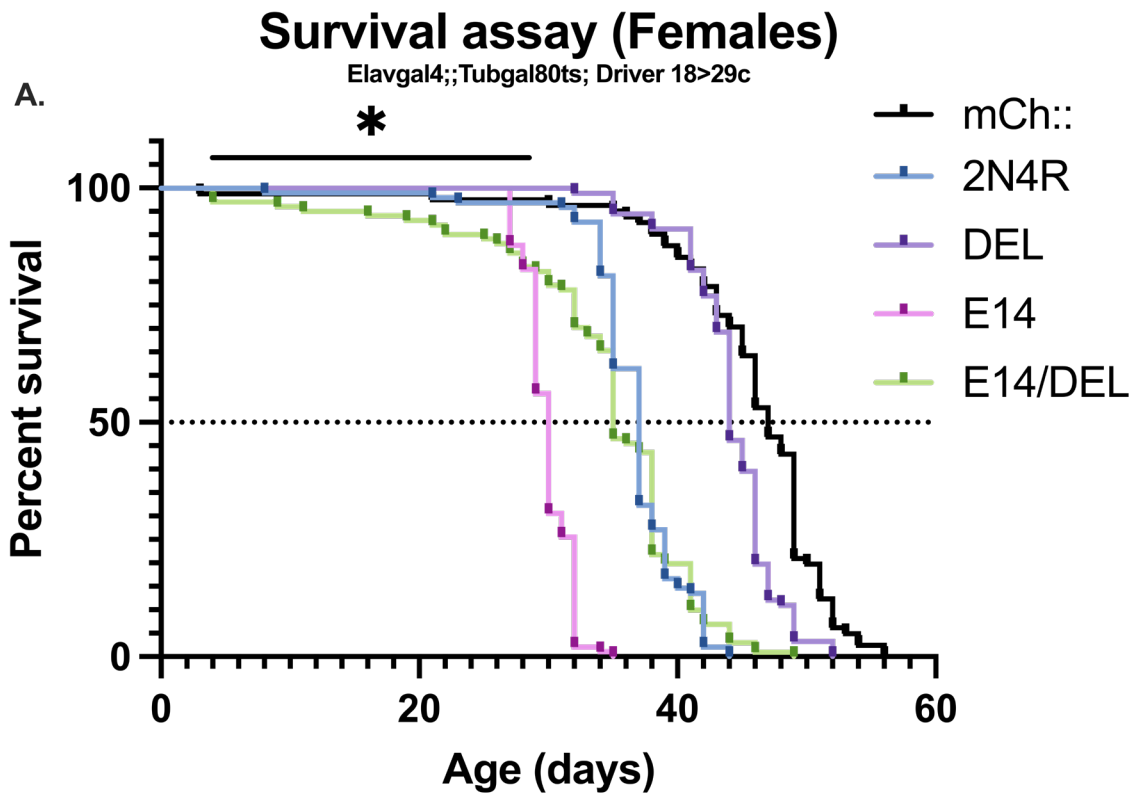


B.

| Median Survival | | | | |
|---|---|---|---|---|
| mCh | 2N4R | DEL | E14 | E14/DEL |
| 47 | 37 | 44 | 30 | 35 |

C.

| | mCherry | 2N4R | DEL | E14 | E14/DEL |
|---|---|---|---|---|---|
| mCherry | | <0.0001 | <0.0001 | <0.0001 | <0.0001 |
| 2N4R | | | <0.0001 | <0.0001 | 0.6802 |
| DEL | | | | <0.0001 | <0.0001 |
| E14 | | | | | <0.0001 |
| E14/DEL | | | | | |

**Figure 40. Survival assay of female Tau-expressing *Drosophila* mutants.**

A) Kaplan Meier survival curves for Elav-Gal4;;TubGal80ts; driven mCherry Tagged Tau mutants: hTau2N4R, hTau2N4R-DEL, hTau2N4R-E14 and hTau2N4R-E14/DEL expressing female flies (n=100). Flies expressing mCherry alone (no Tau) were used as a control. B) Shows median survival age of each genotype. C) Lifespan of flies is significantly different between the Tau variants tested (Log-rank, Mantel-Cox test $p<0.0001$). With a manual Bonferroni correction to correct for 10 multiple comparisons, $*p<0.05/10$ makes corrected p-values $*p<0.005$. All populations except hTau2N4R vs hTau2N4R-E14/DEL were significantly different. Flies expressing hTau2N4R-E14 have a significantly reduced survival rate compared to hTau2N4R (median survival of 30 vs 37 respectively, $p<0.0001$).

A.

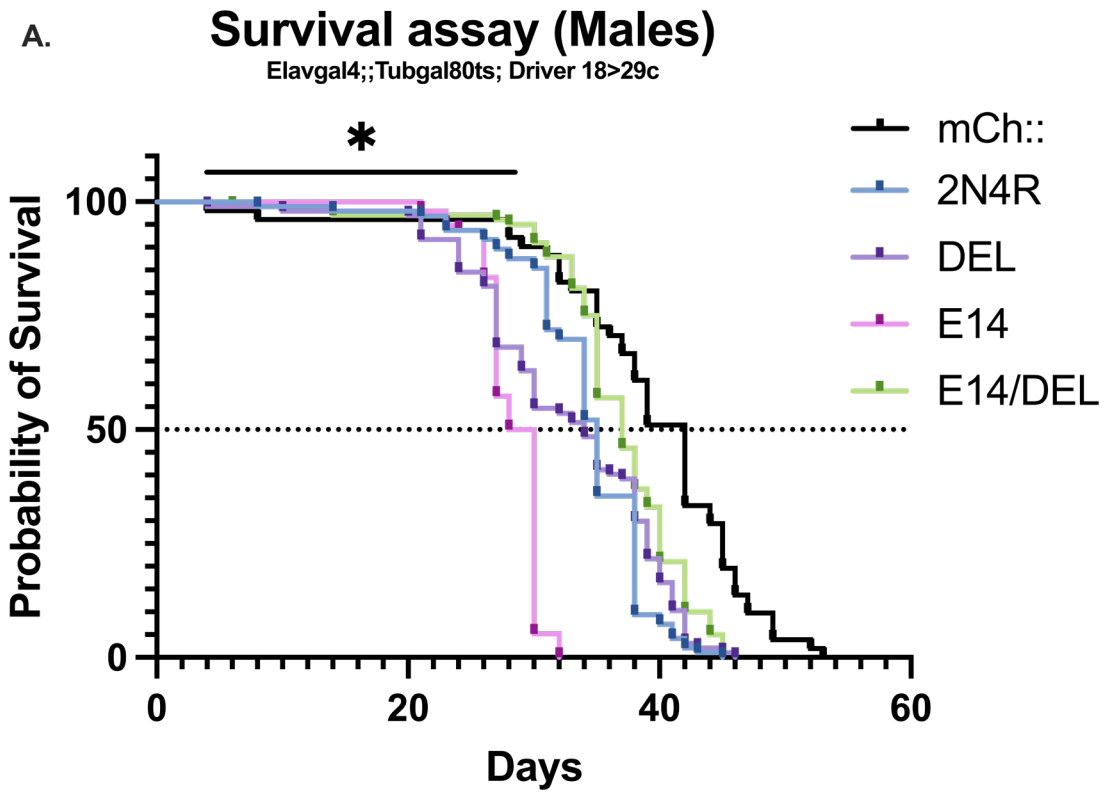


B.

| Median Survival | | | | |
|---|---|---|---|---|
| mCh | 2N4R | DEL | E14 | E14/DEL |
| 42 | 35 | 34 | 29 | 37 |

C.

| | mCherry | 2N4R | DEL | E14 | E14/DEL |
|---|---|---|---|---|---|
| mCherry | | <0.0001 | <0.0001 | <0.0001 | <0.0001 |
| 2N4R | | | 0.5686 | <0.0001 | <0.0001 |
| DEL | | | | <0.0001 | <0.0001 |
| E14 | | | | | <0.0001 |
| E14/DEL | | | | | |

**Figure 41. Survival assay of male Tau-expressing *Drosophila* mutants.**

A) Kaplan Meier survival curves for Elav-Gal4;;TubGal80ts; driven mCherry Tagged Tau mutants: hTau2N4R, hTau2N4R-DEL, hTau2N4R-E14 and hTau2N4R-E14/DEL expressing male flies (n=100). Flies expressing mCherry alone (no Tau) were used as a control. B) Shows median survival age of each genotype. C) Lifespan of flies is significantly different between the Tau variants tested (Log-rank, Mantel-Cox test $p<0.0001$). With a manual Bonferroni correction to correct for 10 multiple comparisons, $*p<0.05/10$ makes corrected p-values $*p<0.005$. All populations except hTau2N4R vs hTau2N4R-DEL were significantly different. Flies expressing hTau2N4R-E14 have a significantly reduced survival rate compared to hTau2N4R (median survival of 29 vs 35 respectively, $p<0.0001$).

## 5.4 Discussion

This Chapter addressed the functional consequences of phospho-mimicking Tau and targeting the $^{306}$VQIVYK$^{311}$ aggregation domain. I demonstrated that deletion of $^{306}$VQIVYK$^{311}$ provides robust functional rescue of pathological Tau-mediated deficits across multiple behavioural assays. This Chapter helps build a comprehensive view that targeting this domain is neuroprotective cellularly and functionally to improve the systemic neurodegenerative effects of pathological Tau.

### 5.4.1 Tau induced functional deficits emerged more clearly in systemic expression models.

Despite several iterations of cognitive assays, all Tau-expressing flies demonstrated intact odour perception and decision-making abilities, with no significant differences observed between Tau mutants. These findings contrast with previous studies showing Tau-mediated cognitive deficits when expressed in higher-order brain centres involved in olfactory learning and memory (Papanikolopoulou et al., 2019, Vourkou et al., 2022), suggesting that my experimental approach was inadequate for detecting cognitive decline.

However, the same flies (which had olfactory-specific Tau expression) also displayed severe motor deficits. This finding suggests either that olfactory circuit dysfunction has downstream functional consequences, for example stress-related responses to tissue degeneration (Jafari et al., 2021), or that other sensory organs like the maxillary palp could be compensating or masking neuron loss during olfactory-based cognitive assessments(de Bruyne et al., 1999). Nonetheless, given that robust functional deficits were observed in the longevity and climbing assays from pan-neuronal expression, it demonstrates that the Tau mutants do cause differential toxicity and functional impairments as previously described (Wittmann et al., 2001). This likely reflects the Tau burden from increased, broader neuronal expression or differential vulnerability across neuronal subtypes.

Previous studies have shown that Tau causes degeneration in a cell-selective manner, with certain neuronal populations being selectively vulnerable or resistant to degeneration than others (Sivanantharajah et al., 2025). The absence of cognitive deficits, but distinct motor and longevity deficits may reflect differential neuronal vulnerability between the olfactory and pan-neuronal circuitry used. Neurons that have motor-related functions could be more vulnerable to Tau burden, possibly due to their functional requirement for axonal transport and cytoskeletal integrity(Richardson et al., 2024, Mudher et al., 2004). Collectively, these findings demonstrate that systemic Tau expression can provide a more sensitive and appropriate model for assessing Tau-mediated functional deficits than cognitive perception.

### 5.4.2 $^{306}$VQIVYK$^{311}$ deletion confers functional neuroprotection against phosphorylation-mediated neuronal deficits.

The functional deficits observed in this Chapter directly validates the cellular toxicity findings from previous Chapters. Consistent with neuronal degeneration demonstrated in **Chapter 3**, pan-neuronal expression of hTau2N4R led to significant reductions in *Drosophila* lifespan and locomotive ability, which was exacerbated by phospho-mimicking Tau. These findings align with previous studies showing that other phospho-mimicking or familial disease-associated mutations exacerbate functional deficits (Prüßing et al., 2013, Wittmann et al., 2001, Talmat-Amar et al., 2011). Other groups have also demonstrated that phosphorylation dramatically reduces survival through physiologically upregulating the expression of GSK-3β kinase *Drosophila* homolog *shaggy* (Sgg) (Veselkina et al., 2023). These findings support the literature that Tau hyperphosphorylation is a key mediator of neuronal dysfunction and degeneration in *Drosophila*, and functionally mirror the cellular degeneration observed in previous results Chapters.

Importantly, deletion of the $^{306}$VQIVYK$^{311}$ aggregation-promoting motif in both hTau2N4R-DEL and hTau2N4R-E14/DEL mutants significantly rescued survival and locomotive deficits, often outperforming the respective hTau2N4R and hTau2N4R-E14 expressing flies. As discussed in **Chapter 4**, $^{306}$VQIVYK$^{311}$ deletion prevents neurodegeneration through multiple possible mechanisms including altering Tau conformational misfolding, aggregation, phosphorylation, microtubule interactions, and changes to the interactome (Martinez et al., 2025, Brotzakis et al., 2021, Passarella and Goedert, 2018, von Bergen et al., 2000). By reducing Tau's ability to misfold or aggregate into seed-competent, toxic species, the ΔVQIVYK mutants may restore cellular integrity, microtubule stability and axonal transport (Katsinelos et al., 2021, Talmat-Amar et al., 2011, Hallinan et al., 2019). Preservation of neuronal function through $^{306}$VQIVYK$^{311}$ deletion is reflected in the rescue of behavioural deficits in Tau-transgenic *Drosophila*, which capture the overall burden and toxicity of the Tau mutants expressed. Importantly, these findings suggest that $^{306}$VQIVYK$^{311}$ deletion successfully mitigates Tau-mediated functional toxicity. This is particularly significant as it demonstrates that the cellularly protective mechanisms translate into meaningful functional neuroprotection. The consistency of rescuing morphological, biochemical and functional Tau-induced deficits strengthens $^{306}$VQIVYK$^{311}$ as a candidate target for therapeutics.

### 5.4.3 Implications for therapeutic design

These findings establish $^{306}$VQIVYK$^{311}$ as a highly promising therapeutic target to holistically mitigate many aspects of Tau-mediated toxicity, including functional degeneration. The comprehensive rescue of survival and locomotor deficits by $^{306}$VQIVYK$^{311}$ deletion suggests that aggregation inhibitors could provide significant clinical benefits. The prevention of functional decline in even severely toxic hTau2N4R-E14 mutants also demonstrates the robustness of this therapeutic efficacy across different disease contexts.

Indeed, several other groups have demonstrated that inhibiting $^{306}$VQIVYK$^{311}$-mediated aggregation promotes longevity and neuronal health in multiple animal models. Peptide and mutagenic aggregation inhibitors have shown to improve survival, locomotive function and cognitive ability in Tau-transgenic *Drosophila* and rodent models, using assays such as longevity, nesting behaviours and the Morris water maze test (Kondo et al., 2021, Zhang et al., 2020b, Aggidis et al., 2024). Notably, Passarella et al., showed that mutagenic deletion of $^{306}$VQIVYK$^{311}$ in transgenic *Drosophila* expressing hTau0N4R-ΔVQIVYK significantly improved both climbing and survival compared to wildtype hTau0N4R flies. Together, there is strong evidence that targeting aggregation via $^{306}$VQIVYK$^{311}$ has great therapeutic potential to mitigating Tau-mediated neurodegeneration across different Tauopathy subtypes, isoforms and disease contexts.

Results from this Chapter also demonstrated gender-specific differences in response to $^{306}$VQIVYK$^{311}$ targeting. Females generally showed greater survival rates, with notable improvement in hTau2N4R-DEL vs hTau2N4R flies which could be explained by hormonal and genetic influences on Tau-mediated toxicity (Lopez-Lee et al., 2024). Importantly, these results may inform therapeutic design strategies to be personalised on a gender basis.

### 5.4.4 Conclusions

In summary, this results Chapter demonstrates that the deletion of $^{306}$VQIVYK$^{311}$ motif confers global protection of neuronal function against Tau-mediated neurodegeneration. Importantly, this Chapter provides compelling evidence that while Tau phosphorylation is a key driver of toxicity, its pathogenic effects are primarily mediated through the $^{306}$VQIVYK$^{311}$ motif. This finding suggests that regardless of whether Tau is hyperphosphorylated in a disease state, inhibiting aggregation early as possible can significantly reduce Tau toxicity, preserve normal neuronal function, and promote longevity.

### 5.4.5 Future directions

To refine the cognitive and olfactory perception assays used in this study, future work should consider using alternative drivers such as a mushroom body driver, which is a selective set of neurons critically involved with learning and memory. This approach would provide a more specific behavioural phenotype of cognitive decline without additional variables such a locomotive dysfunction. *In vivo* imaging techniques such as calcium imaging (Boto and Tomchik, 2024) or electrophysiological recordings may also be an excellent method for directly assessing the functional impact of phosphorylation and targeting $^{306}$VQIVYK$^{311}$ phospho-mimicking, particularly in small neuronal populations like the Or47b circuit.

Additionally, future studies should explore gender-specific molecular mechanisms, such as the influence of hormones on Tau phosphorylation and aggregation, to provide insights into how disease progression may differ between male and female populations. This importantly could inform if treatments could be tailored for better efficacy between genders. Furthermore, the scope of this project should be expanded into a broader range of Tau isoforms to provide deeper understanding of how isoform-specific phosphorylation and aggregation contribute towards neurotoxicity. These findings could influence the design and tailored administration of aggregation therapeutics in distinct Tauopathies.

# Chapter 6 Targeting $^{306}$VQIVYK$^{311}$ with aggregation inhibitor RI-AG03 partially recapitulates neuroprotective effects of ΔVQIVYK mutants.

## 6.1 Introduction

Building on results from Chapters 3-5 demonstrating that mutagenic deletion of $^{306}$VQIVYK$^{311}$ motifs renders Tau pathologically inert, reducing misfolded conformers, neurodegeneration and neuronal dysfunction, this Chapter investigates whether the $^{306}$VQIVYK$^{311}$-targeting peptide aggregation inhibitor "RI-AG03" can pharmacologically recapitulate these protective effects in wildtype and phospho-mimicking Tau-expressing *Drosophila*. These findings would provide clinically relevant insights into which Tau species are likely to respond to aggregation-targeting therapies.

### 6.1.1 Tau aggregation inhibitors as a strategy for mitigating pathology

Tau aggregates, particularly seed-competent small oligomers, are highly toxic and contribute towards neurodegeneration (Mamun et al., 2020, Ward et al., 2012). As such, targeting oligomers is a major focus for developing treatments against Tauopathies as they represent the earliest and possibly most reversible drivers of neurodegeneration. Importantly, findings from previous Chapters demonstrates that preventing aggregation via $^{306}$VQIVYK$^{311}$ deletion is sufficient to rescue Tau-mediated toxicity, which also implies that kinase inhibitors are not required if aggregation can be blocked. Many anti-aggregation strategies are being actively developed to reduce Tau aggregation by a number of different mechanisms. Popular strategies include clearing Tau aggregates through immunotherapy, (Vaz and Silvestre, 2020) reducing the Tau expression available to aggregate through antisense oligonucleotides (Feneberg and Otto, 2020), directly preventing Tau aggregation

through broad-spectrum small molecules (Wischik et al., 1996, Kondo et al., 2021, Necula et al., 2007) or more targeted peptide-inhibitor approaches (Seidler et al., 2018, Zhang et al., 2020b, Sievers et al., 2011).

Therapeutic success is influenced by disease stage, delivery and specificity. Peptide-based aggregation inhibitors are a particularly promising strategy as they offer high sequence and structure specificity unlike other small molecule therapies. By binding to defined aggregation motifs and blocking early aggregate formation, peptide-based inhibitors offer a focused and specific strategy, which in light of the recent cryo-EM evidence for structurally diverse fibril conformations in Tauopathies (Shi et al., 2021), will be broadly effective to the conformational diversity, unlike most small molecule or immunotherapy designs. There are several peptide aggregation inhibitors designed to target and cap $^{275}$VQIINK$^{280}$ and $^{306}$VQIVYK$^{311}$ aggregation motifs (von Bergen et al., 2000) which have had promising results in preclinical studies thus far **(Chapter 1, Table 5).** However, many existing peptide aggregation inhibitors have several challenges when translating *in vitro* design to *in vivo* and clinical applications, including limited specificity, poor target delivery due to the blood-brain-barrier and proteolytic degradation (Aggidis et al., 2024, Aileen Funke et al., 2010, Dominguez-Meijide et al., 2020). RI-AG03 has been designed specifically to overcome these limitations and has shown success in transgenic *Drosophila* models of Tauopathy (Aggidis et al., 2024).

### 6.1.2 Peptide aggregation inhibitor RI-AG03

RI-AG03 [Ac–rrrrrrrrGpkyk(ac)iqvGr–$NH_2$] is a novel retro-inversed, D-amino acid peptide-based Tau aggregation inhibitor designed to bind selectively to $^{306}$VQIVYK$^{311}$. The mechanism by which RI-AG03 works is through binding and capping $^{306}$VQIVYK$^{311}$ and $^{275}$VQIINK$^{280}$ motifs, stabilising non-toxic, off-pathway intermediates, preventing fibril formation without disassembling pre-formed aggregates(Aggidis et al., 2024). RI-AG03 has

proven an effective aggregation inhibitor of full length Tau2N4R *in vitro*, reduced seeding activity in HEK-239 cells, and reduced neurodegenerative phenotypes in Tau2N4R-transgenic *Drosophila* (Aggidis et al., 2024).

| Key design features of RI-AG03 [Ac–rrrrrrrrGpkyk(ac)iqvGr–$NH_2$] |
|---|
| As the peptide is synthesised in a retro-inverted form, it is optimised to be resistant to proteolytic degradation, improving delivery while maintaining binding specificity for Tau. |
| The poly-arginine chain increases the peptides solubility, reduces non-specific aggregation and creates a steric hinderance to block Tau-Tau aggregation. |
| As a capping peptide, its mechanism of action has been optimised to have a sweet-point high-affinity sequence-specific binding capability to $^{306}$VQIVYK$^{311}$, with additional binding to $^{275}$VQIINK$^{280}$ due to sequence conservation between the two motifs. |

Although RI-AG03 has demonstrated efficacy *in vitro* and in hTau2N4R-expressing *Drosophila*, its performance against disease-relevant, conformationally distinct pathological Tau species remains uncharacterised. By testing RI-AG03 in hTau2N4R and phospho-mimicking, aggregation-prone hTau2N4R-E14 flies, this Chapter assesses its ability to reduce Tau accumulation and neurodegeneration in aging neurons, determining whether the protective effects of hTau2N4R-E14/DEL can be recapitulated pharmacologically. *Drosophila* is an ideal model for this assessment because their lack of a stringent blood brain barrier permits efficient compound access to the CNS, which can be utilised in drug testing (Stork et al., 2008).

**Aim**: Investigate the therapeutic potential of the $^{306}$VQIVYK$^{311}$-targeting Tau aggregation inhibitor RI-AG03 in reducing Tau-mediated neurotoxicity.

- **Objective 1.** Determine if RI-AG03 rescues axonal degeneration and Tau accumulation

- **Objective 2.** Assess if RI-AG03 can rescue phosphorylation-mediated neurotoxicity of TauE14 and recapitulate mutagenic deletion of hTau2N4R-E14,DEL *in vivo*.

## 6.2 Methods

See methods **section 2.3** for RI-AG03 drug delivery. See methods **section 2.2** for confocal image acquisition. See methods **section 2.6** for IMARIS 3D image analysis.

## 6.3 Results

### 6.3.1 RI-AG03 selectively reduces Tau accumulation in phospho-mimicking flies.

To explore the translational potential of targeting the $^{306}$VQIVYK$^{311}$ domain, I tested whether the aggregation inhibitor RI-AG03 could suppress Tau accumulation in Or47b neurons. Previous findings from **Chapter 3** demonstrated that deletion of $^{306}$VQIVYK$^{311}$ prevented Tau accumulation, therefore I explored whether pharmacological inhibition of $^{306}$VQIVYK$^{311}$ would similarly reduce the propensity for Tau accumulation. Given that RI-AG03 effectively suppresses aggregation of hTau2N4R *in vitro*, reduced retinal degeneration and improved survival in hTau2N4R-expressing *Drosophila* at 40µM (Aggidis et al., 2024), this dose was chosen for my study. Flies expressing either hTau2N4R or the aggregation prone, phospho-mimicking hTau2N4R-E14 were fed 40µM of an aggregation inhibitor peptide RI-AG03 [Ac–RRRRRRRRGPKYK(Ac)IQVGR–$NH_2$] or 40µm scrambled AG03 control peptide [Ac-RG-QPKIK(Ac)YV-GRRRRRRRR] daily, and Tau accumulates were quantified using the same methods in **Chapter 3**. However, age of analysis was extended to 28 days to assess the effect of prolonged treatment.

Quantification of Tau accumulation density within the axonal compartment showed that the Tau mutants responded differently to RI-AG03 treatment. In hTau2N4R-expressing flies, Tau accumulation increased progressively over 28-days, however treatment with RI-

AG03 did not reduce Tau accumulation at any time point assessed when compared to scramble peptide control (**Figure 42 A1-B3**). In contrast, RI-AG03 treatment reduced the average size and appearance of hTau2N4R-E14 accumulates (arrows, **Figure 42 C2** *versus* **D2**). These morphological improvements are visually subtle in comparison to the dramatic rescue achieved from mutagenic deletion of $^{306}$VQIVYK$^{311}$ in **Chapter 3**. Nonetheless, quantification showed that RI-AG03 treatment reduced average hTau2N4R-E14 Tau accumulation at 14-28 days but was significantly lower by ~30% at 28 days compared to scramble peptide, to levels comparable with scramble-treated hTau2N4R (**Figure 42 B**).

These results show that RI-AG03 works more effectively on hyperphosphorylated Tau species compared to wildtype Tau, indicating that RI-AG03 may preferentially target pathological Tau species. Next, I sought to assess whether the reduction of Tau accumulation also provided protection against neurodegeneration.

### 6.3.2 RI-AG03 shows trending but non-significant improvements in TauE14-induced neuronal degeneration

Given that only hTau2N4R-E14 had a reduction in Tau accumulation following the treatment of RI-AG03, I next examined if treatment would also reduce axonal degeneration as observed in ΔVQIVYK mutants observed in **Chapter 3**.

Similarly to quantification of hTau2N4R accumulation, quantification of axonal swelling density (**Figure 43**) and neuronal bundle volume (**Figure 44**) showed no significant differences between RI-AG03 and scrambled peptide treatments for hTau2N4R expressing flies.

In contrast, similarly to the reduction in hTau2N4R-E14 accumulation, RI-AG03 treatment showed trends towards reduced axonal degeneration. Quantification of axonal swelling density showed that RI-AG03 treated hTau2N4R-E14 expressing flies had 17% less axonal swellings compared to the scrambled treated group at 28 days, though these

trends did not reach statistical significance over 2 biological repeats (**Figure 43**). However, one of the biological replicates showed a significant decrease in hTau2N4R-E14 axonal swelling density at 14 days following RI-AG03 treatment (**Supplementary Figure 21**), but this effect was lost when the biological replicates were combined. This data is encouraging and suggests that RI-AG03 is effective in reducing Tau-mediated toxicity, but implies that a larger sample size is required to achieve statistical significance. Alternatively, the more subtle effect could be limited practically by the penetrance and target engagement of RI-AG03, through pharmacokinetics, delivery and proteolytic stability.

Collectively, this results section demonstrates that RI-AG03 selectively reduces accumulation of phospho-mimicking hTau2N4R-E14 and provides encouraging evidence of protection against neurodegeneration *in vivo*. Unexpectedly RI-AG03 treatment provided no phenotypic protection against wildtype hTau2N4R-mediated neurotoxicity. The trending but non-significant reduction in hTau2N4R-E14 mediated axonal swelling density and neuronal degeneration suggests that either the extent to which RI-AG03 prevented aggregation was inefficient to provide robust neuroprotection, or that the population size was too small to see subtle trends. Nonetheless, this Chapter provides supporting evidence for targeting $^{306}$VQIVYK$^{311}$ against Tau-mediated toxicity. However, further optimisation of dose and delivery methods are needed to more closely recapitulate the neuroprotection observed in the $^{306}$VQIVYK$^{311}$ deletion mutants.

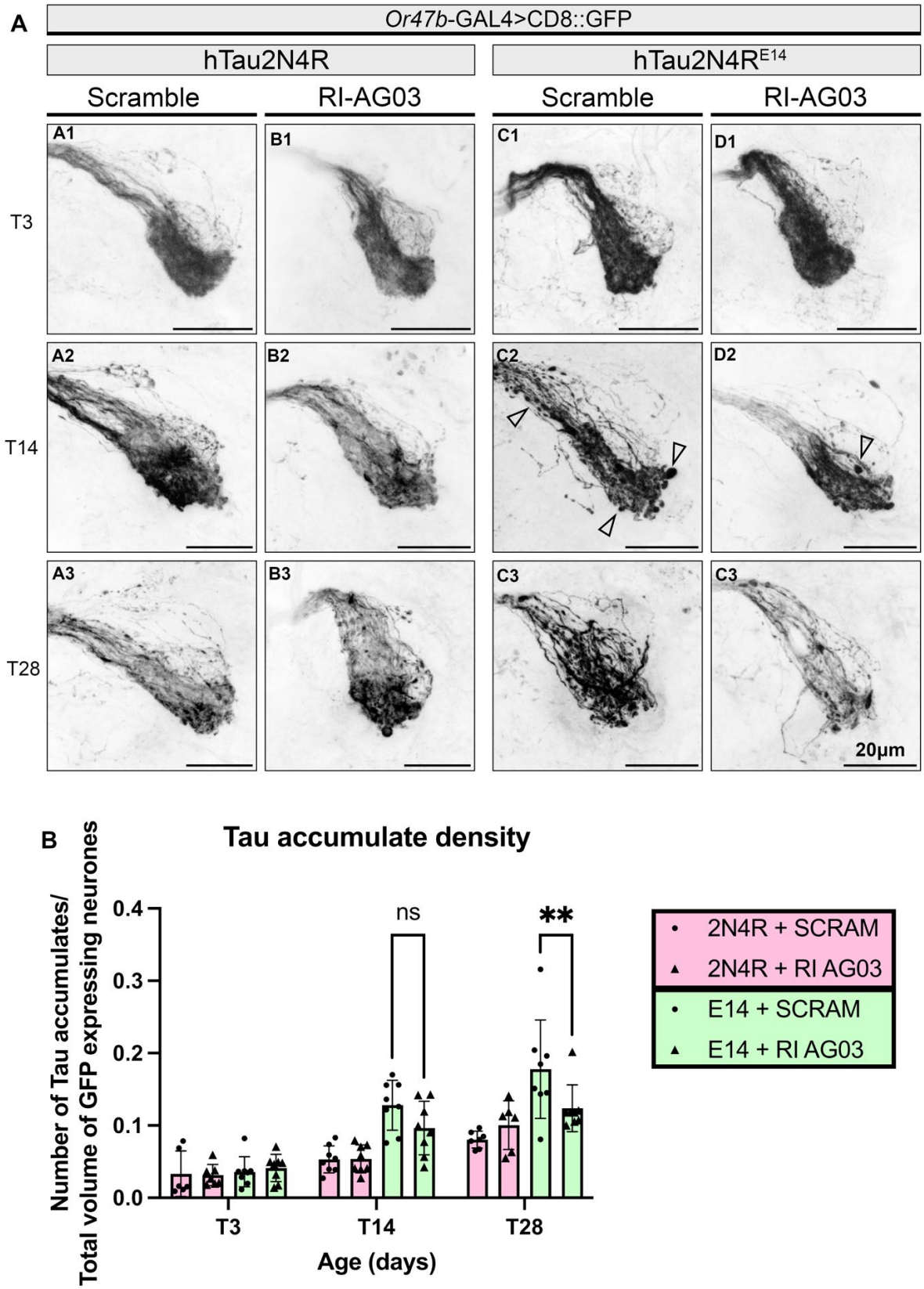


**Figure 42. $^{306}$VQIVYK$^{311}$-targeting RI-AG03 selectively reduces hTau2N4R-E14 accumulation in aged flies.**

A) Maximum projection confocal images (A1-C3) of the brain of flies expressing mCherry::Tau mutants in the Or47b neurons (enhanced with α-hTau Dako). Columns represent genotype (wildtype hTau2N4R *versus* hTau2N4R-E14) and drug treatment condition (40µM Scramble peptide (control) *versus* 40µM RI-AG03) delivered through diet.

Rows represent post-developmental age 3, 14 and 28 days. Arrows point toward beaded Tau accumulates within expressing neurons which increase in frequency and size with age which are exacerbated in hTau2N4R-E14 expressing flies, but reduced after RI-AG03 administration (C2 vs D2). B) Tau accumulate density was quantified using 3D images using IMARIS with a spotting tool (see methods) N=6-8 from two biological repeats. Graphs represent mean ±SD. ** $p<0.001$ (2-way ANOVA with Tukey's multiple comparisons).

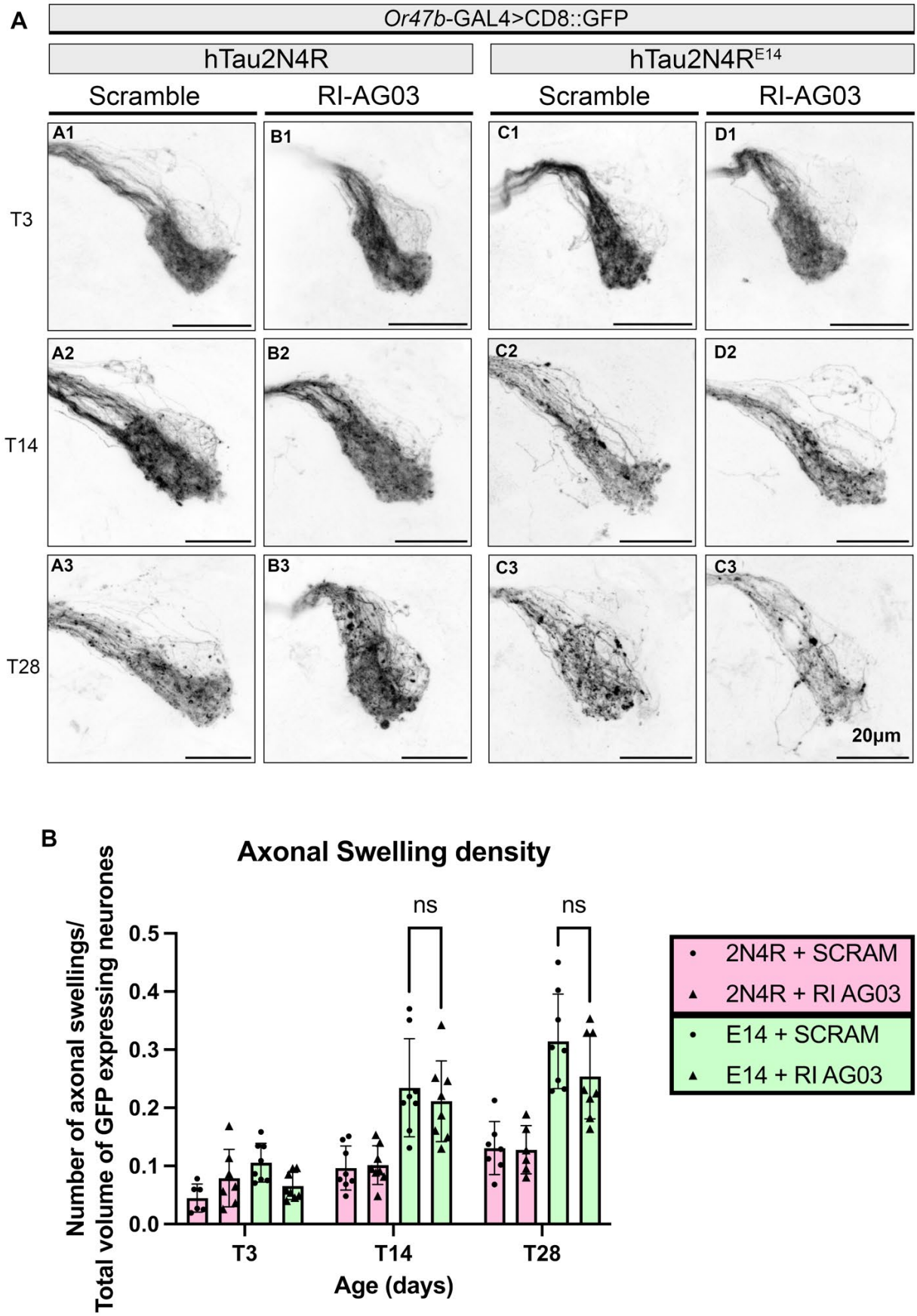


**Figure 43. RI-AG03 treatment does not improve Tau-mediated neuronal degeneration of Or47b neurons.**

**(A)** Maximum projection confocal images (A1-C3) of the brain of flies expressing membrane bound GFP (CD8::GFP) at the Or47b neurons enhanced with α-GFP. Columns represent genotype (wildtype hTau2N4R *versus* hTau2N4R-E14) and drug treatment condition (40µM Scramble peptide (control) *versus* 40µM RI-AG03) delivered through diet. Rows represent post-developmental age 3, 14 and 28 days. Neurons show axonal swellings (dark round structures) that increase with age and are exacerbated in hTau2N4R-E14 expressing flies. **B**) Quantification of axonal swellings were automatically quantified using 3D images with IMARIS (see methods). Graphs represent mean ±SD, and dots represent individual animals. RI-AG03 treatment had no statistical effect on axonal swelling density in either genotype where *p<0.05 (2-way ANOVA with Tukey's multiple comparisons). However, a significant reduction in axonal swelling was observed in hTau2N4R-E14 flies at day 14 in one biological replicate (**Supplementary Figure 21**). N=6-8 brains collected from two biological repeats per genotype.

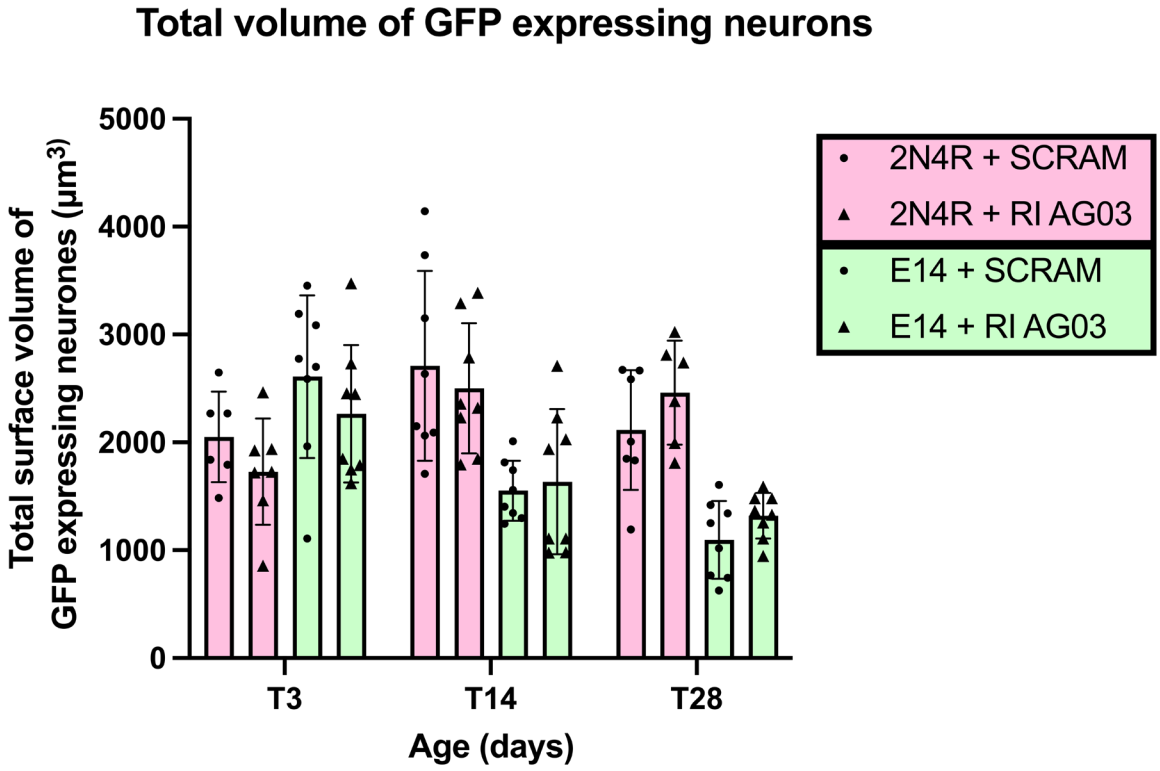


**Figure 44. RI-AG03 does not improve total volume of GFP expressing neurons.**

Quantification of neuron volume was automatically quantified using 3D images with IMARIS (see methods). Flies were fed 40µM Scramble peptide (control) *versus* 40µM RI-AG03 delivered through diet. Graphs represent mean ±SD, and dots represent individual values. *p<0.05 (2-way ANOVA with Tukey's multiple comparisons). RI-AG03 treatment had no statistical effect on neuronal volume in either genotype. N=6-8 brains collected from two biological repeats per genotype.

## 6.4 Discussion

Pharmacological strategies for Tauopathies aim to suppress the formation or persistence of toxic Tau species. In this Chapter, I tested RI-AG03, a retro-inverted peptide inhibitor designed to block the aggregation-promoting $^{306}$VQIVYK$^{311}$ motif. My results show that RI-AG03 selectively reduced accumulation of hyperphosphorylated Tau and showed promising trends in reducing axonal degeneration, though non-significant. Whilst these findings support the targeting of $^{306}$VQIVYK$^{311}$ against pathological Tau species, the modest effects compared to genetic deletion of $^{306}$VQIVYK$^{311}$ highlight the pharmacological limitations of RI-AG03's efficacy. Potential reasons that could account for the comparatively inadequate reduction of neurodegeneration could be due to pharmacokinetics limiting RI-AG03 bioavailability and penetrance. Alternatively, toxic Tau species may persist because pathogenic hTau2N4R-E14 monomers are continuously produced in this overexpression model faster than RI-AG03 can inhibit their aggregation, or because RI-AG03 may fail to neutralise, and may even stabilise, toxic Tau conformations.

### 6.4.1 RI-AG03 supresses accumulation of pseudo-phosphorylated Tau

I have demonstrated that RI-AG03 selectively reduces intracellular accumulation of the phospho-mimicking hTau2N4R-E14 mutant *in vivo*. This supports previous reports that inhibition of the $^{306}$VQIVYK$^{311}$ and $^{275}$VQIINK$^{280}$ motifs reduces Tau aggregation (Zhang et al., 2020b, Sievers et al., 2011, Seidler et al., 2018). However, this study importantly extends this body of literature, demonstrating efficacy against highly toxic disease-relevant hyper-phosphorylated Tau species, whereas previous aggregation inhibitor studies primarily test against wildtype Tau variants (Zhang et al., 2020b, Sievers et al., 2011, Seidler et al., 2018).

In contrast, RI-AG03 did not reduce accumulation of wildtype hTau2N4R. This selectivity demonstrates a Tau species-specific effect likely driven by the distinct

pathological conformations each mutant adopts. Phosphorylation promotes misfolding that exposes the $^{306}$VQIVYK$^{311}$ motif (Jeganathan et al., 2008), which may provide increased binding access for inhibitors such as RI-AG03. In wildtype Tau, this motif may be less exposed, possibly limiting the efficacy of pharmacological targeting.

Collectively, these results validate $^{306}$VQIVYK$^{311}$ as an effective therapeutic target against Tau accumulation *in vivo*, particularly against disease-relevant Tau species, suggesting that inhibitors may act selectively depending on the pathogenic state of Tau. This is an important insight for future therapeutic designs.

### 6.4.2 Pharmacological targeting of $^{306}$VQIVYK$^{311}$ is less effective than genetic deletion

Although RI-AG03 successfully reduced Tau accumulation by up to 30% in hTau2N4R-E14 flies, it did not completely rescue accumulation as observed with genetic deletion of $^{306}$VQIVYK$^{311}$ in previous Chapters, highlighting the fundamental differences between these approaches.

Genetic deletion achieves 100% target elimination, whereas pharmacological inhibition faces inherent limitations. Drug efficacy is highly dependent on its stability, penetration, assimilation and pharmacokinetics (Sigurdsson, 2018). Therefore, the limited efficacy of RI-AG03 likely reflects incomplete drug absorption through feeding, potential drug degradation throughout feeding period, and variable tissue penetration which may have reduced effective concentrations reaching the target neurons. While retro-inverted peptides like RI-AG03 are designed to be protease resistant, they may still be subjected through clearance mechanisms and biological barriers like the *Drosophila* gut which may hinder the drug reaching its target efficiently. Limited efficacy of RI-AG03 could be due to insufficient local delivery concentration to the target tissues, where the $^{306}$VQIVYK$^{311}$ motifs are not saturated effectively. This is particularly relevant in my overexpression model where the Tau is continuously expressed in the target Or47b neurons through the UAS-GAL4 system

(Brand and Perrimon, 1993), as there will already be high local concentration of Tau to target. Moreover, the binding efficiency and half-life of RI-AG03 is unknown. If RI-AG03 does not bind permanently, its dose may be insufficient to maintain high levels of Tau expression in this overexpression model.

Future studies should address these pharmacokinetic concerns by optimising drug dosage, particularly to compensate for pathologically prone Tau species, and consider more direct drug delivery methods, such as injection to forgo biological barriers and reduce proteolytic degradation. Further biochemical analysis of Tau:RI-AG03 binding interaction using surface plasmon resonance (SPR), would provide quantitative information on binding kinetics, affinity and potential degradation which will help guide dose optimisation.

### 6.4.3 Toxic Tau species may persist despite aggregation inhibition

As previously discussed in **Chapter 4**, toxicity in Tauopathies is thought to arise primarily from small, seed-competent Tau conformers which contribute towards impaired axonal transport, synaptic function and neurodegeneration (Ward et al., 2012, Flach et al., 2012, Tian et al., 2013, Santacruz et al., 2005). However, emerging studies demonstrate that control brains contain high molecular weight Tau species and aggregates which lack seeding competency and pathogenic properties (Jury-Garfe et al., 2024, Martinez et al., 2025). This shifts the perspective that conformational structure, rather than relative Tau abundance determines Tau toxicity (Martinez et al., 2025).

Whilst there was a trend toward reduced axonal swelling density in RI-AG03 treated hTau2N4R-E14 flies, quantification analysis did not reach statistical significance. This suggests that RI-AG03 achieved incomplete suppression of pathogenic Tau species, with hTau2N4R-E14 conformations persisting and retaining toxic properties such as disrupting axonal transport, increased motility and enhanced neuronal dysfunction (Hallinan et al., 2019, Hoover et al., 2010, Talmat-Amar et al., 2011, Padmanabhan et al., 2024).

This can be explained by two non-exclusive hypotheses. Either RI-AG03 is not saturating the demand of Tau being produced in this overexpression model, or that RI-AG03 is not effectively neutralising pathogenic conformations of Tau most responsible for conferring toxicity.

As the UAS-GAL4 system continuously drives the expression of Tau, newly synthesised monomers are constantly being produced. RI-AG03 functions by binding to the $^{306}$VQIVYK$^{311}$ motif on Tau to prevent growing aggregation, potentially meaning it can cap many different sizes and stages of the aggregation cascade. However, in this high overexpression model, the rate of Tau production may exceed RI-AG03's ability to bind all available motifs allowing the newly synthesised pathogenic monomers and oligomers to accumulate and induce neuronal degeneration, despite a portion of pathogenic Tau aggregates being capped by RI-AG03 effectively. This could explain why there was a trend but not significant reduction of axonal swelling density in RI-AG03 treated hTau2N4R-E14 expressing flies.

Moreover, the mechanism by which RI-AG03 confers protection may differ from genetic deletion of $^{306}$VQIVYK$^{311}$. By fundamentally altering the primary sequence of Tau, the secondary and tertiary structures of pathological Tau are prevented from forming in ΔVQIVYK mutants, whereas RI-AG03 is not designed to structurally alter the Tau protein itself. Other domains like the N and C terminal work in combination with the $^{306}$VQIVYK$^{311}$-containing microtubule binding domain to influence conformational misfolding in pathological contexts (Jeganathan et al., 2008). Therefore while RI-AG03 works to cap the $^{306}$VQIVYK$^{311}$ domain to prevent further aggregation of toxic Tau species, it may not be able to fundamentally alter the pathological conformation of hTau2N4R-E14, causing the majority of neuronal damage.

Additionally, as the aggregation cascade is dynamic and metastable, and given that RI-AG03 was delivered daily, it is possible that RI-AG03 binds to different types of aggregates, at different stages, potentially stabilising some monomers in pathogenic conformations, or freezing Tau aggregates in pathogenic states. Previously, RI-AG03 has shown to cap Tau fibrils and prevent fibril growth, which reduced seed competence (Aggidis et al., 2024), however it is unknown if these species are toxic in other ways such as disrupting axonal transport, reduced microtubule binding, or induce axonal and synaptic degeneration (Talmat-Amar et al., 2011, Hoover et al., 2010, Hallinan et al., 2019, Mudher et al., 2004). This may possibly explain why RI-AG03 was not as potent at reducing neurodegeneration phenotypes unlike the ΔVQIVYK mutants which prevented misfolded pathogenic Tau conformations, and rescued neurodegeneration phenotypes.

Further experiments staining for misfolded conformers and isolating different fractions of Tau through insolubility assays are needed to quantify how RI-AG03 influences Tau conformation and Tau aggregate formation. If pathological Tau conformations persist despite reduced aggregation, it would suggest that therapies need to combine aggregation inhibitor strategies with strategies to prioritise reducing pathogenic Tau conformers, and reduce total Tau expression.

### 6.4.4 Experimental factors affecting RI-AG03 efficacy

RI-AG03 had no effect on wildtype hTau2N4R mediated neurodegeneration of the Or47b neurons. These results differ from Aggidis et al., who reported improved survival and reduced retinal degeneration with RI-AG03 in *Drosophila* expressing wildtype hTau2N4R. Importantly, these results also do not mirror the significant reduction in neurodegeneration modelled by the Or47b neurons, longevity and climbing assays of hTau2N4R-DEL *versus* hTau2N4R in **Chapter 3** and **Chapter 5.**

Several experimental factors may explain the discrepancy with Aggidis et al. First, their study used a weaker 1X UAS driver, whereas my 10X UAS constructs produced substantially higher Tau levels, which may have exceeded the amount of Tau aggregation that could be supressed by the inhibitor at the same 40µm dose. Second, drug exposure in their system began immediately after eclosion, when Tau levels are lower, whereas in my model aggregates may already have formed during larval and pupal development. Because RI-AG03 prevents further aggregation but does not disassemble existing fibrils, early treatment may be more effective. Third, while RI-AG03 is proteolytically stable *in vitro,* digestion in the fly gut may still reduce bioavailability when delivered through the diet. Together, these factors highlight the need to optimise dose, delivery method to pass biological barriers, and treatment timings to maximise therapeutic efficacy *in vivo.*

### 6.4.5 Conclusion

The findings from this Chapter demonstrate that while pharmacological targeting of $^{306}$VQIVYK$^{311}$ can reduce pathology associated with Tau-mediated neurodegeneration, there are several factors which influence its success including pharmacokinetic limitations and the dynamic nature of Tau toxicity. My results support $^{306}$VQIVYK$^{311}$ as an excellent druggable candidate target for reducing Tau accumulation against pathogenic Tau species, suggesting that $^{306}$VQIVYK$^{311}$ may be appropriate for treating multiple different Tau species at multiple disease stages. Future studies should optimise RI-AG03 delivery and dosing, and focus on how RI-AG03 may affect toxic Tau conformations. This will give future insight to whether target specific drugs like RI-AG03 can be used alone to reduce neurotoxicity, or whether multi-target or cocktail inhibitor approach for treatments, perhaps combining multiple approaches like immunotherapy and anti-sense oligonucleotides to reduce total Tau levels and clear pathogenic species are needed (Vaz and Silvestre, 2020, Feneberg and Otto, 2020).

### 6.4.6 Future directions

To improve and build on the findings of this study, it would be important to explicitly characterise how RI-AG03 affects Tau conformation. This could be achieved by repeating a similar experiment in **Chapter 4,** assessing how RI-AG03 impacted the production of MC1-positive misfolded Tau conformers expressed in the Or47b neurons, and by assessing the production of insoluble aggregates formed in different fractions. This would determine whether RI-AG03 redirects Tau aggregates into inert or pathological species. This would also help define which species of Tau should be targeted before overt aggregation.

Furthermore, the dose of RI-AG03 should be optimised to hyperphosphorylated Tau species. Testing higher doses would determine if drug saturation would be able to improve the efficacy of RI-AG03 in comparison to the ΔVQIVYK mutants. Additionally, further characterisation of RI-AG03's proteolytic stability against proteases should be investigated to assess the efficacy of the drug through feeding. Such results may inform alternative delivery methods such as injection which could read the target neurons more effectively.

# Chapter 7 $^{306}$VQIVYK$^{311}$ mediated toxicity in FTDP-17(*MAPT*) contexts

## 7.1 Introduction

The overarching aim of this thesis is to investigate how aggregation and phosphorylation contribute towards Tau-mediated degeneration to gain better insight into the significant heterogeneity in Tauopathies. Results Chapters so far have provided comprehensive evidence that $^{306}$VQIVYK$^{311}$ is an essential mediator to Tau toxicity and is an excellent candidate for therapeutic targeting to reduce Tau accumulation and formation of toxic conformers even in highly toxic phospho-mimicking mutants.

In this Chapter I investigate how aggregation and phosphorylation contribute towards clinical and pathological heterogeneity observed across different Tau mutants in familial Tauopathies. I aimed to characterise mutation-specific differences in how pathology develops, and to investigate the underlying mechanisms driving mutant-specific degeneration. These findings will also inform whether therapeutic strategies targeting Tau pathology need to be tailored to specific diseases or if common mechanisms like $^{306}$VQIVYK$^{311}$-mediated toxicity can be broadly targeted across the heterogenous Tauopathies.

### 7.1.1 Heterogeneity in Tauopathies

The greatest challenges facing diagnosis and treatment of Tauopathies is their significant clinical, pathological and molecular heterogeneity. Different Tauopathies like AD, PSP, PD and frontotemporal dementia each have distinct clinical profiles, disease progressions, and brain regions effected. Molecularly there are also variabilities in the Tau isoforms compositions and fibril morphologies across diseases (Qi et al., 2025, Shi et al.,

2021, Schweighauser et al., 2025). This heterogeneity implies that each disease has different underlying mechanisms of toxicity despite all being caused primarily by dysfunctional Tau.

### 7.1.2 FTDP-17(*MAPT*) familial Tauopathies

A subset of familial Tauopathies are caused by genetic dysfunction within the *MAPT* gene encoding Tau, called frontotemporal dementia with or without parkinsonism linked to chromosome 17 (FTDP-17(*MAPT*)). Missense, deletion, and splice mutations within the *MAPT* gene were first described in 1998 following human DNA sequence analysis of families with autosomal dominant FTDP-17 (Hutton et al., 1998, Poorkaj et al., 1998, Spillantini et al., 1998). As a collective, these mutations provide clear evidence that dysfunction of the Tau gene directly results in neurodegenerative disorders. This is consistent with other *in vivo* studies showing that neurodegeneration is enhanced by replicated FTDP-17(*MAPT*)-associated mutations (Krishnamurthy and Johnson, 2004).

Despite all sharing Tau pathology patients carrying *MAPT* mutations are clinically, pathologically, and genetically heterogenous. Different Tauopathy strains have previously been classified by cellular pathology and composition of Tau inclusions in the brain. Immunohistochemical slices of tauopathy patients show distinct isoform composition (either 3R or 4R or 3R and 4R) and distinct lesion morphologies (Spillantini et al., 1998). Emerging evidence from cryo-EM studies of Tau fibril ultrastructure suggests that disease-specific fibril conformation may provide new methods for Tauopathy classification, revealing structural diversity which differs from traditional isoform-based classification (Shi et al., 2021, Qi et al., 2025, Schweighauser et al., 2023, Schweighauser et al., 2025). Neuroimaging studies have also shown that *MAPT* mutations generate distinct progression patterns of regional atrophy related to their clinical phenotypes (Whitwell et al., 2009a, Whitwell et al., 2009b) (Young et al., 2021). The significant clinical and molecular heterogeneity between

Tauopathies creates challenges in understanding which pathological mechanisms underscore Tau-mediated degeneration.

### 7.1.3 *MAPT* mutation location determines pathological mechanisms

There are several ways in which Tau mutations can cause disease. Mechanisms underlying Tau-mediated neurodegeneration are primarily determined by their location along the Tau gene, where toxicity is associated with the distinct loss of function of the affected domain. For example, mutations within the microtubule binding domain primarily affect aggregation propensity consequential to loss of microtubule binding and increased intracellular free Tau. Multiple groups have demonstrated that mutations within microtubule binding domain such as ΔK280, P301L, P301S, and V337M directly reduces Tau-microtubule binding and polymerisation and directly increase aggregation propensity compared to controls *in vitro* (Hasegawa et al., 1998, Lee et al., 2001). In contrast, splice-site mutations like IVS10 mutations alter the ratio of 3R:4R Tau isoforms expressed which favour aggregation and disrupts microtubule binding affinity (Spillantini et al., 1998, Lee et al., 2001, Adams et al., 2010).

Other missense mutations have been associated to increase Tau phosphorylation (Alonso Adel et al., 2004), which promotes aggregation and filament assembly across multiple human and animal models (Goedert et al., 1999, Wittmann et al., 2001, Shulman and Feany, 2003).

The distinct pathological effects of different mutations are supported by recent interactome studies. Comparison between different FTDP-17(*MAPT*) mutants and wildtype Tau show distinct interactomes of ribosomal units, translation initiation factors and HNRNPs (Kavanagh et al., 2022). This is further evidence that pathologically distinct Tau species possess distinct interactomes, where interacting proteins bind with distinct Tau conformers

consequential to changes in Tau's primary sequence, contributing to mutant-specific pathological mechanisms.

### 7.1.4 P301S *versus* R406W

In this Chapter, two common FTDP-17(*MAPT*) mutants: P301S and R406W were investigated. They each differ significantly in their clinical and molecular profiles and likely induce pathology through distinct mechanisms. Mutant characteristics are summarised below.

**Table 10. P301S/L versus R406W Tau mutant profiles.**

| Feature | P301S/L | R406W |
|---|---|---|
| Mutation description, loci | Exonic missense mutation in Exon 10 (codon 301, Pro→ Ser or Leu), within the microtubule-binding repeat domain. | Exonic missense mutation in Exon 13 (codon 406, Arg→ Trp), in the C-terminal region. |
| Onset and disease course | Early onset (30s-50s). Aggressive disease with short disease duration and younger age of death. P301S is more aggressive than P301L (Bugiani et al., 1999, Lossos et al., 2003). | Later onset (50s-60s) and slower progression are most common, but early onset with rapid decline has been reported (Ng et al., 2015, Saito et al., 2002). |
| Tau isoform composition | Predominantly 4R Tau inclusions. Mutant Tau dominates over wildtype in brain filaments (Hutton et al., 1998, Rizzu et al., 2000)). | Mixed 3R+4R Tau inclusions, mutant and wildtype deposited in roughly equal amounts. (Spillantini et al., 1998, Ygland et al., 2018) |
| Tau fibril ultrastructure | 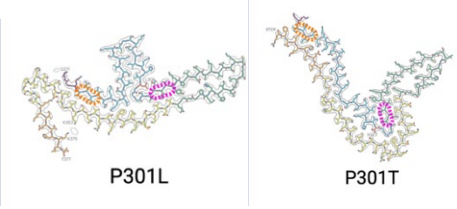 (Schweighauser et al., 2025) For more, see **Figure 9.** | 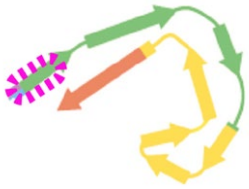 (Qi et al., 2025)For more, see **Figure 9.** |
| Neuropathology: Macroscopy | Marked frontal and temporal cortical atrophy, with subcortical involvement (basal ganglia, brainstem, spinal cord). (Mirra et al., 1999, Miyasaka et al., 2001, Reed et al., 1998, Whitwell et al., 2009a, Whitwell et al., 2009b) | Hippocampal and temporal lobe atrophy, often resembling Alzheimer's. Mirra, 1999 #386}(Miyasaka et al., 2001, Reed et al., 1998, Whitwell et al., 2009a, Whitwell et al., 2009b, Ygland et al., 2018) |

<table>
<tr><td></td><td colspan="2"> 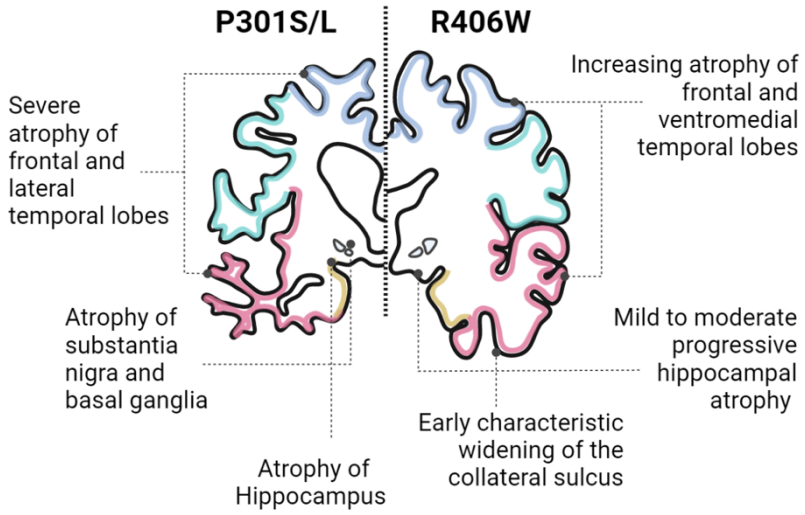

Representative coronal MRI images from two familial FTDP-17(*MAPT*) patients, both with 4-year disease duration at time of examination. Left: P301L mutation patient. Right: R406W mutation patient. Anatomical regions are colour coded as follows: blue = frontal lobe, cyan = parietal lobe, yellow = occipital lobe, pink = temporal lobe. Neuroimages traced from (Whitwell et al., 2009a, Whitwell et al., 2009b, Ygland et al., 2018).</td></tr>
<tr><td>Neuropathology: Microscopy</td><td>Severe neuronal loss, ballooned neurons, pronounced gliosis. Abundant 4R tangles, rod-like and semi-circular inclusions, Pick body-like structures, and extensive hyperphosphorylation (Spillantini et al., 1998, Yasuda et al., 2005).</td><td>Neuronal loss, gliosis, ballooned neurons. Large flame-shaped and globose NFTs, fine neuropil threads, and occasional Pick body-like structures (Miyasaka et al., 2001, Reed et al., 1998, Ygland et al., 2018).</td></tr>
<tr><td>Clinical profile</td><td>Symptoms resemble corticobasal degeneration, with mood, memory, and concentration changes, progressing to rigidity, hallucinations, dystonia, supranuclear palsy (Bugiani et al., 1999). Parkinsonism present in some cases (Sperfeld et al., 1999). Rapid cognitive and motor decline with severe impairment within 3-5 years (Lossos et al., 2003).</td><td>Often mistaken for AD due to memory impairments as the leading symptom, with behavioural changes, language deficits, déjà vu, confabulation, or psychosis also reported (Ikeuchi et al., 2008, Ygland et al., 2018). Parkinsonism is less common but can occur (Hirschbichler et al., 2015). Early onset with delusions and rapid decline described in homozygous cases (Saito et al., 2002, Ng et al., 2015).</td></tr>
<tr><td>Aggregation propensity</td><td>Strongly promotes aggregation. P301S and P301L fibrillise rapidly in vitro (Nacharaju et al., 1999, Arrasate et al., 1999, Strang et al., 2018). Aggregates in brain are dominated by mutant Tau (Hutton et al., 1998, Rizzu et al., 2000).</td><td>Aggregation occurs but with mixed reports. Some studies show increased fibrillisation (Alonso Adel et al., 2004, Strang et al., 2018), others no major kinetic difference (Chang et al., 2008).</td></tr>
<tr><td>Phosphorylation</td><td>Hyperphosphorylation is a consistent feature, inclusions are heavily phosphorylated (Alonso Adel et al., 2004, Delobel et al., 2002).</td><td>Hyperphosphorylated Tau consistently found in patient brains (Alonso Adel et al., 2004, Delobel et al., 2002). In vitro findings are mixed. soluble R406W Tau is less phosphorylated than wildtype, but insoluble fractions are highly</td></tr>
</table>

| | | |
|---|---|---|
| | | phosphorylated (Miyasaka et al., 2001). |
| Microtubule binding | Strongly reduced binding compared to wildtype. Both P301S and P301L disrupt Tau-microtubule interactions, destabilising axonal microtubules (Hutton et al., 1998, Hong et al., 1998). | Reduces binding affinity. R406W alters Tau's C-terminal conformation and charge, impairing microtubule interactions and detaching Tau from membranes (Hasegawa et al., 1998, Gauthier-Kemper et al., 2011). |

### 7.1.5 Chapter aims and objectives

FTDP-17(*MAPT*)-associated mutations differ significantly in the clinical and molecular profiles, and likely induce pathology through distinct mechanisms. Current studies are limited by different experimental paradigms and expression systems, which confounds the understanding of how different mutations influence Tau pathology underlying clinical heterogeneity. Using *Drosophila* I can overcome these experimental limitations by expressing the mutants equally. It is essential to understand which mechanisms are influencing mutant specific degeneration, and whether therapeutic strategies are broadly effective against mutant-specific toxicity.

**Aim 5:** To investigate the mechanisms by which frontotemporal dementia-linked *MAPT* mutations influence Tau accumulation and neuronal degeneration.

- **Objective 1:** Characterise FTDP-17(*MAPT*)-associated Tau mutations P301S and R406W mediated neuronal degeneration and Tau accumulation.
- **Objective 2:** Unpick the mechanisms underlying mutant-specific degeneration.

## 7.2 Methods

See methods **section 2.2** for confocal image acquisition. See methods **section 2.6** for IMARIS 3D image analysis. See methods **section 2.4** for all longevity assays.

## 7.3 Results

### 7.3.1 FTDP-17(*MAPT*)-associated Tau mutant R406W causes increased neurodegeneration.

To investigate whether different FTDP-17(*MAPT*) mutations are neuropathologically distinct, I assessed the impact of hTau2N4R-P301S and hTau2N4R-R406W mutant expression in Or47b neurons. Given their distinct clinical profiles and different locations along the Tau protein, I hypothesised that the mutants would have distinct neuropathological phenotypes in my established *Drosophila* model. These mutants were designed and generated on the same UAS-mCherry::hTau2N4R background and inserted into the same insertion site, *Attp40* to ensure equal expression (as previously established in **Chapter 3-5**).

As seen in **Chapter 3** and from other Tauopathy models, phenotypes of Tau-mediated degeneration are axonal swellings leading to fragmentation and neuronal loss (Lin et al., 2003, Sahara et al., 2014, Probst et al., 2000, Stubbs et al., 2023) due to aging, Tau accumulation and impaired axonal transport (Mudher et al., 2004, Talmat-Amar et al., 2011, Richardson et al., 2024).

Control Or47b neurons expressing no Tau presented as highly compact axon bundles with some evidence of age-related swellings in 14- and 35-day-old animals (**Figure 45 A**). However, the number and size of axonal swellings were greatly increased upon hTau2N4R expression progressively at all ages assayed (**Figure 45 A**), as established in **Chapter 3.**

At day 14, both hTau2N4R-P301S and hTau2N4R-R406W showed similar axonal swelling densities compared to wildtype hTau2N4R. However, by day 35 hTau2N4R-R406W mutants developed a significantly increased axonal swelling density, with quantification showing a 2-fold increase compared to hTau2N4R (**Figure 45 A, B**). Additionally, hTau2N4R-R406W showed a pronounced reduction of total axonal bundle

volume at day 35, which was significantly lower than hTau2N4R-P301S and no Tau control flies by 50% (**Figure 46**). In contrast, hTau2N4R-P301S showed no significant difference in axonal swelling density or neuronal volume loss compared to wildtype hTau2N4R at any timepoint (**Figure 45**, **Figure 46**). In fact, at T14, hTau2N4R-P301S produced the lowest average amount of axonal swellings compared to wildtype and hTau2N4R-R406W expressing flies.

These findings demonstrate that R406W mutation is more toxic than P301S and wildtype hTau2N4R in the Or47b neurons. The age-dependent emergence of differential neuronal degeneration suggests that R406W exerts cumulative toxic effects, indicating distinct pathological mechanisms compared to the other Tau mutants. It is unexpected that P301S is less toxic than both wildtype and R406W mutations, given the current literature describes P301- as highly toxic, aggressive mutants (Bugiani et al., 1999, Xie et al., 2022). Therefore, next I assessed the pathological Tau behaviour of P301S and R406W, and establish if the distinct neuronal degeneration patterns reflected Tau accumulation patterns.

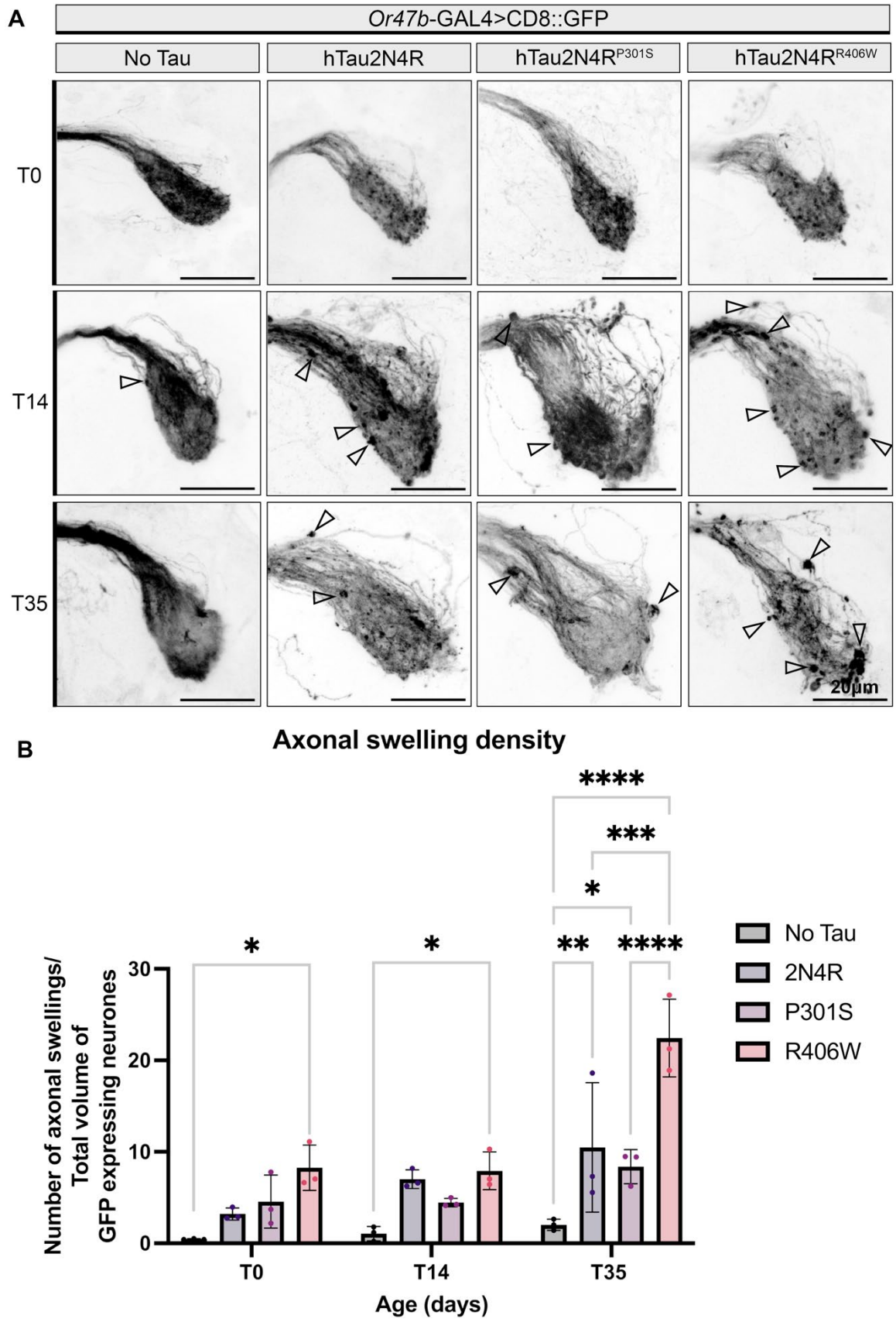


**Figure 45. R406W mutant Tau causes increased progressive axonal degeneration.**

(A) Maximum projection confocal images of flies expressing membrane bound GFP (CD8::GFP) at the Or47b neurons enhanced with α-GFP. Columns represent genotypes

expressing different mCherry-tagged hTau2N4R variants plus the driver expressing GFP only as a control (left most column). Rows represent post-developmental age 0, 14 or 35 days. Normal structure of the neurons shows some axonal swellings (Arrows) that occur with age and are increased in wildtype hTau2N4R flies and more frequent in hTau2N4R-R406W expressing flies. (**B**) Quantification of axonal swellings were automatically quantified using 3D images with IMARIS (see methods). Graphs represent mean ±SD, and dots represent individual values. *p<0.05, **p<0.01, ***p<0.001, ****p<0.0001 (2-way ANOVA with Tukey's multiple comparisons). N= 3 animals.

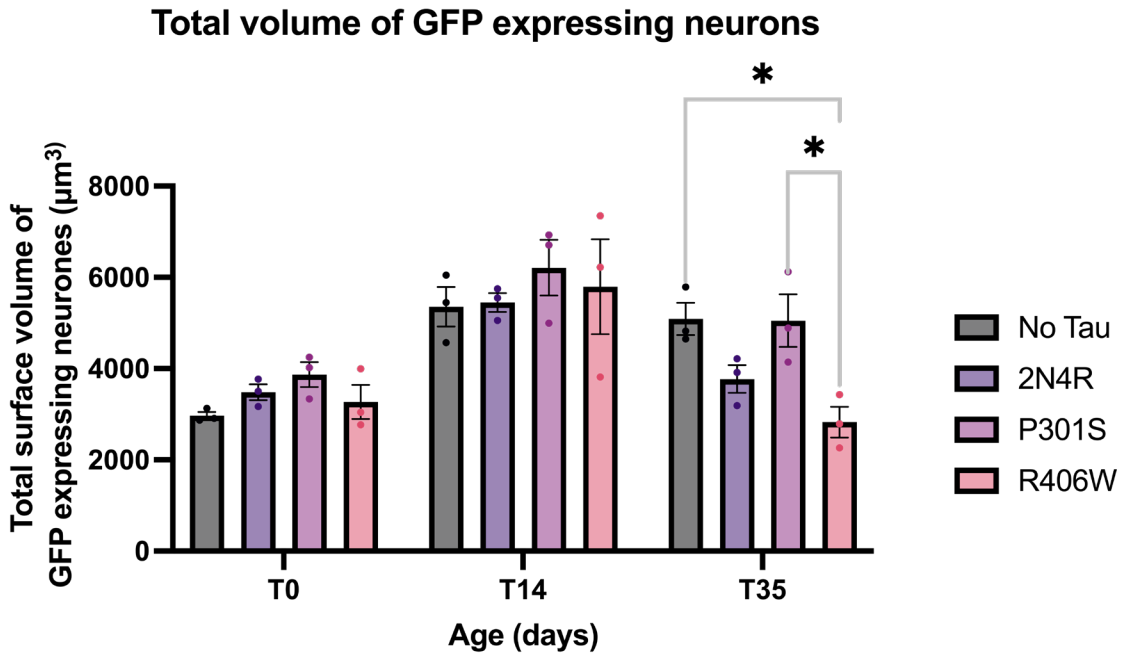


**Figure 46. Total volume of GFP expressing neurons expressing FTDP-17(*MAPT*)-mutant Tau.**

Quantification of neuron volume was automatically quantified using 3D images with IMARIS (see methods). Graphs represent mean ±SD, and dots represent individual values. *p<0.05 (2-way ANOVA with Tukey's multiple comparisons). N= 3 brains collected per genotype.

### 7.3.2 P301S and R406W show distinct Tau accumulation profiles.

Having observed differential axonal degeneration propensities between R406W and P301S mutants, I next investigated how these mutants influenced the pathological behaviour of Tau, assessing their ability to influence Tau accumulation. Understanding how each mutant influenced Tau accumulation would give insight to the mechanism underlying axonal degeneration previously observed.

All Tau mutants were uniformly distributed in Or47b expressing axons and synapses at T0 (**Figure 47 A**). By day 14, the frequency and size of Tau accumulates became prominent, in all mutants tested, and quantification of Tau accumulate density was similar between all mutants. However, by day 35 the density of Tau accumulations had similarly doubled in hTau2N4R and hTau2N4R-R406W compared to respective day 14 levels (**Figure 47 B**). In contrast, hTau2N4R-P301S produced significantly lower Tau accumulate density than both wildtype and hTau2N4R-R406W mutants at day 35 (**Figure 47 B**). This is surprising given that hTau2N4R-R406W and wildtype Tau have similar levels of Tau accumulation despite hTau2N4R-R406W having significantly worse neurodegeneration phenotypes.

Collectively these results demonstrate that the pathological behaviour of Tau is FTDP-17(*MAPT*)-mutant specific, indicating differential mechanisms underlying toxicity. It also implies that mutants like R406W can induce toxicity though mechanisms independent of Tau accumulation. Having established that R406W is the most toxic mutant in this experimental system, I next sought to investigate the molecular mechanisms underlying the enhanced toxicity by assessing the contribution of phosphorylation and aggregation towards R406W-specific toxicity.

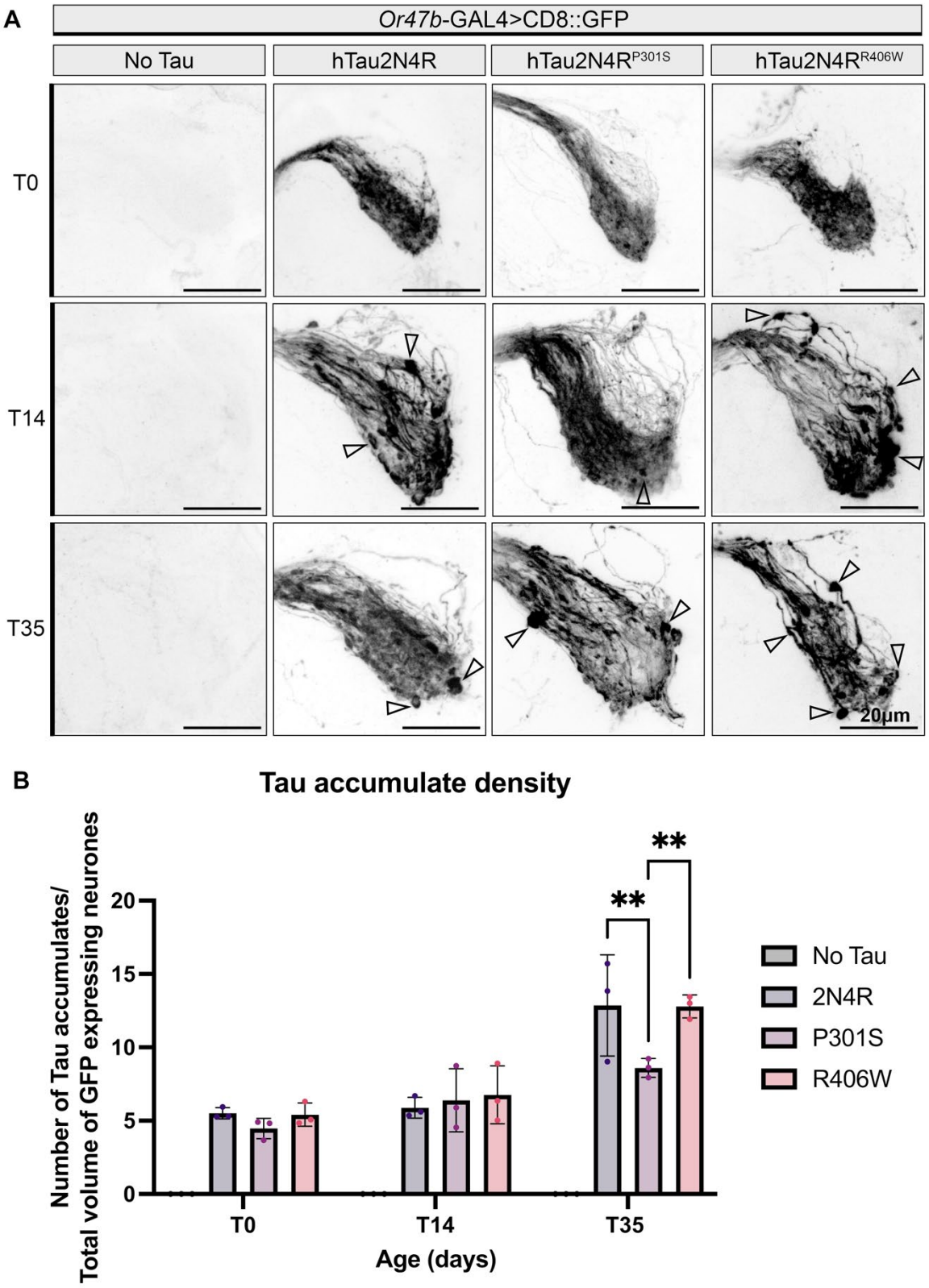


**Figure 47. FTDP-17(*MAPT*)-associated Tau mutants have differential Tau accumulation propensities.**

A) Maximum projection confocal images of the antennal lobe in the brain of 0, 14 and 35 day old flies expressing mCherry::Tau mutants in the Or47b neurons (enhanced with α-hTau Dako). Arrows point toward beaded Tau accumulates within expressing neurons which increase in frequency and size with age. Wildtype hTau2N4R and hTau2N4R-R406W have

the highest density of Tau accumulates. (B) Quantification of the Tau accumulate density were measured using 3D images with IMARIS with a spotting tool (see methods) N=3. Graphs represent mean ±SD. **p<0.01 (2-way ANOVA with Tukey's multiple comparisons).

### 7.3.3 Deletion of aggregation motif $^{306}$VQIVYK$^{311}$ rescues R406W-specific survival deficits.

Having established that R406W causes enhanced toxicity in Or47b neurons, I next sought to unpick the mechanism by R406W-specific enhanced toxicity occurred by. I investigated whether this toxicity was mediated through phosphorylation-dependent or aggregation-dependent mechanisms. I designed two R406W variants: hTau2N4R-R406W/ S2A (phosphorylation-resistant R406W mutant at S262 and S356 by alanine substitutions) and hTau2N4R-R406W/DEL ($^{306}$VQIVYK$^{311}$ deletion mutant) to test which pathological mechanism drives R406W-specific toxicity. I assessed their toxicity using a longevity assay with pan-neuronal expression of these mutants to provide a robust measure of overall toxic Tau burden and reflect the extent of global neuronal dysfunction.

Results showed gender-specific population survival differences. In both male and female cohorts, compared to controls expressing mCherry (no Tau), pan-neuronal expression of hTau2N4R significantly reduced survival and lowered median lifespan by 4 and 7 days in the male and female populations, respectively (**Figure 48** and **Figure 49**).

Notably, longevity results contrast with findings in the Or47b neurons where hTau2N4R-R406W showed enhanced neurodegeneration compared to wildtype hTau2N4R. In the longevity assays, both female and male hTau2N4R-R406W had improved median survival rates compared to wildtype hTau2N4R (**Figure 48** and **Figure 49**).

The phosphorylation-resistant mutant hTau2N4R-R406W/S2A unexpectedly showed significant lethality in both genders, causing the lowest median survival age of all genotypes,

at 30 days in males and 28 days in females (**Figure 48** and **Figure 49**).This indicates that phosphorylation of these sites may provide neuroprotective properties in R406W. In contrast, R406W mutants lacking the $^{306}$VQIVYK$^{311}$ domain significantly improved survival in the male cohort, improving median survival age of 38 days in hTau2N4R-R406W flies versus 46 days in hTau2N4R-R406W/DEL flies (**Figure 48**). The reason for such sharp survival curve from the hTau2N4R-R406W/DEL compared to the other groups was because there was a smaller number of flies assessed, due to low progeny yield from the genetic cross. In the female group, deletion of $^{306}$VQIVYK$^{311}$ did not improve longevity of hTau2N4R-R406W expressing flies, showing gender-specific effects underlying R406W-mediated toxicity (**Figure 49**).

Collectively, these findings reveal several tissue-specific and gender-specific effects of R406W toxicity. Importantly, this chapter shows that R406W mediates toxicity through the $^{306}$VQIVYK$^{311}$ domain. My data also implies that inability to phosphorylate R406W at the S2A epitopes makes the Tau more toxic, and therefore phosphorylation at these sites may provide neuroprotection against R406W-mediated degeneration. However, given such stark contrast with previous studies investigating the effect of S2A mutations, it is difficult to draw and interpret these findings, and further repetitions would be needed before conclusions are made. Nonetheless, these findings support therapeutic targeting of $^{306}$VQIVYK$^{311}$ in wider groups of Tauopathies.

A.

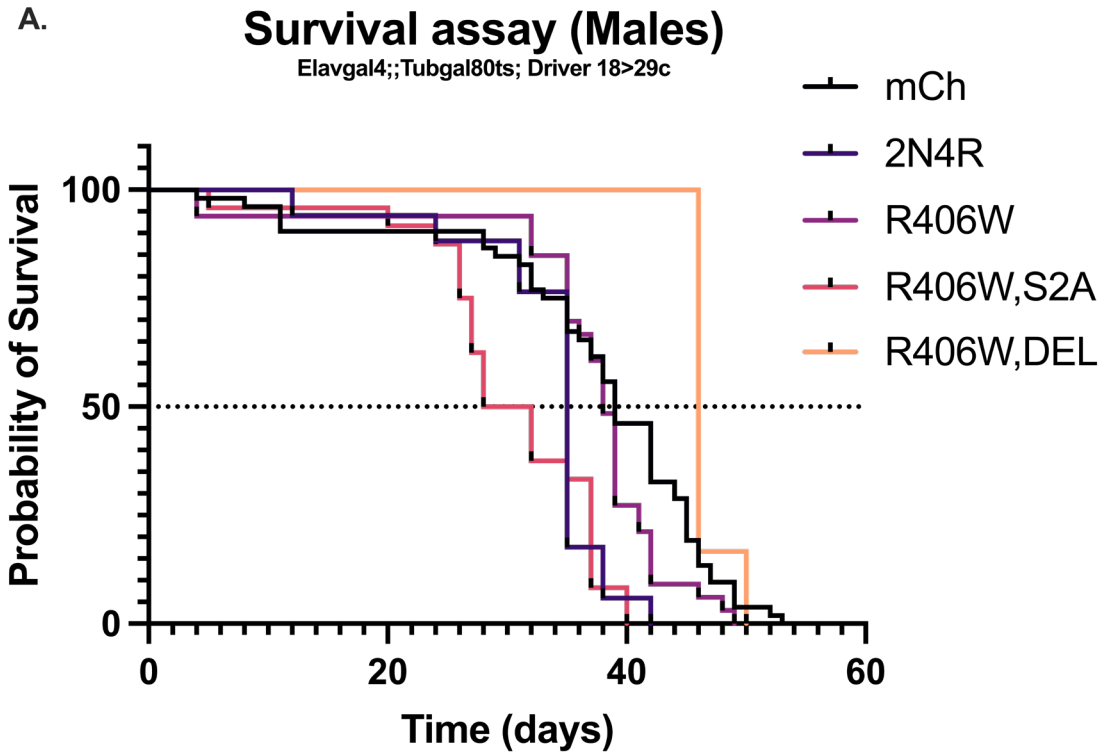


B.

| Median Survival | | | | |
|---|---|---|---|---|
| mCh | 2N4R | R406W | R406W-S2A | R406W-DEL |
| 39 | 35 | 38 | 30 | 46 |

C.

| | mCherry | 2N4R | R406W | R406W,S2A | R406W,DEL |
|---|---|---|---|---|---|
| mCherry | | 0.0009 | 0.1059 | <0.0001 | 0.0452 |
| 2N4R | | | 0.003 | 0.277 | <0.0001 |
| R406W | | | | <0.0001 | 0.0012 |
| R406W,S2A | | | | | <0.0001 |
| R406W,DEL | | | | | |

**Figure 48. Survival assay of male TauR406W mutants.**

A) Kaplan Meier survival curves for Elav-Gal4;;TubGal80ts; driven mCherry Tagged Tau mutants: hTau2N4R, hTau2N4R-R406W hTau2N4R-R406W/S2A and hTau2N4R-R406W/DEL expressing male flies. Flies expressing mCherry alone (no Tau) were used as a control. B) Shows median survival age of each genotype. C) Lifespan of flies is significantly different between the Tau variants tested (Log-rank, Mantel-Cox test $p<0.0001$). With a manual Bonferroni correction to correct for 10 multiple comparisons, $*p<0.05/10$ makes corrected p-values $*p<0.005$. Cells highlighted green are significantly different. Data collected by MSci. Ms Georgia Millner under my supervision.

A.

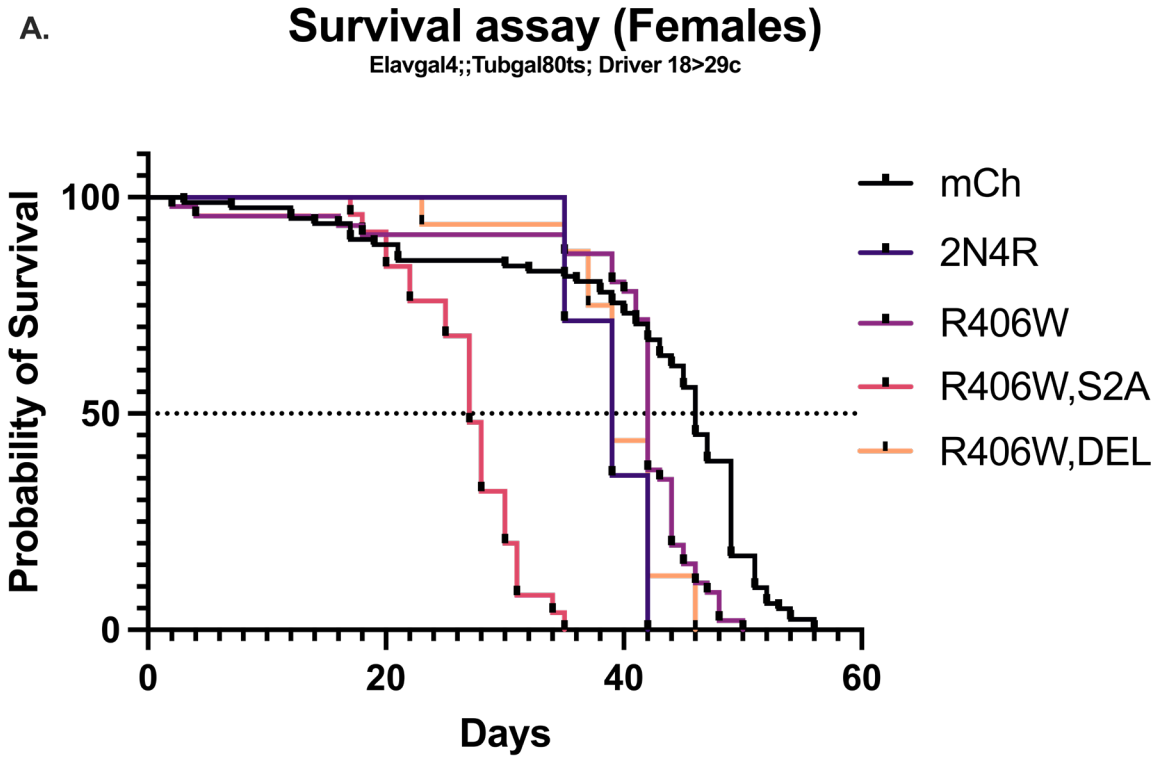


B.

| Median Survival | | | | |
|---|---|---|---|---|
| mCh | 2N4R | R406W | R406W-S2A | R406W-DEL |
| 46 | 39 | 42 | 27 | 39 |

C.

| | mCherry | 2N4R | R406W | R406W,S2A | R406W,DEL |
|---|---|---|---|---|---|
| mCherry | | <0.0001 | <0.0001 | <0.0001 | 0.0001 |
| 2N4R | | | 0.0013 | <0.0001 | 0.4095 |
| R406W | | | | <0.0001 | 0.0455 |
| R406W,S2A | | | | | <0.0001 |
| R406W,DEL | | | | | |

**Figure 49. Survival assay of female TauR406W mutants.**

A) Kaplan Meier survival curves for Elav-Gal4;;TubGal80ts; driven mCherry Tagged Tau mutants: hTau2N4R, hTau2N4R-R406W hTau2N4R-R406W/S2A and hTau2N4R-R406W/DEL expressing female flies. Flies expressing mCherry alone (no Tau) were used as a control. B) Shows median survival age of each genotype. C) Lifespan of flies is significantly different between the Tau variants tested (Log-rank, Mantel-Cox test $p<0.0001$). With a manual Bonferroni correction to correct for 10 multiple comparisons, $*p<0.05/10$ makes corrected p-values $*p<0.005$. Cells highlighted green are significantly different. Data collected by MSci. Ms Georgia Millner under my supervision.

## 7.4 Discussion

This Chapter investigated mutant specific neuropathology of the two most common FTDP-17(*MAPT*)-associated Tau mutants P301S and R406W, to assess whether familial mutations cause neurodegeneration through different mechanisms underlying heterogeneity between Tauopathies. I demonstrate that FTDP-17(*MAPT*) mutants are differentially toxic and provide evidence that the aggregation domain $^{306}$VQIVYK$^{311}$ may represent a universal therapeutic target for treatment of distinct Tauopathies.

### 7.4.1 FTDP-17(*MAPT*) mutants are differentially toxic

Familial *MAPT* mutations have varying clinical and neuropathological profiles, making their diagnosis and treatment challenging (D'Alton and Lewis, 2014). Previous studies across different experimental models show that distinct mutants are differentially toxic, recapitulating clinical heterogeneity observed in patients (Wittmann et al., 2001, Feuillette et al., 2010, Götz et al., 2001, Bodea et al., 2016). Similarly, my findings demonstrate that P301S and R406W mutants influence Tau accumulation and neuronal degeneration differentially. However, in my model whereby the mutants are equally expressed, R406W seems to be far more toxic than P301S which is unusual because R406W is associated later onset and slower disease progression than P301S(Ygland et al., 2018, Whitwell et al., 2009a, Bugiani et al., 1999, Saito et al., 2002). These results provide evidence that FTDP-17(*MAPT*) mutants are distinctly toxic, influenced by either distinct pathological mechanisms or varying propensity for toxicity.

There are two potential explanations for why R406W had enhanced Tau accumulation and neuronal degeneration phenotypes in comparison to the P301S mutation. **1)** The conformations formed from R406W is more pathogenic than those formed in P301S and wildtype Tau and/or **2)** R406W is mediating toxicity through mechanisms independent from P301S.

The enhanced neurotoxicity of the R406W mutant, can be attributed to loss of Tau's function at the mutation loci on the C-terminal domain. Previous studies have shown that the R406W mutation altered protein conformation and charge, reduced microtubule binding and impaired membrane interactions (Hasegawa et al., 1998, Gauthier-Kemper et al., 2011, Qi et al., 2025). Toxicity through these mechanisms would also explain how degeneration was achieved in absence of overt Tau accumulation compared to wildtype Tau. Unlike R406W, the unexpectedly mild phenotypes observed by P301S in my model contradicts the extensive literature which describe P301- mutants as highly toxic, hyperphosphorylated and aggregation-prone variants which accelerates pathology in multiple model systems, including *Drosophila* (Xie et al., 2022, Wittmann et al., 2001, Feuillette et al., 2010, Bugiani et al., 1999, Yoshiyama et al., 2007). Based on the literature, P301S should have promoted Tau accumulate density as observed with other toxic Tau mutants like the phospho-mimicking TauE14 in **Chapter 3**. The reason for this difference could be because Or47b neurons have a particular resistance to P301S-mediated pathology, while being vulnerable to R406W-mediated mechanisms (Sivanantharajah et al., 2025). Alternatively, the pathway of P301S-mediated aggregation may have been restricted in this neuron type in this timeframe.

Interestingly, R406W-expressing flies had twice the amount of axonal swellings and half the amount of neuronal volume compared to wildtype Tau-expressing flies, yet similar quantities of Tau accumulates after 35 days. The difference between accumulation and degeneration severity implies that the conformational state, rather than abundance of Tau accumulates which determines toxicity. Recent cryo-EM studies have demonstrated that R406W and P301S produce distinct ultrastructural conformations of fibril cores (Schweighauser et al., 2025, Qi et al., 2025). As discussed in previous Chapters, different Tau conformations can have different Tau interactomes. This is supported by recent proteomic studies which demonstrate Tau aggregates isolated at the same molecular weight

have distinct conformers between AD and control brains, and have consequential distinct interactomes (Martinez et al., 2025). Similarly, proteomic studies investigating FTDP-17(*MAPT*) mutants show that mutants even within the same domain like V337M and P301L mutations have unique interactome profiles, loosing 184 and 108 interacting proteins respectively, compared to wildtype Tau (Tracy et al., 2022). These distinct patterns of lost and gained binding partners likely contribute significantly towards mechanisms that facilitate or protect against pathological Tau.

### 7.4.2 Targeting $^{306}$VQIVYK$^{311}$ provides neuroprotection across multiple Tau mutants.

The rescue of R406W-mediated survival deficits by deletion of the $^{306}$VQIVYK$^{311}$ motif demonstrates the broad therapeutic potential of this target. Firstly, it shows that targeting this domain can reduce the toxicity in multiple Tau mutants, extending its application to a broader population of Tauopathies, including familial FTDP-17(*MAPT*) variants.

Previous studies have demonstrated that R406W exerts toxicity primarily through reduced microtubule binding and impaired membrane interactions rather than causing overt aggregation (Hasegawa et al., 1998, Gauthier-Kemper et al., 2011). However my results show that R406W increases the density of Tau accumulates compared to the P301S mutant. One potential explanation for this is that R406W-mediated reduced microtubule binding simply favours aggregation indirectly due to increased availability of free, unbound Tau (Kanaan et al., 2020, Wegmann et al., 2018).

Similarly to previous Chapters which have shown that targeting $^{306}$VQIVYK$^{311}$ can mitigate toxicity of phospho-mimicking, aggregation-prone TauE14, the current findings show that $^{306}$VQIVYK$^{311}$ deletion can also mitigate toxicity in R406W. Building on results from **Chapter 4** which showed that deleting $^{306}$VQIVYK$^{311}$ reduces the misfolded Tau conformations, the rescue of R406W toxicity could be through mechanisms beyond Tau accumulation and aggregation. On the R406W background, the deletion of $^{306}$VQIVYK$^{311}$

improving survival could be explained by preventing pathogenic Tau conformations which disrupt Tau physiological Tau function (Jeganathan et al., 2008, Martinez et al., 2025).

These findings implicate $^{306}$VQIVYK$^{311}$ as a multifaceted therapeutic target with broad potential application across diverse Tauopathies which cause toxicity through different pathological mechanisms.

### 7.4.3 Implications and context-dependence of targeting phosphorylation

In contrast to $^{306}$VQIVYK$^{311}$ deletion, targeting phosphorylation at two pathologically linked sites (S2A), did not improve R406W-mediated survival deficits. Instead, unexpectedly it exacerbated R406W-mediated toxicity. This could imply that phosphorylation at these epitopes provides neuroprotection against R406W-mediated pathology. However this finding contradicts the established literature that hyperphosphorylation drives pathology.

As discussed in **Chapter 3**, there is extensive evidence that implicates hyperphosphorylation as toxic, and FTDP-17(*MAPT*) mutants typically are associated with increased Tau phosphorylation which reduces microtubule binding and increases aggregation propensity (Hasegawa et al., 1998, Alonso Adel et al., 2004, Guo and Lee, 2011). Residues S262 and S356 (the S2A epitopes) are particularly associated with toxicity, and when pseudo-phosphorylated strongly promote Tau aggregation and reduce microtubule binding (Augustinack et al., 2002, Biernat et al., 1993, Drewes et al., 1995). Therefore, making these residues phosphorylation resistant should mitigate toxicity. Indeed, previous studies have shown that S2A mutations completely rescues toxicity in transgenic *Drosophila* expressing wildtype Tau2N4R and Tau2N4R-R406W backgrounds in eye and wing disc tissues (Nishimura et al., 2004, Chatterjee et al., 2009, Ramirez-Moreno et al., 2025). However, my results contradict these studies, showing that targeting phosphorylation in pan-neuronally expressed R406W Tau may have pathological consequences.

There are further inconsistencies in the literature regarding the consequence of R406W mutations on phosphorylation patterns. Although most FTDP-17(*MAPT*) mutant carriers usually have increased amounts of hyperphosphorylated Tau in the brain (Delobel et al., 2002, Alonso Adel et al., 2004), analysis of soluble Tau extracted from R406W patients showed that the Tau is moderately *hypophosphorylated* in relation to the control groups (Miyasaka et al., 2001). However, in transgenic *Drosophila* and mouse models expressing R406W Tau, studies often report that R406W is hyperphosphorylated (Williams et al., 2000, Götz and Ittner, 2008). Inconsistencies such as these highlight translational application between human and transgenic expression models and challenges the understanding of how phosphorylation truly contributes to mutant specific pathology. Nonetheless, repeats and/or direct visualisation of neurodegeneration in the Or47b neurons will be needed to ascertain if this is a true result.

My results suggest that R406W-specific neuropathology is mediated through $^{306}$VQIVYK$^{311}$, rather than phosphorylation. The protective effect of phosphorylation at S262 and S356 in the R406W context could stabilise the protein against R406W-specific dysfunction of the C-terminal domain. Phosphorylation at these sites could provide conformational stability which counteracts more toxic conformations from forming or maintain protective protein interactions (Hasegawa et al., 1998, Gauthier-Kemper et al., 2011, Martinez et al., 2025).

This does not exclude the possibility that R406W mediates toxicity through other known disease-associated phosphorylation sites, but it highlights the need for careful evaluation for phosphorylation-targeting therapies in different Tauopathies. The context-dependent nature of phosphorylation has significant implications for future therapeutic design where one strategy may be effective for treating one disease subtype, but detrimental to another. With the emerging ultrastructural characterisation of fibril cores revealing

distinct conformations between different FTDP-17(*MAPT*) mutations, it supports the need for disease-specific therapeutic approaches (Qi et al., 2025, Schweighauser et al., 2025) .

### 7.4.4 Conclusion

This Chapter sought to compare and contrast the pathogenic potential of two mutants in a model that would have no confounding effects from differential expression. In this system it appears that when equivalently expressed, R406W is more toxic than P301S, and that its toxicity is mediated by the $^{306}$VQIVYK$^{311}$ domain. Findings also show that deletion of the $^{306}$VQIVYK$^{311}$ domain confers neuroprotection in R406W, validating it as a therapeutic target with broad applications in different Tauopathies.

### 7.4.5 Future directions

Given that R406W(S2A) has previously demonstrated successful mitigation of degenerative phenotypes in smaller tissue subsets (Nishimura et al., 2004, Chatterjee et al., 2009, Ramirez-Moreno et al., 2025) the hTau2N4R-R406W/S2A and hTau2N4R-R406W/DEL mutants effect on Tau accumulation and neurodegeneration should be assessed in the Or47b neurons. This would clarify whether the toxic effects of the S2A observed in longevity assays reflects a pan-neuronal or tissue selective phenomena.

Additionally, systematic comparative analysis in this model that allows for equal expression of other familial FTDP-17(*MAPT*) mutants could help identify common and distinct pathological mechanisms. This may give more insight into clinical heterogeneity observed within these diseases, and identity which diseases require broad acting therapies or more personalised treatment approaches.

# Chapter 8 General discussion

## 8.1 Introduction and main conclusions

With global aging populations, the number of people being diagnosed with AD is increasing worldwide with huge societal and economical implications. While recent approval of drug Lecanemab show promising strategies for targeting amyloid-β in AD, there is no current disease-modifying treatment for Tau and Tauopathies(van Dyck et al., 2023) (Irizarry et al., 2025). Therefore, better understanding how the mechanisms of Tau mediated toxicity contribute towards pathology and disease heterogeneity is critical to identify therapeutic targets.

This thesis aimed to investigate how phosphorylation and aggregation drive pathology *in vivo* and evaluate the aggregation domain $^{306}$VQIVYK$^{311}$ as a therapeutic target for diverse Tauopathies. I have several key findings. This thesis demonstrates that $^{306}$VQIVYK$^{311}$ is a central mediator of Tau toxicity potentially beyond simply promoting aggregation, which gates toxicity mediated by hyperphosphorylation and controls pathogenic Tau conformations. I show that that phosphorylation enhances toxicity through $^{306}$VQIVYK$^{311}$, but that targeting this domain can rescue pathology even in severely toxic hyperphosphorylated contexts. Furthermore, my results show that distinct FTDP-17(*MAPT*) mutants are differentially toxic, which likely contributes to the clinical heterogeneity observed within Tauopathies. Importantly, targeting $^{306}$VQIVYK$^{311}$ is an effective strategy against distinct Tauopathy contexts, including the FTDP-17(*MAPT*) caused by the R406W mutation. Ultimately, these findings support $^{306}$VQIVYK$^{311}$ as a promising therapeutic target that is effective across multiple disease contexts and contributes to diverse aspects of Tau pathology, but further work must be done to develop and optimise $^{306}$VQIVYK$^{311}$ targeting drugs such as RI-AG03 to overcome pharmacokinetic challenges.

## 8.2 $^{306}$VQIVYK$^{311}$ deletion rescues cellular toxicity

While hyperphosphorylation and aggregation are both hallmarks of Tau pathology, their causal relationship and relative contribution towards neurodegeneration was not clearly understood with evidence in the literature supporting sequential and bi-directional pathways (Alonso et al., 1997, Alonso Adel et al., 2004, Despres et al., 2017, Stefanoska et al., 2022, Perez et al., 2007, Kondo et al., 2021, Zhang et al., 2020b). In **Chapter 3** I showed that mutagenically deleting the aggregation motif $^{306}$VQIVYK$^{311}$ completely eliminated neurodegeneration, Tau accumulation and dendritic mis-localisation of Tau in the *Drosophila* OR47b neurons caused by highly toxic phospho-mimetic TauE14. Additionally, in **Chapter 5** I showed that deleting $^{306}$VQIVYK$^{311}$ confers functional neuroprotection against severe phosphorylation-mediated neuronal deficits. The complete rescue of neurotoxicity was striking as many models have shown that hyperphosphorylation is a primary driver of Tau pathology through multiple mechanisms independent of aggregation like inducing conformational misfolding, reducing microtubule binding and impairing axonal transport (Jeganathan et al., 2008, Mudher et al., 2004, Cowan et al., 2010, Hatch et al., 2017).

The finding that $^{306}$VQIVYK$^{311}$ deletion completely rescues neuropathology, survival and neuronal function despite severe Tau hyperphosphorylation provides novel data which challenges the idea that phosphorylation and aggregation are equally toxic, reciprocal mechanisms. Instead it demonstrates that phosphorylation enhances toxicity through $^{306}$VQIVYK$^{311}$-dependent pathways and reveals a clear hierarchical relationship of phosphorylation and $^{306}$VQIVYK$^{311}$-mediated aggregation. This aligns with structural studies that show that phosphorylation directly alters the conformation of Tau monomers (Jeganathan et al., 2008) and that $^{306}$VQIVYK$^{311}$ forms the core of Tau fibrils (Fitzpatrick et al., 2017) but identifies broader implications of $^{306}$VQIVYK$^{311}$ beyond a simple aggregation promoting motif. This insight of hyperphosphorylation dependence on $^{306}$VQIVYK$^{311}$ may

provide mechanistic explanation as to why current clinical trials of phosphorylation and kinase inhibitors have had limited success (Melchior et al., 2019, Serenó et al., 2009, Lovestone et al., 2015).

This work complements several other groups which have targeted $^{306}$VQIVYK$^{311}$ with success of reducing Tau pathology in other *Drosophila* and murine models of different isoforms (Passarella and Goedert, 2018, Kondo et al., 2021, Zhang et al., 2020b). However, my findings extend this approach to disease relevant, highly pathological contexts, which establishes $^{306}$VQIVYK$^{311}$ as a critical target against Tau in diverse pathological contexts. As the $^{306}$VQIVYK$^{311}$ motif is present in all 6 isoforms of Tau, it may have broad therapeutic potential against many Tauopathies, however further investigation is needed to validate its influence in different isoform backgrounds and disease contexts. Additionally, understanding the hierarchal relationship between $^{306}$VQIVYK$^{311}$ and other equally important PTMs like truncation and ubiquitination will be crucial for identifying other possible mechanisms through which this motif influences toxicity. This will help further therapeutic development of this motif. *Drosophila* provide and excellent model system for generating such mutants due to their genetic tractability and ease of mutant generation.

## 8.3 $^{306}$VQIVYK$^{311}$ controls pathogenic Tau conformations

Understanding the mechanism by which deleting $^{306}$VQIVYK$^{311}$ rescued phosphorylation induced pathology was essential to validate this aggregation-promoting motif as a therapeutic target. Whilst several groups have demonstrated its essential role in fibril formation (von Bergen et al., 2000, von Bergen et al., 2001, Seidler et al., 2018, Sievers et al., 2011), its location within the microtubule binding domain and its striking role in phosphorylation-mediated neurotoxicity suggested more complex and diverse roles in pathology beyond simply facilitating aggregation. In **Chapter 4,** I demonstrated that the deletion of $^{306}$VQIVYK$^{311}$ conferred neuroprotection against hyperphosphorylation

primarily by preventing the formation of pathological misfolded conformations whilst still permitting the formation of non-toxic insoluble Tau species.

This finding fundamentally challenges the current view that Tau aggregation inhibitors confer neuroprotection by solely reducing total accumulate burden (von Bergen et al., 2000, von Bergen et al., 2001, Seidler et al., 2018, Sievers et al., 2011). Whereas my results imply that not all Tau accumulates are equally toxic, and that neuroprotection can be achieved through conformational change into non-toxic conformations, rather than aggregate elimination. These findings align with emerging evidence that conformation, rather than abundance of Tau accumulates determines Tau toxicity (Jury-Garfe et al., 2024, Martinez et al., 2025, Lo Cascio et al., 2025). These studies identify high molecular weight Tau species in control brains which have distinct pathogenic properties and interacting protein partners compared to Tau species isolated from AD brains (Jury-Garfe et al., 2024, Martinez et al., 2025, Lo Cascio et al., 2025). Importantly, this highlights scenarios in which pathological conformations alter Tau's interactome in ways that can promote gain- and loss-of-function mechanisms. Toxic conformers can acquire pathological binding partners which could potentially facilitate mechanisms like somato-dendritic mis-localisation(Diez et al., 2023), aggregation and propagation, whilst also loosing physiological interactions essential for function like microtubule stabilisation and axonal transport(Martinez et al., 2025, Tracy et al., 2022). This dynamic change in gaining toxic function whilst loosing protective and functional interactions provides an explanation for how conformational changes drive neurodegeneration independently of accumulation or insoluble species.

These insights also address ongoing discussion about the efficacy of Tau aggregation inhibitors as treatments. Several groups have proposed that Tau aggregation may actually be a protective mechanism to sequester toxic Tau species, where smaller pre-fibrillar oligomers are the primary drivers of toxicity (Flach et al., 2012, Tian et al., 2013, Ward et al., 2012). Conceptually, this may explain why aggregation inhibitors like methylene blue, showed

limited clinical efficacy in Phase III trials despite reducing aggregate load, suggesting it does not reduce the critical pathogenic conformers of Tau (Schwab et al., 2017, Gauthier et al., 2016, Soeda et al., 2019). In fact one study showed that methylene blue reduced Tau fibrils but increased granular Tau oligomers(Soeda et al., 2019). These findings underscore the importance of targeting toxic Tau conformers and species rather than solely focusing on removing fibrillar aggregates.

Ultimately these findings support $^{306}$VQIVYK$^{311}$ as a therapeutic target for reducing multiple aspects of Tau mediated toxicity, including hyperphosphorylation-induced neurotoxicity and conformational misfolding. As ultrastructural analysis becomes more accessible, it will be critical to understand how Tau-targeting strategies impact the conformation of Tau aggregates, rather than Tau burden alone for therapeutic development.

## 8.4 Pharmacological translation of targeting $^{306}$VQIVYK$^{311}$ using RI-AG03

To test the pharmacological reproducibility of deleting $^{306}$VQIVYK$^{311}$, the peptide aggregation inhibitor RI-AG03 was delivered to *Drosophila* through their diet. **Chapter 6** demonstrated that RI-AG03 successfully reduced phosphorylation-mediated Tau accumulation *in vivo*, and showed promising, though non-significant reductions in axonal degeneration of the Or47b neurons. Fundamentally this Chapter supported the targeting of $^{306}$VQIVYK$^{311}$ against pathogenic Tau species, but revealed critical limitations in translating validated targets to therapeutic efficacy *in vivo*. These limitations include pharmacokinetic challenges such as insufficient dosing for target saturation, biological barriers including gut absorption and the blood brain barrier which may have reduced drug bioavailability. These results support previous reports showing RI-AG03 improved survival and reduced retinal degeneration in *Drosophila* expressing wildtype Tau (Aggidis et al., 2024), but suggest that dosing and delivery regimes may need to be altered to compensate for targeting more pathogenic Tau species.

The selective efficacy of RI-AG03 against hyperphosphorylated Tau accumulation validates that $^{306}$VQIVYK$^{311}$ is a druggable target effective against highly toxic, disease-relevant Tau species (Zhang et al., 2020b, Sievers et al., 2011, Seidler et al., 2018). However, there were substantial differences between the RI-AG03 treated flies and the mutagenic ΔVQIVYK expressing flies, highlighting that drug targeting efficacy, and conformational control are critical factors involved in eliminating Tau toxicity. While genetic deletion of $^{306}$VQIVYK$^{311}$ fundamentally prevents pathological conformations from forming, RI-AG03 may instead cap and/or redirect aggregation pathways without eliminating pathogenic conformation propensity, complementing earlier emerging themes that conformational state, rather than Tau accumulate abundance determines toxicity (Martinez et al., 2025). Importantly, if RI-AG03 does not eliminate toxic conformers, the Tau may retain pathological interactomes with increased pathological binding partners and loss of physiological/protective interactions, thereby limiting therapeutic efficacy against neurodegeneration.

Fundamental pharmacokinetic limitations including incomplete absorption, tissue penetration, and drug degradation during feeding-based delivery methods likely compromised the therapeutic efficacy of RI-AG03. In addition, the high overexpression *Drosophila* model, which continually produces Tau, in combination with inadequate drug dose, delivery and bioavailability likely dampened the efficacy of RI-AG03 in this Chapter. Findings from this thesis validate $^{306}$VQIVYK$^{311}$ as a good therapeutic target but emphasise the need for further optimisation. Potentially conformational targeting approaches may be more effective than simply aiming to reduce total Tau aggregates. However further investigation of misfolded conformation, and Tau aggregate species are needed to define which species and conformations of Tau present after RI-AG03 administration.

## 8.5 Broad potential application of $^{306}$VQIVYK$^{311}$ targeting

The diverse clinical, cellular and molecular heterogeneity between Tauopathies creates ongoing challenges for diagnosing and treating pathological Tau (D'Alton and Lewis, 2014, Congdon and Sigurdsson, 2018, Snowden et al., 2015). A small subcategory of familial frontotemporal dementias caused by mutations within the Tau gene also exhibit significant disease heterogeneity, caused by differential mechanisms of toxicity. In **Chapter 7**, I demonstrate that expression of different FTDP-17(*MAPT*) mutants R406W and P301S influence neuropathology differently independent of Tau accumulation levels, supporting current studies that show that different mutants are differentially toxic (Wittmann et al., 2001).

Critically, R406W-mediated degeneration was also dependent on the $^{306}$VQIVYK$^{311}$ motif, highlighting its broad therapeutic potential across multiple Tauopathies which cause toxicity through distinct mechanisms. This finding complements the research effort in developing Tau therapies against common structural motifs shared by many different Tau mutants and isoforms (Sievers et al., 2011, Seidler et al., 2018, Kondo et al., 2021, Zhang et al., 2020b).

However, findings also revealed mutant-specific therapeutic responses to phosphorylation targeting. Unlike $^{306}$VQIVYK$^{311}$ deletion, inhibiting phosphorylation at pathologically linked sites S262 and S356 (S2A) exacerbated R406W toxicity. These results emphasise that Tau mutations drive pathology through distinct mechanisms and respond differently to phosphorylation-targeting strategies, supporting the need for mutation-specific therapeutic approaches (Qi et al., 2025, Schweighauser et al., 2025).

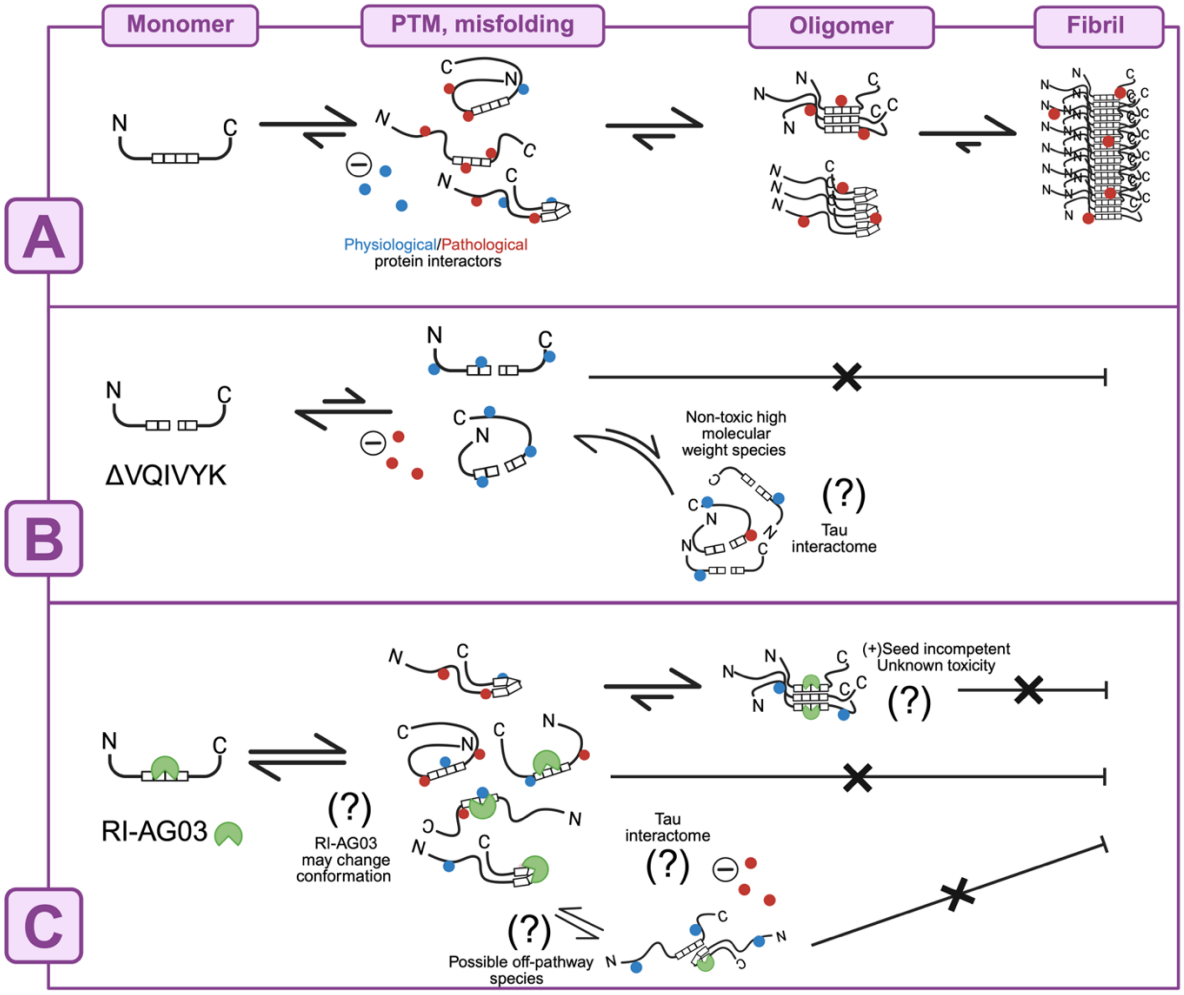


**Figure 50. Schematic summary of how ΔVQIVYK and RI-AG03 treatment alter Tau conformation, aggregation pathway and interactome.**

**A)** Pathological aggregation pathway. Following abnormal post-translational modification (PTM), Tau misfolds into a pathological conformation which promotes aggregation into dimers, oligomers and fibrils. At each stage, the species and conformation of Tau undergoes changes in interacting partners, with a loss of physiological interactions (blue dots) and gain of pathological, disease-specific interactions (red dots). **B)** Deletion of the $^{306}$VQIVYK$^{311}$ motif alters Tau conformation into a non-toxic structure what disrupts the normal aggregation cascade. Some conformations do have MC1 immunoreactivity, however these conformations produce unique non-toxic high molecular weight species which cannot form toxic fibrils. These species may retain protective interactors. **C)** RI-AG03 caps $^{275}$VQIINK$^{280}$ and $^{306}$VQIVYK$^{311}$, preventing elongation of aggregates, preventing fibril formation. These capped Tau species are no longer seed competent, through their toxicity is unknown. RI-AG03 may alter the conformation of Tau and produce off-pathway species. How pharmacological interventions influence Tau's interactome remains unknown and highlights and important area for future research.

### 8.6 Significant findings

This thesis demonstrates that $^{306}$VQIVYK$^{311}$ is essential for hyperphosphorylation-induced Tau toxicity. Deletion of this domain completely rescues severe neurotoxicity, Tau accumulation, mis-localisation and functional deficits caused by phospho-mimicking TauE14.

Mechanistic investigations indicate that $^{306}$VQIVYK$^{311}$ does not mediate toxicity by altering microtubule binding or phosphorylation propensity. The rescue of toxicity also could not be fully explained by reduction of insoluble Tau aggregates alone. Instead, my results suggest that $^{306}$VQIVYK$^{311}$ may mediate toxicity by controlling the misfolding of Tau into pathogenic conformations.

This work shows that heterogeneity between Tauopathies can arise from differential patterns of neurotoxicity rather than simply aggregation mechanisms, but that targeting $^{306}$VQIVYK$^{311}$ can rescue toxicity caused by hyperphosphorylation and FTDP-17(*MAPT*) mutations which are toxic through distinct mechanisms.

Collectively this thesis shows that targeting pathologically linked motifs like $^{306}$VQIVYK$^{311}$ can rescue toxicity across several pathological contexts, which may represent a common therapeutic target across diverse Tauopathies.

## 8.7 Study Limitations

While this thesis provides strong evidence for the therapeutic targeting of $^{306}$VQIVYK$^{311}$, there are some technical limitations which should be addressed in future studies. Conformational analysis of the Tau mutants through MC1 immunoreactivity was informative of misfolded Tau conformers influenced by phosphorylation at disease-linked epitopes (Jeganathan et al., 2008), however there are stronger structural analysis approaches including NMR, Raman spectroscopy and Cryo-EM which could provide more

ultrastructural information on Tau conformation. Cryo-EM is increasingly popular technique used to image the structured fibrillar core of Tau aggregates, however even this approach has limitations. Regions such as the "fuzzy coat" N- and C- terminal cannot be visualised due to their unstructured nature, which leaves them uncharacterised (Lövestam et al., 2022).

Additional biochemical characterisation of insoluble Tau species could also be carried out such as using standard Thioflavin T assays, however there are several inherent challenges in *Drosophila* models where larger mature amyloid fibrils are not common (Gandini et al., 2022), and *in vivo* there are a host of other amyloidogenic proteins which could cause a non-specific signal. Using rodent models may overcome this problem which recapitulate larger Tau aggregates like Tau tangles, which could be labelled with other histological amyloid dyes like pFTAA (Brelstaff et al., 2015).

*Drosophila* models of Tauopathy recapitulate key pathological features observed in mammalian models and human brains, recapitulating early and intermediate stage pathology, forming toxic, hyperphosphorylated Tau species, including oligomers, PHFs and SFs rather than NFTs (Colodner and Feany, 2010, Jackson et al., 2002, Shulman and Feany, 2003, Wittmann et al., 2001). This represents an advantage to using flies, given that the majority of evidence implicates smaller soluble Tau as the most toxic species (Flach et al., 2012, Tian et al., 2013, Ward et al., 2012). However, the precise ultrastructure of fibrils formed in *Drosophila* remains uncharacterised. Establishing whether *Drosophila* models recapitulate AD-like fibril cores is crucial for several reasons. It would provide the field with a clinically relevant and genetically tractable model to interrogate the cellular factors that regulate Tau misfolding *in vivo*. It would also serve as a high-throughput platform for assessing the efficacy of aggregation inhibitors in conformationally relevant Tau species in which this thesis has highlighted critical importance.

## 8.8 Future directions: Therapeutic implications and outstanding questions

This thesis establishes $^{306}$VQIVYK$^{311}$ as a central mediator of Tau toxicity across diverse pathological contexts and validates it as a promising therapeutic target. However future pharmacological development of $^{306}$VQIVYK$^{311}$-centred therapies requires further assessment.

Future drug development must prioritise therapies that conformationally stabilise Tau into inert, non-pathological species rather than only blocking aggregation. Optimising delivery strategies, dose regimens, and conformational stabilisation will be essential for achieving maximum efficacy, and cocktail therapies targeting multiple aspects of Tau pathology may prove necessary for clinical efficacy. Future work developing therapeutics should carefully consider the types of Tauopathies which could benefit from their drug design, and comprehensive assessment of efficacy on a variety of Tau mutants should be assessed as they may respond differently and possibly adversely.

Further investigation on how phosphorylation and $^{306}$VQIVYK$^{311}$-mediated conformational changes influence Tau's interacting protein partners is needed. This is an understudied area of Tau biology of how mechanisms can influence Tau toxicity with significant therapeutic implications. Future studies should compare the interactomes of the designer mutants used in this thesis to determine how RI-AG03, phosphorylation and the $^{306}$VQIVYK$^{311}$ domain shapes the pathological interactome. Clearer understanding of how Tau's interactome changes with pathological changes will be essential form predicting therapeutic mechanism of action.

With the increasing accessibility of ultrastructural analysis of Tau fibrillar conformers, the research effort should continue to characterise all different forms of Tau fibrils formed from diverse Tauopathies. As of now only a few FTDP-17(*MAPT*) mutants have been solved using cryo-EM including R406W, P301F and P301L and V337M (Qi et al., 2025, Shi et al.,

2021). Systematic structural analysis of mutations from different domains affects the conformation and pathogenic mechanism of Tau. Given the significant heterogeneity between different Tauopathies which have distinct isoform composition inclusions (Shi et al., 2021), it should help inform patient stratification and personalised treatment plans.

# Appendix A Supplementary Figures

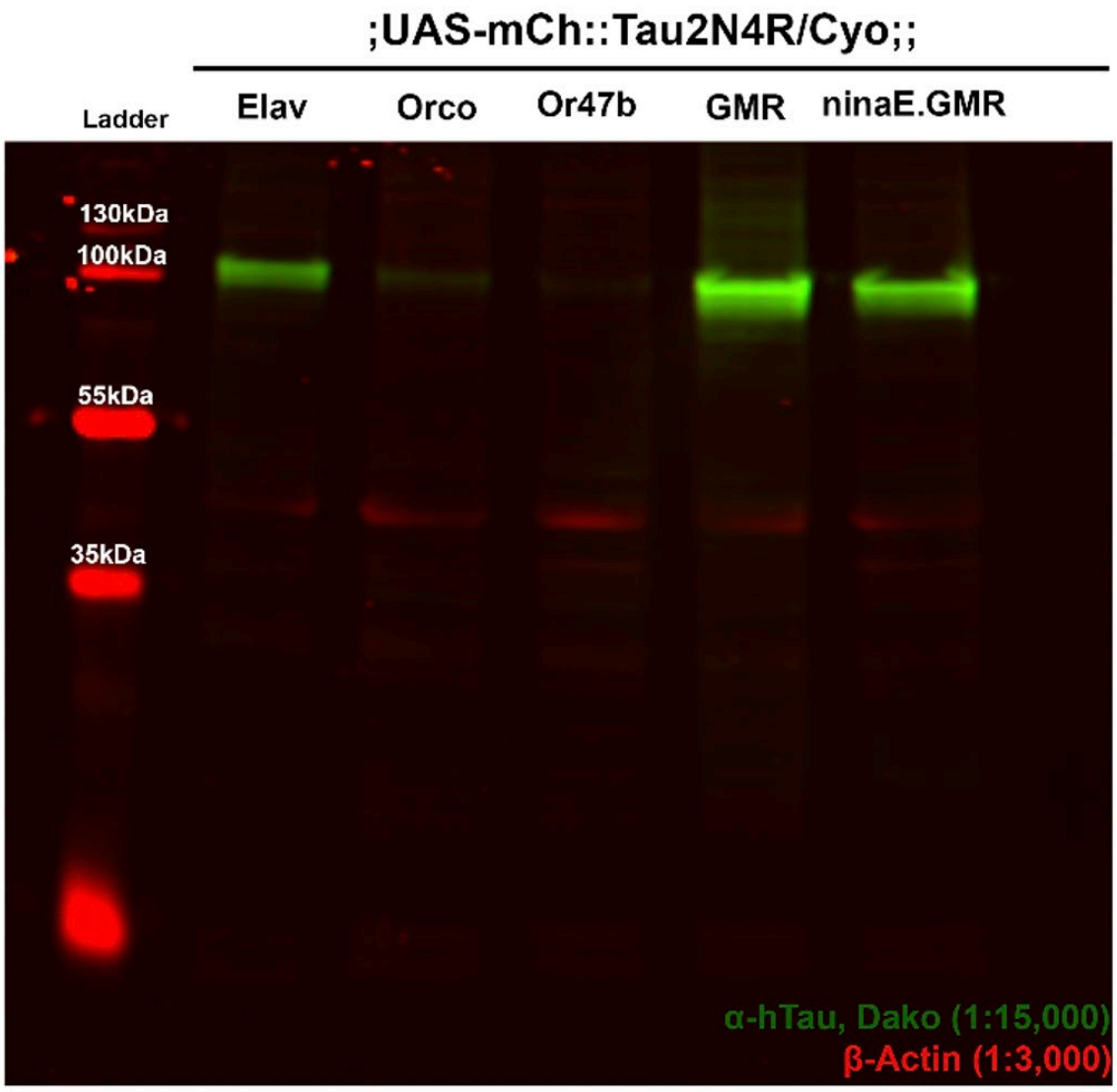


**Supplementary Figure 1. Assessing candidate drivers appropriate for western blot analysis for protein analysis.**

Full blots for 3 day old +/+;UAS.mCherryTau2N4R/Cyo;+/+ (Attp40) male flies driven either pan-neuronally (Elav-Gal4) in the olfactory neurons (Orco-Gal4) or (Or47b-Gal4) or the retinal neurons (GMR-Gal4) or (NinaE.GMR-Gal4). 15 fly heads were used for each lane. Flies were crossed and reared at 25°C. Results show that Elav and both GMR drivers produced the greatest Tau signal, but ninaE.GMR produced the cleanest band.

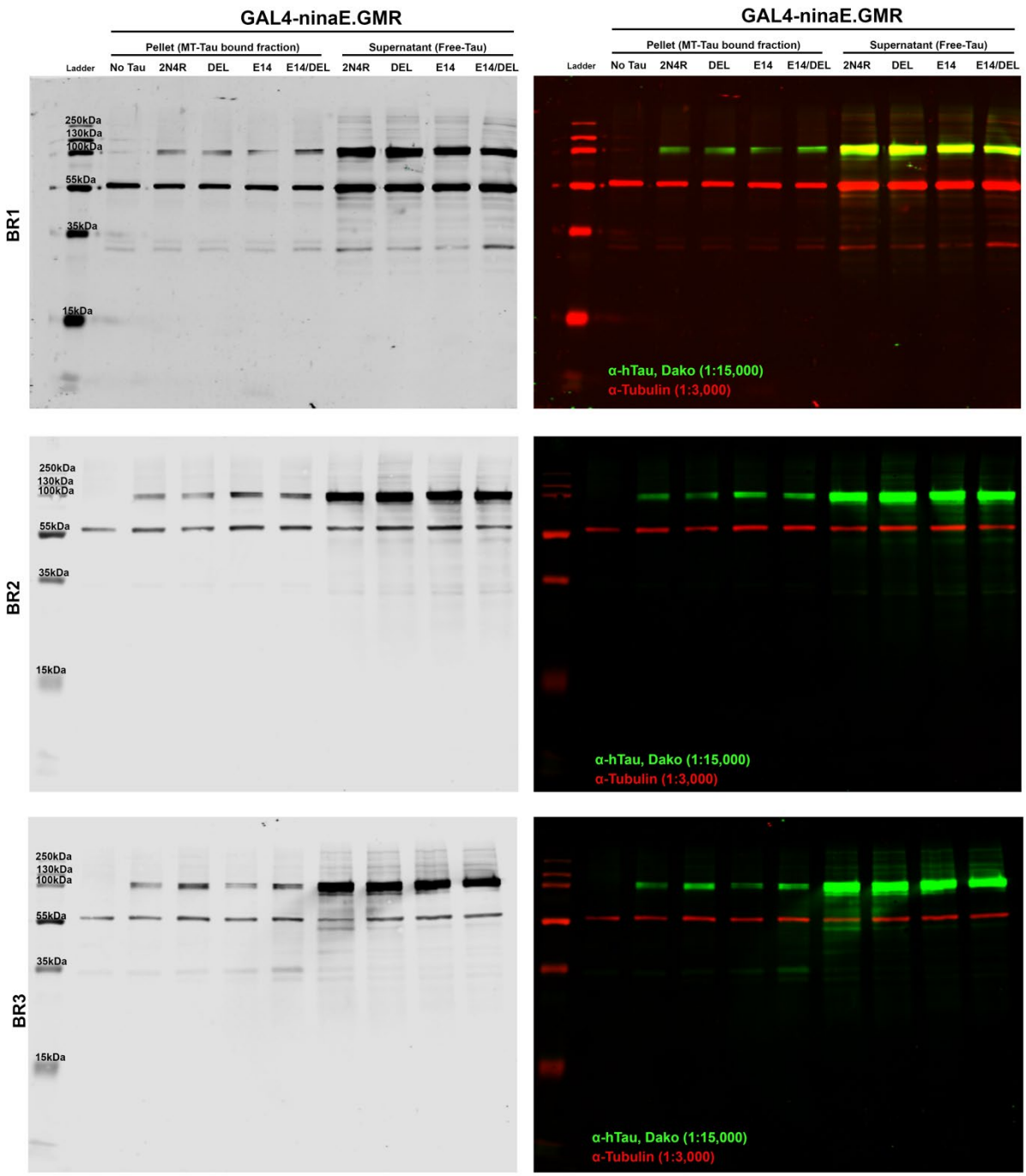


**Supplementary Figure 2. Full western blots of microtubule binding properties of hTau mutants.**

Western blots of *Drosophila* head extracts to demonstrate the microtubule-Tau binding properties of hTau variants (hTau2N4R, hTau2N4R-DEL, hTau2N4R-E14, and hTau2N4R-E14/DEL) expressed in adult retinal neurons using the GAL4-ninaE.GMR driver. Control "no Tau" flies contain the GAL4 driver only. Results show the pelleted microtubule bound to Tau fraction, and also the remaining supernatant, containing the unbound, free Tau. Tau runs at around 100kDa due to the mCherry tag on each construct. α-Tubulin was used as a loading control, and runs at around 50kDa. N=3 biological repeats.

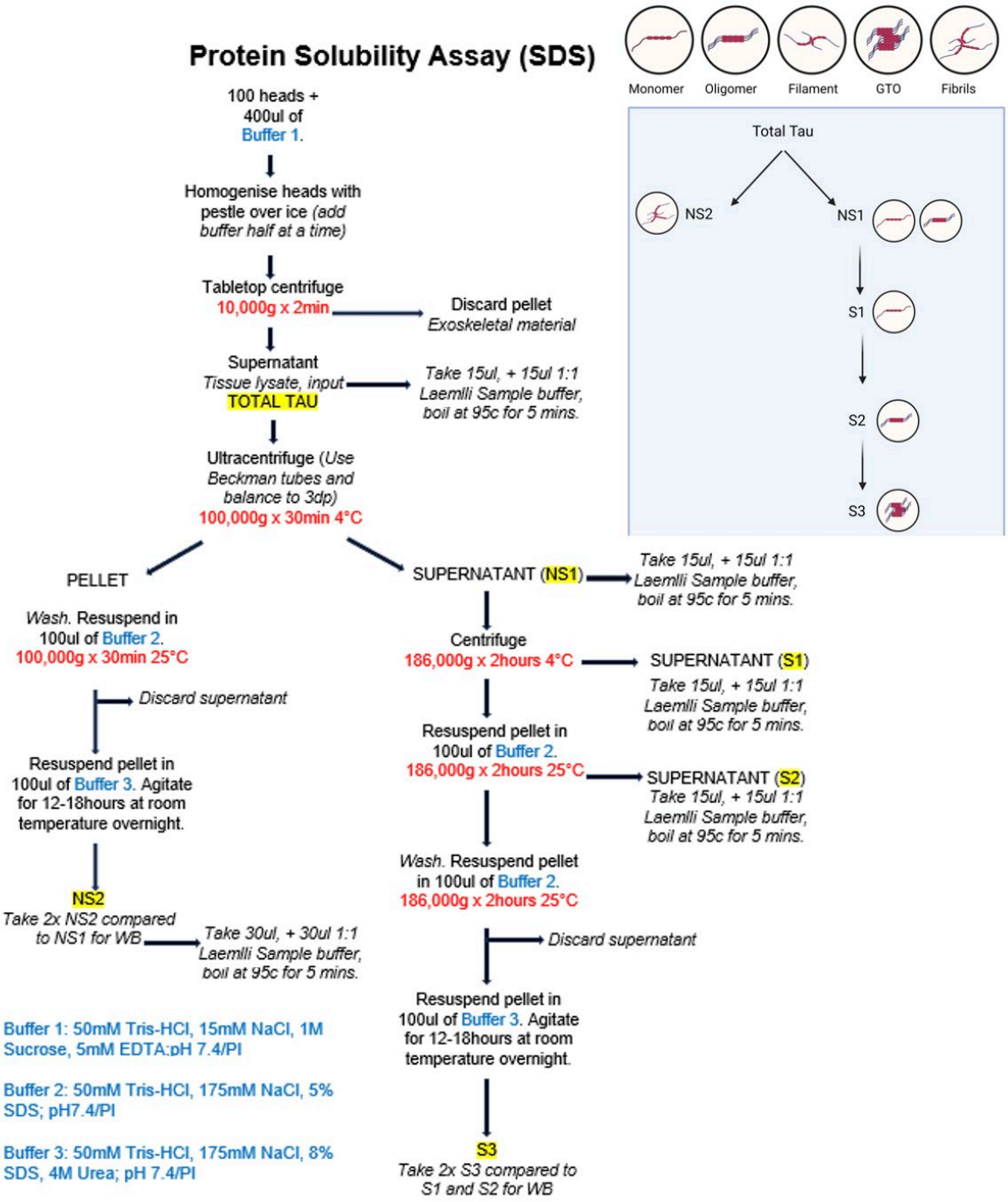


**Supplementary Figure 3. SDS solubility assay methods schematic.**

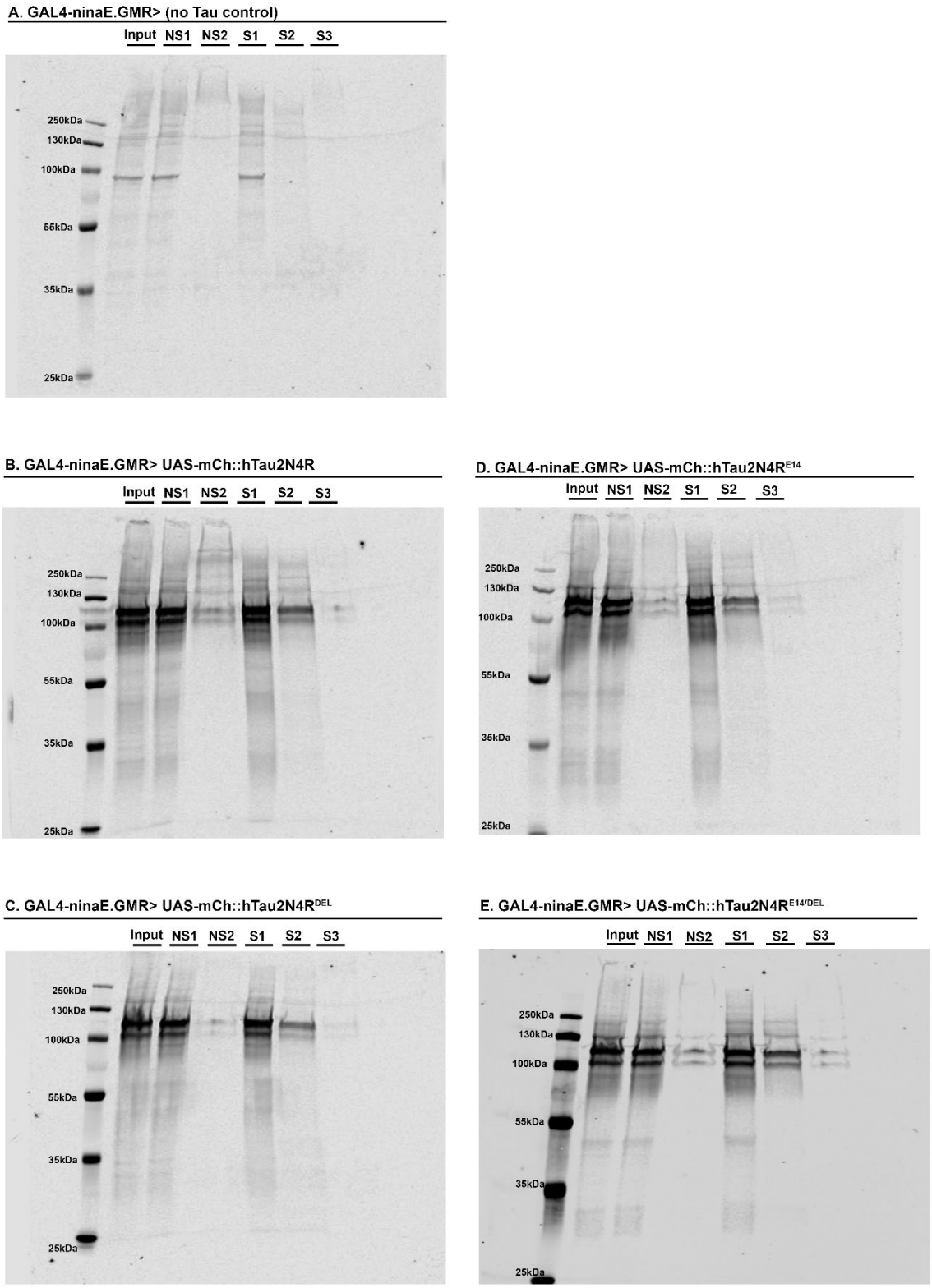


**Supplementary Figure 4. Full western blots for SDS protein solubility assay.**

Comparison of NFT(NS1, NS2) and GTO(S1, S2, S3) enriched fractions between the different transgenic flies tested after 14 days of aging A) undriven GMR.ninaE-GAL4 (no Tau) controls, B) hTau2N4R, C) hTau2N4R-DEL, D)hTau2N4R-E14 and E) hTau2N4R-E14/DEL. Driver used was Gal4-GMR.ninaE. Genetic crosses set up at 18°C and progeny aged at 29°C (n=100 male heads). Each mCherry::hTau mutant fraction runs at ~100kDa, taking into account for the weight of the mCherry Tag.

A.

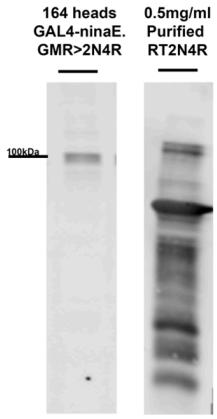


**Calculation of Tau protein expression in 164 GAL4-ninaE.GMR>UAS-mCh::Tau2N4R expressing flies using recombinant Tau as a known constant:**

150µl of 2N4R SN1 sample collected.

15µl of 2N4R SN1 signal (made up of 1:1 sample buffer)= 244000

15µl of 0.5mg/ml 2N4R Recombinant Tau signal = 2510000
→ *0.5 x 15 = 7.5µg of Tau loaded*

Amount of Tau in fly lane (µg) $= \left(\left(\frac{244000}{2510000}\right) \times 7.5\right) = 0.73\mu g$ in 7.5µl of 2N4R SN1.

Amount of Tau in 164 heads (µg)$= \left(\frac{0.73}{7.5}\right) \times 150\mu l = 14.6\mu g$

B.

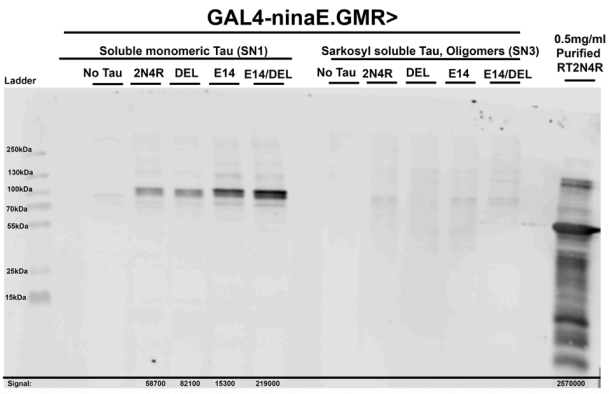


**Supplementary Figure 5. Quantifying amount of Tau expression in 164 GMR>hTau heads.**

**A)** Representative blot used for comparing Tau expression in 164 heads to 0.5mg/ml of 2N4R recombinant Tau. 15ul of input sample (SN1)(from 2.5.3 **Solubility assays**) and Recombinant Tau. GAL4-ninaE.GMR driver was used to express UAS-mCherry::Tau2N4R for 14 days (25ºC>29ºC). Calculation is shown. **B)** Full western blot.

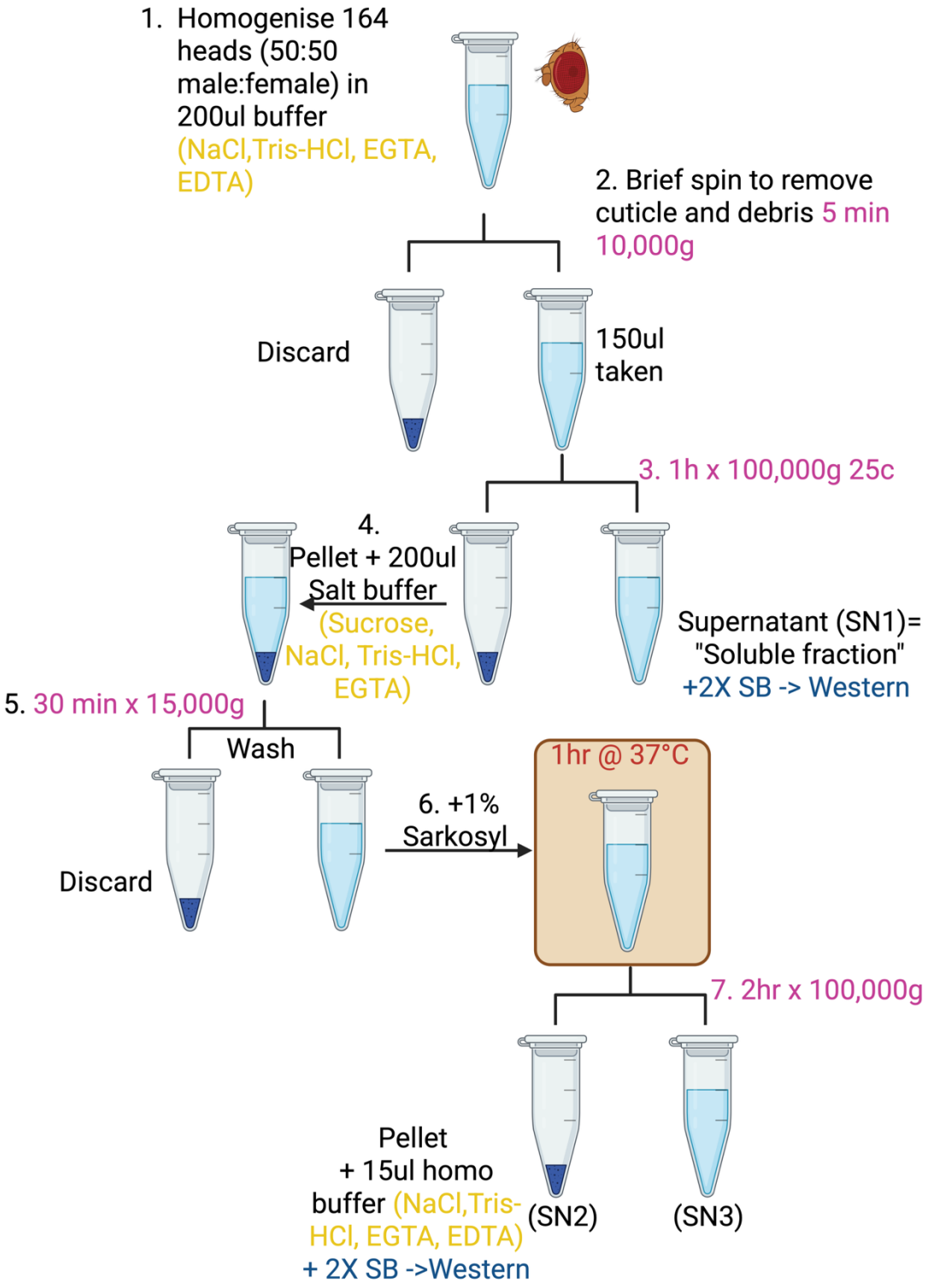


**Supplementary Figure 6. Sarkosyl insolubility methods flowchart. Based on Colodner and Feaney 2010.**

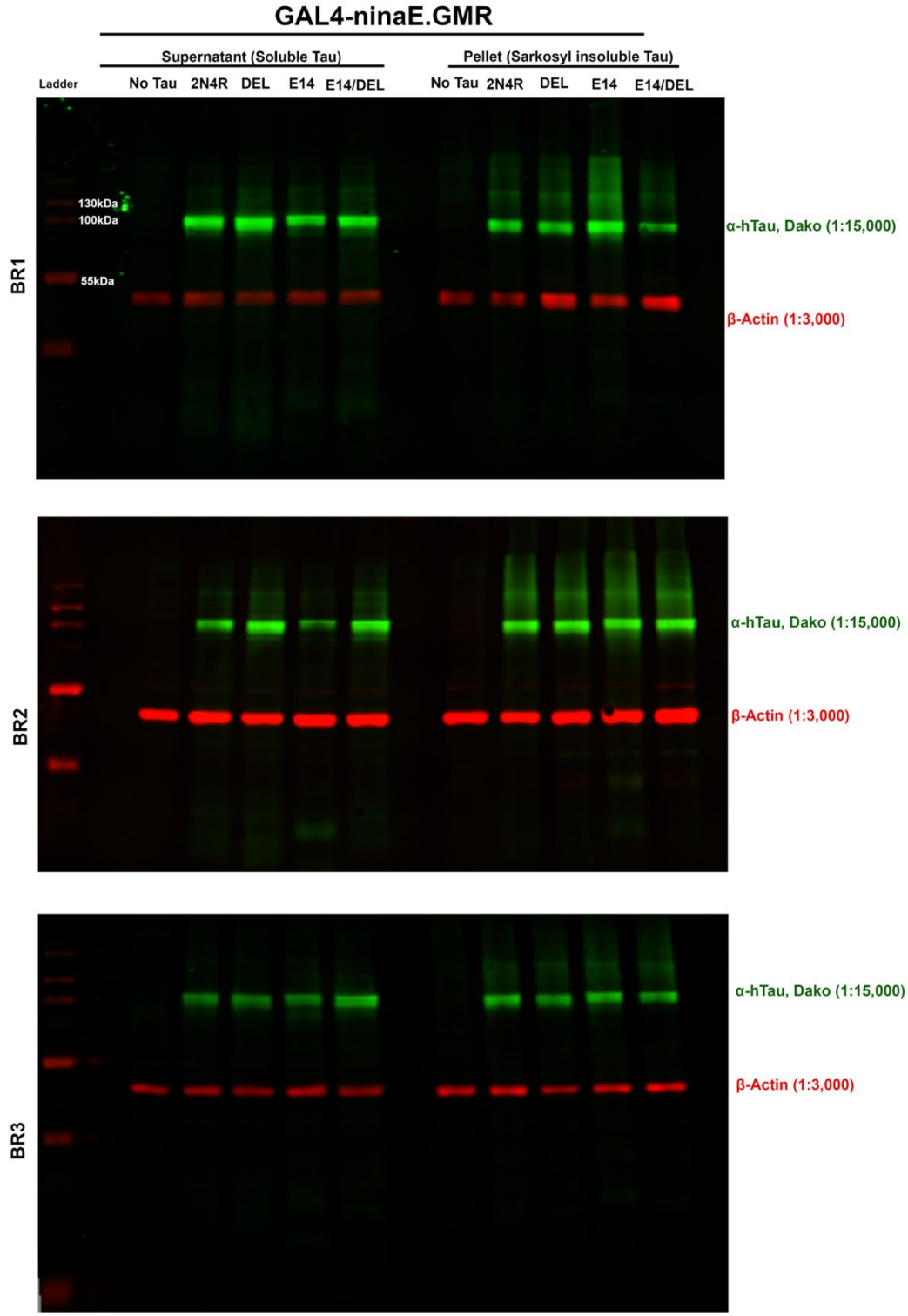


**Supplementary Figure 7. Full western blot of aqueous soluble (SN1) and sarkosyl insoluble fraction (SN2).**

Blotted against a-hTau (DAKO) and β-Actin as a loading control. Driver used was GAL4-GMR.ninaE. Genetic crosses set up at 25°C and progeny aged at 29°C (n=164 heads 50:50 male:female). Loaded with 15µl each.

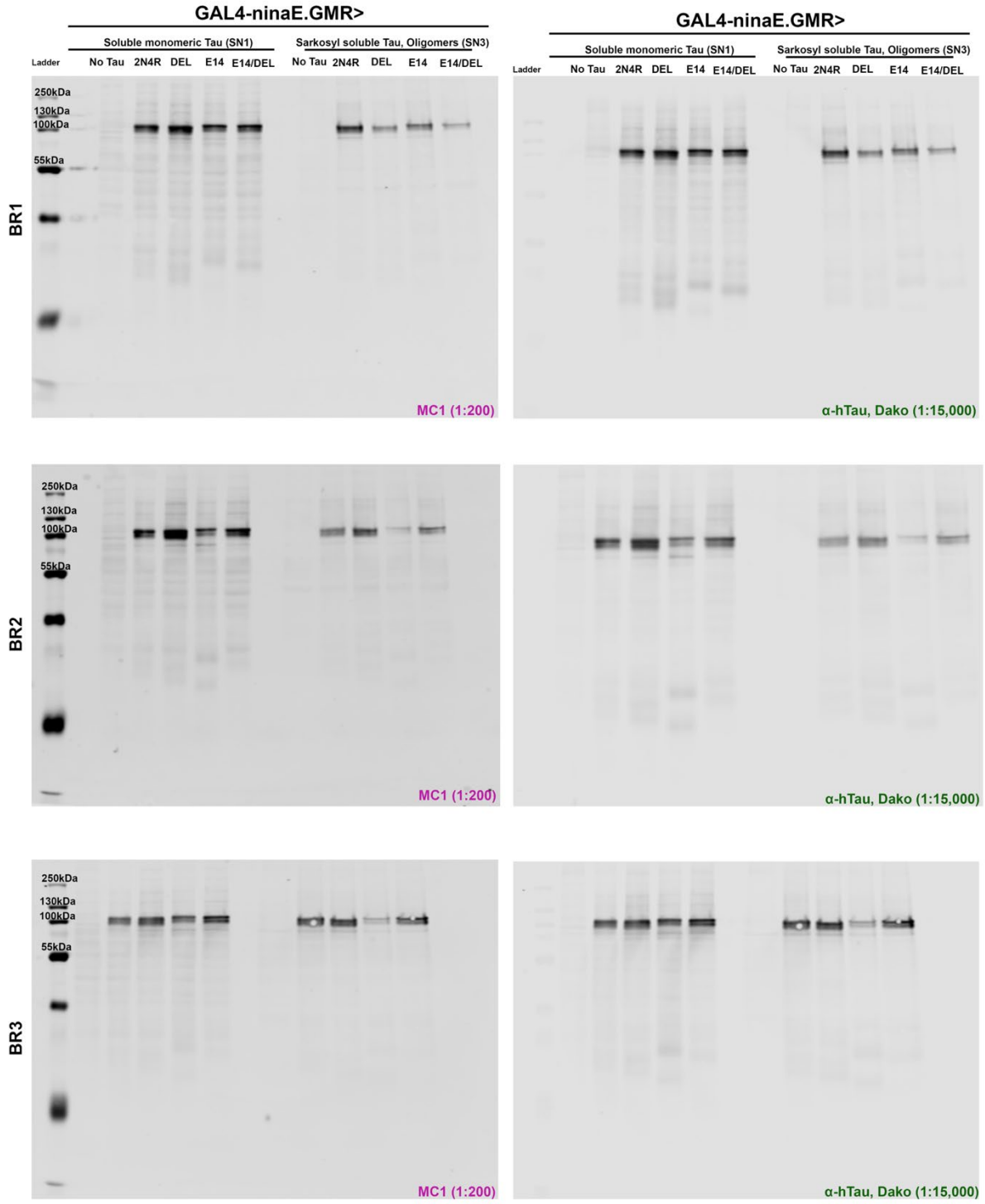


**Supplementary Figure 8. Full western blots of aqueous soluble (SN1) and sarkosyl soluble fraction (SN3).**

Blotted against MC1 for detecting misfolded Tau species (left column) and a-hTau (DAKO) for total Tau (right column). Driver used was GAL4-GMR.ninaE. Genetic crosses set up at 25°C and progeny aged at 29°C (n=164 heads 50:50 male:female). Loaded with 15µl each.

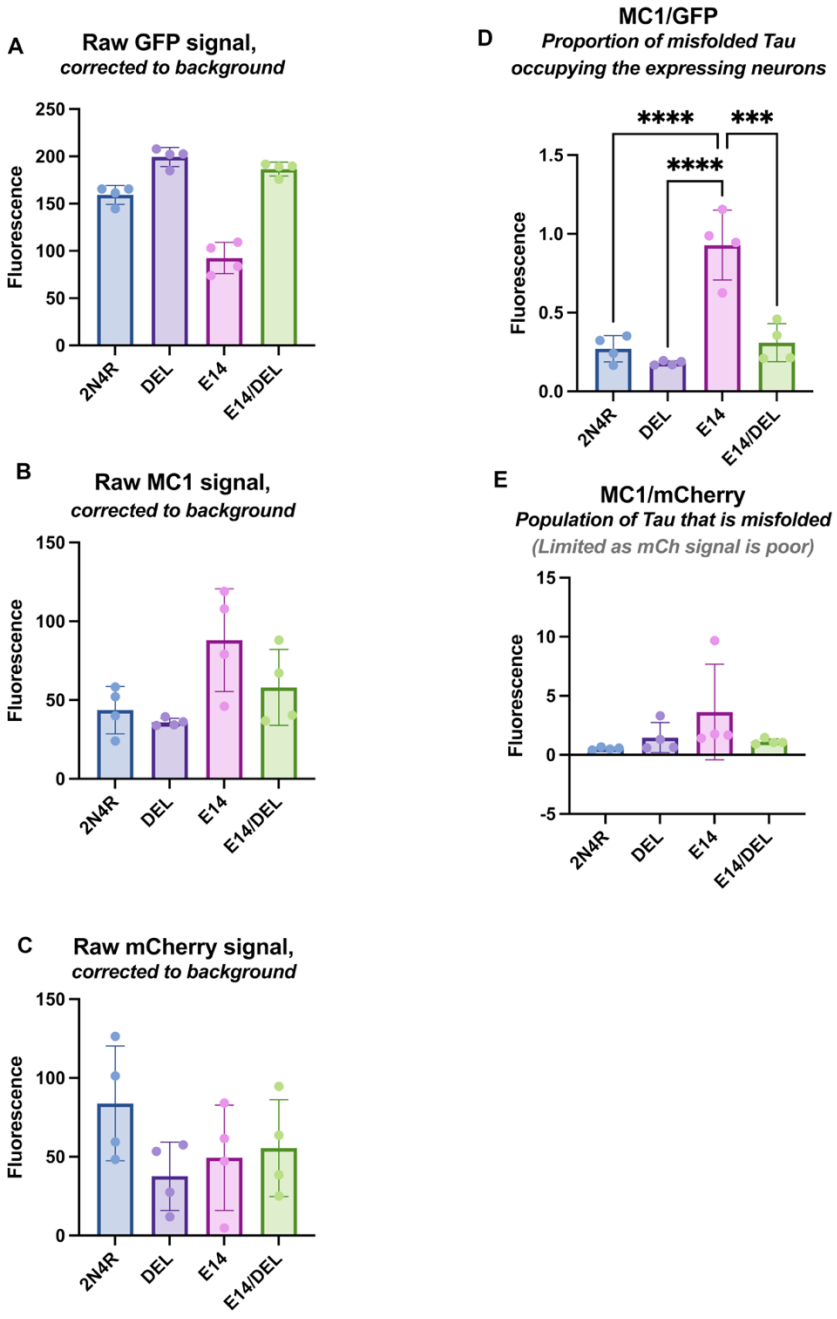


**Supplementary Figure 9. Unadjusted quantification of GFP, Total Tau and MC1 fluorescence signal intensity in Or47b expressing neurons at 14 days old using MATLAB.**

Fluorescence was quantified using automated segmentation of GFP signal using Matlab to separate GFP vs nonGFP pixels. Fluorescence signal is the average MC1 signal of the GFP-positive pixels, minus the average of the GFP-negative pixels (background). MC1/GFP was calculated to represent the proportion of misfolded Tau occupying the expressing Or47b neurons, and MC1/mCherry::Tau signal was calculated to represent the population of Tau that is misfolded, however this measurement was limited as raw mCherry signal was weaker as a-hTau Dako was not used due to antibody interference with MC1. Quantification using this method was carried out by Dr Miguel Ramirez-moreno. N=4 from one biological repeat. Graphs represent mean ±SD. ***=$p<0.001$ and ****= $p<0.0001$ (one-way ANOVA with Tukey's multiple comparisons).

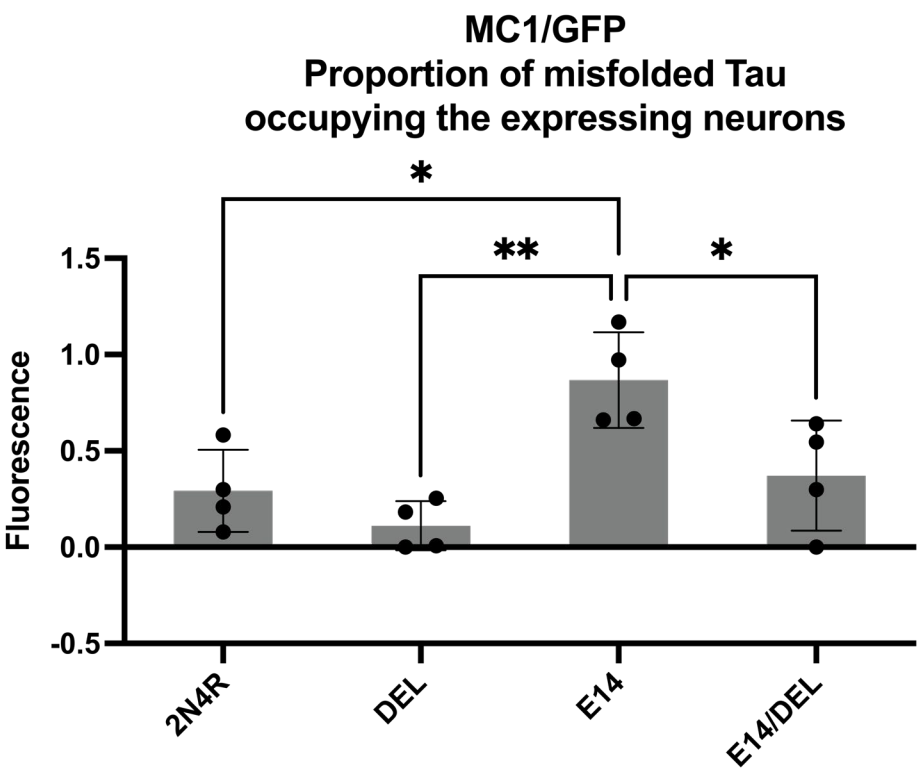


**Supplementary Figure 10. Manual quantification of the proportion of misfolded Tau species occupying the expressing neurons.**

Fluorescence was quantified using manual segmentation of GFP signal using a freehand drawn ROI to separate Or47b-GFP from background. The ROI was then mapped on to the MC1 channel, and the mean gray value of each slice was quantified corrected to background signal. N=4 from one biological repeat. Graphs represent mean ±SD. *p<0.05 and **p<0.01 (one-way ANOVA with Tukey's multiple comparisons). Unadjusted fluorescent values of each channel are shown in **Supplementary Figure 11**. This manual approach yielded trends consistent with automated MATLAB quantification, supporting its validity. Automated methods were used in **Figure 36** due to better robustness and reproducibility.

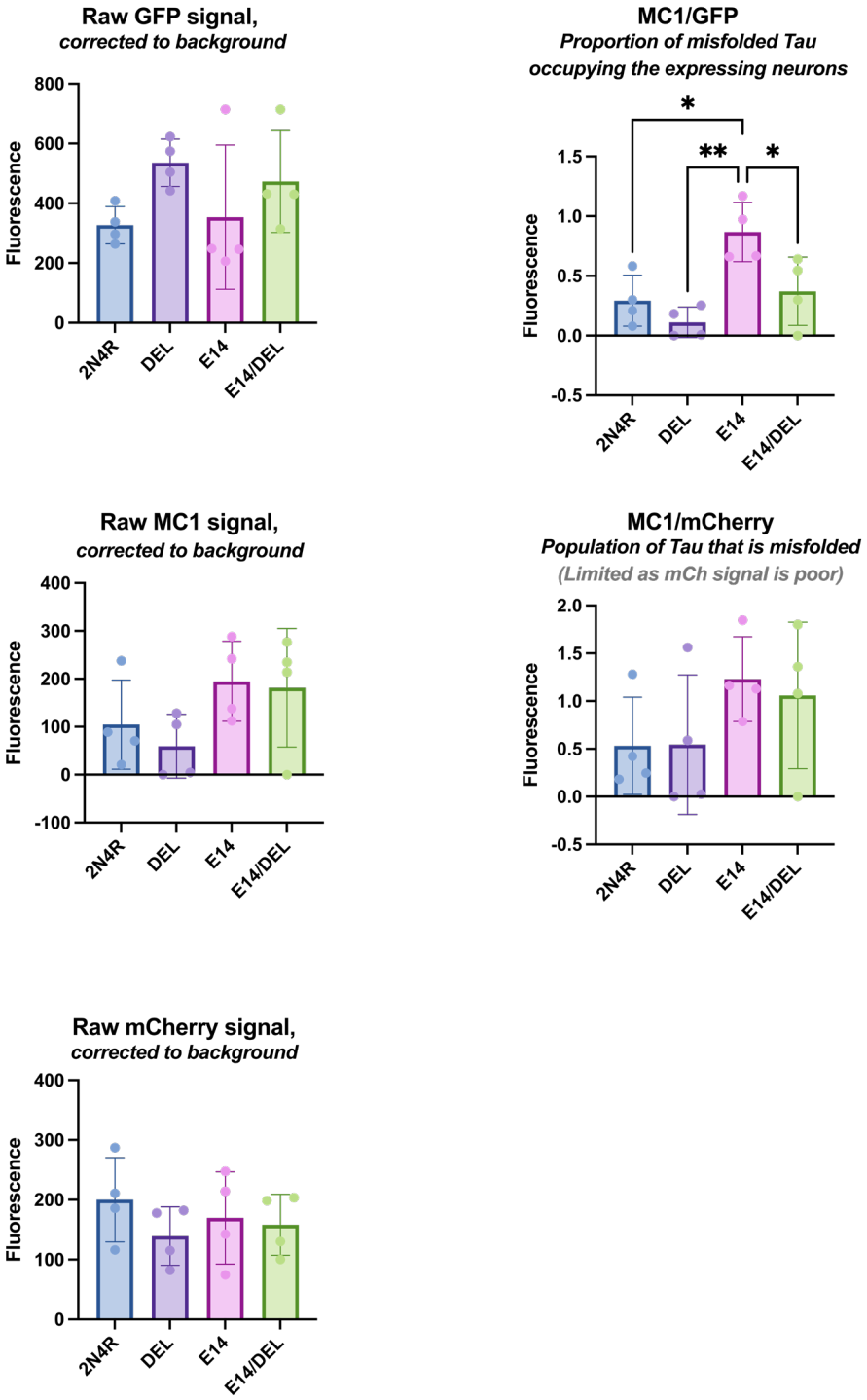


**Supplementary Figure 11. Unadjusted quantification of GFP, Total Tau and MC1 fluorescence signal intensity in Or47b expressing neurons at 14 days old using Image J.**

Fluorescence was quantified using manual segmentation of GFP signal using a freehand drawn ROI to separate GFP from background. The ROI was then mapped on to each other channel, and the mean grey value of each slice, corrected to the average of three background ROIs. MC1/GFP was calculated to represent the proportion of misfolded Tau occupying the expressing Or47b neurons, and MC1/mCherry::Tau signal was calculated to represent the population of Tau that is misfolded, however this measurement was limited as raw mCherry signal was weaker as a-hTau Dako was not used due to antibody interference with MC1. N=4 from one biological repeat. Graphs represent mean ±SD. ***p<0.001 and ****p<0.0001 (one-way ANOVA with Tukey's multiple comparisons).

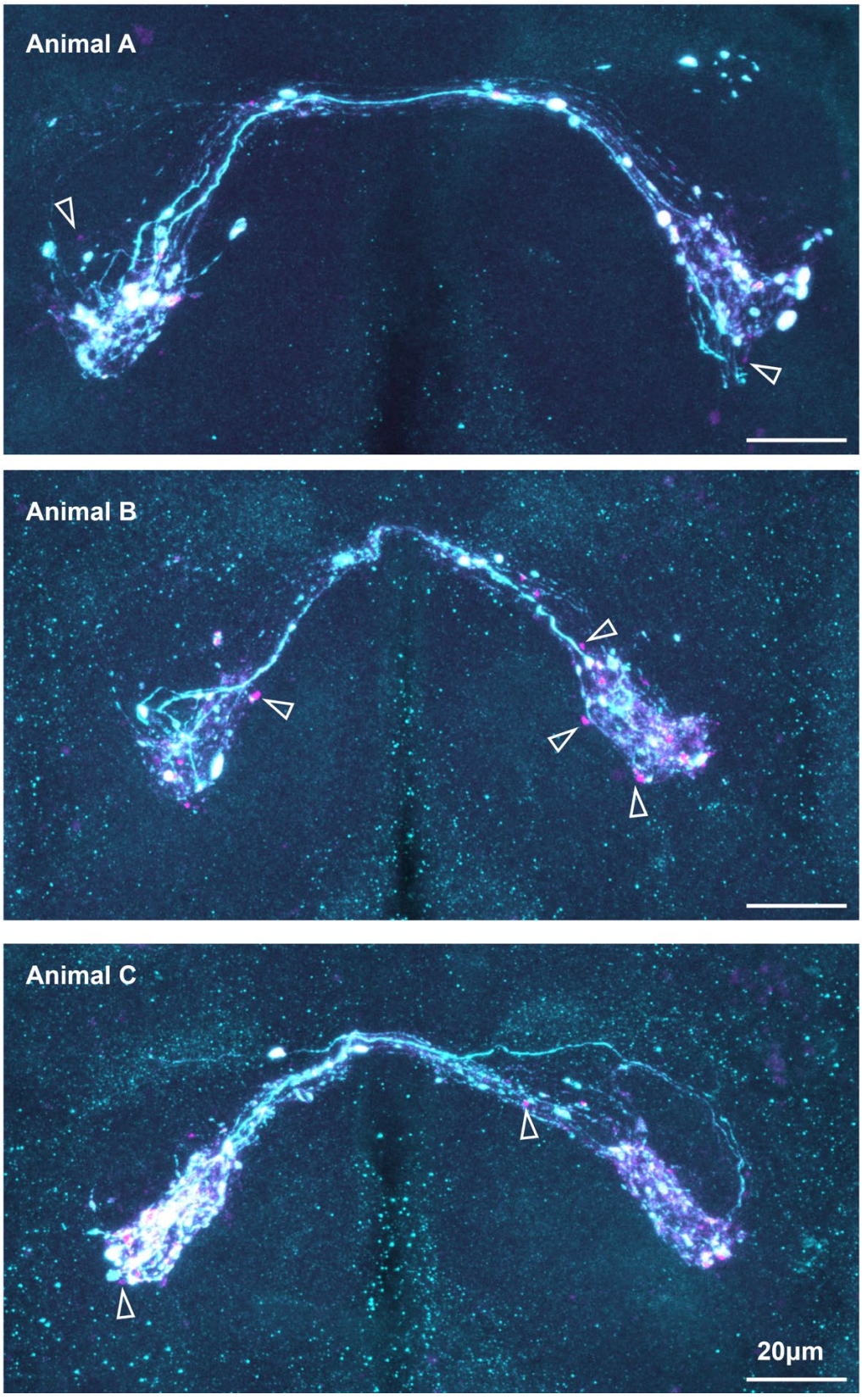


**Supplementary Figure 12. hTau2N4R-E14 accumulates misfolded Tau in Or47b neurons, but not all aggregates are MC1-positive.**

Three examples of Or47b>hTau2N4R-E14 composite images of the full antennal lobe are shown. MC1 staining for misfolded Tau (Cyan) and mCherry::Tau (magenta) images from 14-day-old flies show strong MC1 colocalisation with mCherry::Tau, however there are some Tau aggregates lacking MC1 signal (arrows), indicating that not all Tau is misfolded.

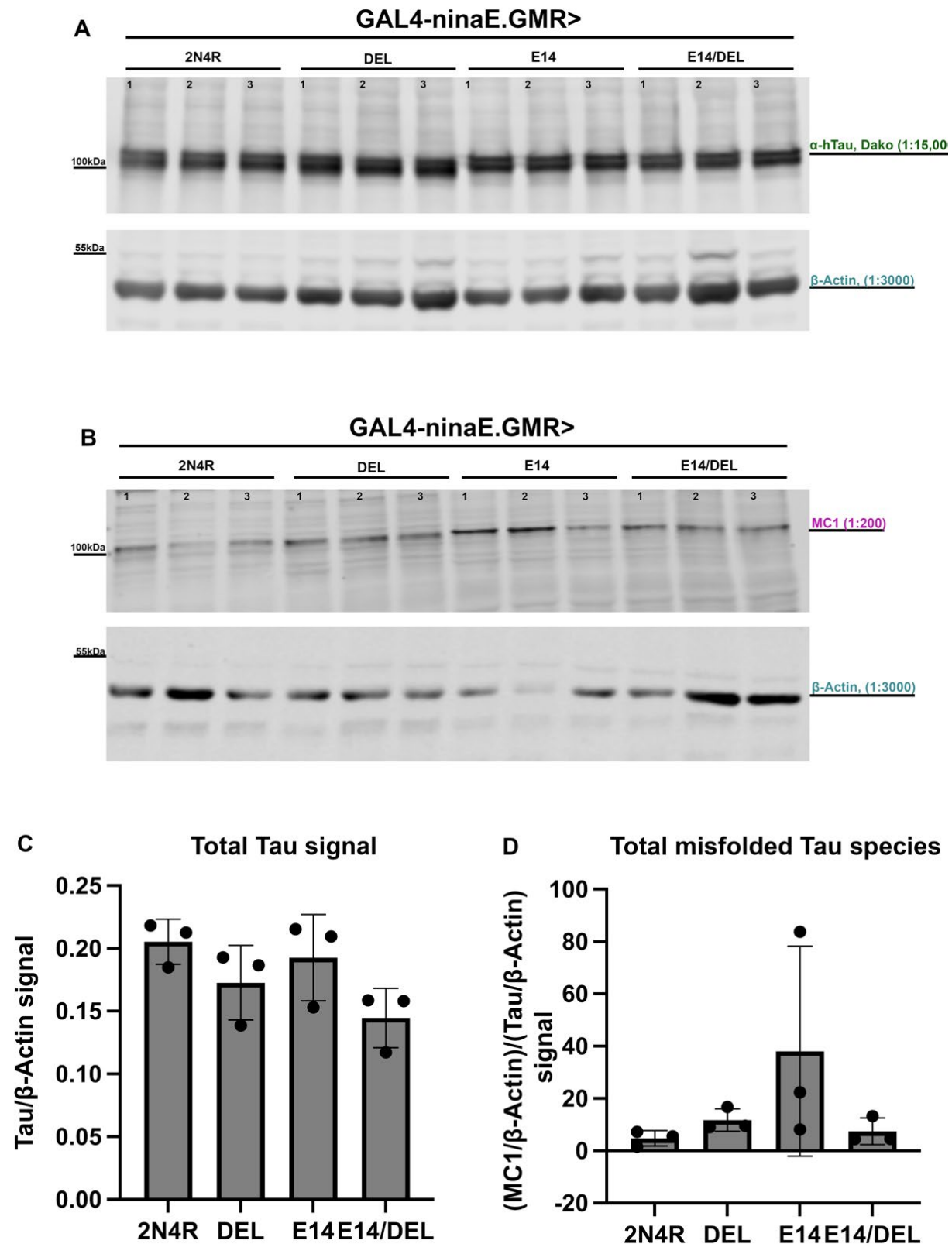


**Supplementary Figure 13. Western blot quantification of misfolded Tau species.**

Comparison of total Tau and misfolded Tau species between different transgenic flies tested after 14 days of aging (mCherry tagged hTau2N4R, hTau2N4R-DEL, hTau2N4R-E14 and hTau2N4R-E14/DEL). Driver used was Gal4-GMR.ninaE. Genetic crosses set up at 25°C and

progeny aged at 29°C (n=15 males). Representative blots comparing the input homogenates for the total Tau blotted against **A)** Dako, α-hTau and **B)** MC1 targeting misfolded Tau conformations. Each Tau mutant fraction runs at ~100kDa, taking into account for the weight of the mCherry Tag. β-Actin was used as a loading control and runs at ~40kDa. Quantification of the **C)** total Tau signal, normalised to actin and the **D)** fraction of misfolded Tau species, normalised to actin and the Dako/actin signal. Full representative blots can be found in **Supplementary Figure 14**. All graphs represent a mean ±SD (n=3). Statistical analysis was performed using a one-way ANOVA, and no statistical significance was reported between genotypes.

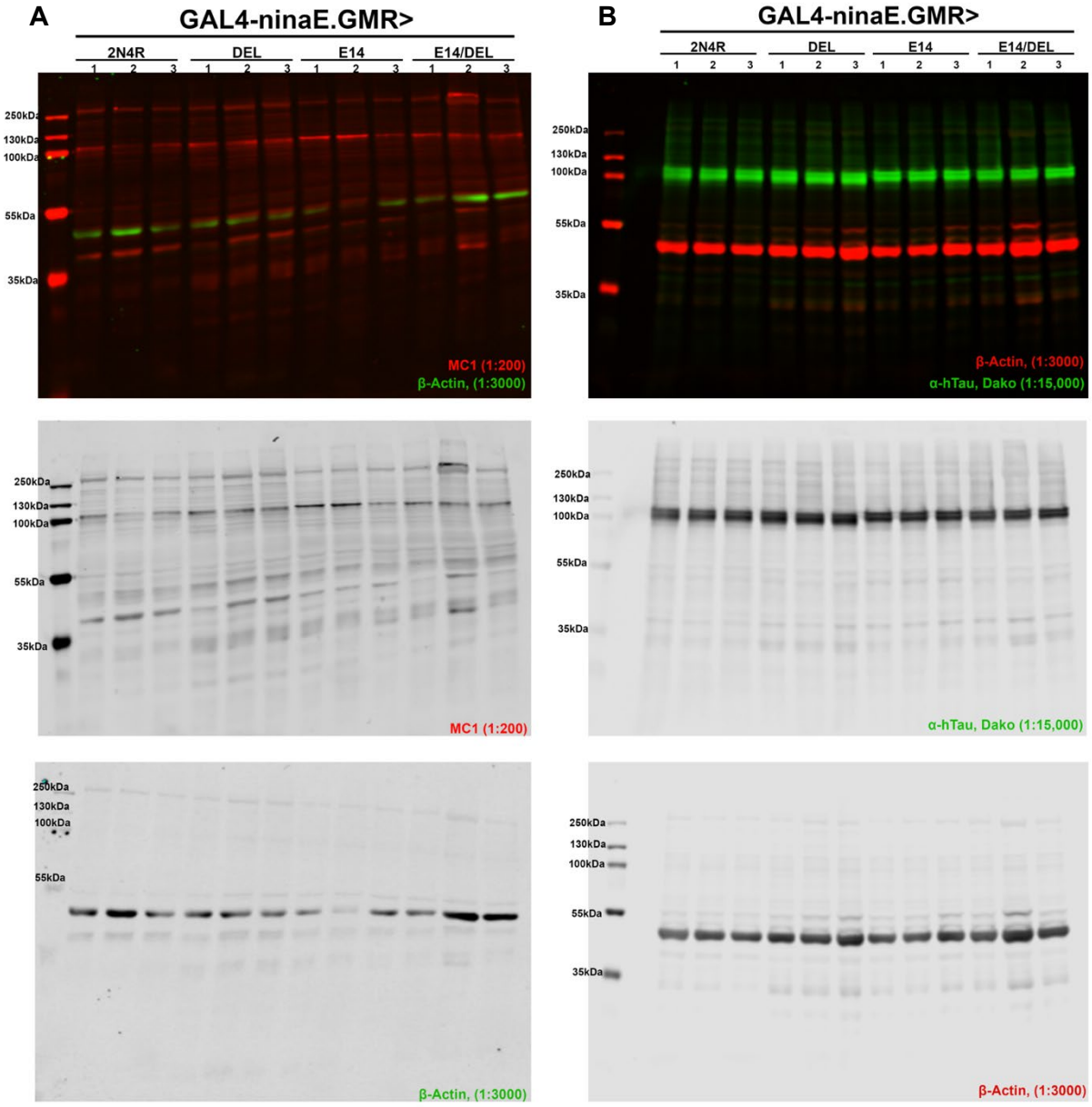


**Supplementary Figure 14. Full western blots of A)Misfolded and B) total Tau species of *Drosophila* brain homogenates, aged fro 14 days, (25>29ºC), 15 male heads.**

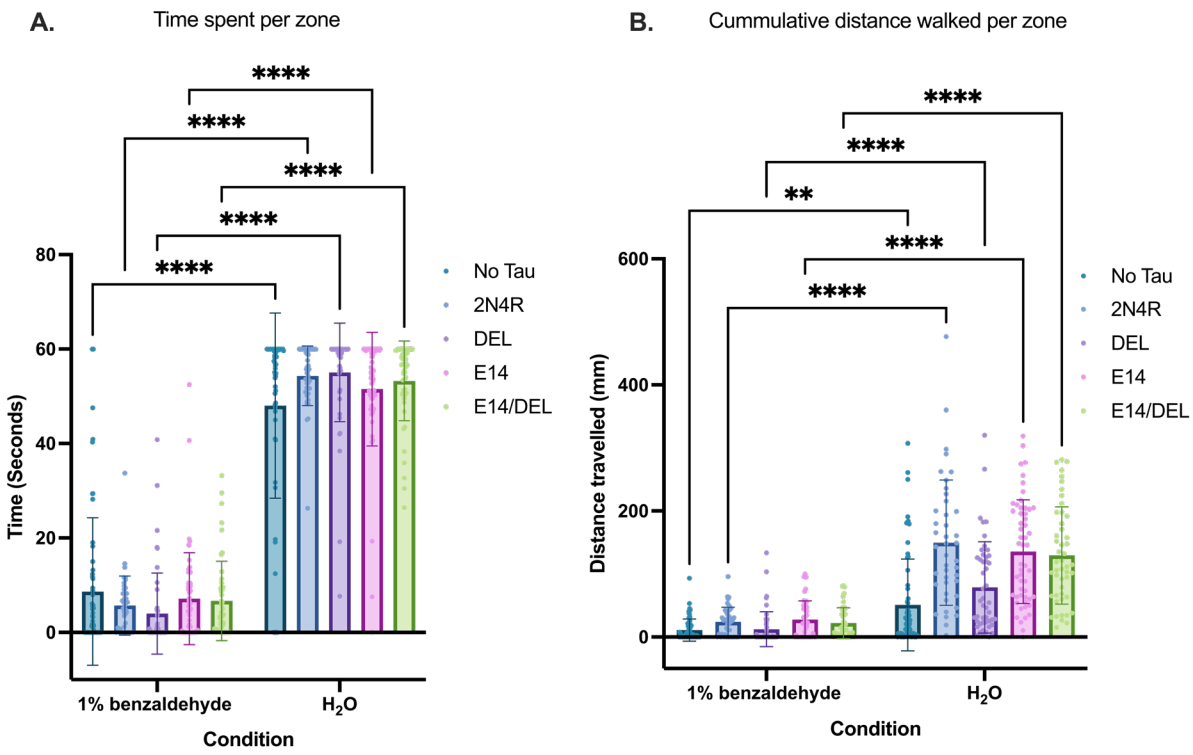


**Supplementary Figure 15. All mutant Tau-expressing flies spend significantly more time away from aversive odour.**

**Odour assay 3.** Aversive choice assay between water and 1% aversive odour benzaldehyde. Only males were used. Each fly's behaviour was quantified using Zantiks. Each animals cumulative distance walked (mm) and time spent per zone (s) was tracked and quantified automatically using Zantiks. Each data point shows an individual animal N= 42-65 per genotype. **A)** Graph represents mean ±SD time spent per zone condition. **D)** Graph shows the mean ±SD cumulative distance walked per condition. *P<0.1, **p<0.01, ***p<0.001 and **** p<0.0001 (non-parametric two-way ANOVA, with Geisser-Greenhouse correction).

Odour Assay 3.
Aversive choice assay using **Zantiks**

A.

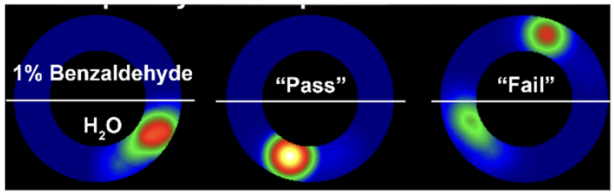


B.

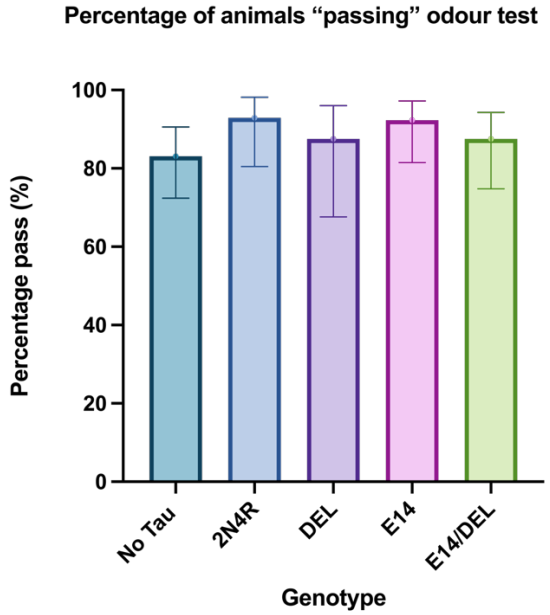


C.

| Genotype | Mean (% Pass) | Lower 95% CI | Upper 95% CI |
|---|---|---|---|
| No Tau | 83.1 | 72.4 | 90.6 |
| 2N4R | 92.9 | 80.5 | 98.2 |
| DEL | 87.5 | 67.6 | 96 |
| E14 | 92.3 | 81.5 | 97.2 |
| E14/DEL | 87.5 | 74.8 | 94.3 |

D.

| Genotype | No Tau | 2N4R | DEL | E14 | E14/DEL |
|---|---|---|---|---|---|
| No Tau | | 0.2395 | 0.7508 | 0.1705 | 0.6009 |
| 2N4R | | | 0.66 | >0.9999 | 0.4943 |
| DEL | | | | 0.6719 | >0.9999 |
| E14 | | | | | 0.5141 |
| E14/DEL | | | | | |

**Supplementary Figure 16. Aversive odour assay 3 Zantiks heatmap analysis.**

Alternative binary quantification for Zantiks odour assay. Each animal was individually assessed for its preference to stay in the control water zone or 1% benzaldehyde aversive odour to assess odorant perception as a functional assessment of the olfactory neurons. A) representative heatmap showing classification for "pass" (positive choice spending most of their time in water) and "fail"(negative choice, spending most of their time in the aversive odour). B-C) Graph and data table is presented as mean pass rate ± 95% confidence intervals (CI). D) Pairwise comparisons of pass/fail outcomes across genotypes. There was no statistical difference between any genotype tested using a two-sided Fishers test in a 2x2 genotype comparison with a Bonferroni correction *p<0.005.

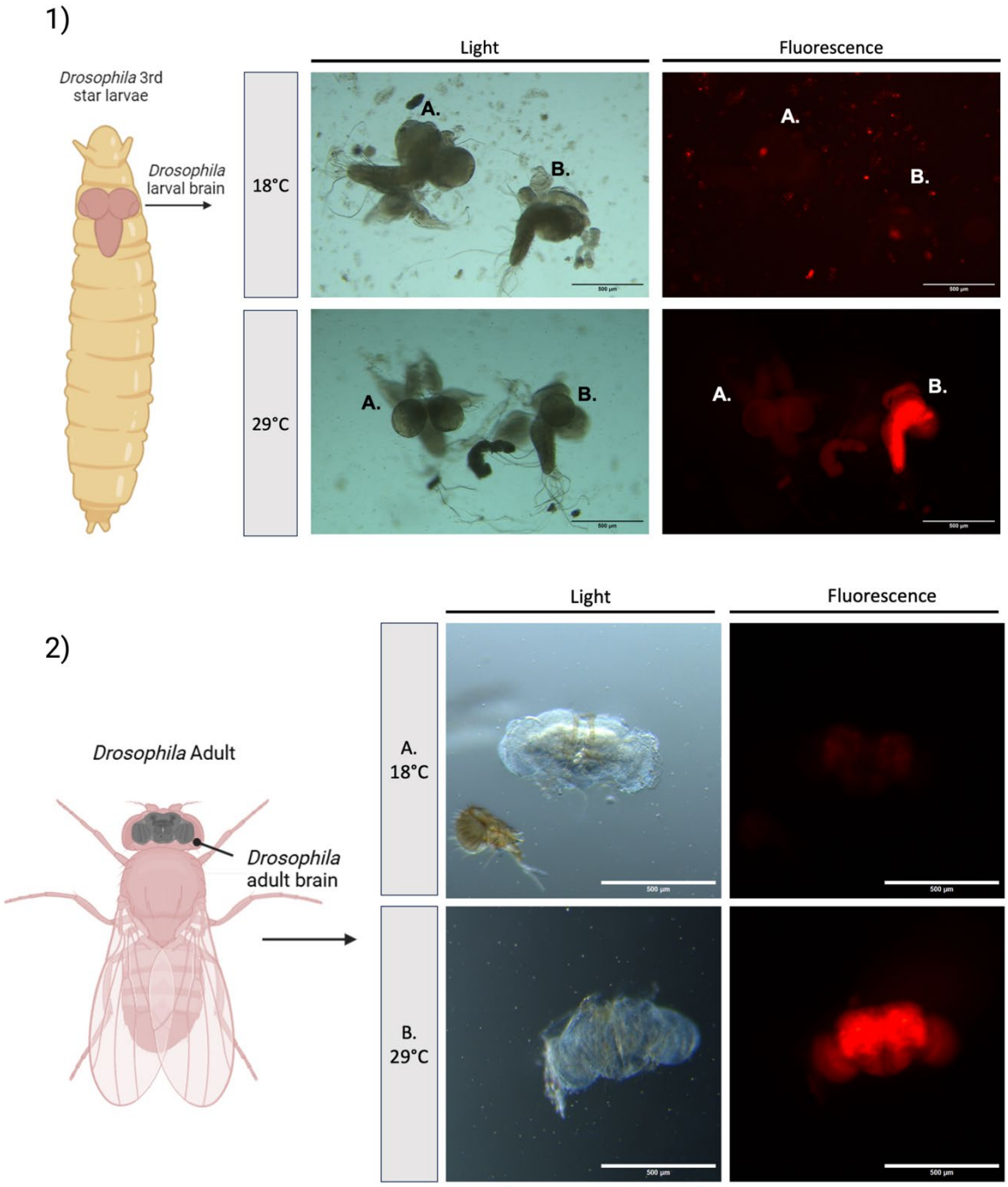


**Supplementary Figure 17. Validating the Elav-GAL4;;Tubulin-GAL80ts; temperature switch driver.**

This system was validated **1)** developmentally using larval brain dissections of A. Control (no Tau/mCherry expression) flies and B. ElavGal4;+;TubGal80ts;x;UAS-mCherry::Tau2N4R(II);; driven flies. mCh::Tau is only expressed at 29ºC, and is suppressed at 18ºC. **2)** shows Adult brain dissections of ElavGal4;+;TubGal80ts; x ;UAS-mCherry::Tau2N4R(E14)(II);; A. adults were collected at 18ºC and dissected at one day old. B. adults were collected at 18ºC, then moved to 29ºC and aged for 2 days. Proper restriction and expression patterns are shown whilst also validating that hTau2N4R-E14 expressing flies do not have pupal lethality due to 18ºC repression.

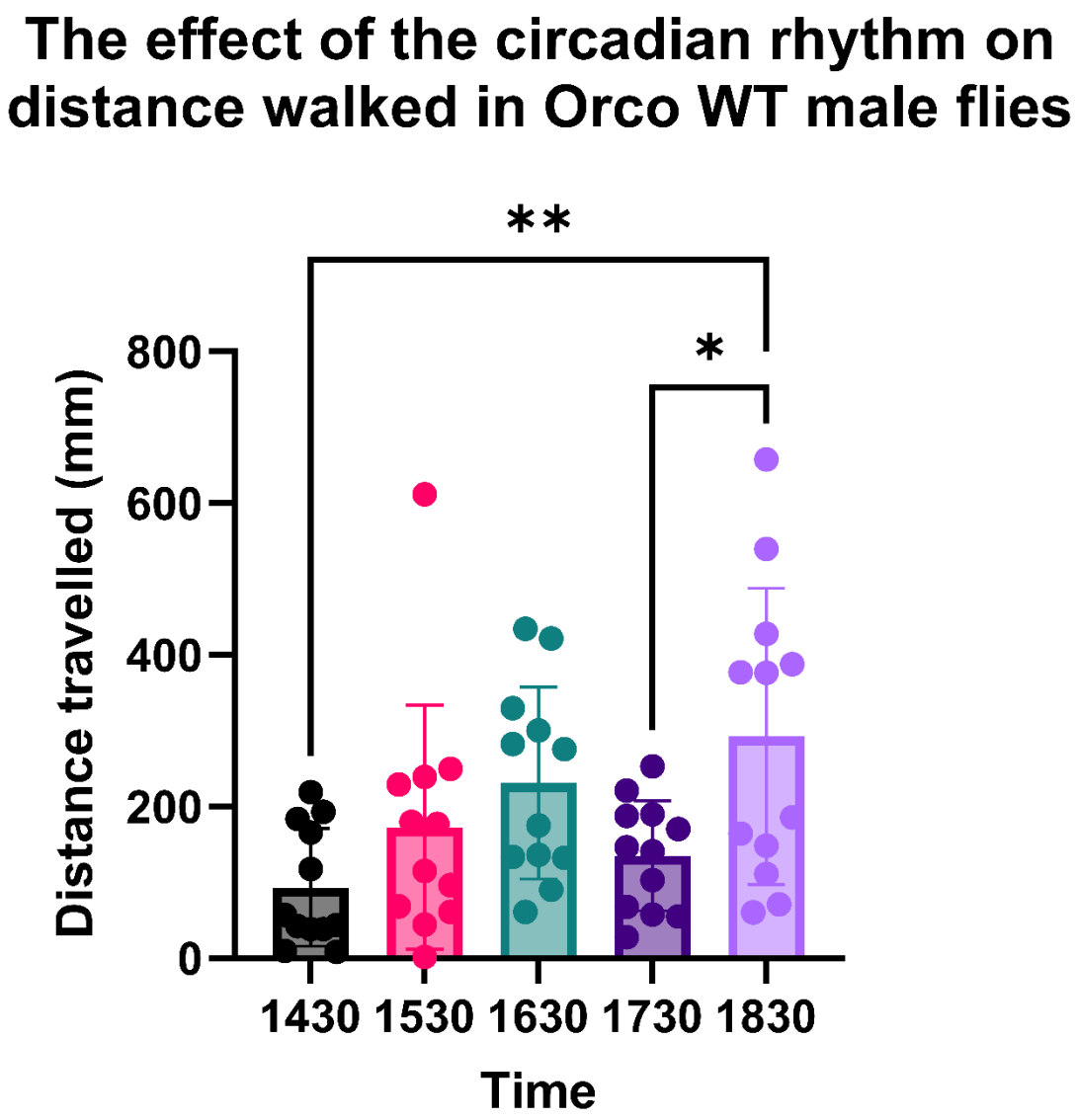


**Supplementary Figure 18. Circadian rhythm affects adult *Drosophila* activity.**

Flies on a 08:00-20:00 24hr L/D cycle are most active after their siesta (mid afternoon nap). Using Zantiks to track the distance walked in an assessment arena over a 10 min period. Graphs represent mean ± SD. Each data point represents an individual animal tested N=12 from 2 biological repeats. Ordinary one-way ANOVA with multiple comparisons was used for statistical analysis. There is a significant increase in locomotive activity from 14:30-18:30 **P=0.058, and from 17:30-18:30 *p=0.0871.

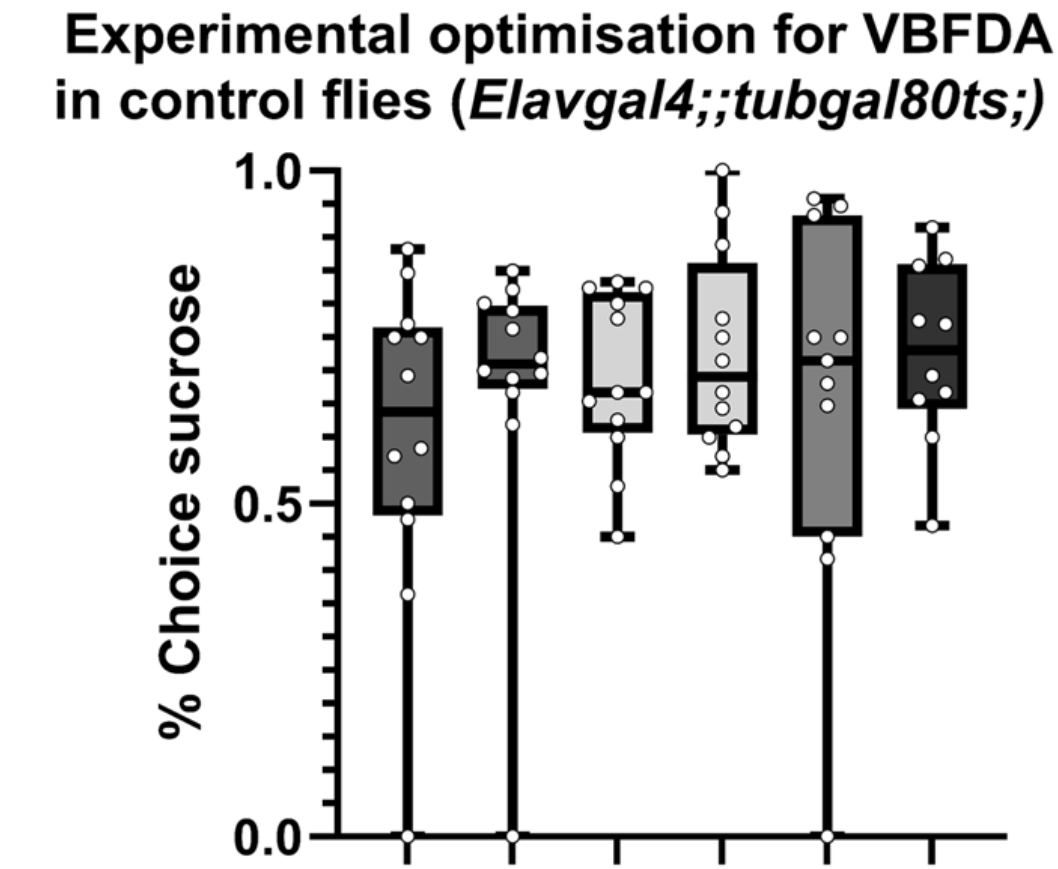


| | | | | | | |
|---|---|---|---|---|---|---|
| Starvation period (hours) | 24 | 24 | 7 | 7 | 16 | 12 |
| Age (days) | 1 | 4 | 4 | 14 | 11 | 14 |
| Time assay performed | 4pm | 4pm | 4pm | 4pm | 9am | 6pm |

**Supplementary Figure 19. Starvation optimisation for Value based feeding decision assay(VBDA).**

Based on the previously published protocol from Yu et al 2021, flies were starved for 24 hours, but this led to high mortality in 14-day-old flies reared at 18ºC and aged at 29ºC. To account for increased metabolic demand under Gal80ts conditions, starvation durations were reduced to 16, 12, or 7 hours. Twelve-hour starvation with testing at 6 pm (6am–6pm) produced the most consistent sucrose preference without excessive mortality. Each data point represents a group of 12 starved male flies. While no statistically significant differences in medians were observed (Kruskal-Wallis test, *$p<0.05$), 12-hour starvation at 6pm had the lowest variance and was used for all VBFDAs.

A.

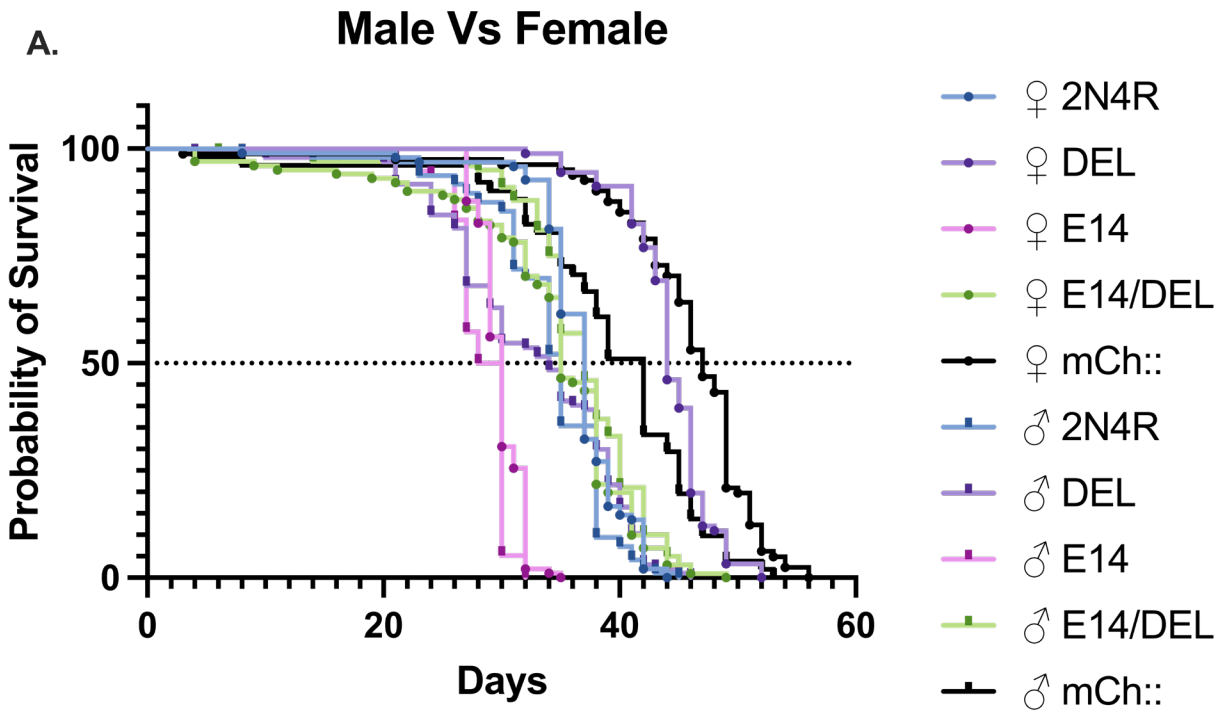


B.

| Median Survival | | | | | |
|---|---|---|---|---|---|
| | mCh | 2N4R | DEL | E14 | E14/DEL |
| ♀ | 47 | 37 | 44 | 30 | 35 |
| ♂ | 42 | 35 | 34 | 29 | 37 |

C.

| | mCherry | 2N4R | DEL | E14 | E14/DEL |
|---|---|---|---|---|---|
| mCherry | <0.0001 | | | | |
| 2N4R | | 0.0036 | | | |
| DEL | | | <0.0001 | | |
| E14 | | | | <0.0001 | |
| E14/DEL | | | | | 0.1359 |

**Supplementary Figure 20. Gender comparison of longevity assay.**

**A)** Kaplan Meier survival curves for Elav-Gal4;;TubGal80ts; driven mCherry Tagged Tau mutants: hTau2N4R, hTau2N4R-DEL, hTau2N4R-E14 and hTau2N4R-E14/DEL expressing male (squares))(n=100) and female flies (circles)(n=100). Flies expressing mCherry alone (no Tau) were used as a control. **B)** Shows median survival age of each genotype and sex. **C)** Lifespan of flies is significantly different between the Tau variants tested (Log-rank, Mantel-Cox test $p<0.0001$). With a manual Bonferroni correction to correct for 5 multiple comparisons, $*p<0.05/5$ makes corrected p-values $<0.01$. All gender populations except E14/DEL were significantly different. Generally, the female population from each genotype would outlive the respective e male populations.

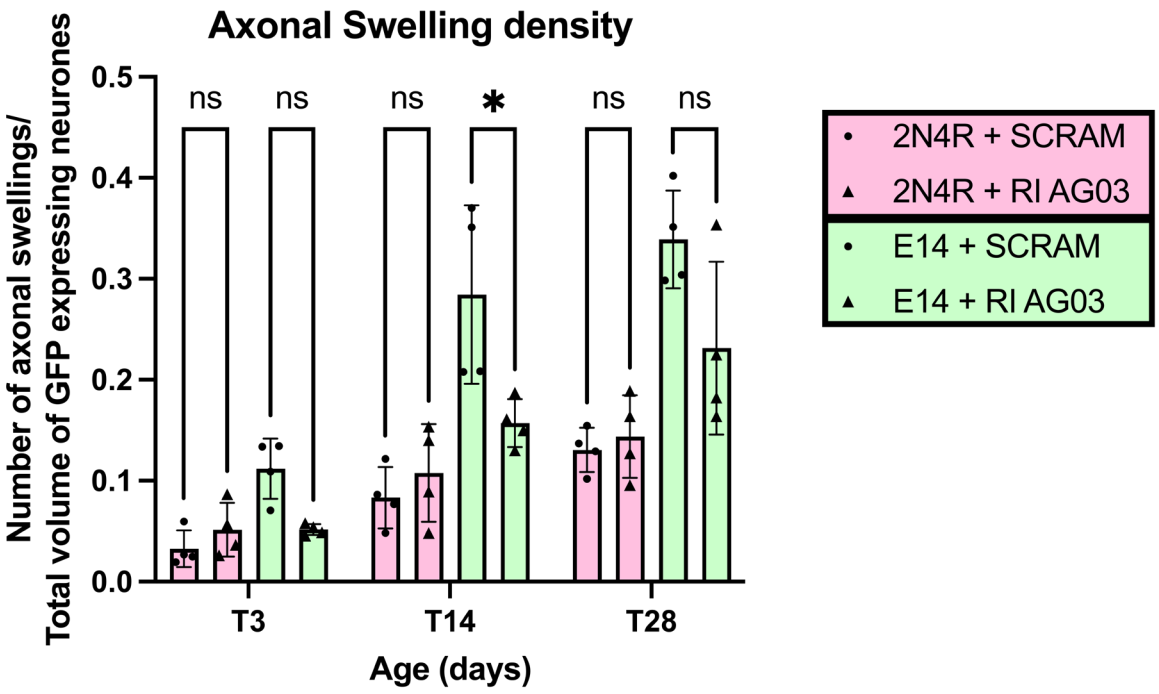


**Supplementary Figure 21. RI-AG03 treatment improves TauE14-mediated neuronal degeneration of Or47b neurons in one biological replicate.**

Quantification of axonal swellings from maximum projection confocal images of Scramble peptide(SCRAM, Control) /RI-AG03 treated hTau2N4R and hTau2N4R-E14 expressing flies within the Or47b neurons. Quantification of axonal swellings were automatically quantified using 3D images with IMARIS. Graph represents mean ±SD, and dots represent individual animals. RI-AG03 significantly improved axonal swelling density in hTau2N4R-E14 expressing flies at T14 only, * $p<0.05$ (2-way ANOVA with Tukey's multiple comparisons). N=4 brains collected from one biological repeat.

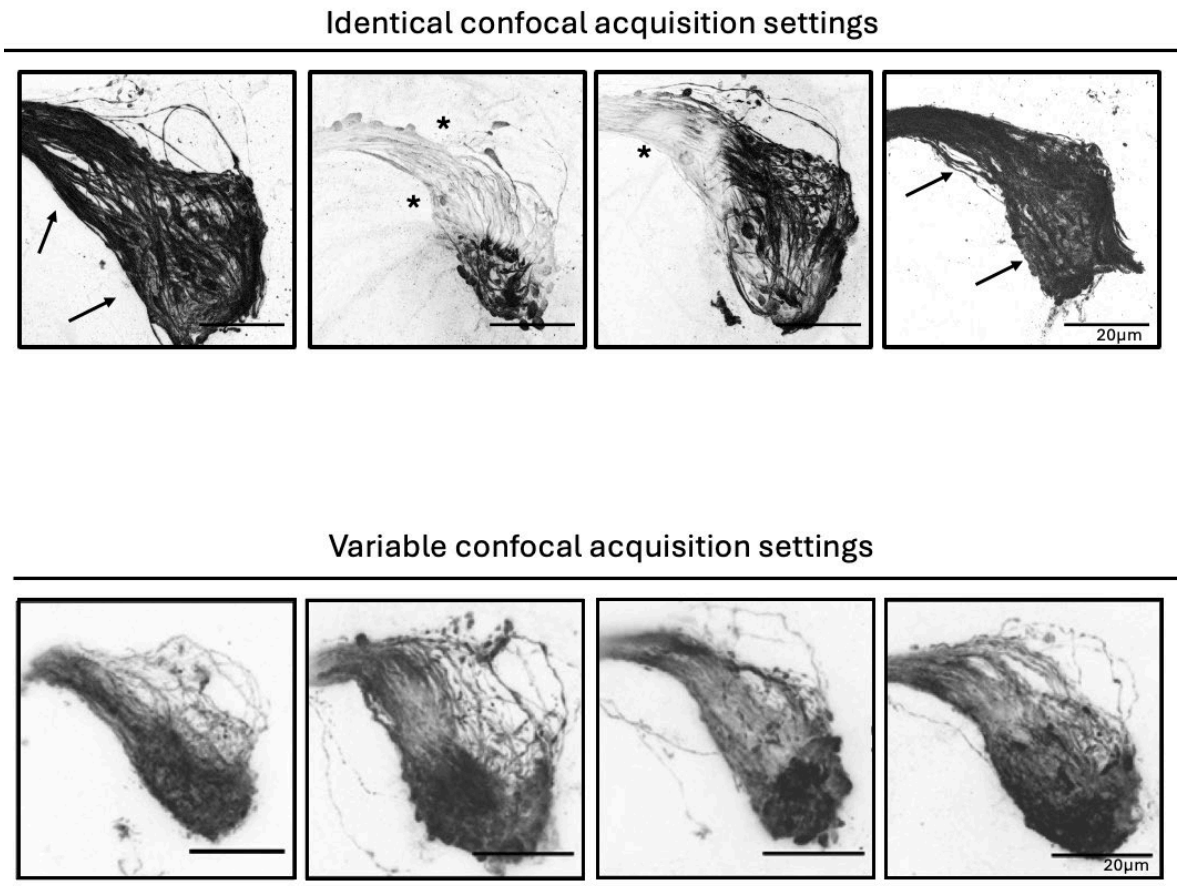


**Supplementary Figure 51. Confocal acquisition optimisation to preserve morphological detail.**

Representative confocal images of Tau signal in 14-day-old Or47b>hTau2N4R-P301S *Drosophila*, showing the variability in fluorescence intensity between animals when identical acquisition settings were applied. In some samples, fixed laser power caused overexposure, obscuring axonal swelling structures or Tau accumulates (Arrows). In other cases, the same settings failed to capture structures that were in fact there (Asterisk's), resulting in loss of morphological information. To maximise morphological information, acquisition parameters were adjusted to avoid saturation and signal loss. All subsequent analyses were quantified using 3D image analysis IMARIS which uses morphological segmentation independent of fluorescence intensity. Although fluorescence intensity can be informative, in this context uniform acquisition would have compromised morphological resolution through signal saturation. Therefore, acquisition settings were adapted between genotypes within 10% range to prioritise structural accuracy over intensity comparability.

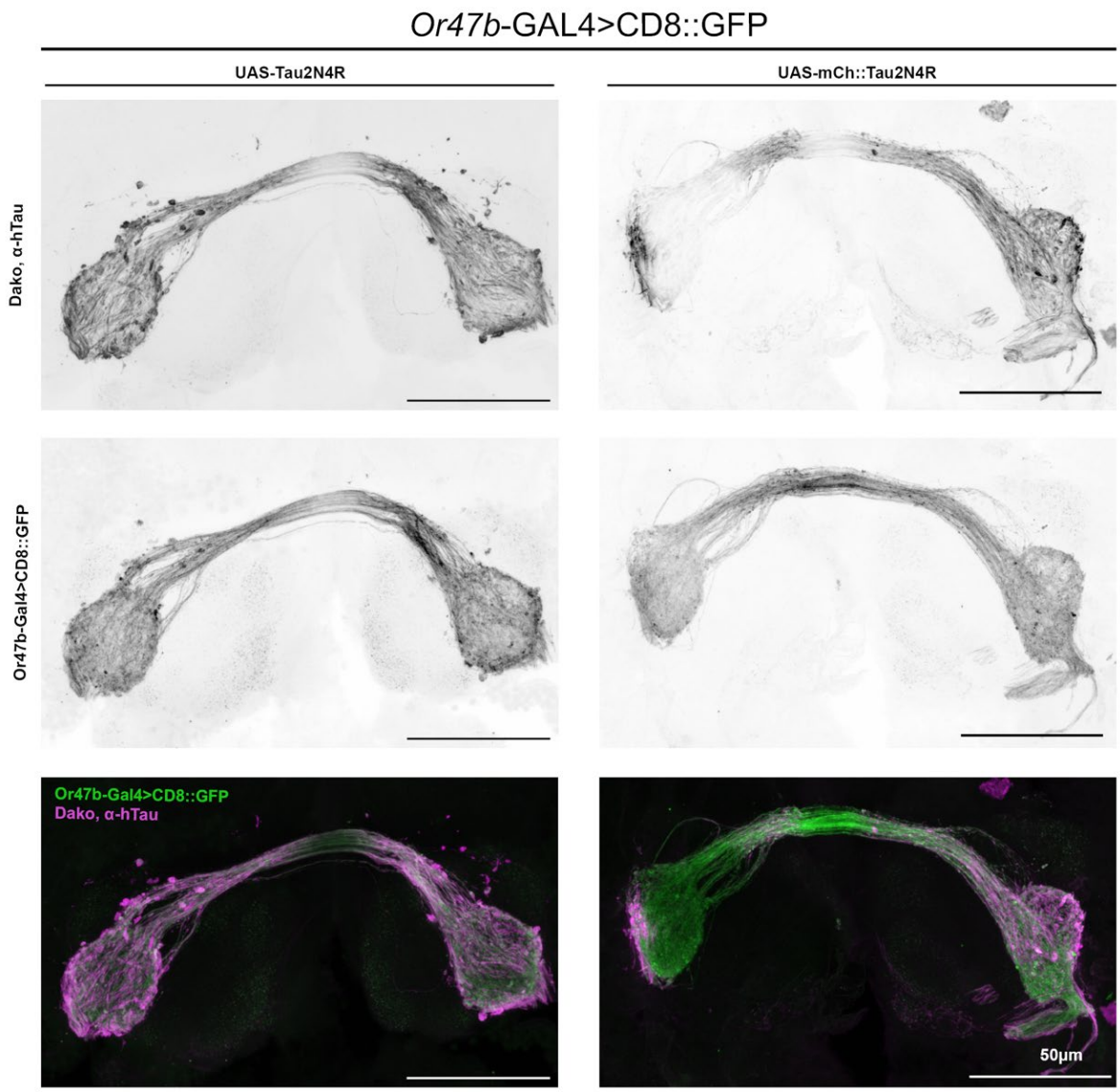


**Supplementary Figure 52. The mCherry tag does not alter Tau accumulation or axonal swelling.**

Sample confocal image of 7-day-old Or47b>hTau2N4R versus Or47b>mCh::hTau2N4R flies, demonstrating that the mCherry Tag does not significantly alter Tau accumulation (visualised using Dako) or axonal swelling (visualised using membrane bound GFP).

# Appendix B Supplementary Tables

**Supplementary Table 1. Commercially available Tau antibodies and their epitopes recognised that detect misfolded Tau conformations at different aggregation stages.**

They recognize discontinuous epitopes along Tau, binding when two distant regions along the Tau protein misfold into close proximity. Although the ultra-structures of misfolded Tau remains undefined, epitope mapping of these antibodies has provided insights into which Tau domains may fold and interact in early pathological conformations.

| Antibody | Epitope mapping (aa) | Tau conformation | Aggregation stage detected | References |
|---|---|---|---|---|
| **MC1** | 7-9, 313-322 | Misfolded Tau | Early (Pre-tangle) | (Jicha et al., 1997) |
| **Alz-50** | 2-10, 312-342 | Misfolded Tau | Early (Pre-tangle) | (Carmel et al., 1996) |
| **Tau-66** | 155-244, 305-314 | Misfolded Tau | Early (pre-tangle/intermediate) | (Ghoshal et al., 2001) |
| **MN423** | Recognises compact fold of PHF core, specifically truncated Tau cleaved at C-terminal Glu391 | Truncated, aggregated Tau | Late-stage tangles, ghost tangles | (Novak et al., 1993) |

**Supplementary Table 2. Fly homologs of Tau-interacting partners associated with $^{306}$VQIVYK$^{311}$.**

Human protein, the *Drosophila* homolog and their function, description copied from FlyBase.

| **Human Protein** | ***Drosophila* Homolog** | **FlyBase ID** | **Function in *Drosophila*** |
|---|---|---|---|
| **Hsp27 (HSPB1)** | Hsp26 | FBgn0001225 | Involved in protein folding. |
| **Hsp70 (HSPA1A)** | Hsp110 | FBgn0026418 | Interacts physically with the product of DnaJ-1 as a chaperone of misfolded proteins. It functions to prevent the toxicity of aggregation-prone proteins. |
| **Hsp90 (HSP90AA1)** | Hsp83 | FBgn0001233 | Molecular chaperone for cell cycle control and signal transduction. |
| **FKBP12 (FKBP1A)** | FKBP12 (CG14768) | FBgn0013954 | Binds the intracellular calcium channel. Loss results in increased calcium leak and reduced muscle function. |
| **G3BP2** | Rasputin (Rin) | FBgn0015778 | Rasputin (Rin) encodes an RNA-binding protein that regulates gene expression. It is involved in eye development and the dorsal/ventral axis specification of the ovary. |

# List of References.

List of References

ABRAHA, A., GHOSHAL, N., GAMBLIN, T. C., CRYNS, V., BERRY, R. W., KURET, J. & BINDER, L. I. 2000. C-terminal inhibition of tau assembly in vitro and in Alzheimer's disease. *J Cell Sci,* 113 Pt 21**,** 3737-45.

ABREHA, M. H., DAMMER, E. B., PING, L., ZHANG, T., DUONG, D. M., GEARING, M., LAH, J. J., LEVEY, A. I. & SEYFRIED, N. T. 2018. Quantitative Analysis of the Brain Ubiquitylome in Alzheimer's Disease. *Proteomics,* 18**,** e1800108.

ABSKHARON, R., PAN, H., SAWAYA, M. R., SEIDLER, P. M., OLIVARES, E. J., CHEN, Y., MURRAY, K. A., ZHANG, J., LANTZ, C., BENTZEL, M., BOYER, D. R., CASCIO, D., NGUYEN, B. A., HOU, K., CHENG, X., PARDON, E., WILLIAMS, C. K., NANA, A. L., VINTERS, H. V., SPINA, S., GRINBERG, L. T., SEELEY, W. W., STEYAERT, J., GLABE, C. G., OGORZALEK LOO, R. R., LOO, J. A. & EISENBERG, D. S. 2023. Structure-based design of nanobodies that inhibit seeding of Alzheimer's patient-extracted tau fibrils. *Proc Natl Acad Sci U S A,* 120**,** e2300258120.

ABUBAKAR, M., GIRI, A., GOEL, F., KHAN, M., GUPTA, J., KUMAR, D., KAUSHIK, M., RAI, S. N. & KUMAR, N. 2025. Diabetes, Alzheimer's Disease Risk Factors, and the Cafeteria Diet: A Comprehensive Review. *Curr Neuropharmacol*.

ACOSTA, D. M., MANCINELLI, C., BRACKEN, C. & ELIEZER, D. 2022. Post-translational modifications within tau paired helical filament nucleating motifs perturb microtubule interactions and oligomer formation. *J Biol Chem,* 298**,** 101442.

ADAMS, S. J., DETURE, M. A., MCBRIDE, M., DICKSON, D. W. & PETRUCELLI, L. 2010. Three repeat isoforms of tau inhibit assembly of four repeat tau filaments. *PLoS One,* 5**,** e10810.

AGGIDIS, A., DEVITT, G., ZHANG, Y., CHATTERJEE, S., TOWNSEND, D., FULLWOOD, N. J., ORTEGA, E. R., TARUTANI, A., HASEGAWA, M., COOPER, A., WILLIAMSON, P., MENDOZA-OLIVA, A., DIAMOND, M. I., MUDHER, A. & ALLSOP, D. 2024. A novel peptide-based tau aggregation inhibitor as a potential therapeutic for Alzheimer's disease and other tauopathies. *Alzheimers Dement,* 20**,** 7788-7804.

AHMED, T., VAN DER JEUGD, A., BLUM, D., GALAS, M. C., D'HOOGE, R., BUEE, L. & BALSCHUN, D. 2014. Cognition and hippocampal synaptic plasticity in mice with a homozygous tau deletion. *Neurobiol Aging,* 35**,** 2474-2478.

AILEEN FUNKE, S., VAN GROEN, T., KADISH, I., BARTNIK, D., NAGEL-STEGER, L., BRENER, O., SEHL, T., BATRA-SAFFERLING, R., MORISCOT, C., SCHOEHN, G., HORN, A. H., MüLLER-SCHIFFMANN, A., KORTH, C., STICHT, H. & WILLBOLD, D. 2010. Oral treatment with the d-enantiomeric peptide D3 improves the pathology and behavior of Alzheimer's Disease transgenic mice. *ACS Chem Neurosci,* 1**,** 639-48.

AILLAUD, I., KANIYAPPAN, S., CHANDUPATLA, R. R., RAMIREZ, L. M., ALKHASHROM, S., EICHLER, J., HORN, A. H. C., ZWECKSTETTER, M., MANDELKOW, E., STICHT, H. & FUNKE, S. A. 2022. A novel D-amino acid peptide with therapeutic potential (ISAD1) inhibits aggregation of neurotoxic disease-relevant mutant Tau and prevents Tau toxicity in vitro. *Alzheimers Res Ther,* 14**,** 15.

AIT-BOUZIAD, N., CHIKI, A., LIMORENKO, G., XIAO, S., ELIEZER, D. & LASHUEL, H. A. 2020. Phosphorylation of the overlooked tyrosine 310 regulates the structure, aggregation, and microtubule- and lipid-binding properties of Tau. *J Biol Chem,* 295**,** 7905-7922.

AJIT, D., TRZECIAKIEWICZ, H., TSENG, J. H., WANDER, C. M., CHEN, Y., AJIT, A., KING, D. P. & COHEN, T. J. 2019. A unique tau conformation generated by an acetylation-mimic substitution modulates P301S-dependent tau pathology and hyperphosphorylation. *J Biol Chem,* 294**,** 16698-16711.

AKALAL, D. B., WILSON, C. F., ZONG, L., TANAKA, N. K., ITO, K. & DAVIS, R. L. 2006. Roles for Drosophila mushroom body neurons in olfactory learning and memory. *Learn Mem,* 13**,** 659-68.

AL-BASSAM, J., OZER, R. S., SAFER, D., HALPAIN, S. & MILLIGAN, R. A. 2002. MAP2 and tau bind longitudinally along the outer ridges of microtubule protofilaments. *J Cell Biol,* 157**,** 1187-96.

ALONSO, A., ZAIDI, T., NOVAK, M., GRUNDKE-IQBAL, I. & IQBAL, K. 2001. Hyperphosphorylation induces self-assembly of tau into tangles of paired helical filaments/straight filaments. *Proc Natl Acad Sci U S A,* 98**,** 6923-8.

ALONSO, A. C., GRUNDKE-IQBAL, I. & IQBAL, K. 1996. Alzheimer's disease hyperphosphorylated tau sequesters normal tau into tangles of filaments and disassembles microtubules. *Nat Med,* 2**,** 783-7.

ALONSO, A. C., ZAIDI, T., GRUNDKE-IQBAL, I. & IQBAL, K. 1994. Role of abnormally phosphorylated tau in the breakdown of microtubules in Alzheimer disease. *Proc Natl Acad Sci U S A,* 91**,** 5562-6.

ALONSO, A. D., COHEN, L. S., CORBO, C., MOROZOVA, V., ELIDRISSI, A., PHILLIPS, G. & KLEIMAN, F. E. 2018. Hyperphosphorylation of Tau Associates With Changes in Its Function Beyond Microtubule Stability. *Front Cell Neurosci,* 12**,** 338.

ALONSO, A. D., DI CLERICO, J., LI, B., CORBO, C. P., ALANIZ, M. E., GRUNDKE-IQBAL, I. & IQBAL, K. 2010. Phosphorylation of tau at Thr212, Thr231, and Ser262 combined causes neurodegeneration. *J Biol Chem,* 285**,** 30851-60.

ALONSO, A. D., GRUNDKE-IQBAL, I., BARRA, H. S. & IQBAL, K. 1997. Abnormal phosphorylation of tau and the mechanism of Alzheimer neurofibrillary degeneration: sequestration of microtubule-associated proteins 1 and 2 and the disassembly of microtubules by the abnormal tau. *Proc Natl Acad Sci U S A,* 94**,** 298-303.

ALONSO ADEL, C., MEDERLYOVA, A., NOVAK, M., GRUNDKE-IQBAL, I. & IQBAL, K. 2004. Promotion of hyperphosphorylation by frontotemporal dementia tau mutations. *J Biol Chem,* 279**,** 34873-81.

AMARAL, A. C., PEREZ-NIEVAS, B. G., SIAO TICK CHONG, M., GONZALEZ-MARTINEZ, A., ARGENTE-ESCRIG, H., RUBIO-GUERRA, S., COMMINS, C., MUFTU, S., EFTEKHARZADEH, B., HUDRY, E., FAN, Z., RAMANAN, P., TAKEDA, S., FROSCH, M. P., WEGMANN, S. & GOMEZ-ISLA, T. 2021. Isoform-selective decrease of glycogen synthase kinase-3-beta (GSK-3β) reduces synaptic tau phosphorylation, transcellular spreading, and aggregation. *iScience,* 24**,** 102058.

ANDORFER, C., ACKER, C. M., KRESS, Y., HOF, P. R., DUFF, K. & DAVIES, P. 2005. Cell-cycle reentry and cell death in transgenic mice expressing nonmutant human tau isoforms. *J Neurosci,* 25**,** 5446-54.

ARAKHAMIA, T., LEE, C. E., CARLOMAGNO, Y., DUONG, D. M., KUNDINGER, S. R., WANG, K., WILLIAMS, D., DETURE, M., DICKSON, D. W., COOK, C. N., SEYFRIED, N. T., PETRUCELLI, L. & FITZPATRICK, A. W. P. 2020. Posttranslational Modifications Mediate the Structural Diversity of Tauopathy Strains. *Cell,* 180**,** 633-644.e12.

ARRASATE, M., PéREZ, M., ARMAS-PORTELA, R. & AVILA, J. 1999. Polymerization of tau peptides into fibrillar structures. The effect of FTDP-17 mutations. *FEBS Lett,* 446**,** 199-202.

AUGUSTINACK, J. C., SCHNEIDER, A., MANDELKOW, E. M. & HYMAN, B. T. 2002. Specific tau phosphorylation sites correlate with severity of neuronal cytopathology in Alzheimer's disease. *Acta Neuropathol,* 103**,** 26-35.

BARBIER, P., ZEJNELI, O., MARTINHO, M., LASORSA, A., BELLE, V., SMET-NOCCA, C., TSVETKOV, P. O., DEVRED, F. & LANDRIEU, I. 2019. Role of Tau as a Microtubule-Associated Protein: Structural and Functional Aspects. *Front Aging Neurosci,* 11**,** 204.

BARDAI, F. H., ORDONEZ, D. G., BAILEY, R. M., HAMM, M., LEWIS, J. & FEANY, M. B. 2018. Lrrk promotes tau neurotoxicity through dysregulation of actin and mitochondrial dynamics. *PLoS Biol,* 16**,** e2006265.

BARGHORN, S., ZHENG-FISCHHöFER, Q., ACKMANN, M., BIERNAT, J., VON BERGEN, M., MANDELKOW, E. M. & MANDELKOW, E. 2000. Structure, microtubule interactions, and paired helical filament aggregation by tau mutants of frontotemporal dementias. *Biochemistry,* 39**,** 11714-21.

BARISH, S. & VOLKAN, P. C. 2015. Mechanisms of olfactory receptor neuron specification in Drosophila. *Wiley Interdiscip Rev Dev Biol,* 4**,** 609-21.

BARTHéLEMY, N. R., MALLIPEDDI, N., MOISEYEV, P., SATO, C. & BATEMAN, R. J. 2019. Tau Phosphorylation Rates Measured by Mass Spectrometry Differ in the Intracellular Brain vs. Extracellular Cerebrospinal Fluid Compartments and Are Differentially Affected by Alzheimer's Disease. *Front Aging Neurosci,* 11**,** 121.

BASHEER, N., BUEE, L., BRION, J. P., SMOLEK, T., MUHAMMADI, M. K., HRITZ, J., HROMADKA, T., DEWACHTER, I., WEGMANN, S., LANDRIEU, I., NOVAK, P., MUDHER, A. & ZILKA, N. 2024. Shaping the future of preclinical development of successful disease-modifying drugs against Alzheimer's disease: a systematic review of tau propagation models. *Acta Neuropathol Commun,* 12**,** 52.

BASURTO-ISLAS, G., GU, J. H., TUNG, Y. C., LIU, F. & IQBAL, K. 2018. Mechanism of Tau Hyperphosphorylation Involving Lysosomal Enzyme Asparagine Endopeptidase in a Mouse Model of Brain Ischemia. *J Alzheimers Dis,* 63**,** 821-833.

BAUGHMAN, H. E. R., CLOUSER, A. F., KLEVIT, R. E. & NATH, A. 2018. HspB1 and Hsc70 chaperones engage distinct tau species and have different inhibitory effects on amyloid formation. *J Biol Chem,* 293**,** 2687-2700.

BEAUDET, D., BERGER, C. L. & HENDRICKS, A. G. 2024. The types and numbers of kinesins and dyneins transporting endocytic cargoes modulate their motility and response to tau. *J Biol Chem,* 300**,** 107323.

BECKMAN, D., CHAKRABARTY, P., OTT, S., DAO, A., ZHOU, E., JANSSEN, W. G., DONIS-COX, K., MULLER, S., KORDOWER, J. H. & MORRISON, J. H. 2021. A novel tau-based rhesus monkey model of Alzheimer's pathogenesis. *Alzheimers Dement,* 17**,** 933-945.

BEHARRY, C., ALANIZ, M. E. & ALONSO ADEL, C. 2013. Expression of Alzheimer-like pathological human tau induces a behavioral motor and olfactory learning deficit in Drosophila melanogaster. *J Alzheimers Dis,* 37**,** 539-50.

BEJANIN, A., SCHONHAUT, D. R., LA JOIE, R., KRAMER, J. H., BAKER, S. L., SOSA, N., AYAKTA, N., CANTWELL, A., JANABI, M., LAURIOLA, M., O'NEIL, J. P., GORNO-TEMPINI, M. L., MILLER, Z. A., ROSEN, H. J., MILLER, B. L., JAGUST, W. J. & RABINOVICI, G. D. 2017. Tau pathology and neurodegeneration contribute to cognitive impairment in Alzheimer's disease. *Brain,* 140**,** 3286-3300.

BELLEN, H. J., TONG, C. & TSUDA, H. 2010. 100 years of Drosophila research and its impact on vertebrate neuroscience: a history lesson for the future. *Nat Rev Neurosci,* 11**,** 514-22.

BEUREL, E., GRIECO, S. F. & JOPE, R. S. 2015. Glycogen synthase kinase-3 (GSK3): regulation, actions, and diseases. *Pharmacol Ther,* 148**,** 114-31.

BIERNAT, J., GUSTKE, N., DREWES, G., MANDELKOW, E. M. & MANDELKOW, E. 1993. Phosphorylation of Ser262 strongly reduces binding of tau to microtubules: distinction between PHF-like immunoreactivity and microtubule binding. *Neuron,* 11**,** 153-63.

BINDER, L. I., FRANKFURTER, A. & REBHUN, L. I. 1985. The distribution of tau in the mammalian central nervous system. *J Cell Biol,* 101**,** 1371-8.

BLARD, O., FRéBOURG, T., CAMPION, D. & LECOURTOIS, M. 2006. Inhibition of proteasome and Shaggy/Glycogen synthase kinase-3beta kinase prevents clearance of phosphorylated tau in Drosophila. *J Neurosci Res,* 84**,** 1107-15.

BODEA, L. G., ECKERT, A., ITTNER, L. M., PIGUET, O. & GöTZ, J. 2016. Tau physiology and pathomechanisms in frontotemporal lobar degeneration. *J Neurochem,* 138 Suppl 1**,** 71-94.

BOTO, T. & TOMCHIK, S. M. 2024. Imaging Olfactory Learning-Induced Plasticity in Vivo in the Drosophila Brain. *Cold Spring Harb Protoc,* 2024**,** pdb.prot108135.

BOULEAU, S. & TRICOIRE, H. 2015. Drosophila models of Alzheimer's disease: advances, limits, and perspectives. *J Alzheimers Dis,* 45**,** 1015-38.

BOXER, A. L., LANG, A. E., GROSSMAN, M., KNOPMAN, D. S., MILLER, B. L., SCHNEIDER, L. S., DOODY, R. S., LEES, A., GOLBE, L. I., WILLIAMS, D. R., CORVOL, J. C., LUDOLPH, A., BURN, D., LORENZL, S., LITVAN, I., ROBERSON, E. D., HöGLINGER,

G. U., KOESTLER, M., JACK, C. R., JR., VAN DEERLIN, V., RANDOLPH, C., LOBACH, I. V., HEUER, H. W., GOZES, I., PARKER, L., WHITAKER, S., HIRMAN, J., STEWART, A. J., GOLD, M. & MORIMOTO, B. H. 2014. Davunetide in patients with progressive supranuclear palsy: a randomised, double-blind, placebo-controlled phase 2/3 trial. *Lancet Neurol,* 13**,** 676-85.

BRAAK, H. & BRAAK, E. 1991. Neuropathological stageing of Alzheimer-related changes. *Acta Neuropathol,* 82**,** 239-59.

BRAAK, H. & DEL TREDICI, K. 2015. The preclinical phase of the pathological process underlying sporadic Alzheimer's disease. *Brain,* 138**,** 2814-33.

BRAND, A. H. & PERRIMON, N. 1993. Targeted gene expression as a means of altering cell fates and generating dominant phenotypes. *Development,* 118**,** 401-15.

BRANDT, R., LéGER, J. & LEE, G. 1995. Interaction of tau with the neural plasma membrane mediated by tau's amino-terminal projection domain. *J Cell Biol,* 131**,** 1327-40.

BRELSTAFF, J., OSSOLA, B., NEHER, J. J., KLINGSTEDT, T., NILSSON, K. P., GOEDERT, M., SPILLANTINI, M. G. & TOLKOVSKY, A. M. 2015. The fluorescent pentameric oligothiophene pFTAA identifies filamentous tau in live neurons cultured from adult P301S tau mice. *Front Neurosci,* 9**,** 184.

BRINER, A., GöTZ, J. & POLANCO, J. C. 2020. Fyn Kinase Controls Tau Aggregation In Vivo. *Cell Rep,* 32**,** 108045.

BROTZAKIS, Z. F., LINDSTEDT, P. R., TAYLOR, R. J., RINAURO, D. J., GALLAGHER, N. C. T., BERNARDES, G. J. L. & VENDRUSCOLO, M. 2021. A Structural Ensemble of a Tau-Microtubule Complex Reveals Regulatory Tau Phosphorylation and Acetylation Mechanisms. *ACS Cent Sci,* 7**,** 1986-1995.

BROUHARD, G. J. & RICE, L. M. 2018. Microtubule dynamics: an interplay of biochemistry and mechanics. *Nature Reviews Molecular Cell Biology,* 19**,** 451-463.

BUGIANI, O., MURRELL, J. R., GIACCONE, G., HASEGAWA, M., GHIGO, G., TABATON, M., MORBIN, M., PRIMAVERA, A., CARELLA, F., SOLARO, C., GRISOLI, M., SAVOIARDO, M., SPILLANTINI, M. G., TAGLIAVINI, F., GOEDERT, M. & GHETTI, B. 1999. Frontotemporal dementia and corticobasal degeneration in a family with a P301S mutation in tau. *J Neuropathol Exp Neurol,* 58**,** 667-77.

BURNOUF, S., GRöNKE, S., AUGUSTIN, H., DOLS, J., GORSKY, M. K., WERNER, J., KERR, F., ALIC, N., MARTINEZ, P. & PARTRIDGE, L. 2016. Deletion of endogenous Tau proteins is not detrimental in Drosophila. *Sci Rep,* 6**,** 23102.

CARMEL, G., MAGER, E. M., BINDER, L. I. & KURET, J. 1996. The Structural Basis of Monoclonal Antibody Alz50's Selectivity for Alzheimer's Disease Pathology*. *Journal of Biological Chemistry,* 271**,** 32789-32795.

CASH, A. D., ALIEV, G., SIEDLAK, S. L., NUNOMURA, A., FUJIOKA, H., ZHU, X., RAINA, A. K., VINTERS, H. V., TABATON, M., JOHNSON, A. B., PAULA-BARBOSA, M., AVíLA, J., JONES, P. K., CASTELLANI, R. J., SMITH, M. A. & PERRY, G. 2003. Microtubule reduction in Alzheimer's disease and aging is independent of tau filament formation. *Am J Pathol,* 162**,** 1623-7.

CASTILLO-CARRANZA, D. L., GERSON, J. E., SENGUPTA, U., GUERRERO-MUñOZ, M. J., LASAGNA-REEVES, C. A. & KAYED, R. 2014. Specific targeting of tau oligomers in Htau mice prevents cognitive impairment and tau toxicity following injection with brain-derived tau oligomeric seeds. *J Alzheimers Dis,* 40 Suppl 1**,** S97-s111.

CHANG, E., KIM, S., SCHAFER, K. N. & KURET, J. 2011. Pseudophosphorylation of tau protein directly modulates its aggregation kinetics. *Biochim Biophys Acta,* 1814**,** 388-95.

CHANG, E., KIM, S., YIN, H., NAGARAJA, H. N. & KURET, J. 2008. Pathogenic missense MAPT mutations differentially modulate tau aggregation propensity at nucleation and extension steps. *J Neurochem,* 107**,** 1113-23.

CHATTERJEE, S., SANG, T. K., LAWLESS, G. M. & JACKSON, G. R. 2009. Dissociation of tau toxicity and phosphorylation: role of GSK-3beta, MARK and Cdk5 in a Drosophila model. *Hum Mol Genet,* 18**,** 164-77.

CHATTERJEE, S., SEALEY, M., RUIZ, E., PEGASIOU, C. M., BROOKES, K., GREEN, S., CRISFORD, A., DUQUE-VASQUEZ, M., LUCKETT, E., ROBERTSON, R., RICHARDSON, P., VAJRAMANI, G., GRUNDY, P., BULTERS, D., PROUD, C., VARGAS-CABALLERO, M. & MUDHER, A. 2023. Age-related changes in tau and autophagy in human brain in the absence of neurodegeneration. *PLoS One,* 18**,** e0262792.

CHAU, K. W., CHAN, W. Y., SHAW, P. C. & CHAN, H. Y. 2006. Biochemical investigation of Tau protein phosphorylation status and its solubility properties in Drosophila. *Biochem Biophys Res Commun,* 346**,** 150-9.

CHAU, M. F., RADEKE, M. J., DE INéS, C., BARASOAIN, I., KOHLSTAEDT, L. A. & FEINSTEIN, S. C. 1998. The microtubule-associated protein tau cross-links to two distinct sites on each alpha and beta tubulin monomer via separate domains. *Biochemistry,* 37**,** 17692-703.

CHEE, F. C., MUDHER, A., CUTTLE, M. F., NEWMAN, T. A., MACKAY, D., LOVESTONE, S. & SHEPHERD, D. 2005. Over-expression of tau results in defective synaptic transmission in Drosophila neuromuscular junctions. *Neurobiol Dis,* 20**,** 918-28.

CHEN, J., KANAI, Y., COWAN, N. J. & HIROKAWA, N. 1992. Projection domains of MAP2 and tau determine spacings between microtubules in dendrites and axons. *Nature,* 360**,** 674-7.

CHEN, X. Q. & MOBLEY, W. C. 2019. Alzheimer Disease Pathogenesis: Insights From Molecular and Cellular Biology Studies of Oligomeric Aβ and Tau Species. *Front Neurosci,* 13**,** 659.

CHERRY, J. D., ESNAULT, C. D., BAUCOM, Z. H., TRIPODIS, Y., HUBER, B. R., ALVAREZ, V. E., STEIN, T. D., DICKSON, D. W. & MCKEE, A. C. 2021. Tau isoforms are differentially expressed across the hippocampus in chronic traumatic encephalopathy and Alzheimer's disease. *Acta Neuropathol Commun,* 9**,** 86.

CHHATWAL, J. P., SCHULTZ, A. P., JOHNSON, K. A., HEDDEN, T., JAIMES, S., BENZINGER, T. L. S., JACK, C., JR., ANCES, B. M., RINGMAN, J. M., MARCUS, D. S., GHETTI, B., FARLOW, M. R., DANEK, A., LEVIN, J., YAKUSHEV, I., LASKE, C., KOEPPE, R. A., GALASKO, D. R., XIONG, C., MASTERS, C. L., SCHOFIELD, P. R., KINNUNEN, K. M., SALLOWAY, S., MARTINS, R. N., MCDADE, E., CAIRNS, N. J., BUCKLES, V. D., MORRIS, J. C., BATEMAN, R. & SPERLING, R. A. 2018. Preferential degradation of cognitive networks differentiates Alzheimer's disease from ageing. *Brain,* 141**,** 1486-1500.

CHI, H., SUN, L., SHIU, R.-H., HAN, R., HSIEH, C.-P., WEI, T.-M., LO, C.-C., CHANG, H.-Y. & SANG, T.-K. 2020. Cleavage of human tau at Asp421 inhibits hyperphosphorylated tau induced pathology in a Drosophila model. *Scientific Reports,* 10**,** 13482.

CHUDOBOVá, J. & ZEMPEL, H. 2023. Microtubule affinity regulating kinase (MARK/Par1) isoforms differentially regulate Alzheimer-like TAU missorting and Aβ-mediated synapse pathology. *Neural Regen Res,* 18**,** 335-336.

CHUNG, D. C., DENG, X., YALAMANCHILI, H. K., REVELLI, J. P., HAN, A. L., TADROS, B., RICHMAN, R., DIAS, M., NAINI, F. A., BOEYNAEMS, S., HYMAN, B. T. & ZOGHBI, H. Y. 2024. The big tau splice isoform resists Alzheimer's-related pathological changes. *bioRxiv*.

CHUNG, D. C., ROEMER, S., PETRUCELLI, L. & DICKSON, D. W. 2021. Cellular and pathological heterogeneity of primary tauopathies. *Mol Neurodegener,* 16**,** 57.

COHEN, T. J., GUO, J. L., HURTADO, D. E., KWONG, L. K., MILLS, I. P., TROJANOWSKI, J. Q. & LEE, V. M. 2011. The acetylation of tau inhibits its function and promotes pathological tau aggregation. *Nat Commun,* 2**,** 252.

COLODNER, K. J. & FEANY, M. B. 2010. Glial fibrillary tangles and JAK/STAT-mediated glial and neuronal cell death in a Drosophila model of glial tauopathy. *J Neurosci,* 30**,** 16102-13.

COMBS, B., TIERNAN, C. T., HAMEL, C. & KANAAN, N. M. 2017. Production of recombinant tau oligomers in vitro. *Methods Cell Biol,* 141**,** 45-64.

CONGDON, E. E., JI, C., TETLOW, A. M., JIANG, Y. & SIGURDSSON, E. M. 2023. Tau-targeting therapies for Alzheimer disease: current status and future directions. *Nat Rev Neurol,* 19**,** 715-736.

CONGDON, E. E. & SIGURDSSON, E. M. 2018. Tau-targeting therapies for Alzheimer disease. *Nat Rev Neurol,* 14**,** 399-415.

COOK, R. K., DEAL, M. E., DEAL, J. A., GARTON, R. D., BROWN, C. A., WARD, M. E., ANDRADE, R. S., SPANA, E. P., KAUFMAN, T. C. & COOK, K. R. 2010. A new resource for characterizing X-linked genes in Drosophila melanogaster: systematic coverage and subdivision of the X chromosome with nested, Y-linked duplications. *Genetics,* 186**,** 1095-109.

COOPER, A., RICHARDSON, B., RUIZ ORTEGA, E., ZHANG, Y., BATCHELOR, B., VAIKAKKARA CHITHRAN, A., LIU, J., LIAN, T., RAMíREZ MORENO, M., BOEHME, B., ABTAHI, L., DEVITT, G., SIVANANTHARAJAH, L., SKOULAKIS, E. M. C., ALLAN, D. W. & MUDHER, A. 2024. Aggregation promoting sequences rather than phosphorylation are essential for Tau-mediated toxicity in Drosophila. *bioRxiv***,** 2024.12.22.629946.

COWAN, C. M., BOSSING, T., PAGE, A., SHEPHERD, D. & MUDHER, A. 2010. Soluble hyper-phosphorylated tau causes microtubule breakdown and functionally compromises normal tau in vivo. *Acta Neuropathol,* 120**,** 593-604.

COWAN, C. M. & MUDHER, A. 2013. Are tau aggregates toxic or protective in tauopathies? *Front Neurol,* 4**,** 114.

COWAN, C. M., QURAISHE, S., HANDS, S., SEALEY, M., MAHAJAN, S., ALLAN, D. W. & MUDHER, A. 2015. Rescue from tau-induced neuronal dysfunction produces insoluble tau oligomers. *Scientific Reports,* 5**,** 17191.

CRIPPS, D., THOMAS, S. N., JENG, Y., YANG, F., DAVIES, P. & YANG, A. J. 2006. Alzheimer disease-specific conformation of hyperphosphorylated paired helical filament-Tau is polyubiquitinated through Lys-48, Lys-11, and Lys-6 ubiquitin conjugation. *J Biol Chem,* 281**,** 10825-38.

CROWTHER, D. C., PAGE, R., CHANDRARATNA, D. & LOMAS, D. A. 2006. A Drosophila model of Alzheimer's disease. *Methods Enzymol,* 412**,** 234-55.

CROWTHER, R. A. & GOEDERT, M. 2000. Abnormal tau-containing filaments in neurodegenerative diseases. *J Struct Biol,* 130**,** 271-9.

D'ALTON, S. & LEWIS, J. 2014. Therapeutic and diagnostic challenges for frontotemporal dementia. *Front Aging Neurosci,* 6**,** 204.

DAEBEL, V., CHINNATHAMBI, S., BIERNAT, J., SCHWALBE, M., HABENSTEIN, B., LOQUET, A., AKOURY, E., TEPPER, K., MüLLER, H., BALDUS, M., GRIESINGER, C., ZWECKSTETTER, M., MANDELKOW, E., VIJAYAN, V. & LANGE, A. 2012. β-Sheet core of tau paired helical filaments revealed by solid-state NMR. *J Am Chem Soc,* 134**,** 13982-9.

DAMMERS, C., YOLCU, D., KUKUK, L., WILLBOLD, D., PICKHARDT, M., MANDELKOW, E., HORN, A. H., STICHT, H., MALHIS, M. N., WILL, N., SCHUSTER, J. & FUNKE, S. A. 2016. Selection and Characterization of Tau Binding ᴅ-Enantiomeric Peptides with Potential for Therapy of Alzheimer Disease. *PLoS One,* 11**,** e0167432.

DAVID, D. C., LAYFIELD, R., SERPELL, L., NARAIN, Y., GOEDERT, M. & SPILLANTINI, M. G. 2002. Proteasomal degradation of tau protein. *J Neurochem,* 83**,** 176-85.

DE ANCOS, J. G. & AVILA, J. 1993. Differential distribution in white and grey matter of tau phosphoisoforms containing four tubulin-binding motifs. *Biochem J,* 296 ( Pt 2)**,** 351-4.

DE BRUYNE, M., CLYNE, P. J. & CARLSON, J. R. 1999. Odor coding in a model olfactory organ: the Drosophila maxillary palp. *J Neurosci,* 19**,** 4520-32.

DE CALIGNON, A., POLYDORO, M., SUáREZ-CALVET, M., WILLIAM, C., ADAMOWICZ, D. H., KOPEIKINA, K. J., PITSTICK, R., SAHARA, N., ASHE, K. H., CARLSON, G. A., SPIRES-JONES, T. L. & HYMAN, B. T. 2012. Propagation of tau pathology in a model of early Alzheimer's disease. *Neuron,* 73**,** 685-97.

DEANHARDT, B., DUAN, Q., DU, C., SOEDER, C., MORLOTE, A., GARG, D., SAHA, A., JONES, C. D. & VOLKAN, P. C. 2023. Social experience and pheromone receptor activity reprogram gene expression in sensory neurons. *G3 (Bethesda),* 13.

DECKER, Y., NéMETH, E., SCHOMBURG, R., CHEMLA, A., FüLöP, L., MENGER, M. D., LIU, Y. & FASSBENDER, K. 2021. Decreased pH in the aging brain and Alzheimer's disease. *Neurobiol Aging,* 101**,** 40-49.

DEL MAR FARINAS LUCAS, I., AL-HILALY, Y. K., LUTTER, L., XUE, W.-F. & SERPELL, L. C. 2025. The architecture of amyloid fibrils formed by a human tau-derived hexapeptide VQIVYK. *bioRxiv***,** 2025.03.11.642642.

DELOBEL, P., FLAMENT, S., HAMDANE, M., JAKES, R., ROUSSEAU, A., DELACOURTE, A., VILAIN, J. P., GOEDERT, M. & BUéE, L. 2002. Functional characterization of FTDP-17 tau gene mutations through their effects on Xenopus oocyte maturation. *J Biol Chem,* 277**,** 9199-205.

DESPRES, C., BYRNE, C., QI, H., CANTRELLE, F. X., HUVENT, I., CHAMBRAUD, B., BAULIEU, E. E., JACQUOT, Y., LANDRIEU, I., LIPPENS, G. & SMET-NOCCA, C. 2017. Identification of the Tau phosphorylation pattern that drives its aggregation. *Proc Natl Acad Sci U S A,* 114**,** 9080-9085.

DEVOS, S. L., MILLER, R. L., SCHOCH, K. M., HOLMES, B. B., KEBODEAUX, C. S., WEGENER, A. J., CHEN, G., SHEN, T., TRAN, H., NICHOLS, B., ZANARDI, T. A., KORDASIEWICZ, H. B., SWAYZE, E. E., BENNETT, C. F., DIAMOND, M. I. & MILLER, T. M. 2017. Tau reduction prevents neuronal loss and reverses pathological tau deposition and seeding in mice with tauopathy. *Sci Transl Med,* 9.

DIAS-SANTAGATA, D., FULGA, T. A., DUTTAROY, A. & FEANY, M. B. 2007. Oxidative stress mediates tau-induced neurodegeneration in Drosophila. *J Clin Invest,* 117**,** 236-45.

DIEZ, L., KAPINOS, L. E., LIM, R. Y. H. & WEGMANN, S. 2023. Analysis of Tau/Nucleoporin Interactions by Surface Plasmon Resonance Spectroscopy. *Methods Mol Biol,* 2551**,** 95-109.

DOMINGUEZ-MEIJIDE, A., VASILI, E. & OUTEIRO, T. F. 2020. Pharmacological Modulators of Tau Aggregation and Spreading. *Brain Sci,* 10.

DRECHSEL, D. N., HYMAN, A. A., COBB, M. H. & KIRSCHNER, M. W. 1992. Modulation of the dynamic instability of tubulin assembly by the microtubule-associated protein tau. *Mol Biol Cell,* 3**,** 1141-54.

DRECHSLER, H., XU, Y., GEYER, V. F., ZHANG, Y. & DIEZ, S. 2019. Multivalent electrostatic microtubule interactions of synthetic peptides are sufficient to mimic advanced MAP-like behavior. *Mol Biol Cell,* 30**,** 2953-2968.

DREGNI, A. J., MANDALA, V. S., WU, H., ELKINS, M. R., WANG, H. K., HUNG, I., DEGRADO, W. F. & HONG, M. 2019. In vitro 0N4R tau fibrils contain a monomorphic β-sheet core enclosed by dynamically heterogeneous fuzzy coat segments. *Proc Natl Acad Sci U S A,* 116**,** 16357-16366.

DREWES, G., TRINCZEK, B., ILLENBERGER, S., BIERNAT, J., SCHMITT-ULMS, G., MEYER, H. E., MANDELKOW, E. M. & MANDELKOW, E. 1995. Microtubule-associated protein/microtubule affinity-regulating kinase (p110mark). A novel protein kinase that regulates tau-microtubule interactions and dynamic instability by phosphorylation at the Alzheimer-specific site serine 262. *J Biol Chem,* 270**,** 7679-88.

DWECK, H. K., EBRAHIM, S. A., FARHAN, A., HANSSON, B. S. & STENSMYR, M. C. 2015. Olfactory proxy detection of dietary antioxidants in Drosophila. *Curr Biol,* 25**,** 455-66.

ECKERMANN, K., MOCANU, M. M., KHLISTUNOVA, I., BIERNAT, J., NISSEN, A., HOFMANN, A., SCHöNIG, K., BUJARD, H., HAEMISCH, A., MANDELKOW, E., ZHOU, L., RUNE, G. & MANDELKOW, E. M. 2007. The beta-propensity of Tau determines aggregation and synaptic loss in inducible mouse models of tauopathy. *J Biol Chem,* 282**,** 31755-65.

ERCAN-HERBST, E., EHRIG, J., SCHöNDORF, D. C., BEHRENDT, A., KLAUS, B., GOMEZ RAMOS, B., PRAT ORIOL, N., WEBER, C. & EHRNHOEFER, D. E. 2019. A post-translational modification signature defines changes in soluble tau correlating with oligomerization in early stage Alzheimer's disease brain. *Acta Neuropathol Commun,* 7**,** 192.

ESTERAS, N. & ABRAMOV, A. Y. 2020. Mitochondrial Calcium Deregulation in the Mechanism of Beta-Amyloid and Tau Pathology. *Cells,* 9.

FATH, T., EIDENMüLLER, J. & BRANDT, R. 2002. Tau-mediated cytotoxicity in a pseudohyperphosphorylation model of Alzheimer's disease. *J Neurosci,* 22**,** 9733-41.

FENEBERG, E. & OTTO, M. 2020. [Gene-specific treatment approaches in Alzheimer's disease and other tauopathies]. *Nervenarzt,* 91**,** 312-317.

FEUILLETTE, S., MIGUEL, L., FRéBOURG, T., CAMPION, D. & LECOURTOIS, M. 2010. Drosophila models of human tauopathies indicate that Tau protein toxicity in vivo is mediated by soluble cytosolic phosphorylated forms of the protein. *J Neurochem,* 113**,** 895-903.

FISCHER, D., MUKRASCH, M. D., BIERNAT, J., BIBOW, S., BLACKLEDGE, M., GRIESINGER, C., MANDELKOW, E. & ZWECKSTETTER, M. 2009. Conformational changes specific for pseudophosphorylation at serine 262 selectively impair binding of tau to microtubules. *Biochemistry,* 48**,** 10047-55.

FISCHER, I. 2023. Big Tau: What We Know, and We Need to Know. *eNeuro,* 10.

FITZPATRICK, A. W. P., FALCON, B., HE, S., MURZIN, A. G., MURSHUDOV, G., GARRINGER, H. J., CROWTHER, R. A., GHETTI, B., GOEDERT, M. & SCHERES, S. H. W. 2017. Cryo-EM structures of tau filaments from Alzheimer's disease. *Nature,* 547**,** 185-190.

FLACH, K., HILBRICH, I., SCHIFFMANN, A., GäRTNER, U., KRüGER, M., LEONHARDT, M., WASCHIPKY, H., WICK, L., ARENDT, T. & HOLZER, M. 2012. Tau oligomers impair artificial membrane integrity and cellular viability. *J Biol Chem,* 287**,** 43223-33.

FORLENZA, O. V., RADANOVIC, M., TALIB, L. L. & GATTAZ, W. F. 2019. Clinical and biological effects of long-term lithium treatment in older adults with amnestic mild cognitive impairment: randomised clinical trial. *Br J Psychiatry,* 215**,** 668-674.

FORTINI, M. E. & BONINI, N. M. 2000. Modeling human neurodegenerative diseases in Drosophila: on a wing and a prayer. *Trends Genet,* 16**,** 161-7.

FRENKEL-PINTER, M., RICHMAN, M., BELOSTOZKY, A., ABU-MOKH, A., GAZIT, E., RAHIMIPOUR, S. & SEGAL, D. 2016. Selective Inhibition of Aggregation and Toxicity of a Tau-Derived Peptide using Its Glycosylated Analogues. *Chemistry,* 22**,** 5945-52.

FRENKEL-PINTER, M., TAL, S., SCHERZER-ATTALI, R., ABU-HUSSIEN, M., ALYAGOR, I., EISENBAUM, T., GAZIT, E. & SEGAL, D. 2017. Cl-NQTrp Alleviates Tauopathy Symptoms in a Model Organism through the Inhibition of Tau Aggregation-Engendered Toxicity. *Neurodegener Dis,* 17**,** 73-82.

FRIEDHOFF, P., SCHNEIDER, A., MANDELKOW, E. M. & MANDELKOW, E. 1998. Rapid assembly of Alzheimer-like paired helical filaments from microtubule-associated protein tau monitored by fluorescence in solution. *Biochemistry,* 37**,** 10223-30.

FULGA, T. A., ELSON-SCHWAB, I., KHURANA, V., STEINHILB, M. L., SPIRES, T. L., HYMAN, B. T. & FEANY, M. B. 2007. Abnormal bundling and accumulation of F-actin mediates tau-induced neuronal degeneration in vivo. *Nat Cell Biol,* 9**,** 139-48.

GANDINI, A., GONçALVES, A. E., STROCCHI, S., ALBERTINI, C., JANOčKOVá, J., TRAMARIN, A., GRIFONI, D., POETA, E., SOUKUP, O., MUñOZ-TORRERO, D., MONTI, B., SABATé, R., BARTOLINI, M., LEGNAME, G. & BOLOGNESI, M. L. 2022. Discovery of Dual Aβ/Tau Inhibitors and Evaluation of Their Therapeutic Effect on a Drosophila Model of Alzheimer's Disease. *ACS Chem Neurosci,* 13**,** 3314-3329.

GAUTHIER, S., FELDMAN, H. H., SCHNEIDER, L. S., WILCOCK, G. K., FRISONI, G. B., HARDLUND, J. H., MOEBIUS, H. J., BENTHAM, P., KOOK, K. A., WISCHIK, D. J., SCHELTER, B. O., DAVIS, C. S., STAFF, R. T., BRACOUD, L., SHAMSI, K., STOREY, J. M., HARRINGTON, C. R. & WISCHIK, C. M. 2016. Efficacy and safety of tau-aggregation inhibitor therapy in patients with mild or moderate Alzheimer's disease: a randomised, controlled, double-blind, parallel-arm, phase 3 trial. *Lancet,* 388**,** 2873-2884.

GAUTHIER-KEMPER, A., WEISSMANN, C., GOLOVYASHKINA, N., SEBö-LEMKE, Z., DREWES, G., GERKE, V., HEINISCH, J. J. & BRANDT, R. 2011. The frontotemporal dementia mutation R406W blocks tau's interaction with the membrane in an annexin A2-dependent manner. *J Cell Biol,* 192**,** 647-61.

GENG, J., XIA, L., LI, W. & DOU, F. 2015. The C-terminus of tau protein plays an important role in its stability and toxicity. *J Mol Neurosci,* 55**,** 251-259.

GERKE, V., CREUTZ, C. E. & MOSS, S. E. 2005. Annexins: linking Ca2+ signalling to membrane dynamics. *Nature Reviews Molecular Cell Biology,* 6**,** 449-461.

GERSON, J. E. & KAYED, R. 2013. Formation and propagation of tau oligomeric seeds. *Front Neurol,* 4**,** 93.

GHEYARA, A. L., PONNUSAMY, R., DJUKIC, B., CRAFT, R. J., HO, K., GUO, W., FINUCANE, M. M., SANCHEZ, P. E. & MUCKE, L. 2014. Tau reduction prevents disease in a mouse model of Dravet syndrome. *Ann Neurol,* 76**,** 443-56.

GHOSHAL, N., GARCíA-SIERRA, F., FU, Y., BECKETT, L. A., MUFSON, E. J., KURET, J., BERRY, R. W. & BINDER, L. I. 2001. Tau-66: evidence for a novel tau conformation in Alzheimer's disease. *J Neurochem,* 77**,** 1372-85.

GINSBERG, S. D., CRINO, P. B., LEE, V. M., EBERWINE, J. H. & TROJANOWSKI, J. Q. 1997. Sequestration of RNA in Alzheimer's disease neurofibrillary tangles and senile plaques. *Ann Neurol,* 41**,** 200-9.

GOEDERT, M., CROWTHER, R. A. & SPILLANTINI, M. G. 1998. Tau mutations cause frontotemporal dementias. *Neuron,* 21**,** 955-8.

GOEDERT, M., EISENBERG, D. S. & CROWTHER, R. A. 2017. Propagation of Tau Aggregates and Neurodegeneration. *Annu Rev Neurosci,* 40**,** 189-210.

GOEDERT, M., JAKES, R. & CROWTHER, R. A. 1999. Effects of frontotemporal dementia FTDP-17 mutations on heparin-induced assembly of tau filaments. *FEBS Lett,* 450**,** 306-11.

GOEDERT, M., JAKES, R., SPILLANTINI, M. G., HASEGAWA, M., SMITH, M. J. & CROWTHER, R. A. 1996. Assembly of microtubule-associated protein tau into Alzheimer-like filaments induced by sulphated glycosaminoglycans. *Nature,* 383**,** 550-3.

GOEDERT, M., SPILLANTINI, M. G., CAIRNS, N. J. & CROWTHER, R. A. 1992. Tau proteins of Alzheimer paired helical filaments: abnormal phosphorylation of all six brain isoforms. *Neuron,* 8**,** 159-68.

GOEDERT, M., SPILLANTINI, M. G., JAKES, R., RUTHERFORD, D. & CROWTHER, R. A. 1989. Multiple isoforms of human microtubule-associated protein tau: sequences and localization in neurofibrillary tangles of Alzheimer's disease. *Neuron,* 3**,** 519-26.

GOGUEL, V., BELAIR, A. L., AYAZ, D., LAMPIN-SAINT-AMAUX, A., SCAPLEHORN, N., HASSAN, B. A. & PREAT, T. 2011. Drosophila amyloid precursor protein-like is required for long-term memory. *J Neurosci,* 31**,** 1032-7.

GOHAR, M., YANG, W., STRONG, W., VOLKENING, K., LEYSTRA-LANTZ, C. & STRONG, M. J. 2009. Tau phosphorylation at threonine-175 leads to fibril formation and enhanced cell death: implications for amyotrophic lateral sclerosis with cognitive impairment. *J Neurochem,* 108**,** 634-43.

GOLD, M., LORENZL, S., STEWART, A. J., MORIMOTO, B. H., WILLIAMS, D. R. & GOZES, I. 2012. Critical appraisal of the role of davunetide in the treatment of progressive supranuclear palsy. *Neuropsychiatr Dis Treat,* 8**,** 85-93.

GóMEZ-ISLA, T., HOLLISTER, R., WEST, H., MUI, S., GROWDON, J. H., PETERSEN, R. C., PARISI, J. E. & HYMAN, B. T. 1997. Neuronal loss correlates with but exceeds neurofibrillary tangles in Alzheimer's disease. *Ann Neurol,* 41**,** 17-24.

GOODE, B. L. & FEINSTEIN, S. C. 1994. Identification of a novel microtubule binding and assembly domain in the developmentally regulated inter-repeat region of tau. *J Cell Biol,* 124**,** 769-82.

GöTZ, J. 2001. Tau and transgenic animal models. *Brain Res Brain Res Rev,* 35**,** 266-86.

GöTZ, J., CHEN, F., BARMETTLER, R. & NITSCH, R. M. 2001. Tau filament formation in transgenic mice expressing P301L tau. *J Biol Chem,* 276**,** 529-34.

GöTZ, J. & ITTNER, L. M. 2008. Animal models of Alzheimer's disease and frontotemporal dementia. *Nat Rev Neurosci,* 9**,** 532-44.

GUNAWARDANA, C. G., MEHRABIAN, M., WANG, X., MUELLER, I., LUBAMBO, I. B., JONKMAN, J. E., WANG, H. & SCHMITT-ULMS, G. 2015. The Human Tau Interactome: Binding to the Ribonucleoproteome, and Impaired Binding of the Proline-to-Leucine Mutant at Position 301 (P301L) to Chaperones and the Proteasome. *Mol Cell Proteomics,* 14**,** 3000-14.

GUO, J. L. & LEE, V. M. 2011. Seeding of normal Tau by pathological Tau conformers drives pathogenesis of Alzheimer-like tangles. *J Biol Chem,* 286**,** 15317-31.

GUO, T., NOBLE, W. & HANGER, D. P. 2017. Roles of tau protein in health and disease. *Acta Neuropathol,* 133**,** 665-704.

HAASE, C., STIELER, J. T., ARENDT, T. & HOLZER, M. 2004. Pseudophosphorylation of tau protein alters its ability for self-aggregation. *J Neurochem,* 88**,** 1509-20.

HAJ-YAHYA, M., GOPINATH, P., RAJASEKHAR, K., MIRBAHA, H., DIAMOND, M. I. & LASHUEL, H. A. 2020. Site-Specific Hyperphosphorylation Inhibits, Rather than Promotes, Tau Fibrillization, Seeding Capacity, and Its Microtubule Binding. *Angew Chem Int Ed Engl,* 59**,** 4059-4067.

HALL, A. M., THROESCH, B. T., BUCKINGHAM, S. C., MARKWARDT, S. J., PENG, Y., WANG, Q., HOFFMAN, D. A. & ROBERSON, E. D. 2015. Tau-dependent Kv4.2 depletion and dendritic hyperexcitability in a mouse model of Alzheimer's disease. *J Neurosci,* 35**,** 6221-30.

HALLINAN, G. I., VARGAS-CABALLERO, M., WEST, J. & DEINHARDT, K. 2019. Tau Misfolding Efficiently Propagates between Individual Intact Hippocampal Neurons. *J Neurosci,* 39**,** 9623-9632.

HANGER, D. P., ANDERTON, B. H. & NOBLE, W. 2009. Tau phosphorylation: the therapeutic challenge for neurodegenerative disease. *Trends Mol Med,* 15**,** 112-9.

HANGER, D. P., BYERS, H. L., WRAY, S., LEUNG, K. Y., SAXTON, M. J., SEEREERAM, A., REYNOLDS, C. H., WARD, M. A. & ANDERTON, B. H. 2007. Novel phosphorylation sites in tau from Alzheimer brain support a role for casein kinase 1 in disease pathogenesis. *J Biol Chem,* 282**,** 23645-54.

HAROUTUNIAN, V., DAVIES, P., VIANNA, C., BUXBAUM, J. D. & PUROHIT, D. P. 2007. Tau protein abnormalities associated with the progression of alzheimer disease type dementia. *Neurobiol Aging,* 28**,** 1-7.

HARRIS, G. A., HIRSCHFELD, L. R., GONZALEZ, M. I., PRITCHARD, M. C. & MAY, P. C. 2025. Revisiting the therapeutic landscape of tauopathies: assessing the current pipeline and clinical trials. *Alzheimer's Research & Therapy,* 17**,** 129.

HASEGAWA, M., SMITH, M. J. & GOEDERT, M. 1998. Tau proteins with FTDP-17 mutations have a reduced ability to promote microtubule assembly. *FEBS Lett,* 437**,** 207-10.

HATCH, R. J., WEI, Y., XIA, D. & GöTZ, J. 2017. Hyperphosphorylated tau causes reduced hippocampal CA1 excitability by relocating the axon initial segment. *Acta Neuropathol,* 133**,** 717-730.

HEIDARY, G. & FORTINI, M. E. 2001. Identification and characterization of the Drosophila tau homolog. *Mech Dev,* 108**,** 171-8.

HERNANDEZ, F., LUCAS, J. J. & AVILA, J. 2013. GSK3 and tau: two convergence points in Alzheimer's disease. *J Alzheimers Dis,* 33 Suppl 1**,** S141-4.

HERNáNDEZ-VEGA, A., BRAUN, M., SCHARREL, L., JAHNEL, M., WEGMANN, S., HYMAN, B. T., ALBERTI, S., DIEZ, S. & HYMAN, A. A. 2017. Local Nucleation of Microtubule Bundles through Tubulin Concentration into a Condensed Tau Phase. *Cell Rep,* 20**,** 2304-2312.

HIRATA, A., SUGIMOTO, K., KONNO, T. & MORII, T. 2007. Amyloid-forming propensity of the hydrophobic non-natural amino acid on the fibril-forming core peptide of human tau. *Bioorg Med Chem Lett,* 17**,** 2971-4.

HIROTA, Y., SAKAKIBARA, Y., IBARAKI, K., TAKEI, K., IIJIMA, K. M. & SEKIYA, M. 2022. Distinct brain pathologies associated with Alzheimer's disease biomarker-related phospho-tau 181 and phospho-tau 217 in App knock-in mouse models of amyloid-β amyloidosis. *Brain Commun,* 4**,** fcac286.

HIRSCHBICHLER, S. T., ERRO, R., BATLA, A. & BHATIA, K. P. 2015. Classic PD-like rest tremor associated with the tau p.R406W mutation. *Parkinsonism Relat Disord,* 21**,** 1002-4.

HOCHGRäFE, K., SYDOW, A., MATENIA, D., CADINU, D., KöNEN, S., PETROVA, O., PICKHARDT, M., GOLL, P., MORELLINI, F., MANDELKOW, E. & MANDELKOW, E. M. 2015. Preventive methylene blue treatment preserves cognition in mice expressing full-length pro-aggregant human Tau. *Acta Neuropathol Commun,* 3**,** 25.

HöGLINGER, G. U., RESPONDEK, G., STAMELOU, M., KURZ, C., JOSEPHS, K. A., LANG, A. E., MOLLENHAUER, B., MüLLER, U., NILSSON, C., WHITWELL, J. L., ARZBERGER, T., ENGLUND, E., GELPI, E., GIESE, A., IRWIN, D. J., MEISSNER, W. G., PANTELYAT, A., RAJPUT, A., VAN SWIETEN, J. C., TROAKES, C., ANTONINI, A., BHATIA, K. P., BORDELON, Y., COMPTA, Y., CORVOL, J. C., COLOSIMO, C., DICKSON, D. W., DODEL, R., FERGUSON, L., GROSSMAN, M., KASSUBEK, J., KRISMER, F., LEVIN, J., LORENZL, S., MORRIS, H. R., NESTOR, P., OERTEL, W. H., POEWE, W., RABINOVICI, G., ROWE, J. B., SCHELLENBERG, G. D., SEPPI, K., VAN EIMEREN, T., WENNING, G. K., BOXER, A. L., GOLBE, L. I. & LITVAN, I. 2017. Clinical diagnosis of progressive supranuclear palsy: The movement disorder society criteria. *Mov Disord,* 32**,** 853-864.

HOLTH, J. K., BOMBEN, V. C., REED, J. G., INOUE, T., YOUNKIN, L., YOUNKIN, S. G., PAUTLER, R. G., BOTAS, J. & NOEBELS, J. L. 2013. Tau loss attenuates neuronal network hyperexcitability in mouse and Drosophila genetic models of epilepsy. *J Neurosci,* 33**,** 1651-9.

HONG, M., ZHUKAREVA, V., VOGELSBERG-RAGAGLIA, V., WSZOLEK, Z., REED, L., MILLER, B. I., GESCHWIND, D. H., BIRD, T. D., MCKEEL, D., GOATE, A., MORRIS, J. C., WILHELMSEN, K. C., SCHELLENBERG, G. D., TROJANOWSKI, J. Q. & LEE, V. M. 1998. Mutation-specific functional impairments in distinct tau isoforms of hereditary FTDP-17. *Science,* 282**,** 1914-7.

HOOVER, B. R., REED, M. N., SU, J., PENROD, R. D., KOTILINEK, L. A., GRANT, M. K., PITSTICK, R., CARLSON, G. A., LANIER, L. M., YUAN, L. L., ASHE, K. H. & LIAO, D. 2010.

Tau mislocalization to dendritic spines mediates synaptic dysfunction independently of neurodegeneration. *Neuron,* 68**,** 1067-81.

HORIE, K., BARTHéLEMY, N. R., SPINA, S., VANDEVREDE, L., HE, Y., PATERSON, R. W., WRIGHT, B. A., DAY, G. S., DAVIS, A. A., KARCH, C. M., SEELEY, W. W., PERRIN, R. J., KOPPISETTI, R. K., SHAIKH, F., LAGO, A. L., HEUER, H. W., GHOSHAL, N., GABELLE, A., MILLER, B. L., BOXER, A. L., BATEMAN, R. J. & SATO, C. 2022. CSF tau microtubule-binding region identifies pathological changes in primary tauopathies. *Nature Medicine,* 28**,** 2547-2554.

HU, W., ZHANG, X., TUNG, Y. C., XIE, S., LIU, F. & IQBAL, K. 2016. Hyperphosphorylation determines both the spread and the morphology of tau pathology. *Alzheimers Dement,* 12**,** 1066-1077.

HUESTON, C. E., OLSEN, D., LI, Q., OKUWA, S., PENG, B., WU, J. & VOLKAN, P. C. 2016. Chromatin Modulatory Proteins and Olfactory Receptor Signaling in the Refinement and Maintenance of Fruitless Expression in Olfactory Receptor Neurons. *PLoS Biol,* 14**,** e1002443.

HUTTON, M., LENDON, C. L., RIZZU, P., BAKER, M., FROELICH, S., HOULDEN, H., PICKERING-BROWN, S., CHAKRAVERTY, S., ISAACS, A., GROVER, A., HACKETT, J., ADAMSON, J., LINCOLN, S., DICKSON, D., DAVIES, P., PETERSEN, R. C., STEVENS, M., DE GRAAFF, E., WAUTERS, E., VAN BAREN, J., HILLEBRAND, M., JOOSSE, M., KWON, J. M., NOWOTNY, P., CHE, L. K., NORTON, J., MORRIS, J. C., REED, L. A., TROJANOWSKI, J., BASUN, H., LANNFELT, L., NEYSTAT, M., FAHN, S., DARK, F., TANNENBERG, T., DODD, P. R., HAYWARD, N., KWOK, J. B., SCHOFIELD, P. R., ANDREADIS, A., SNOWDEN, J., CRAUFURD, D., NEARY, D., OWEN, F., OOSTRA, B. A., HARDY, J., GOATE, A., VAN SWIETEN, J., MANN, D., LYNCH, T. & HEUTINK, P. 1998. Association of missense and 5'-splice-site mutations in tau with the inherited dementia FTDP-17. *Nature,* 393**,** 702-5.

IKEUCHI, T., KANEKO, H., MIYASHITA, A., NOZAKI, H., KASUGA, K., TSUKIE, T., TSUCHIYA, M., IMAMURA, T., ISHIZU, H., AOKI, K., ISHIKAWA, A., ONODERA, O., KUWANO, R. & NISHIZAWA, M. 2008. Mutational analysis in early-onset familial dementia in the Japanese population. The role of PSEN1 and MAPT R406W mutations. *Dement Geriatr Cogn Disord,* 26**,** 43-9.

INOUE, M., HIRATA, A., TAINAKA, K., MORII, T. & KONNO, T. 2008. Charge-pairing mechanism of phosphorylation effect upon amyloid fibrillation of human tau core peptide. *Biochemistry,* 47**,** 11847-57.

IRIZARRY, M., DYCK, C., LI, D., DHADDA, S., HERSCH, S., REYDERMAN, L. & KRAMER, L. 2025. The Lecanemab Clarity AD Open-Label Extension in Early Alzheimer's Disease (P1-3.003). *Neurology,* 104**,** 4158.

IRWIN, D. J., LEE, V. M. & TROJANOWSKI, J. Q. 2013. Parkinson's disease dementia: convergence of α-synuclein, tau and amyloid-β pathologies. *Nat Rev Neurosci,* 14**,** 626-36.

IYER, J., WANG, Q., LE, T., PIZZO, L., GRöNKE, S., AMBEGAOKAR, S. S., IMAI, Y., SRIVASTAVA, A., TROISí, B. L., MARDON, G., ARTERO, R., JACKSON, G. R., ISAACS, A. M., PARTRIDGE, L., LU, B., KUMAR, J. P. & GIRIRAJAN, S. 2016. Quantitative Assessment of Eye Phenotypes for Functional Genetic Studies Using Drosophila melanogaster. *G3 (Bethesda),* 6**,** 1427-37.

JACKSON, G. R., WIEDAU-PAZOS, M., SANG, T. K., WAGLE, N., BROWN, C. A., MASSACHI, S. & GESCHWIND, D. H. 2002. Human wild-type tau interacts with wingless pathway components and produces neurofibrillary pathology in Drosophila. *Neuron,* 34**,** 509-19.

JAFARI, S., HENRIKSSON, J., YAN, H. & ALENIUS, M. 2021. Stress and odorant receptor feedback during a critical period after hatching regulates olfactory sensory neuron differentiation in Drosophila. *PLoS Biol,* 19**,** e3001101.

JANELIDZE, S., MATTSSON, N., PALMQVIST, S., SMITH, R., BEACH, T. G., SERRANO, G. E., CHAI, X., PROCTOR, N. K., EICHENLAUB, U., ZETTERBERG, H., BLENNOW, K., REIMAN, E. M., STOMRUD, E., DAGE, J. L. & HANSSON, O. 2020a. Plasma P-tau181 in Alzheimer's disease: relationship to other biomarkers, differential diagnosis, neuropathology and longitudinal progression to Alzheimer's dementia. *Nat Med,* 26**,** 379-386.

JANELIDZE, S., PALMQVIST, S., LEUZY, A., STOMRUD, E., VERBERK, I. M. W., ZETTERBERG, H., ASHTON, N. J., PESINI, P., SARASA, L., ALLUé, J. A., TEUNISSEN, C. E., DAGE, J. L., BLENNOW, K., MATTSSON-CARLGREN, N. & HANSSON, O. 2022. Detecting amyloid positivity in early Alzheimer's disease using combinations of plasma Aβ42/Aβ40 and p-tau. *Alzheimers Dement,* 18**,** 283-293.

JANELIDZE, S., STOMRUD, E., SMITH, R., PALMQVIST, S., MATTSSON, N., AIREY, D. C., PROCTOR, N. K., CHAI, X., SHCHERBININ, S., SIMS, J. R., TRIANA-BALTZER, G., THEUNIS, C., SLEMMON, R., MERCKEN, M., KOLB, H., DAGE, J. L. & HANSSON, O. 2020b. Cerebrospinal fluid p-tau217 performs better than p-tau181 as a biomarker of Alzheimer's disease. *Nat Commun,* 11**,** 1683.

JEFFERIS, G. S., VYAS, R. M., BERDNIK, D., RAMAEKERS, A., STOCKER, R. F., TANAKA, N. K., ITO, K. & LUO, L. 2004. Developmental origin of wiring specificity in the olfactory system of Drosophila. *Development,* 131**,** 117-30.

JEGANATHAN, S., HASCHER, A., CHINNATHAMBI, S., BIERNAT, J., MANDELKOW, E. M. & MANDELKOW, E. 2008. Proline-directed pseudo-phosphorylation at AT8 and PHF1 epitopes induces a compaction of the paperclip folding of Tau and generates a pathological (MC-1) conformation. *J Biol Chem,* 283**,** 32066-76.

JEGANATHAN, S., VON BERGEN, M., BRUTLACH, H., STEINHOFF, H. J. & MANDELKOW, E. 2006. Global hairpin folding of tau in solution. *Biochemistry,* 45**,** 2283-93.

JIANG, L., CHAKRABORTY, P., ZHANG, L., WONG, M., HILL, S. E., WEBBER, C. J., LIBERA, J., BLAIR, L. J., WOLOZIN, B. & ZWECKSTETTER, M. 2023. Chaperoning of specific tau structure by immunophilin FKBP12 regulates the neuronal resilience to extracellular stress. *Sci Adv,* 9**,** eadd9789.

JIANG, L., LIN, W., ZHANG, C., ASH, P. E. A., VERMA, M., KWAN, J., VAN VLIET, E., YANG, Z., CRUZ, A. L., BOUDEAU, S., MAZIUK, B. F., LEI, S., SONG, J., ALVAREZ, V. E., HOVDE, S., ABISAMBRA, J. F., KUO, M. H., KANAAN, N., MURRAY, M. E., CRARY, J. F., ZHAO, J., CHENG, J. X., PETRUCELLI, L., LI, H., EMILI, A. & WOLOZIN, B. 2021. Interaction of tau with HNRNPA2B1 and N(6)-methyladenosine RNA mediates the progression of tauopathy. *Mol Cell,* 81**,** 4209-4227.e12.

JICHA, G. A., BERENFELD, B. & DAVIES, P. 1999. Sequence requirements for formation of conformational variants of tau similar to those found in Alzheimer's disease. *J Neurosci Res,* 55**,** 713-23.

JICHA, G. A., LANE, E., VINCENT, I., OTVOS, L., JR., HOFFMANN, R. & DAVIES, P. 1997. A conformation- and phosphorylation-dependent antibody recognizing the paired helical filaments of Alzheimer's disease. *J Neurochem,* 69**,** 2087-95.

JIN, N., YIN, X., YU, D., CAO, M., GONG, C.-X., IQBAL, K., DING, F., GU, X. & LIU, F. 2015. Truncation and activation of GSK-3β by calpain I: a molecular mechanism links to tau hyperphosphorylation in Alzheimer's disease. *Scientific Reports,* 5**,** 8187.

JUNG, H. J., KIM, Y. J., EGGERT, S., CHUNG, K. C., CHOI, K. S. & PARK, S. A. 2013. Age-dependent increases in tau phosphorylation in the brains of type 2 diabetic rats correlate with a reduced expression of p62. *Exp Neurol,* 248**,** 441-50.

JURY-GARFE, N., REDDING-OCHOA, J., YOU, Y., MARTíNEZ, P., KARAHAN, H., CHIMAL-JUáREZ, E., JOHNSON, T. S., ZHANG, J., RESNICK, S., KIM, J., TRONCOSO, J. C. & LASAGNA-REEVES, C. A. 2024. Enhanced microglial dynamics and a paucity of tau seeding in the amyloid plaque microenvironment contribute to cognitive resilience in Alzheimer's disease. *Acta Neuropathol,* 148**,** 15.

KADAVATH, H., HOFELE, R. V., BIERNAT, J., KUMAR, S., TEPPER, K., URLAUB, H., MANDELKOW, E. & ZWECKSTETTER, M. 2015. Tau stabilizes microtubules by binding at the interface between tubulin heterodimers. *Proc Natl Acad Sci U S A,* 112**,** 7501-6.

KAMETANI, F., YOSHIDA, M., MATSUBARA, T., MURAYAMA, S., SAITO, Y., KAWAKAMI, I., ONAYA, M., TANAKA, H., KAKITA, A., ROBINSON, A. C., MANN, D. M. A. & HASEGAWA, M. 2020. Comparison of Common and Disease-Specific Post-translational Modifications of Pathological Tau Associated With a Wide Range of Tauopathies. *Front Neurosci,* 14**,** 581936.

KAMPERS, T., FRIEDHOFF, P., BIERNAT, J., MANDELKOW, E. M. & MANDELKOW, E. 1996. RNA stimulates aggregation of microtubule-associated protein tau into Alzheimer-like paired helical filaments. *FEBS Lett,* 399**,** 344-9.

KANAAN, N. M., HAMEL, C., GRABINSKI, T. & COMBS, B. 2020. Liquid-liquid phase separation induces pathogenic tau conformations in vitro. *Nat Commun,* 11**,** 2809.

KANDEL, E. R. S., J.H.; JESSELL, T.M.; SIEGELBAUM, S.A.; HUDSPETH, A.J.; AND MACK, S. 2021. *Principles of Neural Science,* New York, McGraw-Hill Medical.

KAR, S., FAN, J., SMITH, M. J., GOEDERT, M. & AMOS, L. A. 2003. Repeat motifs of tau bind to the insides of microtubules in the absence of taxol. *Embo j,* 22**,** 70-7.

KARAGAS, N., YOUNG, J. E., BLUE, E. E. & JAYADEV, S. 2025. The Spectrum of Genetic Risk in Alzheimer Disease. *Neurol Genet,* 11**,** e200224.

KATSINELOS, T., MCEWAN, W. A., JAHN, T. R. & NICKEL, W. 2021. Identification of cis-acting determinants mediating the unconventional secretion of tau. *Sci Rep,* 11**,** 12946.

KATSUNO, T., MORISHIMA-KAWASHIMA, M., SAITO, Y., YAMANOUCHI, H., ISHIURA, S., MURAYAMA, S. & IHARA, Y. 2005. Independent accumulations of tau and amyloid beta-protein in the human entorhinal cortex. *Neurology,* 64**,** 687-92.

KAVANAGH, T., HALDER, A. & DRUMMOND, E. 2022. Tau interactome and RNA binding proteins in neurodegenerative diseases. *Mol Neurodegener,* 17**,** 66.

KERAMIDIS, I., VOURKOU, E., PAPANIKOLOPOULOU, K. & SKOULAKIS, E. M. C. 2020. Functional Interactions of Tau Phosphorylation Sites That Mediate Toxicity and Deficient Learning in Drosophila melanogaster. *Front Mol Neurosci,* 13**,** 569520.

KHURANA, V., LU, Y., STEINHILB, M. L., OLDHAM, S., SHULMAN, J. M. & FEANY, M. B. 2006. TOR-mediated cell-cycle activation causes neurodegeneration in a Drosophila tauopathy model. *Curr Biol,* 16**,** 230-41.

KIM, J., TADROS, B., LIANG, Y. H., KIM, Y., LASAGNA-REEVES, C., SONN, J. Y., CHUNG, D.-E. C., HYMAN, B., HOLTZMAN, D. M. & ZOGHBI, H. Y. 2024. TYK2 regulates tau levels, phosphorylation and aggregation in a tauopathy mouse model. *Nature Neuroscience,* 27**,** 2417-2429.

KIRIS, E., VENTIMIGLIA, D., SARGIN, M. E., GAYLORD, M. R., ALTINOK, A., ROSE, K., MANJUNATH, B. S., JORDAN, M. A., WILSON, L. & FEINSTEIN, S. C. 2011. Combinatorial Tau pseudophosphorylation: markedly different regulatory effects on microtubule assembly and dynamic instability than the sum of the individual parts. *J Biol Chem,* 286**,** 14257-70.

KONDO, K., IKURA, T., TANAKA, H., FUJITA, K., TAKAYAMA, S., YOSHIOKA, Y., TAGAWA, K., HOMMA, H., LIU, S., KAWASAKI, R., HUANG, Y., ITO, N., TATE, S. I. & OKAZAWA, H. 2021. Hepta-Histidine Inhibits Tau Aggregation. *ACS Chem Neurosci,* 12**,** 3015-3027.

KöPKE, E., TUNG, Y. C., SHAIKH, S., ALONSO, A. C., IQBAL, K. & GRUNDKE-IQBAL, I. 1993. Microtubule-associated protein tau. Abnormal phosphorylation of a non-paired helical filament pool in Alzheimer disease. *J Biol Chem,* 268**,** 24374-84.

KOSMIDIS, S., GRAMMENOUDI, S., PAPANIKOLOPOULOU, K. & SKOULAKIS, E. M. 2010. Differential effects of Tau on the integrity and function of neurons essential for learning in Drosophila. *J Neurosci,* 30**,** 464-77.

KOSS, D. J., JONES, G., CRANSTON, A., GARDNER, H., KANAAN, N. M. & PLATT, B. 2016. Soluble pre-fibrillar tau and β-amyloid species emerge in early human Alzheimer's disease and track disease progression and cognitive decline. *Acta Neuropathol,* 132**,** 875-895.

KOVACS, G. G. 2015. Invited review: Neuropathology of tauopathies: principles and practice. *Neuropathol Appl Neurobiol,* 41**,** 3-23.

KRISHNAMURTHY, P. K. & JOHNSON, G. V. 2004. Mutant (R406W) human tau is hyperphosphorylated and does not efficiently bind microtubules in a neuronal cortical cell model. *J Biol Chem,* 279**,** 7893-900.

KUBO, A., MISONOU, H., MATSUYAMA, M., NOMORI, A., WADA-KAKUDA, S., TAKASHIMA, A., KAWATA, M., MURAYAMA, S., IHARA, Y. & MIYASAKA, T. 2019. Distribution of endogenous normal tau in the mouse brain. *J Comp Neurol,* 527**,** 985-998.

KUMAR, H. & UDGAONKAR, J. B. 2021. The Lys 280 → Gln mutation mimicking disease-linked acetylation of Lys 280 in tau extends the structural core of fibrils and modulates their catalytic properties. *Protein Sci,* 30**,** 785-803.

KYALU NGOIE ZOLA, N., BALTY, C., PYR DIT RUYS, S., VANPARYS, A. A. T., HUYGHE, N. D. G., HERINCKX, G., JOHANNS, M., BOYER, E., KIENLEN-CAMPARD, P., RIDER, M. H., VERTOMMEN, D. & HANSEEUW, B. J. 2023. Specific post-translational modifications of soluble tau protein distinguishes Alzheimer's disease and primary tauopathies. *Nat Commun,* 14**,** 3706.

LAMPRECHT, R. & LEDOUX, J. 2004. Structural plasticity and memory. *Nature Reviews Neuroscience,* 5**,** 45-54.

LANE-DONOVAN, C. & BOXER, A. L. 2024. Disentangling tau: One protein, many therapeutic approaches. *Neurotherapeutics,* 21**,** e00321.

LAU, D. H., HOGSETH, M., PHILLIPS, E. C., O'NEILL, M. J., POOLER, A. M., NOBLE, W. & HANGER, D. P. 2016. Critical residues involved in tau binding to fyn: implications for tau phosphorylation in Alzheimer's disease. *Acta Neuropathol Commun,* 4**,** 49.

LAURETTI, E. & PRATICò, D. 2020. Alzheimer's disease: phenotypic approaches using disease models and the targeting of tau protein. *Expert Opin Ther Targets,* 24**,** 319-330.

LEBOUVIER, T., SCALES, T. M., WILLIAMSON, R., NOBLE, W., DUYCKAERTS, C., HANGER, D. P., REYNOLDS, C. H., ANDERTON, B. H. & DERKINDEREN, P. 2009. The microtubule-associated protein tau is also phosphorylated on tyrosine. *J Alzheimers Dis,* 18**,** 1-9.

LEE, G., NEWMAN, S. T., GARD, D. L., BAND, H. & PANCHAMOORTHY, G. 1998. Tau interacts with src-family non-receptor tyrosine kinases. *J Cell Sci,* 111 ( Pt 21)**,** 3167-77.

LEE, V. M., GOEDERT, M. & TROJANOWSKI, J. Q. 2001. Neurodegenerative tauopathies. *Annu Rev Neurosci,* 24**,** 1121-59.

LESLIE, S. N., KANYO, J., DATTA, D., WILSON, R. S., ZEISS, C., DUQUE, A., LAM, T. T., ARNSTEN, A. F. T. & NAIRN, A. C. 2021. Simple, Single-Shot Phosphoproteomic Analysis of Heat-Stable Tau Identifies Age-Related Changes in pS235- and pS396-Tau Levels in Non-human Primates. *Front Aging Neurosci,* 13**,** 767322.

LEVEILLE, E., ROSS, O. A. & GAN-OR, Z. 2021. Tau and MAPT genetics in tauopathies and synucleinopathies. *Parkinsonism & Related Disorders,* 90**,** 142-154.

LEVY, S. A., ZUNIGA, G., GONZALEZ, E. M., BUTLER, D., TEMPLE, S. & FROST, B. 2022. Tau(LUM), an in vivo Drosophila sensor of tau multimerization, identifies neuroprotective interventions in tauopathy. *Cell Rep Methods,* 2**,** 100292.

LI, W. & LEE, V. M. 2006. Characterization of two VQIXXK motifs for tau fibrillization in vitro. *Biochemistry,* 45**,** 15692-701.

LIMORENKO, G. & LASHUEL, H. A. 2022. Revisiting the grammar of Tau aggregation and pathology formation: how new insights from brain pathology are shaping how we study and target Tauopathies. *Chem Soc Rev,* 51**,** 513-565.

LIN, W. L., LEWIS, J., YEN, S. H., HUTTON, M. & DICKSON, D. W. 2003. Ultrastructural neuronal pathology in transgenic mice expressing mutant (P301L) human tau. *J Neurocytol,* 32**,** 1091-105.

LIU, F., IQBAL, K., GRUNDKE-IQBAL, I., HART, G. W. & GONG, C. X. 2004. O-GlcNAcylation regulates phosphorylation of tau: a mechanism involved in Alzheimer's disease. *Proc Natl Acad Sci U S A,* 101**,** 10804-9.

LLORENS-MARTíN, M., JURADO, J., HERNáNDEZ, F. & AVILA, J. 2014. GSK-3β, a pivotal kinase in Alzheimer disease. *Front Mol Neurosci,* 7**,** 46.

LO CASCIO, F., PARK, S., SENGUPTA, U., PUANGMALAI, N., BHATT, N., SHCHANKIN, N., JEREZ, C., MORENO, N., BITTAR, A., XAVIER, R., ZHAO, Y., WANG, C., FU, H., MA, Q., MONTALBANO, M. & KAYED, R. 2025. Brain-derived tau oligomer polymorphs: distinct aggregations, stability profiles, and biological activities. *Commun Biol,* 8**,** 53.

LOPEZ-LEE, C., KODAMA, L., FAN, L., ZHU, D., ZHU, J., WONG, M. Y., YE, P., NORMAN, K., FOXE, N. R., IJAZ, L., YU, F., CHEN, H., CARLING, G. K., TORRES, E. R., KIM, R. D., DUBAL, D. B., LIDDELOW, S. A., SINHA, S. C., LUO, W. & GAN, L. 2024. Tlr7 drives sex differences in age- and Alzheimer's disease-related demyelination. *Science,* 386**,** eadk7844.

LOSSOS, A., RECHES, A., GAL, A., NEWMAN, J. P., SOFFER, D., GOMORI, J. M., BOHER, M., EKSTEIN, D., BIRAN, I., MEINER, Z., ABRAMSKY, O. & ROSENMANN, H. 2003. Frontotemporal dementia and parkinsonism with the P301S tau gene mutation in a Jewish family. *J Neurol,* 250**,** 733-40.

LöVESTAM, S., KOH, F. A., VAN KNIPPENBERG, B., KOTECHA, A., MURZIN, A. G., GOEDERT, M. & SCHERES, S. H. W. 2022. Assembly of recombinant tau into filaments identical to those of Alzheimer's disease and chronic traumatic encephalopathy. *Elife,* 11.

LöVESTAM, S., LI, D., WAGSTAFF, J. L., KOTECHA, A., KIMANIUS, D., MCLAUGHLIN, S. H., MURZIN, A. G., FREUND, S. M. V., GOEDERT, M. & SCHERES, S. H. W. 2024. Disease-specific tau filaments assemble via polymorphic intermediates. *Nature,* 625**,** 119-125.

LöVESTAM, S., WAGSTAFF, J. L., KATSINELOS, T., SHI, J., FREUND, S. M. V., GOEDERT, M. & SCHERES, S. H. W. 2025. Twelve phosphomimetic mutations induce the assembly of recombinant full-length human tau into paired helical filaments. eLife Sciences Publications, Ltd.

LOVESTONE, S., BOADA, M., DUBOIS, B., HüLL, M., RINNE, J. O., HUPPERTZ, H. J., CALERO, M., ANDRéS, M. V., GóMEZ-CARRILLO, B., LEóN, T. & DEL SER, T. 2015. A phase II trial of tideglusib in Alzheimer's disease. *J Alzheimers Dis,* 45**,** 75-88.

LUCAS, J. J., HERNáNDEZ, F., GóMEZ-RAMOS, P., MORáN, M. A., HEN, R. & AVILA, J. 2001. Decreased nuclear beta-catenin, tau hyperphosphorylation and neurodegeneration in GSK-3beta conditional transgenic mice. *Embo j,* 20**,** 27-39.

LUNA-MUñOZ, J., CHáVEZ-MACíAS, L., GARCíA-SIERRA, F. & MENA, R. 2007. Earliest stages of tau conformational changes are related to the appearance of a sequence of specific phospho-dependent tau epitopes in Alzheimer's disease. *J Alzheimers Dis,* 12**,** 365-75.

MACDONALD, J. A., BRONNER, I. F., DRYNAN, L., FAN, J., CURRY, A., FRASER, G., LAVENIR, I. & GOEDERT, M. 2019. Assembly of transgenic human P301S Tau is necessary for neurodegeneration in murine spinal cord. *Acta Neuropathol Commun,* 7**,** 44.

MAIR, W., MUNTEL, J., TEPPER, K., TANG, S., BIERNAT, J., SEELEY, W. W., KOSIK, K. S., MANDELKOW, E., STEEN, H. & STEEN, J. A. 2016. FLEXITau: Quantifying Post-translational Modifications of Tau Protein in Vitro and in Human Disease. *Anal Chem,* 88**,** 3704-14.

MALHIS, M., KANIYAPPAN, S., AILLAUD, I., CHANDUPATLA, R. R., RAMIREZ, L. M., ZWECKSTETTER, M., HORN, A. H. C., MANDELKOW, E., STICHT, H. & FUNKE, S. A. 2021. Potent Tau Aggregation Inhibitor D-Peptides Selected against Tau-Repeat 2 Using Mirror Image Phage Display. *Chembiochem,* 22**,** 3049-3059.

MAMSA, S. S. A. & MELONI, B. P. 2021. Arginine and Arginine-Rich Peptides as Modulators of Protein Aggregation and Cytotoxicity Associated With Alzheimer's Disease. *Front Mol Neurosci,* 14**,** 759729.

MAMUN, A. A., UDDIN, M. S., MATHEW, B. & ASHRAF, G. M. 2020. Toxic tau: structural origins of tau aggregation in Alzheimer's disease. *Neural Regen Res,* 15**,** 1417-1420.

MANCUSO, R., FRYATT, G., CLEAL, M., OBST, J., PIPI, E., MONZóN-SANDOVAL, J., RIBE, E., WINCHESTER, L., WEBBER, C., NEVADO, A., JACOBS, T., AUSTIN, N., THEUNIS, C., GRAUWEN, K., DANIELA RUIZ, E., MUDHER, A., VICENTE-RODRIGUEZ, M., PARKER, C. A., SIMMONS, C., CASH, D., RICHARDSON, J., JONES, D. N. C., LOVESTONE, S., GóMEZ-NICOLA, D. & PERRY, V. H. 2019. CSF1R inhibitor JNJ-40346527 attenuates microglial proliferation and neurodegeneration in P301S mice. *Brain,* 142**,** 3243-3264.

MANDELKOW, E. M. & MANDELKOW, E. 1998. Tau in Alzheimer's disease. *Trends Cell Biol,* 8**,** 425-7.

MARTIN, L., LATYPOVA, X. & TERRO, F. 2011. Post-translational modifications of tau protein: implications for Alzheimer's disease. *Neurochem Int,* 58**,** 458-71.

MARTINEZ, P., PATEL, H., YOU, Y., LOPES, D., AMARO, A., JURY-GARFE, N., MIN, Y., REDDING-OCHOA, J., DUTTA, S., ROCHET, J. C., ERTEKIN-TANER, N., TRONCOSO, J. C. & LASAGNA-REEVES, C. A. 2025. Tau-seed interactome analysis reveals distinct functional signatures in Alzheimer's disease across model systems. *bioRxiv*.

MARVIAN, A. T., STRAUSS, T., TANG, Q., TUCK, B. J., KEELING, S., RüDIGER, D., MIRZAZADEH DIZAJI, N., MOHAMMAD-BEIGI, H., NUSCHER, B., CHAKRABORTY, P., SUTHERLAND, D. S., MCEWAN, W. A., KöGLSPERGER, T., ZAHLER, S., ZWECKSTETTER, M., LICHTENTHALER, S. F., WURST, W., SCHWARZ, S. & HöGLINGER, G. 2024. Distinct regulation of Tau Monomer and aggregate uptake and intracellular accumulation in human neurons. *Mol Neurodegener,* 19**,** 100.

MATSUOKA, Y., GRAY, A. J., HIRATA-FUKAE, C., MINAMI, S. S., WATERHOUSE, E. G., MATTSON, M. P., LAFERLA, F. M., GOZES, I. & AISEN, P. S. 2007. Intranasal NAP administration reduces accumulation of amyloid peptide and tau hyperphosphorylation in a transgenic mouse model of Alzheimer's disease at early pathological stage. *J Mol Neurosci,* 31**,** 165-70.

MCGUIRE, S. E., LE, P. T., OSBORN, A. J., MATSUMOTO, K. & DAVIS, R. L. 2003. Spatiotemporal rescue of memory dysfunction in Drosophila. *Science,* 302**,** 1765-8.

MCINNES, J., WIERDA, K., SNELLINX, A., BOUNTI, L., WANG, Y. C., STANCU, I. C., APóSTOLO, N., GEVAERT, K., DEWACHTER, I., SPIRES-JONES, T. L., DE STROOPER, B., DE WIT, J., ZHOU, L. & VERSTREKEN, P. 2018. Synaptogyrin-3 Mediates Presynaptic Dysfunction Induced by Tau. *Neuron,* 97**,** 823-835.e8.

MCKIBBEN, K. M. & RHOADES, E. 2019. Independent tubulin binding and polymerization by the proline-rich region of Tau is regulated by Tau's N-terminal domain. *J Biol Chem,* 294**,** 19381-19394.

MEINERTZHAGEN, I. A. & LEE, C. H. 2012. The genetic analysis of functional connectomics in Drosophila. *Adv Genet,* 80**,** 99-151.

MELCHIOR, B., MITTAPALLI, G. K., LAI, C., DUONG-POLK, K., STEWART, J., GüNER, B., HOFILENA, B., TJITRO, A., ANDERSON, S. D., HERMAN, D. S., DELLAMARY, L., SWEARINGEN, C. J., SUNIL, K. C. & YAZICI, Y. 2019. Tau pathology reduction with SM07883, a novel, potent, and selective oral DYRK1A inhibitor: A potential therapeutic for Alzheimer's disease. *Aging Cell,* 18**,** e13000.

MENG, J. X., ZHANG, Y., SAMAN, D., HAIDER, A. M., DE, S., SANG, J. C., BROWN, K., JIANG, K., HUMPHREY, J., JULIAN, L., HIDARI, E., LEE, S. F., BALMUS, G., FLOTO, R. A., BRYANT, C. E., BENESCH, J. L. P., YE, Y. & KLENERMAN, D. 2022. Hyperphosphorylated tau self-assembles into amorphous aggregates eliciting TLR4-dependent responses. *Nat Commun,* 13**,** 2692.

MERSHIN, A., PAVLOPOULOS, E., FITCH, O., BRADEN, B. C., NANOPOULOS, D. V. & SKOULAKIS, E. M. 2004. Learning and memory deficits upon TAU accumulation in Drosophila mushroom body neurons. *Learn Mem,* 11**,** 277-87.

MIGUEL, L., ROVELET-LECRUX, A., FEYEUX, M., FREBOURG, T., NASSOY, P., CAMPION, D. & LECOURTOIS, M. 2019. Detection of all adult Tau isoforms in a 3D culture model of iPSC-derived neurons. *Stem Cell Res,* 40**,** 101541.

MIN, S. W., CHEN, X., TRACY, T. E., LI, Y., ZHOU, Y., WANG, C., SHIRAKAWA, K., MINAMI, S. S., DEFENSOR, E., MOK, S. A., SOHN, P. D., SCHILLING, B., CONG, X., ELLERBY, L., GIBSON, B. W., JOHNSON, J., KROGAN, N., SHAMLOO, M., GESTWICKI, J., MASLIAH, E., VERDIN, E. & GAN, L. 2015. Critical role of acetylation in tau-mediated neurodegeneration and cognitive deficits. *Nat Med,* 21**,** 1154-62.

MIRBAHA, H., HOLMES, B. B., SANDERS, D. W., BIESCHKE, J. & DIAMOND, M. I. 2015. Tau Trimers Are the Minimal Propagation Unit Spontaneously Internalized to Seed Intracellular Aggregation. *J Biol Chem,* 290**,** 14893-903.

MIRRA, S. S., MURRELL, J. R., GEARING, M., SPILLANTINI, M. G., GOEDERT, M., CROWTHER, R. A., LEVEY, A. I., JONES, R., GREEN, J., SHOFFNER, J. M., WAINER, B. H., SCHMIDT, M. L., TROJANOWSKI, J. Q. & GHETTI, B. 1999. Tau pathology in a family with dementia and a P301L mutation in tau. *J Neuropathol Exp Neurol,* 58**,** 335-45.

MIYASAKA, T., MORISHIMA-KAWASHIMA, M., RAVID, R., KAMPHORST, W., NAGASHIMA, K. & IHARA, Y. 2001. Selective deposition of mutant tau in the FTDP-17 brain affected by the P301L mutation. *J Neuropathol Exp Neurol,* 60**,** 872-84.

MOHAMED, T., HOANG, T., JELOKHANI-NIARAKI, M. & RAO, P. P. 2013. Tau-derived-hexapeptide 306VQIVYK311 aggregation inhibitors: nitrocatechol moiety as a pharmacophore in drug design. *ACS Chem Neurosci,* 4**,** 1559-70.

MöLLER, H. J. & GRAEBER, M. B. 1998. The case described by Alois Alzheimer in 1911. Historical and conceptual perspectives based on the clinical record and neurohistological sections. *Eur Arch Psychiatry Clin Neurosci,* 248**,** 111-22.

MOLONEY, C. M., LOWE, V. J. & MURRAY, M. E. 2021. Visualization of neurofibrillary tangle maturity in Alzheimer's disease: A clinicopathologic perspective for biomarker research. *Alzheimers Dement,* 17**,** 1554-1574.

MONASTIRIOTI, M. 1999. Biogenic amine systems in the fruit fly Drosophila melanogaster. *Microsc Res Tech,* 45**,** 106-21.

MORRIS, M., KNUDSEN, G. M., MAEDA, S., TRINIDAD, J. C., IOANOVICIU, A., BURLINGAME, A. L. & MUCKE, L. 2015. Tau post-translational modifications in wild-type and human amyloid precursor protein transgenic mice. *Nat Neurosci,* 18**,** 1183-9.

MORSCH, R., SIMON, W. & COLEMAN, P. D. 1999. Neurons may live for decades with neurofibrillary tangles. *J Neuropathol Exp Neurol,* 58**,** 188-97.

MROCZKO, B., GROBLEWSKA, M. & LITMAN-ZAWADZKA, A. 2019. The Role of Protein Misfolding and Tau Oligomers (TauOs) in Alzheimer's Disease (AD). *Int J Mol Sci,* 20.

MUDHER, A., COLIN, M., DUJARDIN, S., MEDINA, M., DEWACHTER, I., ALAVI NAINI, S. M., MANDELKOW, E. M., MANDELKOW, E., BUéE, L., GOEDERT, M. & BRION, J. P. 2017. What is the evidence that tau pathology spreads through prion-like propagation? *Acta Neuropathol Commun,* 5**,** 99.

MUDHER, A., SHEPHERD, D., NEWMAN, T. A., MILDREN, P., JUKES, J. P., SQUIRE, A., MEARS, A., DRUMMOND, J. A., BERG, S., MACKAY, D., ASUNI, A. A., BHAT, R. & LOVESTONE, S. 2004. GSK-3beta inhibition reverses axonal transport defects and behavioural phenotypes in Drosophila. *Mol Psychiatry,* 9**,** 522-30.

MUKRASCH, M. D., BIERNAT, J., VON BERGEN, M., GRIESINGER, C., MANDELKOW, E. & ZWECKSTETTER, M. 2005. Sites of tau important for aggregation populate {beta}-structure and bind to microtubules and polyanions. *J Biol Chem,* 280**,** 24978-86.

MUMMERY, C. J., BöRJESSON-HANSON, A., BLACKBURN, D. J., VIJVERBERG, E. G. B., DE DEYN, P. P., DUCHARME, S., JONSSON, M., SCHNEIDER, A., RINNE, J. O., LUDOLPH, A. C., BODENSCHATZ, R., KORDASIEWICZ, H., SWAYZE, E. E., FITZSIMMONS, B., MIGNON, L., MOORE, K. M., YUN, C., BAUMANN, T., LI, D., NORRIS, D. A., CREAN, R., GRAHAM, D. L., HUANG, E., RATTI, E., BENNETT, C. F., JUNGE, C. & LANE, R. M. 2023. Tau-targeting antisense oligonucleotide MAPT(Rx) in mild Alzheimer's disease: a phase 1b, randomized, placebo-controlled trial. *Nat Med,* 29**,** 1437-1447.

NACHARAJU, P., LEWIS, J., EASSON, C., YEN, S., HACKETT, J., HUTTON, M. & YEN, S. H. 1999. Accelerated filament formation from tau protein with specific FTDP-17 missense mutations. *FEBS Lett,* 447**,** 195-9.

NECULA, M., KAYED, R., MILTON, S. & GLABE, C. G. 2007. Small molecule inhibitors of aggregation indicate that amyloid beta oligomerization and fibrillization pathways are independent and distinct. *J Biol Chem,* 282**,** 10311-24.

NG, A. S., SIAS, A. C., PRESSMAN, P. S., FONG, J. C., KARYDAS, A. M., ZANTO, T. P., DE MAY, M., COPPOLA, G., GESCHWIND, D. H., MILLER, B. L. & LEE, S. E. 2015. Young-onset frontotemporal dementia in a homozygous tau R406W mutation carrier. *Ann Clin Transl Neurol,* 2**,** 1124-8.

NISHIMURA, I., YANG, Y. & LU, B. 2004. PAR-1 kinase plays an initiator role in a temporally ordered phosphorylation process that confers tau toxicity in Drosophila. *Cell,* 116**,** 671-82.

NOBLE, W., PLANEL, E., ZEHR, C., OLM, V., MEYERSON, J., SULEMAN, F., GAYNOR, K., WANG, L., LAFRANCOIS, J., FEINSTEIN, B., BURNS, M., KRISHNAMURTHY, P., WEN, Y., BHAT, R., LEWIS, J., DICKSON, D. & DUFF, K. 2005. Inhibition of glycogen synthase kinase-3 by lithium correlates with reduced tauopathy and degeneration in vivo. *Proc Natl Acad Sci U S A,* 102**,** 6990-5.

NOVAK, M., KABAT, J. & WISCHIK, C. M. 1993. Molecular characterization of the minimal protease resistant tau unit of the Alzheimer's disease paired helical filament. *Embo j,* 12**,** 365-70.

NOVAK, P., KOVACECH, B., KATINA, S., SCHMIDT, R., SCHELTENS, P., KONTSEKOVA, E., ROPELE, S., FIALOVA, L., KRAMBERGER, M., PAULENKA-IVANOVOVA, N., SMISEK, M., HANES, J., STEVENS, E., KOVAC, A., SUTOVSKY, S., PARRAK, V., KOSON, P., PRCINA, M., GALBA, J., CENTE, M., HROMADKA, T., FILIPCIK, P., PIESTANSKY, J., SAMCOVA, M., PRENN-GOLOGRANC, C., SIVAK, R., FROELICH, L., FRESSER, M., RAKUSA, M., HARRISON, J., HORT, J., OTTO, M., TOSUN, D., ONDRUS, M., WINBLAD, B., NOVAK, M. & ZILKA, N. 2021. ADAMANT: a placebo-controlled randomized phase 2 study of AADvac1, an active immunotherapy against pathological tau in Alzheimer's disease. *Nat Aging,* 1**,** 521-534.

NUNES, M. A., VIEL, T. A. & BUCK, H. S. 2013. Microdose lithium treatment stabilized cognitive impairment in patients with Alzheimer's disease. *Curr Alzheimer Res,* 10**,** 104-7.

O'CONNOR, A., KARIKARI, T. K., POOLE, T., ASHTON, N. J., LANTERO RODRIGUEZ, J., KHATUN, A., SWIFT, I., HESLEGRAVE, A. J., ABEL, E., CHUNG, E., WESTON, P. S. J., PAVISIC, I. M., RYAN, N. S., BARKER, S., ROSSOR, M. N., POLKE, J. M., FROST, C., MEAD, S., BLENNOW, K., ZETTERBERG, H. & FOX, N. C. 2021. Plasma phospho-tau181 in presymptomatic and symptomatic familial Alzheimer's disease: a longitudinal cohort study. *Mol Psychiatry,* 26**,** 5967-5976.

OJELADE, S. A., ACEVEDO, S. F. & ROTHENFLUH, A. 2013. The role of the actin cytoskeleton in regulating Drosophila behavior. *Rev Neurosci,* 24**,** 471-84.

ONYIKE, C. U. & DIEHL-SCHMID, J. 2013. The epidemiology of frontotemporal dementia. *Int Rev Psychiatry,* 25**,** 130-7.

PADMANABHAN, P., KNEYNSBERG, A., CRUZ, E., BRINER, A. & GöTZ, J. 2024. Single-molecule imaging of Tau reveals how phosphorylation affects its movement and confinement in living cells. *Molecular Brain,* 17**,** 7.

PALMQVIST, S., JANELIDZE, S., QUIROZ, Y. T., ZETTERBERG, H., LOPERA, F., STOMRUD, E., SU, Y., CHEN, Y., SERRANO, G. E., LEUZY, A., MATTSSON-CARLGREN, N., STRANDBERG, O., SMITH, R., VILLEGAS, A., SEPULVEDA-FALLA, D., CHAI, X., PROCTOR, N. K., BEACH, T. G., BLENNOW, K., DAGE, J. L., REIMAN, E. M. & HANSSON, O. 2020. Discriminative Accuracy of Plasma Phospho-tau217 for Alzheimer Disease vs Other Neurodegenerative Disorders. *Jama,* 324**,** 772-781.

PAPANIKOLOPOULOU, K., ROUSSOU, I. G., GOUZI, J. Y., SAMIOTAKI, M., PANAYOTOU, G., TURIN, L. & SKOULAKIS, E. M. C. 2019. Drosophila Tau Negatively Regulates Translation and Olfactory Long-Term Memory, But Facilitates Footshock Habituation and Cytoskeletal Homeostasis. *J Neurosci,* 39**,** 8315-8329.

PARK, S., LEE, J. H., JEON, J. H. & LEE, M. J. 2018. Degradation or aggregation: the ramifications of post-translational modifications on tau. *BMB Rep,* 51**,** 265-273.

PARRA BRAVO, C., NAGUIB, S. A. & GAN, L. 2024. Cellular and pathological functions of tau. *Nature Reviews Molecular Cell Biology,* 25**,** 845-864.

PASSARELLA, D. & GOEDERT, M. 2018. Beta-sheet assembly of Tau and neurodegeneration in Drosophila melanogaster. *Neurobiol Aging,* 72**,** 98-105.

PéREZ, M., HERNáNDEZ, F., LIM, F., DíAZ-NIDO, J. & AVILA, J. 2003. Chronic lithium treatment decreases mutant tau protein aggregation in a transgenic mouse model. *J Alzheimers Dis,* 5**,** 301-8.

PEREZ, M., SANTA-MARíA, I., TORTOSA, E., CUADROS, R., DEL VALLE, M., HERNáNDEZ, F., MORENO, F. J. & AVILA, J. 2007. The role of the VQIVYK peptide in tau protein phosphorylation. *J Neurochem,* 103**,** 1447-60.

PERRY, G., FRIEDMAN, R., SHAW, G. & CHAU, V. 1987. Ubiquitin is detected in neurofibrillary tangles and senile plaque neurites of Alzheimer disease brains. *Proc Natl Acad Sci U S A,* 84**,** 3033-6.

PLASCENCIA-VILLA, G. & PERRY, G. 2022. Neuropathologic Changes Provide Insights into Key Mechanisms of Alzheimer Disease and Related Dementia. *Am J Pathol,* 192**,** 1340-1346.

PLáTENíK, J., FIšAR, Z., BUCHAL, R., JIRáK, R., KITZLEROVá, E., ZVěřOVá, M. & RABOCH, J. 2014. GSK3β, CREB, and BDNF in peripheral blood of patients with Alzheimer's disease and depression. *Prog Neuropsychopharmacol Biol Psychiatry,* 50**,** 83-93.

POORKAJ, P., BIRD, T. D., WIJSMAN, E., NEMENS, E., GARRUTO, R. M., ANDERSON, L., ANDREADIS, A., WIEDERHOLT, W. C., RASKIND, M. & SCHELLENBERG, G. D. 1998. Tau is a candidate gene for chromosome 17 frontotemporal dementia. *Ann Neurol,* 43**,** 815-25.

POUNOT, K., PIERSSON, C., GORING, A. K., ROSU, F., GABELICA, V., WEIK, M., HAN, S. & FICHOU, Y. 2024. Mutations in Tau Protein Promote Aggregation by Favoring Extended Conformations. *JACS Au,* 4**,** 92-100.

POVELLATO, G., TUXWORTH, R. I., HANGER, D. P. & TEAR, G. 2014. Modification of the Drosophila model of in vivo Tau toxicity reveals protective phosphorylation by GSK3β. *Biol Open,* 3**,** 1-11.

PRIETO-GODINO, L. L., DIEGELMANN, S. & BATE, M. 2012. Embryonic origin of olfactory circuitry in Drosophila: contact and activity-mediated interactions pattern connectivity in the antennal lobe. *PLoS Biol,* 10**,** e1001400.

PROBST, A., GöTZ, J., WIEDERHOLD, K. H., TOLNAY, M., MISTL, C., JATON, A. L., HONG, M., ISHIHARA, T., LEE, V. M., TROJANOWSKI, J. Q., JAKES, R., CROWTHER, R. A., SPILLANTINI, M. G., BüRKI, K. & GOEDERT, M. 2000. Axonopathy and amyotrophy in mice transgenic for human four-repeat tau protein. *Acta Neuropathol,* 99**,** 469-81.

PRUSINER, S. B. 1982. Novel proteinaceous infectious particles cause scrapie. *Science,* 216**,** 136-44.

PRüßING, K., VOIGT, A. & SCHULZ, J. B. 2013. Drosophila melanogaster as a model organism for Alzheimer's disease. *Mol Neurodegener,* 8**,** 35.

QI, C., LöVESTAM, S., MURZIN, A. G., PEAK-CHEW, S., FRANCO, C., BOGDANI, M., LATIMER, C., MURRELL, J. R., CULLINANE, P. W., JAUNMUKTANE, Z., BIRD, T. D., GHETTI, B., SCHERES, S. H. W. & GOEDERT, M. 2025. Tau filaments with the Alzheimer fold in human MAPT mutants V337M and R406W. *Nat Struct Mol Biol,* 32**,** 1297-1304.

QURAISHE, S., COWAN, C. M. & MUDHER, A. 2013. NAP (davunetide) rescues neuronal dysfunction in a Drosophila model of tauopathy. *Mol Psychiatry,* 18**,** 834-42.

RAMIREZ-MORENO, M., COOPER, A. S., LIAN, T., LIU, J., ABTAHI, S., SKOULAKIS, E. M. C., SIVANANTHARAJAH, L., ALLAN, D. & MUDHER, A. 2025. The *Drosophila* wing is a high-throughput and versatile screening tool for Tau-mediated disease mechanisms and drug discovery. *bioRxiv***,** 2025.05.21.655273.

RAMSDEN, M., KOTILINEK, L., FORSTER, C., PAULSON, J., MCGOWAN, E., SANTACRUZ, K., GUIMARAES, A., YUE, M., LEWIS, J., CARLSON, G., HUTTON, M. & ASHE, K. H. 2005. Age-dependent neurofibrillary tangle formation, neuron loss, and memory impairment in a mouse model of human tauopathy (P301L). *J Neurosci,* 25**,** 10637-47.

RANKIN, C. A., SUN, Q. & GAMBLIN, T. C. 2005. Pseudo-phosphorylation of tau at Ser202 and Thr205 affects tau filament formation. *Brain Res Mol Brain Res,* 138**,** 84-93.

REED, L. A., SCHMIDT, M. L., WSZOLEK, Z. K., BALIN, B. J., SOONTORNNIYOMKIJ, V., LEE, V. M., TROJANOWSKI, J. Q. & SCHELPER, R. L. 1998. The neuropathology of a chromosome 17-linked autosomal dominant parkinsonism and dementia ("pallido-ponto-nigral degeneration"). *J Neuropathol Exp Neurol,* 57**,** 588-601.

RICHARDSON, B., GOEDERT, T., QURAISHE, S., DEINHARDT, K. & MUDHER, A. 2024. How do neurons age? A focused review on the aging of the microtubular cytoskeleton. *Neural Regen Res,* 19**,** 1899-1907.

RISSMAN, R. A., POON, W. W., BLURTON-JONES, M., ODDO, S., TORP, R., VITEK, M. P., LAFERLA, F. M., ROHN, T. T. & COTMAN, C. W. 2004. Caspase-cleavage of tau is an early event in Alzheimer disease tangle pathology. *J Clin Invest,* 114**,** 121-30.

RIZZU, P., JOOSSE, M., RAVID, R., HOOGEVEEN, A., KAMPHORST, W., VAN SWIETEN, J. C., WILLEMSEN, R. & HEUTINK, P. 2000. Mutation-dependent aggregation of tau protein and its selective depletion from the soluble fraction in brain of P301L FTDP-17 patients. *Hum Mol Genet,* 9**,** 3075-82.

ROBERTSON, H. M., WARR, C. G. & CARLSON, J. R. 2003. Molecular evolution of the insect chemoreceptor gene superfamily in Drosophila melanogaster. *Proc Natl Acad Sci U S A,* 100 Suppl 2**,** 14537-42.

RODRíGUEZ-MARTíN, T., CUCHILLO-IBáñEZ, I., NOBLE, W., NYENYA, F., ANDERTON, B. H. & HANGER, D. P. 2013. Tau phosphorylation affects its axonal transport and degradation. *Neurobiol Aging,* 34**,** 2146-57.

ROSENBERG, K. J., ROSS, J. L., FEINSTEIN, H. E., FEINSTEIN, S. C. & ISRAELACHVILI, J. 2008. Complementary dimerization of microtubule-associated tau protein: Implications for microtubule bundling and tau-mediated pathogenesis. *Proc Natl Acad Sci U S A,* 105**,** 7445-50.

SAHARA, N., LEWIS, J., DETURE, M., MCGOWAN, E., DICKSON, D. W., HUTTON, M. & YEN, S. H. 2002. Assembly of tau in transgenic animals expressing P301L tau: alteration of phosphorylation and solubility. *J Neurochem,* 83**,** 1498-508.

SAHARA, N., REN, Y., WARD, S., BINDER, L. I., SUHARA, T. & HIGUCHI, M. 2014. Tau oligomers as potential targets for early diagnosis of tauopathy. *J Alzheimers Dis,* 40 Suppl 1**,** S91-6.

SAITO, Y., GEYER, A., SASAKI, R., KUZUHARA, S., NANBA, E., MIYASAKA, T., SUZUKI, K. & MURAYAMA, S. 2002. Early-onset, rapidly progressive familial tauopathy with R406W mutation. *Neurology,* 58**,** 811-3.

SANTA-MARíA, I., PéREZ, M., HERNáNDEZ, F., MUñOZ, V., MORENO, F. J. & AVILA, J. 2006. In vitro tau fibrillization: mapping protein regions. *Biochim Biophys Acta,* 1762**,** 683-92.

SANTACRUZ, K., LEWIS, J., SPIRES, T., PAULSON, J., KOTILINEK, L., INGELSSON, M., GUIMARAES, A., DETURE, M., RAMSDEN, M., MCGOWAN, E., FORSTER, C., YUE, M., ORNE, J., JANUS, C., MARIASH, A., KUSKOWSKI, M., HYMAN, B., HUTTON, M. & ASHE, K. H. 2005. Tau suppression in a neurodegenerative mouse model improves memory function. *Science,* 309**,** 476-81.

SAWAYA, M. R., SAMBASHIVAN, S., NELSON, R., IVANOVA, M. I., SIEVERS, S. A., APOSTOL, M. I., THOMPSON, M. J., BALBIRNIE, M., WILTZIUS, J. J., MCFARLANE, H. T., MADSEN, A., RIEKEL, C. & EISENBERG, D. 2007. Atomic structures of amyloid cross-beta spines reveal varied steric zippers. *Nature,* 447**,** 453-7.

SAYAS, C. L. & ÁVILA, J. 2021. GSK-3 and Tau: A Key Duet in Alzheimer's Disease. *Cells,* 10.

SCHERES, S. H., ZHANG, W., FALCON, B. & GOEDERT, M. 2020. Cryo-EM structures of tau filaments. *Curr Opin Struct Biol,* 64**,** 17-25.

SCHLATTERER, S. D., TREMBLAY, M. A., ACKER, C. M. & DAVIES, P. 2011. Neuronal c-Abl overexpression leads to neuronal loss and neuroinflammation in the mouse forebrain. *J Alzheimers Dis,* 25**,** 119-33.

SCHNEIDER, A., BIERNAT, J., VON BERGEN, M., MANDELKOW, E. & MANDELKOW, E. M. 1999. Phosphorylation that detaches tau protein from microtubules (Ser262, Ser214) also protects it against aggregation into Alzheimer paired helical filaments. *Biochemistry,* 38**,** 3549-58.

SCHöLL, M., LOCKHART, S. N., SCHONHAUT, D. R., O'NEIL, J. P., JANABI, M., OSSENKOPPELE, R., BAKER, S. L., VOGEL, J. W., FARIA, J., SCHWIMMER, H. D., RABINOVICI, G. D. & JAGUST, W. J. 2016. PET Imaging of Tau Deposition in the Aging Human Brain. *Neuron,* 89**,** 971-982.

SCHWAB, K., FRAHM, S., HORSLEY, D., RICKARD, J. E., MELIS, V., GOATMAN, E. A., MAGBAGBEOLU, M., DOUGLAS, M., LEITH, M. G., BADDELEY, T. C., STOREY, J. M. D., RIEDEL, G., WISCHIK, C. M., HARRINGTON, C. R. & THEURING, F. 2017. A Protein Aggregation Inhibitor, Leuco-Methylthioninium Bis(Hydromethanesulfonate), Decreases α-Synuclein Inclusions in a Transgenic Mouse Model of Synucleinopathy. *Front Mol Neurosci,* 10**,** 447.

SCHWEERS, O., SCHöNBRUNN-HANEBECK, E., MARX, A. & MANDELKOW, E. 1994. Structural studies of tau protein and Alzheimer paired helical filaments show no evidence for beta-structure. *J Biol Chem,* 269**,** 24290-7.

SCHWEIGHAUSER, M., MURZIN, A. G., MACDONALD, J., LAVENIR, I., CROWTHER, R. A., SCHERES, S. H. W. & GOEDERT, M. 2023. Cryo-EM structures of tau filaments from the brains of mice transgenic for human mutant P301S Tau. *Acta Neuropathol Commun,* 11**,** 160.

SCHWEIGHAUSER, M., SHI, Y., MURZIN, A. G., GARRINGER, H. J., VIDAL, R., MURRELL, J. R., ERRO, M. E., SEELAAR, H., FERRER, I., VAN SWIETEN, J. C., GHETTI, B., SCHERES, S. H. W. & GOEDERT, M. 2025. Distinct tau filament folds in human MAPT mutants P301L and P301T. *Nat Struct Mol Biol,* 32**,** 1470-1478.

SEALEY, M. A., VOURKOU, E., COWAN, C. M., BOSSING, T., QURAISHE, S., GRAMMENOUDI, S., SKOULAKIS, E. M. C. & MUDHER, A. 2017. Distinct phenotypes of three-repeat and four-repeat human tau in a transgenic model of tauopathy. *Neurobiol Dis,* 105**,** 74-83.

SEIDLER, P. M., BOYER, D. R., RODRIGUEZ, J. A., SAWAYA, M. R., CASCIO, D., MURRAY, K., GONEN, T. & EISENBERG, D. S. 2018. Structure-based inhibitors of tau aggregation. *Nat Chem,* 10**,** 170-176.

SENGUPTA, A., KABAT, J., NOVAK, M., WU, Q., GRUNDKE-IQBAL, I. & IQBAL, K. 1998. Phosphorylation of tau at both Thr 231 and Ser 262 is required for maximal inhibition of its binding to microtubules. *Arch Biochem Biophys,* 357**,** 299-309.

SERENó, L., COMA, M., RODRíGUEZ, M., SáNCHEZ-FERRER, P., SáNCHEZ, M. B., GICH, I., AGULLó, J. M., PéREZ, M., AVILA, J., GUARDIA-LAGUARTA, C., CLARIMóN, J., LLEó, A. & GóMEZ-ISLA, T. 2009. A novel GSK-3beta inhibitor reduces Alzheimer's pathology and rescues neuronal loss in vivo. *Neurobiol Dis,* 35**,** 359-67.

SERRANO, L., MONTEJO DE GARCINI, E., HERNáNDEZ, M. A. & AVILA, J. 1985. Localization of the tubulin binding site for tau protein. *Eur J Biochem,* 153**,** 595-600.

SHI, Y., ZHANG, W., YANG, Y., MURZIN, A. G., FALCON, B., KOTECHA, A., VAN BEERS, M., TARUTANI, A., KAMETANI, F., GARRINGER, H. J., VIDAL, R., HALLINAN, G. I., LASHLEY, T., SAITO, Y., MURAYAMA, S., YOSHIDA, M., TANAKA, H., KAKITA, A., IKEUCHI, T., ROBINSON, A. C., MANN, D. M. A., KOVACS, G. G., REVESZ, T., GHETTI, B., HASEGAWA, M., GOEDERT, M. & SCHERES, S. H. W. 2021. Structure-based classification of tauopathies. *Nature,* 598**,** 359-363.

SHIMURA, H., SCHWARTZ, D., GYGI, S. P. & KOSIK, K. S. 2004. CHIP-Hsc70 complex ubiquitinates phosphorylated tau and enhances cell survival. *J Biol Chem,* 279**,** 4869-76.

SHULMAN, J. M. & FEANY, M. B. 2003. Genetic modifiers of tauopathy in Drosophila. *Genetics,* 165**,** 1233-42.

SIEVERS, S. A., KARANICOLAS, J., CHANG, H. W., ZHAO, A., JIANG, L., ZIRAFI, O., STEVENS, J. T., MüNCH, J., BAKER, D. & EISENBERG, D. 2011. Structure-based design of non-natural amino-acid inhibitors of amyloid fibril formation. *Nature,* 475**,** 96-100.

SIGURDSSON, E. M. 2018. Tau Immunotherapies for Alzheimer's Disease and Related Tauopathies: Progress and Potential Pitfalls. *J Alzheimers Dis,* 64**,** S555-s565.

SIVANANTHARAJAH, L., MUDHER, A. & SHEPHERD, D. 2019. An evaluation of Drosophila as a model system for studying tauopathies such as Alzheimer's disease. *J Neurosci Methods,* 319**,** 77-88.

SIVANANTHARAJAH, L., MUDHER, A. & SHEPHERD, D. 2025. Examining the vulnerability of adult neuron subtypes to tau-mediated toxicity in Drosophila. *Transl Psychiatry,* 15**,** 127.

SNOWDEN, J. S., ADAMS, J., HARRIS, J., THOMPSON, J. C., ROLLINSON, S., RICHARDSON, A., JONES, M., NEARY, D., MANN, D. M. & PICKERING-BROWN, S. 2015. Distinct clinical and pathological phenotypes in frontotemporal dementia associated with MAPT, PGRN and C9orf72 mutations. *Amyotroph Lateral Scler Frontotemporal Degener,* 16**,** 497-505.

SOEDA, Y., SAITO, M., MAEDA, S., ISHIDA, K., NAKAMURA, A., KOJIMA, S. & TAKASHIMA, A. 2019. Methylene Blue Inhibits Formation of Tau Fibrils but not of Granular Tau Oligomers: A Plausible Key to Understanding Failure of a Clinical Trial for Alzheimer's Disease. *J Alzheimers Dis,* 68**,** 1677-1686.

SOL, O., MERMOUD, J., HALLIKAINEN, M., KURL, S., RINNE, J., DAUTZENBERG, P., VIJVERBERG, E. G. B., MUMMERY, C., BöRJESSON-HANSON, A., JONSSON, M., RITCHIE, C., PENNINGTON, C., VUKICEVIC, M., GOLLWITZER, E., FIORINI, E., HICKMAN, D. T., HLIVA, V., GRAY, J., GERASYMCHUK, V., WAGG, J., FOURNIER, N., Lê, B., KEZIC, I., STEUKERS, L., TRIANA-BALTZER, G., THEUNIS, C., STREFFER, J.,

KOSCO-VILBOIS, M., PFEIFER, A. & SCHELTENS, P. 2025. Safety and immunogenicity of two Tau-targeting active immunotherapies, ACI-35.030 and JACI-35.054, in participants with early Alzheimer's disease: a phase 1b/2a, multicentre, double-blind, randomised, placebo-controlled study. *EBioMedicine,* 120**,** 105940.

SONTAG, J. M. & SONTAG, E. 2014. Protein phosphatase 2A dysfunction in Alzheimer's disease. *Front Mol Neurosci,* 7**,** 16.

SPERFELD, A. D., COLLATZ, M. B., BAIER, H., PALMBACH, M., STORCH, A., SCHWARZ, J., TATSCH, K., RESKE, S., JOOSSE, M., HEUTINK, P. & LUDOLPH, A. C. 1999. FTDP-17: an early-onset phenotype with parkinsonism and epileptic seizures caused by a novel mutation. *Ann Neurol,* 46**,** 708-15.

SPILLANTINI, M. G., MURRELL, J. R., GOEDERT, M., FARLOW, M. R., KLUG, A. & GHETTI, B. 1998. Mutation in the tau gene in familial multiple system tauopathy with presenile dementia. *Proc Natl Acad Sci U S A,* 95**,** 7737-41.

STEFANOSKA, K., GAJWANI, M., TAN, A. R. P., AHEL, H. I., ASIH, P. R., VOLKERLING, A., POLJAK, A. & ITTNER, A. 2022. Alzheimer's disease: Ablating single master site abolishes tau hyperphosphorylation. *Sci Adv,* 8**,** eabl8809.

STEINHILB, M. L., DIAS-SANTAGATA, D., FULGA, T. A., FELCH, D. L. & FEANY, M. B. 2007a. Tau phosphorylation sites work in concert to promote neurotoxicity in vivo. *Mol Biol Cell,* 18**,** 5060-8.

STEINHILB, M. L., DIAS-SANTAGATA, D., MULKEARNS, E. E., SHULMAN, J. M., BIERNAT, J., MANDELKOW, E. M. & FEANY, M. B. 2007b. S/P and T/P phosphorylation is critical for tau neurotoxicity in Drosophila. *J Neurosci Res,* 85**,** 1271-8.

STORK, T., ENGELEN, D., KRUDEWIG, A., SILIES, M., BAINTON, R. J. & KLäMBT, C. 2008. Organization and function of the blood-brain barrier in Drosophila. *J Neurosci,* 28**,** 587-97.

STRANG, K. H., CROFT, C. L., SORRENTINO, Z. A., CHAKRABARTY, P., GOLDE, T. E. & GIASSON, B. I. 2018. Distinct differences in prion-like seeding and aggregation between Tau protein variants provide mechanistic insights into tauopathies. *J Biol Chem,* 293**,** 2408-2421.

STRANG, K. H., GOLDE, T. E. & GIASSON, B. I. 2019a. MAPT mutations, tauopathy, and mechanisms of neurodegeneration. *Laboratory Investigation,* 99**,** 912-928.

STRANG, K. H., GOODWIN, M. S., RIFFE, C., MOORE, B. D., CHAKRABARTY, P., LEVITES, Y., GOLDE, T. E. & GIASSON, B. I. 2017. Generation and characterization of new monoclonal antibodies targeting the PHF1 and AT8 epitopes on human tau. *Acta Neuropathol Commun,* 5**,** 58.

STRANG, K. H., SORRENTINO, Z. A., RIFFE, C. J., GORION, K. M., VIJAYARAGHAVAN, N., GOLDE, T. E. & GIASSON, B. I. 2019b. Phosphorylation of serine 305 in tau inhibits aggregation. *Neurosci Lett,* 692**,** 187-192.

STUBBS, K., BATCHELOR, B., SIVANANTHARAJAH, L., SEALEY, M., RAMIREZ-MORENO, M., RUIZ, E., RICHARDSON, B., PERRY, V. H., NEWMAN, T. A. & MUDHER, A. 2023. Tau-mediated axonal degeneration is prevented by activation of the Wld(S) pathway. *Brain Commun,* 5**,** fcad052.

SULTAN, A., NESSLANY, F., VIOLET, M., BéGARD, S., LOYENS, A., TALAHARI, S., MANSUROGLU, Z., MARZIN, D., SERGEANT, N., HUMEZ, S., COLIN, M., BONNEFOY, E., BUéE, L. & GALAS, M. C. 2011. Nuclear tau, a key player in neuronal DNA protection. *J Biol Chem,* 286**,** 4566-75.

SUN, Q. & GAMBLIN, T. C. 2009. Pseudohyperphosphorylation causing AD-like changes in tau has significant effects on its polymerization. *Biochemistry,* 48**,** 6002-11.

TALMAT-AMAR, Y., ARRIBAT, Y., REDT-CLOUET, C., FEUILLETTE, S., BOUGé, A. L., LECOURTOIS, M. & PARMENTIER, M. L. 2011. Important neuronal toxicity of microtubule-bound Tau in vivo in Drosophila. *Hum Mol Genet,* 20**,** 3738-45.

TAN, W., THIRUPPATHI, J., HONG, S. H., PUTH, S., PHENG, S., MUN, B.-R., CHOI, W.-S., LEE, K.-H., PARK, H.-S., NGUYEN, D. T., LEE, M.-C., JEONG, K., ZHENG, J. H., KIM, Y., LEE, S. E. & RHEE, J. H. 2024. Development of an anti-tauopathy mucosal vaccine specifically targeting pathologic conformers. *npj Vaccines,* 9**,** 108.

TANIGUCHI, T., DOE, N., MATSUYAMA, S., KITAMURA, Y., MORI, H., SAITO, N. & TANAKA, C. 2005. Transgenic mice expressing mutant (N279K) human tau show mutation dependent cognitive deficits without neurofibrillary tangle formation. *FEBS Lett,* 579**,** 5704-12.

TAO, Y. & LI, D. 2023. Acetylation encodes Tau aggregation. *Structure,* 31**,** 1005-1007.

TESI, N., VAN DER LEE, S., HULSMAN, M., VAN SCHOOR, N. M., HUISMAN, M., PIJNENBURG, Y., VAN DER FLIER, W. M., REINDERS, M. & HOLSTEGE, H. 2024. Cognitively healthy centenarians are genetically protected against Alzheimer's disease. *Alzheimers Dement,* 20**,** 3864-3875.

TIAN, H., DAVIDOWITZ, E., LOPEZ, P., EMADI, S., MOE, J. & SIERKS, M. 2013. Trimeric tau is toxic to human neuronal cells at low nanomolar concentrations. *Int J Cell Biol,* 2013**,** 260787.

TOLOSA, E., LITVAN, I., HöGLINGER, G. U., BURN, D., LEES, A., ANDRéS, M. V., GóMEZ-CARRILLO, B., LEóN, T. & DEL SER, T. 2014. A phase 2 trial of the GSK-3 inhibitor tideglusib in progressive supranuclear palsy. *Mov Disord,* 29**,** 470-8.

TRABZUNI, D., WRAY, S., VANDROVCOVA, J., RAMASAMY, A., WALKER, R., SMITH, C., LUK, C., GIBBS, J. R., DILLMAN, A., HERNANDEZ, D. G., AREPALLI, S., SINGLETON, A. B., COOKSON, M. R., PITTMAN, A. M., DE SILVA, R., WEALE, M. E., HARDY, J. & RYTEN, M. 2012. MAPT expression and splicing is differentially regulated by brain region: relation to genotype and implication for tauopathies. *Hum Mol Genet,* 21**,** 4094-103.

TRACY, T. E., MADERO-PéREZ, J., SWANEY, D. L., CHANG, T. S., MORITZ, M., KONRAD, C., WARD, M. E., STEVENSON, E., HüTTENHAIN, R., KAUWE, G., MERCEDES, M., SWEETLAND-MARTIN, L., CHEN, X., MOK, S. A., WONG, M. Y., TELPOUKHOVSKAIA, M., MIN, S. W., WANG, C., SOHN, P. D., MARTIN, J., ZHOU, Y., LUO, W., TROJANOWSKI, J. Q., LEE, V. M. Y., GONG, S., MANFREDI, G., COPPOLA, G., KROGAN, N. J., GESCHWIND, D. H. & GAN, L. 2022. Tau interactome maps synaptic and mitochondrial processes associated with neurodegeneration. *Cell,* 185**,** 712-728.e14.

TSUCHIDA, T., SUSA, K., KIBIKI, T., TSUCHIYA, T., MIYAMOTO, K., IN, Y., MINOURA, K., TANIGUCHI, T., ISHIDA, T. & TOMOO, K. 2020. Crystal structure of the human tau PHF core domain VQIINK complexed with the Fab domain of monoclonal antibody Tau2r3. *FEBS Lett*.

UBHI, K. K., SHAIBAH, H., NEWMAN, T. A., SHEPHERD, D. & MUDHER, A. 2007. A comparison of the neuronal dysfunction caused by Drosophila tau and human tau in a Drosophila model of tauopathies. *Invert Neurosci,* 7**,** 165-71.

VAN DYCK, C. H., NYGAARD, H. B., CHEN, K., DONOHUE, M. C., RAMAN, R., RISSMAN, R. A., BREWER, J. B., KOEPPE, R. A., CHOW, T. W., RAFII, M. S., GESSERT, D., CHOI, J., TURNER, R. S., KAYE, J. A., GALE, S. A., REIMAN, E. M., AISEN, P. S. & STRITTMATTER, S. M. 2019. Effect of AZD0530 on Cerebral Metabolic Decline in Alzheimer Disease: A Randomized Clinical Trial. *JAMA Neurol,* 76**,** 1219-1229.

VAN DYCK, C. H., SWANSON, C. J., AISEN, P., BATEMAN, R. J., CHEN, C., GEE, M., KANEKIYO, M., LI, D., REYDERMAN, L., COHEN, S., FROELICH, L., KATAYAMA, S., SABBAGH, M., VELLAS, B., WATSON, D., DHADDA, S., IRIZARRY, M., KRAMER, L. D. & IWATSUBO, T. 2023. Lecanemab in Early Alzheimer's Disease. *N Engl J Med,* 388**,** 9-21.

VAZ, M. & SILVESTRE, S. 2020. Alzheimer's disease: Recent treatment strategies. *Eur J Pharmacol,* 887**,** 173554.

VESELKINA, E. R., TROSTNIKOV, M. V., ROSHINA, N. V. & PASYUKOVA, E. G. 2023. The Effect of the Tau Protein on D. melanogaster Lifespan Depends on GSK3 Expression and Sex. *Int J Mol Sci,* 24.

VIOLET, M., DELATTRE, L., TARDIVEL, M., SULTAN, A., CHAUDERLIER, A., CAILLIEREZ, R., TALAHARI, S., NESSLANY, F., LEFEBVRE, B., BONNEFOY, E., BUéE, L.

& GALAS, M. C. 2014. A major role for Tau in neuronal DNA and RNA protection in vivo under physiological and hyperthermic conditions. *Front Cell Neurosci,* 8**,** 84.

VOELZMANN, A., OKENVE-RAMOS, P., QU, Y., CHOJNOWSKA-MONGA, M., DEL CAñO-ESPINEL, M., PROKOP, A. & SANCHEZ-SORIANO, N. 2016. Tau and spectraplakins promote synapse formation and maintenance through Jun kinase and neuronal trafficking. *Elife,* 5.

VOGEL, J. W., ITURRIA-MEDINA, Y., STRANDBERG, O. T., SMITH, R., LEVITIS, E., EVANS, A. C. & HANSSON, O. 2020. Spread of pathological tau proteins through communicating neurons in human Alzheimer's disease. *Nat Commun,* 11**,** 2612.

VON BERGEN, M., BARGHORN, S., BIERNAT, J., MANDELKOW, E. M. & MANDELKOW, E. 2005. Tau aggregation is driven by a transition from random coil to beta sheet structure. *Biochim Biophys Acta,* 1739**,** 158-66.

VON BERGEN, M., BARGHORN, S., JEGANATHAN, S., MANDELKOW, E. M. & MANDELKOW, E. 2006. Spectroscopic approaches to the conformation of tau protein in solution and in paired helical filaments. *Neurodegener Dis,* 3**,** 197-206.

VON BERGEN, M., BARGHORN, S., LI, L., MARX, A., BIERNAT, J., MANDELKOW, E. M. & MANDELKOW, E. 2001. Mutations of tau protein in frontotemporal dementia promote aggregation of paired helical filaments by enhancing local beta-structure. *J Biol Chem,* 276**,** 48165-74.

VON BERGEN, M., FRIEDHOFF, P., BIERNAT, J., HEBERLE, J., MANDELKOW, E. M. & MANDELKOW, E. 2000. Assembly of tau protein into Alzheimer paired helical filaments depends on a local sequence motif ((306)VQIVYK(311)) forming beta structure. *Proc Natl Acad Sci U S A,* 97**,** 5129-34.

VOSSHALL, L. B. & STOCKER, R. F. 2007. Molecular architecture of smell and taste in Drosophila. *Annu Rev Neurosci,* 30**,** 505-33.

VOURKOU, E., PASPALIARIS, V., BOUROULITI, A., ZERVA, M. C., PRIFTI, E., PAPANIKOLOPOULOU, K. & SKOULAKIS, E. M. C. 2022. Differential Effects of Human Tau Isoforms to Neuronal Dysfunction and Toxicity in the Drosophila CNS. *Int J Mol Sci,* 23.

WANG, C., FAN, L., KHAWAJA, R. R., LIU, B., ZHAN, L., KODAMA, L., CHIN, M., LI, Y., LE, D., ZHOU, Y., CONDELLO, C., GRINBERG, L. T., SEELEY, W. W., MILLER, B. L., MOK, S.-A., GESTWICKI, J. E., CUERVO, A. M., LUO, W. & GAN, L. 2022. Microglial NF-κB drives tau spreading and toxicity in a mouse model of tauopathy. *Nature Communications,* 13**,** 1969.

WANG, C., TERRIGNO, M., LI, J., DISTLER, T., PANDYA, N. J., EBELING, M., TYANOVA, S., HOOZEMANS, J. J. M., DIJKSTRA, A. A., FUCHS, L., XIANG, S., BONNI, A., GRüNINGER, F. & JAGASIA, R. 2023. Increased G3BP2-Tau interaction in tauopathies is a natural defense against Tau aggregation. *Neuron,* 111**,** 2660-2674.e9.

WANG, C. K., NORTHFIELD, S. E., HUANG, Y. H., RAMOS, M. C. & CRAIK, D. J. 2016. Inhibition of tau aggregation using a naturally-occurring cyclic peptide scaffold. *Eur J Med Chem,* 109**,** 342-9.

WANG, J. Z., XIA, Y. Y., GRUNDKE-IQBAL, I. & IQBAL, K. 2013. Abnormal hyperphosphorylation of tau: sites, regulation, and molecular mechanism of neurofibrillary degeneration. *J Alzheimers Dis,* 33 Suppl 1**,** S123-39.

WANG, Y. & MANDELKOW, E. 2016. Tau in physiology and pathology. *Nat Rev Neurosci,* 17**,** 5-21.

WANI, W. Y., CHATHAM, J. C., DARLEY-USMAR, V., MCMAHON, L. L. & ZHANG, J. 2017. O-GlcNAcylation and neurodegeneration. *Brain Res Bull,* 133**,** 80-87.

WARD, S. M., HIMMELSTEIN, D. S., LANCIA, J. K. & BINDER, L. I. 2012. Tau oligomers and tau toxicity in neurodegenerative disease. *Biochem Soc Trans,* 40**,** 667-71.

WEAVER, C. L., ESPINOZA, M., KRESS, Y. & DAVIES, P. 2000. Conformational change as one of the earliest alterations of tau in Alzheimer's disease. *Neurobiol Aging,* 21**,** 719-27.

WEGMANN, S., EFTEKHARZADEH, B., TEPPER, K., ZOLTOWSKA, K. M., BENNETT, R. E., DUJARDIN, S., LASKOWSKI, P. R., MACKENZIE, D., KAMATH, T., COMMINS, C., VANDERBURG, C., ROE, A. D., FAN, Z., MOLLIEX, A. M., HERNANDEZ-VEGA, A., MULLER, D., HYMAN, A. A., MANDELKOW, E., TAYLOR, J. P. & HYMAN, B. T. 2018. Tau protein liquid-liquid phase separation can initiate tau aggregation. *Embo j,* 37.

WEISSMANN, C., REYHER, H. J., GAUTHIER, A., STEINHOFF, H. J., JUNGE, W. & BRANDT, R. 2009. Microtubule binding and trapping at the tip of neurites regulate tau motion in living neurons. *Traffic,* 10**,** 1655-68.

WESSELING, H., MAIR, W., KUMAR, M., SCHLAFFNER, C. N., TANG, S., BEEREPOOT, P., FATOU, B., GUISE, A. J., CHENG, L., TAKEDA, S., MUNTEL, J., ROTUNNO, M. S., DUJARDIN, S., DAVIES, P., KOSIK, K. S., MILLER, B. L., BERRETTA, S., HEDREEN, J. C., GRINBERG, L. T., SEELEY, W. W., HYMAN, B. T., STEEN, H. & STEEN, J. A. 2020. Tau PTM Profiles Identify Patient Heterogeneity and Stages of Alzheimer's Disease. *Cell,* 183**,** 1699-1713.e13.

WHITWELL, J. L., JACK, C. R., JR., BOEVE, B. F., SENJEM, M. L., BAKER, M., IVNIK, R. J., KNOPMAN, D. S., WSZOLEK, Z. K., PETERSEN, R. C., RADEMAKERS, R. & JOSEPHS, K. A. 2009a. Atrophy patterns in IVS10+16, IVS10+3, N279K, S305N, P301L, and V337M MAPT mutations. *Neurology,* 73**,** 1058-65.

WHITWELL, J. L., PRZYBELSKI, S. A., WEIGAND, S. D., IVNIK, R. J., VEMURI, P., GUNTER, J. L., SENJEM, M. L., SHIUNG, M. M., BOEVE, B. F., KNOPMAN, D. S., PARISI, J. E., DICKSON, D. W., PETERSEN, R. C., JACK, C. R., JR. & JOSEPHS, K. A. 2009b. Distinct anatomical subtypes of the behavioural variant of frontotemporal dementia: a cluster analysis study. *Brain,* 132**,** 2932-46.

WILLIAMS, D. W., TYRER, M. & SHEPHERD, D. 2000. Tau and tau reporters disrupt central projections of sensory neurons in Drosophila. *J Comp Neurol,* 428**,** 630-40.

WILSON, D. M. & BINDER, L. I. 1997. Free fatty acids stimulate the polymerization of tau and amyloid beta peptides. In vitro evidence for a common effector of pathogenesis in Alzheimer's disease. *Am J Pathol,* 150**,** 2181-95.

WISCHIK, C. M., BENTHAM, P., GAUTHIER, S., MILLER, S., KOOK, K. & SCHELTER, B. O. 2022. Oral Tau Aggregation Inhibitor for Alzheimer's Disease: Design, Progress and Basis for Selection of the 16 mg/day Dose in a Phase 3, Randomized, Placebo-Controlled Trial of Hydromethylthionine Mesylate. *J Prev Alzheimers Dis,* 9**,** 780-790.

WISCHIK, C. M., EDWARDS, P. C., LAI, R. Y., ROTH, M. & HARRINGTON, C. R. 1996. Selective inhibition of Alzheimer disease-like tau aggregation by phenothiazines. *Proc Natl Acad Sci U S A,* 93**,** 11213-8.

WITTMANN, C. W., WSZOLEK, M. F., SHULMAN, J. M., SALVATERRA, P. M., LEWIS, J., HUTTON, M. & FEANY, M. B. 2001. Tauopathy in Drosophila: neurodegeneration without neurofibrillary tangles. *Science,* 293**,** 711-4.

WU, L., MADHAVAN, S. S., TAN, C. & XU, B. 2022. Hexameric Aggregation Nucleation Core Sequences and Diversity of Pathogenic Tau Strains. *Pathogens,* 11.

WU, X., YANG, Z., ZOU, J., GAO, H., SHAO, Z., LI, C. & LEI, P. 2025. Protein kinases in neurodegenerative diseases: current understandings and implications for drug discovery. *Signal Transduction and Targeted Therapy,* 10**,** 146.

XIA, Y., PROKOP, S. & GIASSON, B. I. 2021. "Don't Phos Over Tau": recent developments in clinical biomarkers and therapies targeting tau phosphorylation in Alzheimer's disease and other tauopathies. *Mol Neurodegener,* 16**,** 37.

XIA, Y., PROKOP, S., GORION, K. M., KIM, J. D., SORRENTINO, Z. A., BELL, B. M., MANAOIS, A. N., CHAKRABARTY, P., DAVIES, P. & GIASSON, B. I. 2020. Tau Ser208 phosphorylation promotes aggregation and reveals neuropathologic diversity in Alzheimer's disease and other tauopathies. *Acta Neuropathol Commun,* 8**,** 88.

XIE, J. Z., ZHANG, Y., LI, S. H., WEI, H., YU, H. L., ZHOU, Q. Z., WEI, L. Y., KE, D., WANG, Q., YANG, Y. & WANG, J. Z. 2022. P301S-hTau acetylates KEAP1 to trigger synaptic toxicity via inhibiting NRF2/ARE pathway: A novel mechanism underlying hTau-induced synaptic toxicities. *Clin Transl Med,* 12**,** e1003.

YANG, Y., TAPIAS, V., ACOSTA, D., XU, H., CHEN, H., BHAWAL, R., ANDERSON, E. T., IVANOVA, E., LIN, H., SAGDULLAEV, B. T., CHEN, J., KLEIN, W. L., VIOLA, K. L., GANDY, S., HAROUTUNIAN, V., BEAL, M. F., ELIEZER, D., ZHANG, S. & GIBSON, G. E. 2022. Altered succinylation of mitochondrial proteins, APP and tau in Alzheimer's disease. *Nat Commun,* 13**,** 159.

YASUDA, M., NAKAMURA, Y., KAWAMATA, T., KANEYUKI, H., MAEDA, K. & KOMURE, O. 2005. Phenotypic heterogeneity within a new family with the MAPT p301s mutation. *Ann Neurol,* 58**,** 920-8.

YGLAND, E., VAN WESTEN, D., ENGLUND, E., RADEMAKERS, R., WSZOLEK, Z. K., NILSSON, K., NILSSON, C., LANDQVIST WALDö, M., ALAFUZOFF, I., HANSSON, O., GUSTAFSON, L. & PUSCHMANN, A. 2018. Slowly progressive dementia caused by MAPT R406W mutations: longitudinal report on a new kindred and systematic review. *Alzheimers Res Ther,* 10**,** 2.

YOKOYAMA, M., KOBAYASHI, H., TATSUMI, L. & TOMITA, T. 2022. Mouse Models of Alzheimer's Disease. *Front Mol Neurosci,* 15**,** 912995.

YOSHIYAMA, Y., HIGUCHI, M., ZHANG, B., HUANG, S. M., IWATA, N., SAIDO, T. C., MAEDA, J., SUHARA, T., TROJANOWSKI, J. Q. & LEE, V. M. 2007. Synapse loss and microglial activation precede tangles in a P301S tauopathy mouse model. *Neuron,* 53**,** 337-51.

YOUNG, A. L., BOCCHETTA, M., RUSSELL, L. L., CONVERY, R. S., PEAKMAN, G., TODD, E., CASH, D. M., GREAVES, C. V., VAN SWIETEN, J., JISKOOT, L., SEELAAR, H., MORENO, F., SANCHEZ-VALLE, R., BORRONI, B., LAFORCE, R., JR., MASELLIS, M., TARTAGLIA, M. C., GRAFF, C., GALIMBERTI, D., ROWE, J. B., FINGER, E., SYNOFZIK, M., VANDENBERGHE, R., DE MENDONçA, A., TAGLIAVINI, F., SANTANA, I., DUCHARME, S., BUTLER, C., GERHARD, A., LEVIN, J., DANEK, A., OTTO, M., SORBI, S., WILLIAMS, S. C. R., ALEXANDER, D. C. & ROHRER, J. D. 2021. Characterizing the Clinical

Features and Atrophy Patterns of MAPT-Related Frontotemporal Dementia With Disease Progression Modeling. *Neurology,* 97**,** e941-e952.

YU, A., FOX, S. G., CAVALLINI, A., KERRIDGE, C., O'NEILL, M. J., WOLAK, J., BOSE, S. & MORIMOTO, R. I. 2019. Tau protein aggregates inhibit the protein-folding and vesicular trafficking arms of the cellular proteostasis network. *J Biol Chem,* 294**,** 7917-7930.

YU, C.-C., CHANG, F.-C., HONG, Y.-H., LI, J.-C., CHEN, P.-L., CHEN, C.-H., CHIU, T.-W., LU, T.-T., WANG, Y.-M. & KAO, C.-F. 2021. Assessing the cognitive status of Drosophila by the value-based feeding decision. *npj Aging and Mechanisms of Disease,* 7**,** 24.

YUZWA, S. A., SHAN, X., MACAULEY, M. S., CLARK, T., SKOROBOGATKO, Y., VOSSELLER, K. & VOCADLO, D. J. 2012. Increasing O-GlcNAc slows neurodegeneration and stabilizes tau against aggregation. *Nat Chem Biol,* 8**,** 393-9.

ZABIK, N. L., IMHOF, M. M. & MARTIC-MILNE, S. 2017. Structural evaluations of tau protein conformation: methodologies and approaches. *Biochem Cell Biol,* 95**,** 338-349.

ZARS, T., FISCHER, M., SCHULZ, R. & HEISENBERG, M. 2000. Localization of a short-term memory in Drosophila. *Science,* 288**,** 672-5.

ZEMPEL, H. & MANDELKOW, E. 2014. Lost after translation: missorting of Tau protein and consequences for Alzheimer disease. *Trends Neurosci,* 37**,** 721-32.

ZHANG, B., MAITI, A., SHIVELY, S., LAKHANI, F., MCDONALD-JONES, G., BRUCE, J., LEE, E. B., XIE, S. X., JOYCE, S., LI, C., TOLEIKIS, P. M., LEE, V. M. & TROJANOWSKI, J. Q. 2005. Microtubule-binding drugs offset tau sequestration by stabilizing microtubules and reversing fast axonal transport deficits in a tauopathy model. *Proc Natl Acad Sci U S A,* 102**,** 227-31.

ZHANG, M. Y., LEAR, B. C. & ALLADA, R. 2022a. The microtubule-associated protein Tau suppresses the axonal distribution of PDF neuropeptide and mitochondria in circadian clock neurons. *Hum Mol Genet,* 31**,** 1141-1150.

ZHANG, S., ZHU, Y., LU, J., LIU, Z., LOBATO, A. G., ZENG, W., LIU, J., QIANG, J., ZENG, S., ZHANG, Y., LIU, C., LIU, J., HE, Z., ZHAI, R. G. & LI, D. 2022b. Specific binding of Hsp27 and phosphorylated Tau mitigates abnormal Tau aggregation-induced pathology. *Elife,* 11.

ZHANG, W., TARUTANI, A., NEWELL, K. L., MURZIN, A. G., MATSUBARA, T., FALCON, B., VIDAL, R., GARRINGER, H. J., SHI, Y., IKEUCHI, T., MURAYAMA, S., GHETTI, B., HASEGAWA, M., GOEDERT, M. & SCHERES, S. H. W. 2020a. Novel tau filament fold in corticobasal degeneration. *Nature,* 580**,** 283-287.

ZHANG, X., ZHANG, X., ZHONG, M., ZHAO, P., GUO, C., LI, Y., WANG, T. & GAO, H. 2020b. Selection of a d-Enantiomeric Peptide Specifically Binding to PHF6 for Inhibiting Tau Aggregation in Transgenic Mice. *ACS Chem Neurosci,* 11**,** 4240-4253.

ZHENG, J., LIU, C., SAWAYA, M. R., VADLA, B., KHAN, S., WOODS, R. J., EISENBERG, D., GOUX, W. J. & NOWICK, J. S. 2011. Macrocyclic β-sheet peptides that inhibit the aggregation of a tau-protein-derived hexapeptide. *J Am Chem Soc,* 133**,** 3144-57.

ZIV, Y., BIELOPOLSKI, D., GALANTY, Y., LUKAS, C., TAYA, Y., SCHULTZ, D. C., LUKAS, J., BEKKER-JENSEN, S., BARTEK, J. & SHILOH, Y. 2006. Chromatin relaxation in response to DNA double-strand breaks is modulated by a novel ATM- and KAP-1 dependent pathway. *Nat Cell Biol,* 8**,** 870-6.